AN ANALYSIS OF QUANTITATIVE ASPECTS OF ULTRASONIC PULSE - ECHO TECHNIQUES IN MEDICAL DIAGNOSIS

by

John Christopher Gore

Thesis submitted for the degree of Doctor of Philosophy in the University of London

1977

Department of Medical Physics
Royal Postgraduate Medical School

ROYAL POST GRADUATE MEDICAL SCHOOL
WELLCOME
- 6 DEC 1977
LIBRARY

ROYAL POST GRADUATE MEDICAL SCHOOL
WELLCOME
- 6 DEC 1977
LIBRARY

Abstract of Thesis

The basic physics of ultrasound methods is reviewed and their use in the extraction of quantitative measurements is illustrated by particular reference to cardiological applications. Methods of evaluating scanners are reviewed and the inadequacy of the tests in current usage is demonstrated by results obtained with conventional B scanners and a multi-element array system.

General problems of ultrasonic image formation are discussed and the formation of both A and B scan images is described in terms of linear filter theory. A specification of the scanner performance is derived in terms of spatial frequency responses, and suitable criteria for resolution and accuracy are developed in these terms. A relationship between the resolution achieved under non-ideal conditions and the intrinsic properties of the scanner is obtained, and by derivation of the transfer functions of each component, this intrinsic ability is related to the practical design of scanners.

A discussion of the significance of echo amplitude is illustrated with measurements made of the effect of changes in angle, size and roughness of the reflector, and of the behaviour of the transducer in reception. The concept of pulse structure, derived from considering the scattering integral for transient fields, is related to a theoretical model of scattering based upon the formation of sequences of replica pulses.

The statistical properties of echoes from inhomogeneous media are discussed and illustrated with measurements, and the results are related to the ultrasonic scanners' parameters and to the characteristics of the medium. A possible method

of tissue differentiation is outlined.

Finally, the imaging process is summarised in terms of an overall model which relates the final image to the parameters of importance in both the object and the ultrasonic system.

Acknowledgements

I would like to record my sincere thanks to Sidney Leeman for all his continuing advice and guidance, and for the many discussions which, besides occasionally generating heat, have often shed some light.

I thank Dr. E.W. Emery for his many helpful criticisms and encouragement in preparing this thesis.

I am grateful to Dr. Ronald Pridie for providing many hours of enjoyable clinical collaboration and discussion, and to Keith Willson for his advice and expertise in all matters of instrumentation.

The Medical Physics Workshop under Bill Coupland provided me with considerable help in constructing apparatus and I particularly appreciate the helpfulness of everyone there.

I was lucky to find an understanding typist, Jenny Eckford, whose skills have considerably improved the final presentation of this thesis.

I thankfully acknowledge the financial support of the Science Research Council and Hammersmith Hospital.

I thank my parents for all their support during and before these studies; and I am grateful to my wife, Joyce, for the understanding and encouragement which have helped me immensely.

Finally, I would like to pay tribute to the inspiration given to me by the late Professor R. Oliver, who suggested many of the problems considered here, who was an enthusiastic teacher and skilful supervisor, whose advice was always wise, and whose humility and courage will long be remembered.

Contents

	Page
Abstract	1
Acknowledgements	3
Contents	4
Preface	9
Chapter 1 Physical principles of ultrasonic diagnosis	
1.1 Introduction	11
1.2 Physical principles of ultrasound	15
1.3 Principles of pulse-echo techniques	22
1.4 Information content of ultrasonic images	26
Chapter 2 Ultrasound in cardiac diagnosis	
2.1 Introduction	33
2.2 Techniques used in cardiac diagnosis	35
2.3 Geometrical information from echocardiography	39
2.4 Physical information from echocardiography	46
2.5 Some limitations of echocardiography	51
Chapter 3 Methods of evaluating ultrasonic scanners	
3.1 Introduction	54
3.2 Review of methods	55
3.3 Ultrasonic equipment at Hammersmith Hospital	64

3.4 An assessment of an NE4102 Diasonograph 68

a Registration errors 68

b Velocity calibrations 69

c Transmitter characteristics and output calibrations 72

d Receiver frequency response 75

e Swept gain and dynamic range measurements 78

f Amplitude transfer functions and dynamic ranges 82

g Measurement of lateral resolution 88

h Measurement of axial resolution 100

3.5 An assessment of a Multiscan 104

a Technical description 104

b Measurements of lateral resolution 106

c Range precision and resolution 124

3.6 An assessment of distortions in Multiscan images 129

Chapter 4 The resolution of ultrasonic A scanners

4.1 Introduction 144

4.2 Formulation of the problem 147

4.3 Description of the object 150

4.4 Description of the A scan as a linear filter 154

4.5 Discussion of linearity and stationarity 159

4.6 Single index of resolution 164

4.7 Approximations for real functions 168

4.8 Estimates of achieved resolution 178
a Effect of attenuation or gain 178
b Effect of frequency dependent attenuation 181
c Effect of time dependent gain 186
d Effect of threshold 189
e Effect of differentiation 195
f Summary 202
4.9 Axial resolution of the B mode: the TP scan 203
4.10 Intrinsic range accuracy of the A scan 212
4.11 A consideration of A scan design 218
4.12 Transfer functions of piezoelectric transducers 220
a Solutions for transducers in transmission 221
b Solutions for transducers in reception 226

Chapter 5 The resolution of ultrasonic B scanners
5.1 The formation of B scan images 231
5.2 Scanner transfer functions 242
5.3 The point spread function 247
5.4 Measurements of point spread functions 259
5.5 Some factors affecting the Equivalent Frequency 265
a Effect of threshold 265
b Effect of non-linear amplification 266
c Effect of bistable displays 267
d Effect of focussing 267

5.6 A consideration of factors that determine the intrinsic point spread function 270

a The sound field from a pulsed transducer 270

b Design considerations for pulsed fields 280

5.7 A reconsideration of the A scan 286

Chapter 6 A consideration of echo amplitudes

6.1 Introduction 288

6.2 Factors that affect echo amplitude 290

6.3 Factors that affect apparent reflection coefficients 295

a Echo structure in pulsed conditions 295

b Effect of angle 297

c Effect of reflector area 310

d Effect of sampling the echo field 316

6.4 Conclusions 323

Chapter 7 An analysis of grey scale images

7.1 Methods of tissue characterisation 325

7.2 The inhomogeneous wave equation 328

7.3 Solution for backscattering of pulses 331

7.4 Implications for tissue characterisation by B scanning 340

7.5 A possible method of tissue characterisation 343

7.6 Conclusions 352

Chapter 8 Some further problems 354

Appendix A The Nuclear Enterprises NE4102 Diasonograph 361

Appendix B Derivation of the transient response of a piezoelectric transducer

B.1 General equations 366

B.2 Transmission transfer functions 371

a Weakly coupled transducers 372

b Rigidly backed transducers 374

B.3 Receiver transfer functions 377

a Open circuit response 377

b Response for finite loading and rigid backing 380

Appendix C The structure of the transient sound field from a plane transducer

a Near Field 381

b Far Field 385

References 390

Preface

The central problem considered in this thesis is the extraction of quantitative information from images produced with ultrasonic pulse-echo scanners, and the thesis aims to explore some of the limitations placed on this information by instrumental characteristics and by the fundamental properties of ultrasound. Many phenomena are not considered either because not enough is known about them or because they vary widely according to the circumstances in which a scanner is used and so they cannot be described easily in general.

The first three chapters are not essential to the later discussion of the principal problems, and much of their content is available elsewhere but is included to illustrate the approach that has generally been followed by other people. Chapters 1 and 2 set the physical and clinical backgrounds for readers who may not be familiar with medical ultrasonic methods, whilst the first part of Chapter 3 is included to help formulate some of the problems considered later and to summarise some measurements of scanner characteristics that were performed at the outset of this study in order to obtain an appreciation of the problems of importance. The second half of Chapter 3 contains observations of the behaviour of a new type of scanner, and highlights some of the distortions obtainable with real time multielement arrays.

The crucial problem of defining and measuring scanner resolution is discussed in Chapters 4 and 5 where some novel concepts of resolution are introduced and basic problems of image formation are discussed. Here the principal aim is to describe the intrinsic characteristics of a scanner and to discuss some of the other factors that influence the resolution

achieved in practice. The electromechanical response of a piezoelectric transducer, and the structure of a sound field from a pulsed transducer, are included for completeness and to emphasise the transient character of pulse-echo phenomena, although much of the theoretical analysis is available elsewhere.

Chapters 6 and 7 are concerned with the extraction of information other than interface position and the concept of echo structure is given some quantitative basis. Chapter 6 considers the information contained in the shape and size of single echoes from well defined interfaces, whilst Chapter 7 discusses the information contained in echo ensembles produced by weak backscattering from inside inhomogeneous tissues and suggests criteria for tissue characterisation.

The mathematical notation is consistent within each chapter: symbols which are used to denote more than one quantity in the thesis are defined for each context and no confusion should arise when cross referring.

Chapter 1: Physical Principles of Ultrasonic Diagnosis

1.1 Introduction

It is not the purpose of this thesis to clarify uncertainties in the history of applications of ultrasonic pulse echo techniques in medicine, nor to identify the significant advances made in the diagnosis of diseases using such methods. Several good reviews of the evolution of ultrasonic techniques have been published (for example, Holmes (1974)), but the precise dating of various advances remains a minor controversy. It is clear, however, that since the realisation, soon after the peace settlement of 1945, that ultrasonic depth sounding and flaw detection could be used to identify changes in soft tissue characteristics, that pulse echo techniques have gradually become an accepted addition to the range of methods available in medicine for diagnosis. Indeed, in some areas of their application, ultrasonic methods are established as routine, preferred procedures that provide reliable information sufficient to obviate tests which were previously considered essential. In obstetrics, for example, the monitoring of fetal development without hazard by ultrasonic scanning is an important adjunct to the handling of ante-natal patients, whilst the information obtained by echocardiography may be used to decide between alternative surgical procedures and often replaces the need for catheterisation and angiography. As with all other methods of obtaining information, ultrasonic techniques have limited accuracy and are not universally applicable. Although the pulse echo technique produces images of internal structures of the body non-invasively, the information contained in these images

is different and sometimes less useful than that obtained by other imaging techniques (e.g. information on physiological function obtained by scintigraphy), whilst the image itself may contain inaccuracies or distortions that can give rise to spurious conclusions. Any method of producing an image is necessarily imperfect, and the information obtainable by ultrasonic techniques is subject to the constraints imposed by distortion, noise and artefacts, arising from various sources, that are encountered in all other forms of image. It is one of the aims of this thesis to identify some of these limitations, and particularly to clarify some of the factors that influence the quantitative accuracy of the information obtainable.

The extent of the use of ultrasonic pulse echo techniques is determined partly by the nature of the information obtained and its relevance to genuine problems, partly by the ease with which such information is obtained, and partly by the reliability that such information is not spurious. The nature of the information and its reliability are dependent on many factors some of which are inherent in the physics of ultrasound and some of which are determined by the choice of operating characteristics of the equipment used.

The nature of the information obtainable has seldom been the subject of any detailed discussion in the literature, and few definitive statements have been made that describe the types of information that can be derived by different techniques. Little discussion has appeared which relates the information obtainable to basic physical parameters of tissues or of

ultrasound, or to the equipment used for scanning. Such considerations are referred to later in this chapter and they recur throughout this thesis.

The ease of obtaining information depends on the tissues investigated and the equipment used, and with the present generation of scanners, it is strongly dependent on the equipment operator, although there is some basis for believing that the technical expertise of the operator will be less important with future developments. An overall limitation is that many regions of the body cannot be examined with ultrasound because of the nature of the overlying tissues, especially when a region of interest is in the acoustic shadow of a region of bone or air filled cavity. An important consideration that underlies some of the analysis produced in this thesis is the extent to which quantitative information is sacrificed by the introduction of design features which allow images to be produced more easily.

The reliability of the information produced by ultrasonic methods depends on the nature of the information itself, since this determines the type of artefact or noise that can produce spurious results. It also depends on the equipment used in any measurement. This thesis attempts to clarify some of the problems associated with measuring the usefulness of different techniques and different types of information. By describing the information obtainable in terms of measurable physical parameters of the tissue and the equipment used, realistic limits can be set on the reliability of results, and suitable design criteria can then be established. However, before defining more exactly the problems that require attention, a

brief review is given of the methods which this thesis analyses. In discussing some of the techniques used, the nomenclature used throughout this thesis is introduced.

1.2 Physical Principles of Ultrasound

Ultrasonic pulse echo techniques utilise the phenomenon that longitudinal waves with frequencies of a few MegaHertz propagate in soft tissues with velocities of the order of 1½ mm/μsec. The precise behaviour of compressional waves in tissues is not well documented but for many purposes an adequate description is afforded by the homogeneous wave equation

$$\nabla^2 \phi - \frac{1}{c^2} \frac{\partial^2 \phi}{\partial t^2} = 0$$

where ϕ = the velocity potential

c = the sound velocity.

This equation is derived from linearised equations of motion by assuming that the medium is continuous, homogenous, non-attenuating and perfectly elastic and that it undergoes small amplitude oscillations. As a result of such oscillations, the medium's density and pressure change adiabatically, and the condition that these changes are small is satisfied if the velocity of the elements of the medium, v, satisfies

$$v \ll c$$

The homogeneous equation may be replaced by a more suitable equation when required to allow for changes in the medium's properties. For example, when the thermal conductivity is not zero then some of the energy in the wave is absorbed by the medium, and the wavelength is a complex function of the frequency. For simple (so called classical) absorption the wave equation reduces to the equation of diffusion (Landau and Lifshitz, 1970). Similarly, when the medium in which the

sound propagates is non-uniform, the acoustic properties vary with position and the effects of inhomogeneities must be considered. An inhomogeneous wave equation is considered in Chapter 7.

There have been few attempts at measuring the basic physical parameters of tissues systematically so that an exact description of sound in tissues cannot be given. It is not apparent, for example, whether it is necessary to use a general stress tensor to describe the elastic properties of tissues or whether they can be adequately described as extended fluids that are unable to support shear stresses. Such considerations are important when considering the precise behaviour of a wave at a reflecting boundary, but the only relevant theoretical work has been directed to analysing mode conversions at solid intrusions in liquids. In this thesis, no attempt is made to determine the importance of such conversions, since it may be generally assumed that energy removed by transverse waves does not contribute significantly to the echo signal. The validity of this does not prejudice the applicability of any of the results of this thesis, and leads to a simplification of the equations of motion. The relevant solid description assumes that the wave induces only pure longitudinal strain in the medium. The second Lame constant (the shear modulus), defined as the ratio of shear stress to shear strain, is then effectively zero, whilst the first Lame constant is numerically equal to the Bulk Modulus, K. This description is then identically equal to the description of an isotropic extended fluid. The relevant physical parameters which describe the motion are the

particle displacement, $\underline{u}$, from which we obtain the particle velocity, $\underline{v}$.

$$\underline{v} = \frac{d\underline{u}}{dt}$$

The fractional change in the volume of any element is the condensation, s

$$s = - \text{div } \underline{u}$$

which is everywhere small. The locally varying excess pressure is the acoustic pressure, p, and it is proportional to the condensation

$$p = K s$$

K = the adiabatic Bulk Modulus or Volume Stiffness, whose reciprocal is the Compressibility. The wave velocity c is given by

$$c^2 = \frac{K}{\rho}$$

where ρ = the ambient density.

It is often convenient to use the velocity potential ϕ, such that

$$\underline{v} = -\underline{\nabla} \phi$$

The pressure p is then

$$p = \rho \frac{\partial \phi}{\partial t}$$

whilst the condensation s

$$\frac{\partial s}{\partial t} = \frac{1}{c^2} \frac{\partial^2 \phi}{\partial t^2}$$

The Specific Impedance Z is the ratio of p to v

$$Z = - \frac{\rho \frac{\partial \phi}{\partial t}}{\nabla \phi}$$

Various types of wave may be propagated. A particularly useful approximation to some real waves is a plane wave of the form

$$\phi = A \cos(wt - kx)$$

in which case $Z = \rho c$.

For a plane wave in a lossless medium, Z is real and depends only on the medium, so that it is called the Characteristic Impedance. Another type of wave often encountered is a spherical wave of the form

$$\phi = \frac{A}{r} \cos(wt - kr)$$

For such a wave,

$$Z = \rho c\left(1 + \frac{j}{kr}\right)\left(1 + \frac{1}{k^2r^2}\right)^{-1}$$

For a spherical wave, there is a phase shift between the velocity potential and particle displacement. This phase angle is ψ where

$$\tan \psi = \frac{1}{kr}$$

When a sound wave is incident on a boundary between two different media it undergoes reflection and refraction. This means that in addition to the incident wave there appears a reflected wave propagating back into the first medium from the surface of separation, and a refracted wave in the second medium. The relation between these waves is determined by the boundary conditions at the surface of separation which require the pressures and normal velocity components to be equal. For a plane wave incident on a plane boundary, separating

media 1 and 2, if θ_1 = the angle of incidence

θ_2 = the angle of reflection

θ_3 = the angle of the refracted wave

then

$$\sin \theta_1 = \frac{c1}{c2} \sin \theta_2 ,$$

where c_1, c_2 are the velocities in the two media.

The Reflection Coefficient, the ratio of the time averaged energy flux densities in the reflected and the incident waves, is R

$$R = \left(\frac{\rho_2 c_2 \cos \theta_1 - \rho_1 (c_1^2 - c_2^2 \sin^2 \theta_1)^{\frac{1}{2}}}{\rho_2 c_2 \cos \theta_1 + \rho_1 (c_1^2 - c_2^2 \sin^2 \theta_1)^{\frac{1}{2}}}\right)^2$$

At normal incidence, $\theta_1 = 0$, and

$$R = \left(\frac{Z_2 - Z_1}{Z_2 + Z_1}\right)^2$$

However, many boundaries are not plane, so that the effective impedance change depends on factors other than the Characteristic Impedance difference, and such factors are considered in Chapter 6.

It is usual to describe the waves deflected by objects in terms that depend arbitrarily on the object size. The difference between the actual wave produced with the object present and the undisturbed wave is the scattered wave, and for a plane wave incident on an object there is produced a scattered wave that spreads in all directions from the obstacle, distorting and interfering with the incident plane wave. The distinctions between obstacles that are large

compared to the wavelength, which create sharp edged shadows and are describable using the approximations of geometrical optics, and those that are very small compared with the wavelength, from which the scattered wave propagates in all directions can often be usefully drawn, but many of the objects of interest in medical ultrasonics belong to an intermediate class where the object has dimensions of only a few wavelengths, giving rise to a variety of interference phenomena. Where such objects are considered, the ray approximations that are valid elsewhere cannot be used. However, calculations of the distributions of pressure caused by surface sources of sound can be performed using suitable expressions of Huyghens principle. An important result of Kirchoff's Diffraction Theory (Born and Wolf, 1975) expresses the velocity potential at a point in terms of a surface integral of point and dipole sources. If $\phi(x,y,z,t)$ is a solution of the equation

$$\nabla^2 \phi = \frac{1}{c^2} \frac{\partial^2 \phi}{\partial t^2}$$

whose partial derivatives of the first and second orders are continuous within and on a closed surface S, and if (x',y',z') is a point within S

$$\phi(x',y',z',t) = \frac{1}{4\pi} \iint_S \left(\underset{\sim}{\phi} \frac{\partial}{\partial n}\left(\frac{1}{r}\right) - \frac{1}{cr} \frac{\partial r}{\partial n} \left(\underset{\sim}{\frac{\partial \phi}{\partial t}}\right) - \frac{1}{r}\left(\underset{\sim}{\frac{\partial \phi}{\partial n}}\right) \right) dS$$

where r is the distance from the point (x',y',z') to a point on S

$\frac{\partial}{\partial n}$ denotes differentiation along the inward normal to S

$\underset{\sim}{(\ )}$ indicate retarded values.

If (x',y',z') lies outside S, $\phi = 0$.

This particular formulation of Huyghens Principle reduces to the formulae of Poisson, Rayleigh and Helmholtz if further assumptions are made (Baker and Copson, 1950). The formula derived by Rayleigh (1896) is useful when considering the radiation from a bounded plane surface. This gives, for monochromatic excitations of the surface,

$$p(x',y',z',t) = \frac{i\rho w\, e^{jwt}}{2\pi} \iint_S \frac{e^{-jkr}}{r} V_n(S)\, dS$$

where V_n = the maximum normal velocity of the surface.

1.3 Principles of Pulse Echo Techniques

Ultrasonic scanners use piezoelectric transducers to generate pulses which are short in duration (typically a few cycles of their fundamental frequency) and which have diameters of several millimetres. Such pulses are produced by the heavily damped mechanical ringing of a ceramic element which is typically 20 to 30 wavelengths in diameter and which is excited by a transient voltage. A description of the design and operation of transducers is given in Appendix B whilst the characteristics of the sound field produced by a wide bandwidth large aperture radiator are considered in Appendix C.

Sound pulses propagating in tissues are partially reflected at changes in the acoustic properties of the medium, and echoes are received at the transducer where they produce electrical signals whose precise characteristics depend on the transfer properties of the transducer. The voltage at the receiver is an amplitude modulated Radio Frequency signal which can be processed in various ways. The receiver contains an amplifier, usually tuned to give low noise levels with restricted frequency response, and a detection stage, from where the envelope of the signals (video signal) may be reshaped (for example by differentiation) amplified and displayed on a cathode ray oscilloscope. This elementary display is the A scan and it records the variation of received signal amplitude with time. The receiver acts as a clock which compares the times taken for echoes to return from reflecting interfaces with the time base velocity of the CRO. By assuming a suitable average velocity for sound in tissues, the A scan display can be calibrated in terms of distance in tissues.

Other modes of display can be derived from the A scan. The intensity of a CRO may be modulated by the video waveform or by signals derived from it to give a B-mode display. The nature of the signal processing fundamentally affects the information content of the display. Intensity modulated displays can be usefully employed to investigate the characteristic motions of structures. By displacing a single B-mode line of echoes uniformly with time, an image is produced on which stationary structures trace out straight lines but moving structures give displacement - time curves (Figure 1.1). Such Time Position (TP) scans are particularly useful in investigating the heart. Two dimensional images of cross sections through the body can be obtained by moving the transducer over the body surface, changing its direction and position, whilst simultaneously deflecting the B-mode line of echoes in exactly the same geometry. This produces a B scan which can be recorded either on to a film or on a storage tube. The pattern of transducer movement distinguishes the type of B scan produced - usually it is either a Linear scan, a Sector scan or a hybrid Compound scan - whilst a variety of techniques are used for moving the transducer and monitoring its position. These include mechanical couplings which require the operator to move the transducer over the surface of interest, automated scanners which scan in a fixed geometry (e.g. Brown, 1973, Hill, 1976), and real time mechanical scanners which produce cross sections in fractions of a second (e.g. the Siemens Vidoson). Increasing interest is being shown in techniques which deflect the sound beam but which do not move the transducer physically. The sound beam can be moved over the patient by sequentially exciting

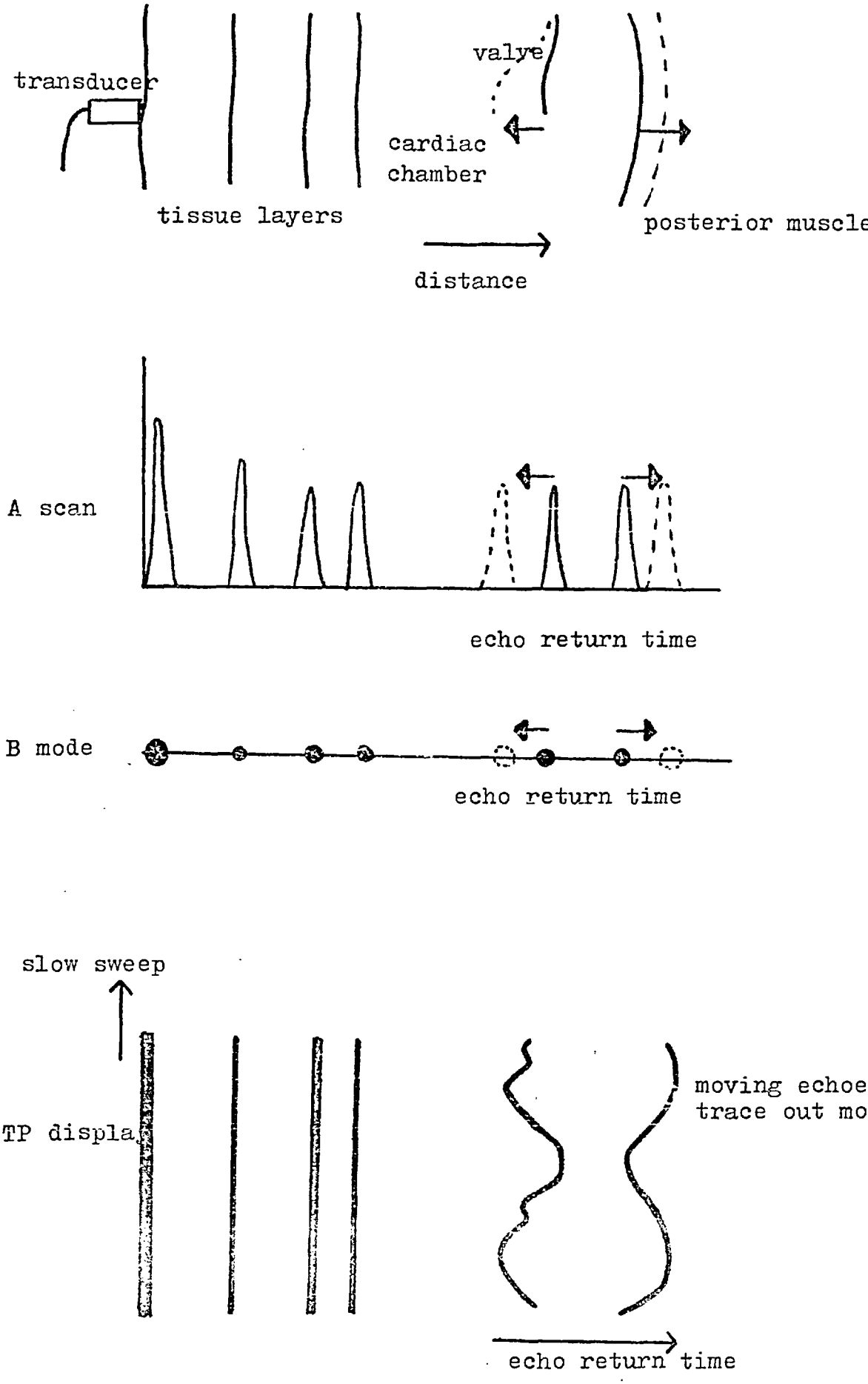


Figure 1.1 Principle of A and TP scan techniques.

the elements of an array of transducers (e.g. the Multiscan of Bom, 1972), or it can be deflected inside tissues by using several elements excited with small phase differences (e.g. Somer, 1968).

A more comprehensive review of current techniques has been given, for example, by McDicken (1976). A description of a B scanner which is extensively used in hospitals is given in Appendix A.

1.4 Information content of ultrasonic images

One of the purposes of this thesis is to investigate the extent to which quantitative information may be derived from ultrasonic A, B or TP scans. Some illustrations of the uses of this information are given in Chapter 2 where the requirements for quantitative measurements in echocardiography are discussed. However, the general nature of the information derived for such application may first be described.

Irrespective of the mode of the final display, or the design of the scanner, all pulse echo techniques measure times of return of echoes, and estimates of distance are then made by assuming an appropriate velocity and direction for the emitted sound pulse. The precise nature of the image depends on many other parameters, such as the signal processing of the receiver, whilst B scans by their very nature require the monitoring of other variables, but a considerable amount of information originates from estimates of interface distances only. An A scan, for example, may be used to measure distances or separations along a single direction, whilst TP scans allow the time derivatives[iv] of A scan dimensions to be estimated. A B scan provides measurements of distances along any direction in the plane of scan, thereby conveying two dimensional information about the positions of reflecting interfaces. Accurate measurements obtained with an A scan can produce information about organ sizes and tissue thicknesses, and examples of these are given in Chapter 2. The natural uses of B scans for measuring cross sectional areas, for studying organ shapes and sizes in three dimensions, or for determining

the velocities and accelerations of moving organs, are examples of the extraction of quantitative information from knowing only the positions of interfaces. Such information may be called Geometrical Information, and it requires no other property of the echo to be depicted in the image than the position in the object from whence the echo was derived. Geometrical Information is lost whenever there are errors in the positions of interfaces in the display.

Another type of information may be described as Physical Information, which can be obtained by considering features of echoes other than their times of arrival at the transducer. Such information may be related to the physical composition of interfaces and must be derived by analysing echo amplitudes and shapes. Such analyses may be performed in the A or B mode, on single echoes or echo complexes, in the time domain or after Fourier Transformation, but all are related in that they attempt to portray information about characteristics of interfaces other than just their positions.

The information obtainable by existing pulse echo techniques may therefore be separated into at least four classes. These are

(1) Qualitative Geometrical Information - this is derived from our subjective perception of shapes and positions of objects and those features of general anatomy which are not measured precisely but which contribute to any diagnosis or classification of the object.

(2) Quantitative Geometrical Information - this is obtained from precise measurements of dimensions, rates of change, etc.,

which describe the detailed anatomy of an object.

(3) Qualitative Physical Information - this is obtained by using echo shape and size cosmetically to enhance images, which may improve our perception of shapes and boundaries and our recognition of different media.

(4) Quantitative Physical Information - this is obtainable from quantitative analyses of echo shapes, distributions, or other suitable features, and should provide an objective description of the physical condition of any region.

This classification is arbitrary but conveniently matches our intuitive appreciation of the information conveyed in ultrasonic images. For example, Class 1 information might provide the basis for the detection and recognition of a fetus in utero, and a qualitative description of its general presentation and condition, whereas measurements of fetal dimensions (Class 2 information) produce a description of the degree to which the condition or abnormality (in this case pregnancy) has progressed. Such quantitative information is often useful because it enables a direct comparison of a patient's data with tabulated normal values. Class 3 information might correspond, in this example, to the use of grey-scale 'speckle' patterns to aid the identification of the placenta, whilst Class 4 information could perhaps be used to assess any degree of placental insufficiency. Quantitative information is often required not to establish the general nature of a complaint but to assess the degree or severity of abnormality or disease.

The four classes may not always be separable or independent. The distinction between qualitative and quantitative information

is somewhat artificial in present imaging contexts because the eye and brain of an observer undoubtedly use semi-quantitative analyses of an image to produce qualitative judgements, but such visual perception effects are not considered here. Each type of information may impose different requirements on scanner design and use, and some conflicting requirements are considered later. In practice, it may not be possible to maximise all four types of information simultaneously, although this should be the aim of scanner design. However, many of the characteristics of scanners which affect the amount of information obtainable may be identified on the basis of the classification above.

The derivation of quantitative geometrical information must obviously depend on the range accuracy of a scanner, a concept which is required to describe the capacity of any scanner to obtain accurate estimates of distances along the path of the sound pulse. This parameter is also a fundamental limitation on the accuracy with which possible movements may be monitored because it affects the errors included in measurements of velocity or acceleration. Similarly, range resolution is obviously important because it affects the ability of a scanner to display closely spaced interfaces, so that it is an inherent constraint on the detail included in the image. Range resolution and accuracy are likely to be extremely significant when considering the positions of interfaces for deriving quantitative Geometrical information from A and B scans. The amount of information obtained from a B scan also depends on the ability to place interfaces in their correct positions in a

two dimensional display which requires that a scanner measure relative positions accurately. The usefulness of a B-scan image is therefore dependent on variations of range accuracy with transducer angle or position, which are conventionally described in terms of scanner registration errors and image distortions. The quantity lateral resolution is also necessary to describe a scanner's ability to record detail in the B mode. Furthermore, it is evident that both the qualitative and the quantitative Geometrical information contained in any scan depends on the number of interfaces detected and displayed, and this is partly determined by scanner sensitivity.

The requirements for optimal extraction of Physical Information are less clear because it requires a more detailed description of the physical processes involved in pulse echo techniques to determine what features of echoes should be analysed. One of the purposes of the second part of this thesis is to investigate the formation of echoes to help establish suitable methods of extracting Physical Information.

It can be recognised that many independent factors can affect each type of information. Certainly the design of a scanner and the method of its use are important. The calibration of a scanner and the expertise of its operator must however be considered of secondary significance here, although both can seriously affect the usefulness of the result of a scan. Some attention is given to calibration errors in Chapter 3. In general, there can be little knowledge available about effects such as refraction errors, which may cause range errors and distortion, or many types of artefact which contribute to

the noise in an image, since these depend on the precise nature of the object investigated and are limitations only in particular circumstances. Similarly, echo amplitude changes caused by attenuation in tissue are limitations of the pulse echo technique itself and we can have no previous knowledge of their importance. In this thesis, it is those features of scanner design which limit the information obtainable which are of interest. In the discussion later, factors which are inherent in the pulse echo technique itself or which arise only with particular media, are specifically excluded although the significance of some may be mentioned. The discussion is intended to consider the features of scanner design which are important for the potential derivation of Geometrical or Physical information.

Although much has been written about the relative merits of different forms of display, Information Theory does not yet provide a satisfactory description of the subjective use of the qualitative content of images. In this thesis therefore the primary consideration will be the evaluation of quantitative information, and of particular interest are the conflicting requirements of different classes of information.

A further consideration of all image science must be the specification of suitable criteria by which to assess images, from which follows a practical requirement for methods of comparing different scanners. A basic description of scanner performance should enable the degree of quantitation obtainable to be estimated. Some of these considerations are already understood and some are summarised by the authors cited in

Chapter 3, but in this thesis a further attempt is made to specify the ability of scanners to obtain quantitative information in the absence of extrinsic influences. In this way some poorly understood design features can be properly described and a more comprehensive appreciation of the uses of quantitative pulse echo techniques can be obtained.

Chapter 2: Ultrasound in cardiac diagnosis

2.1 Introduction

It is illustrative to consider the applications of ultrasonic pulse echo techniques in a particular field of clinical interest in order to demonstrate some of the problems associated with scanning and to clarify some of the concepts introduced in Chapter 1. The example discussed below is the heart which is especially interesting not only because it is an important organ to study but also because it poses novel problems for scanner designers and clinicians. There have been several comprehensive treatises published on echocardiography (e.g. Gramiak and Waag, 1975, Feigenbaum, 1972) which adequately describe details of the various clinical techniques and the characteristic presentations of different heart conditions which have been detected with ultrasound. Here we are not concerned with emulating any of these summaries of the present state of echocardiography. The plethora of publications in this field is evidence of the snowballing of the applications of echo techniques of recent years, but a few particular applications can be used to illustrate general features of the way that pulse echo techniques provide information.

The heart is important because its pumping action is vital to normal body functions, and the widespread occurrence of heart disease in Western society has made it a prime concern of modern medicine. There are a large number of different types of heart disease - some acquired, others congenital - which may affect the anatomy, physiology or histology of the heart, and which can present themselves clinically in diverse ways. Many heart complaints can be remedied if they are detected

early enough, so there is a demand for a routine method of screening the population to diagnose diseases in their early stages. In order to be useful, such a technique must evaluate parameters which are indicators of the state of the heart, and at present echocardiography provides several such parameters more conveniently than any other method. Electrical signals from the heart are routinely monitored by electrocardiography but ECG traces are often difficult to interpret especially when there are conduction defects. Phonocardiography and auscultation are useful for diagnosing haemodynamic irregularities but considerable skill is required to use a stethoscope successfully, and the information provided is only qualitative. Radiological (or even radioisotope) methods of producing images of the heart are not without risk; the use of catheters is itself traumatic, there is a relatively high X-ray dose to the patient and despite the use of image intensification and contrast enhancement the image quality is not good. Angiocardiography cannot therefore be routinely used or repeated, and is expensive in terms of hospital beds and personnel. Echocardiography provides an inexpensive, repeatable non-invasive screening technique which is hazard free yet which provides information about a wide range of heart conditions.

2.2 Techniques used in cardiac diagnosis

Improvements in the equipment used for cardiac ultrasonography are continually being described. Conventional A scans are still used however, often because it is easier to recognise moving echoes in the A mode. The TP scan is used most extensively to display echoes from a single direction through the heart which are recorded continuously either with a storage cathode ray tube, polaroid film, video tape, or most commonly a strip chart recorder. Various techniques have been described in the literature for obtaining additional information by angling the transducer in a standard manner (the 'M' scan), whilst reports have been made of attempts to use advanced signal processing, computer analysis and pattern recognition to enhance the value of TP scans (e.g. McSherry, 1973, Waag and Gramiak, 1973). Gramiak and Waag (1973) described a method of recombining samples of many TP scans taken at different phases and orientations to produce a distorted but dynamic two dimensional image.

One of the major limitations of the single dimension technique is that it requires a specialist appreciation of the orientation of the heart which is not normally encountered in conventional medical training. This limitation is largely overcome by the use of two dimensional images which are more easily recognised. Conventional B scanning of the heart is not very useful because cardiac motion blurs the image during the scan unless the transducer is moved continuously, in which case different regions of the heart are recorded at different phases. Such a continuous sweep technique has been used (Gehkre, 1975) to obtain limited useful information and it has

the advantage that true anatomic relationships may be derived with unmodified B scanners. A method of synchronising B scanners to display only those echoes received during one phase of the heart's cycle, which is determined by reference to the R wave of the ECG, has been used to provide B scans of single phases of the cardiac motion (Gehkre, 1975, King, 1973) but there are disadvantages in the use of this technique. It is tedious, it provides little information about the dynamics of the heart, and is unsuitable for studying arrythmic hearts because it averages over the movements of many cycles. However, it is less inconvenient to use if many separate phases can be recorded simultaneously, and this has been achieved using a video tape (Unirad, 1973) and digital recording (Willson et al. 1975). A computer interface for producing images of 50 different phases of the heart's cycle, which can be displayed sequentially after processing, has been developed at Hammersmith Hospital.

More information is potentially available from real time two dimensional scanners such as the Multiscan of Bom (1972). Linear arrays of this type suffer from different distortions and artefacts than phased arrays which produce sector scans. Several phased arrays have been described which are particularly suited to cardiac imaging (Somer, 1973, Thurstone et al. 1973).

Mechanical scanners have been used to investigate the moving heart. Some use water baths and image the whole heart (e.g. Gehkre, 1975) whilst others use a rocking transducer to obtain echoes from a small section of the heart (e.g. McDicken et al. 1974).

There have also been attempts to produce three dimensional images of the heart although it is not yet clear whether it is more satisfactory to produce a scanner that can scan in any direction (Meindl, 1976) or to reconstruct a three dimensional image from several two dimensional sections (Dekker, 1974). Few clinical applications have yet been reported of intracardiac transducers such as those developed by Bom (1972) or Eggleton et al (1970), although these have proven useful in studies on experimental animals and could be useful if introduced into the thoracic cavity without trauma.

In trying to obtain information about the dynamic geometry of the heart, a basic limitation of echocardiography is that the heart is only accessible through a relatively small acoustic window. The front of the heart is normally covered by the lungs and pleura except for a small triangular area in the left parasternal region extending down from the third or fourth intercostal cartilage, and it is through this acoustic window that sound may pass backwards through the skin, the subcutaneous fatty tissue, intercostal muscles, the two layers of the pericardium, the anterior heart wall, the cavity of the Right Ventricle, the Interventricular Septum, the Left Ventricle, the posterior heart wall, and finally the pericardium posteriorly. Often the beam enters the Left Ventricle by traversing the Interventricular Septum without first passing through the Right Ventricle, and it may encounter other cardiac structures such as valves, papillary muscles, or other chambers such as the Left Atrium. The exact course varies considerably because of variations in heart orientation and probe position.

The most important echo producing interfaces are the front of the heart, the septum and the posterior wall, as well as the heart valves. The mitral valve, and particularly its anterior cusp, has been studied most extensively and is generally accepted to supply useful information even in some conditions which show no valve disease. Similarly, the Left Ventricle has been explored more thoroughly than any other chamber, not only because it is more accessible but also because left ventricular dysfunction is a significant indicator of disease.

2.3 Geometrical Information from Echocardiography

A regularly beating normal heart contains structures which move in well defined regular patterns with fixed phase relationships. For example, the walls of the Left Ventricle move towards each other in systole and away in diastole, whereas the Mitral Valve executes a characteristic M shaped movement with two openings and closures per cycle, one partial and one complete. When these characteristic movements are not observed a qualitative assessment of the abnormality can be made from a TP scan, and often this is sufficient. Abnormal motions may be more clearly seen sometimes in real time two dimensional images which also provide an impression of the anatomic relations between different structures. A sweep with a single transducer (M scan) can also give a useful indication of relative positions of structures. Some particular examples of abnormalities which can be diagnosed from the qualitative appearance of scans are aneurysms, which show as irregularities in the shape of the heart walls; pericardial effusions produce clear spaces in the pericardial sac separating the chest wall from the front of the heart; immobile or regurgitant valves produce unusual movements; in many cases of obstructive cardiomyopathy, the overgrowth of the myocardial muscle can be delineated, obstructions to the outflow tract can be detected and paradoxical movements investigated. There are a large number of such qualitative features in cardiac scans which an experienced clinician can use to great effect, but they do not generally provide an accurate assessment of the degree to which disease has advanced which is the purpose of quantitative information.

The Quantitative Geometrical Information which is derived from heart scans includes precise measurements of single dimensions of chambers, especially the short axis of the Left Ventricle. Several conclusions can be drawn from accurate measurements of the size of the pumping chambers at different phases, and some examples of these are given below. The thickness of the heart walls and the interventricular septum are commonly measured, and when fluid is present in the pericardium the depth of the effusion volume is measured. When echoes are obtained from the mitral valve, measurements can be made of the valve leaflet velocity when it opens or closes and the amplitude of its excursion, and similar parameters can be measured for different regions of the posterior wall of the Left Ventricle. Measurements of chamber dimensions obtained either by B or TP scan can be used to estimate chamber volumes, rates of change of volume, stroke volumes and ejection fractions, whilst by measuring B scan sections with a planimeter the internal surface area of a ventricle and its true perimeter length in the plane of scanning can be found.

The value of many of these quantitative descriptions of the heart has yet to be established in clinical practice but such measurements will become increasingly significant as a proper understanding of cardiac function is developed. At present, normal and abnormal hearts may often be classified by the sizes of single chambers alone and the degree of cardiac dysfunction is known to be reflected in the ventricular wall motion and velocity as well as in the rate of change of volume and Ejection Fraction. The Ejection Fraction alone is often used as an indicator of abnormal function. It is likely that

increasing use will be made of perimeter measurements particularly as they can be used to obtain estimates of the circumferential fibre shortening velocity of myocardial segments which is a significant indicator of the contractile state of the heart muscle (Greene et al. 1973). Clearly, however, further work is required to provide a better understanding of cardiac mechanics, but notable advances in this field have been made (e.g. Bellhouse, 1972, Taylor and Wade 1973) and the precise measurements of real hearts provided by echocardiography have themselves added considerably to our experimental capabilities in vivo. Quantitative Geometrical Information from pulse echo measurements may be most useful when considered simultaneously with other information such as ECG or pressure measurements. Absolute measurements of heart volume, which coupled with wall thickness measurements can be used to estimate the mass of the cardiac muscle, are often essential normalising constants in comparisons between different hearts. Accurate measurements of the internal dimensions of the left Ventricle may be differentiated and the turning points accurately pinpointed. These mechanical points of inflexion can be compared to known electrical events depicted by the ECG to show up irregular muscle contractions and measure intervals of isovolumic change. Pressure - Volume curves produce closed loops which portray the work of the heart as a pump, and their shapes are dependent on the phase relationships between events in the heart.

The mitral valve's motion has been exhaustively described but it is analysed quantitatively only in relatively few conditions. Its motion reflects the prevailing haemodynamic

conditions of the left side of the heart and it is dependent on the size and condition of the mitral orifice. Normally the valve opens at the onset of ventricular diastole when the Left Ventricle relaxes and blood rushes through the mitral orifice, but it is then forced to close by forces created by the blood flow and by ventricular elongation. A second opening movement follows left atrial contraction and a second rapid closure is produced by systolic contractions of the Left Ventricle. The closure of the valve in diastole is caused by more than one mechanism. Pridie (1972) supposes that pressure equalisation occurs between the Left Atrium and Left Ventricle when blood passes rapidly into the Ventricle, distending the chamber and carrying the apex away from the mitral ring. The cusps of mitral valve are attached to the mitral ring superiorly whilst the free margins attach to the papillary muscles of the apical myocardium by the chordae tendinae. Distension of the ventricle tenses the chordae and pulls the valve back to the semi-closed position. Pridie cites two other effects that may be important: a Venturi effect produced by blood flowing through the mitral orifice and a vorticeal effect caused by blood directed around the ventricular wall, which agrees with observations on model heart valves (Bellhouse, 1972). The relative importance of these mechanisms remain to be established, whilst mathematical analyses of the kinetics of valve leaflets (e.g. Ghista and Rao, 1972) may help in extracting maximum information from valve echograms but it follows from the explanation above that the diastolic closure rate is related to the speed of left ventricular filling. Leyton et al (1972) showed that in normal subjects the diastolic closure rate (DCR)

is a function of left atrial pressure and left ventricular compliance, and in conditions of high ventricular filling rates (e.g. ventricular septal defects) the DCR reflects the degree of abnormality (Madeira et al. 1972).

In mitral stenosis, rapid equalisation of pressure between atrium and ventricle does not occur when the valve opens because the blood flow is obstructed. The valve orifice may be narrowed and the mitral cusps thickened by fibrosis. Rapid distension of the ventricle at the start of the diastole does not occur to close the valve, there is an increased atrial pressure arising from the need to maintain cardiac output, and the cusps may be quite rigid. Consequently, the DCR is lowered and the valve remains open throughout diastole. Edler and Hertz (1956) showed that the DCR was reduced in patients with stenosis. This condition is an example in which quantitative geometrical information obtained by echocardiography can contribute to a diagnosis of the severity of the disease. Joyner et al (1963) showed there was a good correlation between the DCR and the mitral orifice area estimated at surgery, and similar findings have been reported by others (e.g. Segal et al. 1966, Gustafson, 1967, Winters et al. 1967). Effert et al. (1964) categorised 2156 patients with mitral stenosis as trivial stenosis (DCR above 35 $mm.sec^{-1}$), mild stenosis (DCR = 25 - 35 $mm.sec^{-1}$) tight stenosis (10 - 25 $mm.sec^{-1}$) and very severe stenosis (DCR less than 10 $mm.sec^{-1}$).

The mitral valve mobility varies directly with the amplitude of its movement. The normal systolic traverse is between 1.7 and 2.5 cms. (Ross, 1972) but this is considerably

reduced in rheumatic disease when the chordae tendinae are shortened. Quantitative analysis of echograms may also be used to decide which of several lesions is dominant. For example, when mitral regurgitation and stenosis are present, the elevated left atrial pressure at the end of systole, which is caused by the reflux of blood from the Left Ventricle, produces an initial rapid movement of blood into the Ventricle but the stenosis delays complete pressure equalisation, and the valve remains open. The diastolic trace therefore has two phases, an accelerated partial closure followed by a slow closure until the ventricle contracts. The exact shape depends on which of the lesions is dominant.

There are several other conditions in which the dynamics of the anterior leaflet of the mitral valve can provide quantitative information about other parameters associated with the mechanics of the left heart. In Hypertrophic Obstructive Cardiomyopathy (HOCM), which is characterised by an overgrowth of the myocardial muscle mass, there is often mitral regurgitation, the severity of which is directly proportional to the degree of Left Ventricle outflow tract obstruction (Rachly et al. 1966, Wigle et al. 1967). The abnormal systolic opening movements of the mitral valve, in which the anterior cusp moves towards the hypertrophied septum allowing regurgitation back into the Left Atrium and reducing the Left Ventricle outflow tract, may cause the cusp to touch the septum. The reduced DCR of HOCM reflects the reduced compliance of the ventricular wall.

Quantitative geometrical information is thus routinely obtained from measurements of distances or areas in TP or B scans, and with proper interpretation of this information and correlation with other clinical signs, accurate diagnoses can be made.

2.4 Physical Information from Echocardiography

Physical information is relatively unimportant in echocardiography especially when compared to its role in, for example, liver investigation. However, there are several specific echocardiographic signs derived from analysing echo amplitudes and distributions which constitute examples of Physical Information.

Qualitative information is provided by the increased amplitudes of some echoes which generally indicate strongly reflecting interfaces whose physical compositions have been changed by disease. For example, regions of ischaemic myocardium produce stronger echoes than the surrounding tissue whilst calcified mitral cusps return echoes which are displayed as bright regions characteristic of valve disease. Bright echoes from the septum have been used successfully as a diagnostic sign of hypertrophy (Gehkre, 1975). In severe mitral stenosis, the anterior leaflet may be thickened to such an extent that multiple echoes from inside the leaflet are displayed on a TP scan as parallel lines, and their presence is a good indicator of the nature of the disease.

Decreased echo amplitudes arise when the curvature of the heart is unfavourable for producing strong echoes, as for example when an aneurysm is present, or when septal defects reflect less energy back to the transducer.

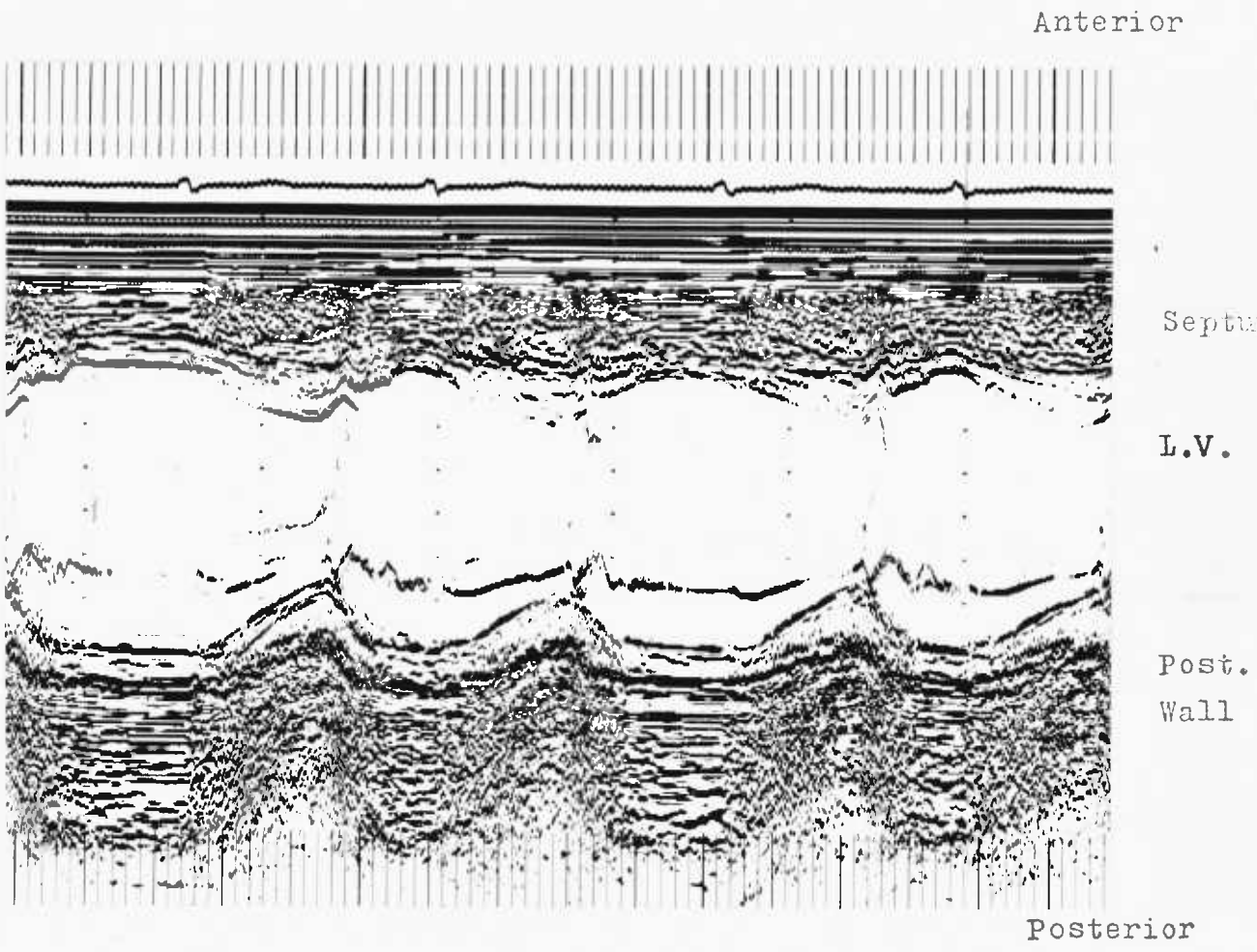
The blood behind the anterior cusp of the mitral valve normally produces no echoes, but when a myxoma is present in the Left Atrium it may produce a spotty area on the echogram

in which the distribution of echoes is determined by the tumour structure and mobility, and several consistent recordings of these echoes have been made (Effert et al. 1959, Pridie, 1971). A few reports of quantitative analyses of echo sizes or shapes have been made but little clinical significance is at present attached to these. For example, an analysis of the amplitude of echoes from valves could be used to describe the degree of calcification but this is generally considered unnecessary. Lele (1975) has shown that the attenuation of sound in heart muscle depends on the frequency and claims to be able to characterise tissues by analysing the Fourier components of echoes scattered from the posterior wall of the Left Ventricular myocardium. By quantitative analysis of spectra he distinguishes between different types of normal, ischemic, infarcted and necrotic tissues. Spectral analysis may therefore produce histological diagnoses not yet available non-invasively.

A proposal for the analysis of the elastic state of cardiac muscle has been put forward by Leeman (private communication). The pattern of echoes from within the walls of the heart chambers, such as those from the Interventricular Septum shown in Figure 2.1, changes at different stages of the heart's cycle. The echo distribution reflects changes in the shape and/or the elastic condition of the heart muscle, and a quantitative analysis of the echo pattern, perhaps using the mathematical techniques described in Chapter 7, may give useful information about the compliance of the ventricular walls. Similar "echo density" changes are apparent in the tracings of

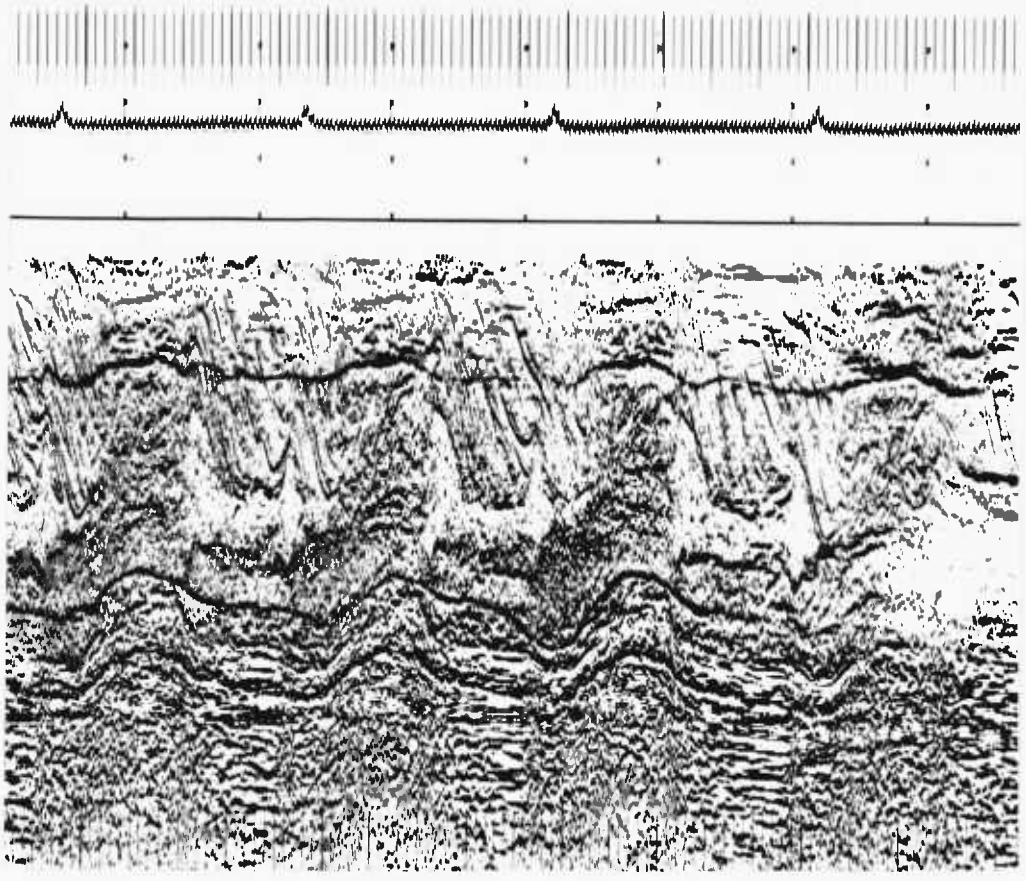
Figure 2.2, which show the result of injecting radio-opaque contrast fluid into the circulation. These echoes are produced by reflections from the many microbubbles in the injected bolus, and the changes in their distribution correspond to pressure changes in the ventricle. It may be postulated that a quantitative analysis of the density of echoes in such traces will provide information of the pressure in the ventricle at different heart phases.

Figure 2.1 Echocardiogram recorded on a strip chart recorder.



This TP scan shows the cavity of the Left Ventricle (L.V.) expanding and contracting with time. The pattern of echoes from inside the muscular walls changes in systole .

Figure 2.2 Echocardiogram taken after the injection of radio-opaque contrast fluid.



The multitude of echoes from within the Left Ventricle is produced by the injection of the contrast fluid, and the changing size and packing density of scatterers is reflected in the changes in echo density observed throughout the cardiac cycle.

2.5 Some limitations of Echocardiography.

The discussion above illustrates the clinical significance of some of the information provided by ultrasonic scanning of the heart. When attempting to derive quantitative information from scans there are limitations imposed by the performance of the scanner used and by the technique itself. A basic error is introduced into measurements of distances along the sound beam by uncertainties in the velocity of sound in the medium; for example, there is an appreciable difference between the system velocity chosen for most scanners and the velocity of sound in the blood pool of the Left Ventricle (Gehkre et al. 1975). A serious limitation is imposed by the small size of the window through which the heart can be viewed ultrasonically, which in practice restricts the number of structures that can be shown in any image. Furthermore, when using long arrays of elements, it is inevitable that some of the sound beams traverse the ribs or sternum in front of the heart. These structures have a much higher velocity of sound than soft tissues so that all structures that lie in their shadows appear anomalously close. This artefact can give misleading images (Gehkre, 1975). A limitation of a single transducer technique is that it gives no indication of the behaviour of the heart in directions other than the sound axis. B scan images are obviously preferable for measuring posterior wall movements if diskinesis occurs only in small areas, and they should produce more reliable estimates of chamber volumes than TP scans, although all echo techniques are still limited by the necessity to assume a particular symmetry of ventricular shape.

Since most of the information derived from echocardiograms depends on measuring distances between interfaces, then a basic requirement of a scanner is good range accuracy. Inherent errors in measuring single dimensions are multiplied threefold when calculating volumes and are included in estimates of velocities. Similarly, the apparent degree of calcification of a valve (as determined by measurements of cusp thicknesses), the apparent muscle mass of the heart (calculated from wall thicknesses) or the apparent severity of pericardial effusion, will depend on the accuracy with which scanners measure distances.

The range resolution of a scanner is a limitation when studying small separations and becomes particularly important when trying to image different layers of the posterior wall of the Left Ventricle. It also affects the ability to detect small clear spaces in the pericardial sac which is essential for an early diagnosis of effusion. In a B-scan image, it is important to precisely locate the position of the mitral valve cusp, especially when using a multielement linear array which also produces a TP scan from any single element. The ability to pinpoint interfaces in directions orthogonal to the transducer axis depends on the lateral resolution as shown in later chapters. This lateral resolution also affects estimates of the areas of abnormalities such as infarcted muscle, and with multielement arrays is particularly important when imaging ventricular septal defects. These show as echo free spaces with high resolution but are depicted as weak interfaces with poor resolution.

When echoes are not placed in their correct positions the image is distorted so that an object's true shape is not faithfully depicted. This can be of considerable importance in images of the Left Ventricle as the shape of the chamber may itself be used as an indicator of abnormality. The shape also affects the errors included in estimating chamber volumes from cross-sections, and in real time B scans shape distortions alter the apparent velocity of structures so that it is not the true velocity which is measured. Gibson (1976) has used a shape index to describe cardiac function: its specification depends on the relationship between chamber volume and cross sectional area. Any such shape index which is measured echocardiographically will be affected by the inherent distortions of the scanner.

An overall limitation on the information obtainable from scans is sensitivity. A particular example of interest occurs when scanning the long axis of the Left Ventricle, where the unfavourable geometry of the chamber at the apex reduces the amplitudes of echoes from the lower part of the ventricle. With poor sensitivity it can therefore be extremely difficult to image the whole heart in a single scan.

Thus, it is clear from the discussion above that echocardiography can contribute to the accuracy of diagnosis of many types of heart disease, and the information obtained by pulse echo methods has been surveyed. By considering the nature of this information, the importance of some features of ultrasonic scanners has been indicated by intuitive reasoning.

Chapter 3: Methods of evaluating ultrasonic scanners

3.1 Introduction

There exists a need for methods by which different scanners may be compared and with which any scanner's characteristics can be specified. Prospective purchasers, scanner designers and clinicians each require to know which scanner gives the 'best' performance in any application, and this requires suitable standards to determine what performance is 'best'. It is also necessary to know the limitations of any scanner and whether or not a scanner is achieving its optimal performance within its limitations.

Several criteria for evaluating scanners have been proposed by previous workers, but they have generally suffered from an inadequate specification of the problems to be solved. Before considering these problems in detail, which is the purpose of much of this thesis, the methods currently available to analyse the performance of ultrasonic imaging devices are discussed, and the use and limitations of these methods are illustrated with measurements made with particular types of equipment.

3.2 Review of methods

Previous workers have generally taken a practical but somewhat arbitrary approach to evaluating scanners and have measured various equipment characteristics in special circumstances in order to enable quantitative comparisons to be made. They have not attempted to relate such characteristics to a scanner's ability to obtain quantitative information in general circumstances. In some evaluation programmes, the test procedures have been deliberately modified to test only those characteristics of specialist interest. Others have failed to produce a general programme, and in the absence of any meaningful criteria to specify performance, have opted to measure certain parameters, arbitrarily chosen, under standard conditions.

A review of the practical requirements for a B scanner was attempted by Blackwell (1972). He identified some of the conditions necessary to obtain a good scan, stipulating that the electronics must be sensitive, that the scanning plane must be easily changeable, and that the B mode processor must be able to register a fine spot with a good range of grey scale. In this 1972 paper he suggested a simple phantom to check the registration of a B scanner, but otherwise made no attempt to specify the scanner capability. His 1973 paper (Blackwell et al., 1973) listed ten requirements for a B scanner all of which are merely points of convenience for operator use, such as types of display and recorders.

Mallard and Christie (1968) illustrated some of those physical characteristics of the medium and of the scanner that contribute to the information displayed in a B scan. They concluded that factors such as reflector inclination, tissue scattering, and absorption, each degrade the signal. They measured the received echo from a 1 mm diameter spherical target at various positions, for various transducers, and suggested that resolution of two similar point targets may be defined as the separation of two such beam profiles 'at a given depth, which overlap at half of their maximum height.' They further suggested that the beam width at some chosen level (the Full Width at Half Maximum, for example) 'is related in some way to the spatial resolution at that depth which can be displayed without complex scanning procedures and without electronically applied swept gain'. They also observed, as will be verified later in this thesis, that 'there is a considerable measure of variability and uncertainty concerning swept gain and beam width'. They concluded that one difficulty appeared to be the definition of transducer beamwidth since 'it depends on how it is measured, and whether one means actual or displayed resolution. It is not yet certain what is meant by resolution.'

Hall and Fleming (1972) were concerned with illustrating various effects that can occur to limit or enhance the usefulness of a B scan, basing their findings on the experience they acquired with the Nuclear Enterprises' scanners. They were particulary concerned with artefacts arising from such effects as too much sensitivity, swept gain settings, blooming

of tubes, registration errors and tube astigmatism. Thus, again the emphasis was placed on operator usage and convenience, and they made no real attempt to relate their findings to fundamental design limitations, but merely illustrated how incorrect usage may influence the degree of success of scanning. However, they concluded that registration errors are the most common electronic faults encountered and suggested that a wire phantom, scanned from different angles, is sufficient to illustrate these. More recently they have produced a more sophisticated method of measuring registration errors (Hall and Fleming, (1975).

Critical assessments of technique in similar vein have been put forward by Christie (1973), Whittingham (1973) and most recently by Watmough (1974), all with particular reference to measurements of biparietal diameters. Their primary concern was to evaluate the types of distortion and measurement error obtained in a clinical situation, due either to the scanning technique or to operator error. They were not therefore primarily concerned with the inherent capabilities of their scanning systems, and do not therefore concern their critical assessments with those limitations coming from the scanner design. However, Watmough suggested that the distortions he observed on scanning aborted fetuses' heads and perspex cylinders were derived from side lobe effects from the transducer, and therefore quantitative interpretation is related to this beam profile.

Kossoff (1964) attempted to identify those parameters that are relevant to obtaining good echograms; he considered only B scans and attempted to relate all sources of error to the oscilloscope spot size. In this and other papers, he has described his attempts to obtain improved axial and lateral resolutions by designing transducers to give minimal beamwidth over a region of interest, and minimal pulse length. He has also demonstrated the advantage of compound scanning, logarithmic amplifiers and various signal processing techniques, for certain purposes. However, although these early papers report his attempts to measure useful characteristics of isolated parts of the system, they do not produce a comprehensive evaluation programme with which to compare scanner performances. Moreover, his criterion of displayed spot size as a measure of performance is less valid now: Wells (1969) has pointed out that spot size is rarely the limitation on resolution. It is a unit of measurement in terms of which other parameters can be measured, but it does not relate to A scan capability. However, in a more recent paper (Kossoff, 1972) Kossoff has described a series of performance tests for use "in the objective comparison of machine performance". Whilst deliberately keeping the necessary tests simple, without requiring complicated apparatus, he has attempted "to provide data which the technician can easily relate to system performance and which indicate the effect of the measured performance parameters on the echogram". The tests described are intended to provide comparisons of different machines before purchase, to allow standardisation of clinical machines for obtaining consistent results, and to describe equipment when work is

published. This latter objective is certainly to be commended when the wide variety of applications that involve ultrasonic equipment are considered. It is rare for an author to specify more than the manufacturer's name and ultrasonic frequency employed, which is an insufficient description of equipment or conditions to enable other workers to repeat the work. Kossoff identifies four major parameters that are meaningful to the user and which provide enough information to give the clinician a clear picture of the performance and resolution of his equipment. These parameters (overall sensitivity, resolution along and across the beam, and beam deflection accuracy), are assessed in a series of nine tests using a simple grid of wires and a glass block as phantoms. The tests suggested by Kossoff are discussed later in this chapter when clinical equipment is actually evaluated using similar criteria. It will be demonstrated then that, whilst these tests are valuable in restricted circumstances, they are inadequate for fully describing the limitations of performance of a scanner. However, the tests do enable a clinician to compare the abilities of two systems under certain defined conditions, and the test cage has now been adopted by the American Institute of Ultrasound in Medicine as its standard test object for measuring performance.

More recently, (September 1972) the Department of Health and Social Security have collaborated with the UKAEA-AWRE Applied Physics Division to develop techniques to evaluate medical ultrasound equipment, and their methods are

summarised in a report by Montgomery (1972). The objectives of Montgomery's study were to supply equipment users with information to assist them in their choice of equipment, and at a later date, to correlate laboratory and clinical findings to act as a basis for the specification of a manufactured system. The particular areas of interest were the ability of an A-scan to detect midlines, and the value of a B scan in Obstetrics. Montgomery describes the AWRE programme as an assessment of straightforward electrical and engineering features. Under controlled conditions he measured the ability to identify two interfaces both longitudinally and laterally, depth accuracy and transducer beam profiles. Particular aspects of this report will also be referred to later, but here it is noted that whereas Montgomery intended to measure basic physical parameters of the system, using materials that were similar acoustically to tissue where possible, he resorted to adopting quite arbitrary definitions of several parameters that he measured. For example. he adopted criteria of lateral and longitudinal resolution based on the degree of interaction of echoes from two reflectors. It is illustrative to note that he measured the peak to valley ratio between echo peaks, and for lateral resolution said that this should be 'at least 4:1 but preferably 10:1 : for identification only of two targets, at least 2:1 but preferably 4:1'. For longitudinal resolution, 'there should be no interaction between two displayed signals'. He also measured the resolution for three classes of object, for blocks, spheres and wires, all of arbitrary dimensions, and

no one of them purporting to be a representative phantom. In discussing measurements of beam profiles, Montgomery noted that there is no generally accepted standard of measuring beam parameters, concluding that individuals must express them in their own terms, and thereby pinpointing the absence of a sound theoretical basis for these and previous procedures. Whilst these tests illustrate a system's capability under controlled conditions, they do not describe a systems's capability in more general conditions, and they do not present measurements of overall limitations.

Wells (1969) discusses those parameters necessary for producing a good scan. He also describes the effect of poor design and behaviour of various components, and discusses methods of measuring some features of a system's performance.

The parameters to be measured in a complete evaluation of a system, as suggested by various authors, and their methods for measuring these parameters, are summarised in Table 3.1. There is obviously a general concensus as to what parameters are important and quite specific guidance as to how they may be measured. Montgomery observes in his report that, after all his tests, no new factors were revealed which would alter the essential requirements of a good machine as advocated by workers in the field for the past decade. In essence therefore, part of the objective of this thesis would seem to have been reached by previous workers, but little justification for previous work has been offered, and little theoretical explanation of performance criteria given. In addition, little attention has been paid to a proper identi-

Table 3.1

Summary of methods used by other workers to evaluate scanners

Measurement	Kossoff	Montgomery	Others
Sensitivity	Referred to glass water interface	Referred to depth of castor oil for echo to fall to 1/3	Mentioned by Blackwell, Wells
Swept Gain	Uses wire reflector in water to check	..... Use calibrated attenuators.....	
Registration	Uses wires	Uses wires	Electromechanical device of Hall (1975) Perspex block of Blackwell
Depth Accuracy	Measures separation of two wires	Measures distance of plane	
Depth Resolution	Two 0.2 mm steel wires, central minimum = 0.7	No interaction for 2 planes	-
Lateral Resolution	Two wires, central minimum 0.7	Wires or balls, central minimum 0.25 or 0.1	Mallard and Christie: two balls, central minimum 0.5

fication of those parameters in the object which are important in the formation of an image by the pulse echo technique. Consequently, evaluation programmes have not enjoyed general applicability. Furthermore, definitions of various characteristics, in particular resolution and beamwidth, have differed from author to author, each one using quite arbitrary criteria. An interesting verification of the lack of guidance offered on proper measurement of resolution is given by examination of the data supplied by equipment manufacturers; in a recent survey by the author of the manuals supplied by fifteen leading manufacturers of A and B scan equipment, no manufacturer gave an indication of the quantitative abilities of his system, and no manufacturer actually quotes a value for the resolution of his system, a peculiar state of affairs for an industry concerned with image formation.

Thus, although there appears to be a degree of agreement about those properties of scanners that are important and which must be measured or calibrated, previous workers have failed to evolve clear guidelines for the assessment of scanner performance.

3.3 Ultrasonic Equipment at Hammersmith Hospital

There has been a requirement for quantitative methods of evaluating scanners at Hammersmith Hospital since 1972 when B scan equipment was first commissioned there for clinical use. In particular, various facilities for cardiac ultrasonography have been available. These have included a Multiscan system, as described by Bom et al (1972), facilities for ECG-triggered and conventional section scanning with a Nuclear Enterprises NE 4102 and a Picker Laminograph IV, Ekoline 20 A/TP systems (from Smith Kline Instruments Ltd.) and a Siemens Vidoson Real Time Mechanical scanner. These systems, together with their associated equipment (such as strip chart recorders for the Ekolines) are typical of the equipment used routinely in most clinical centres, and are comprehensive enough to be able to cover all aspects of echo-cardiography in use to date. In addition, some experience has been obtained in the use of novel techniques, including the use of digital techniques to record and process cardiac cross sections and the use of video recording of the transducer received RF signals. (Willson 1975, 1974).

The primary requirement from a user's viewpoint when a scanner is commissioned is an assessment of the operating characteristics of the system. This must include a knowledge of the ultimate capabilities of the scanner, in order to understand and quantify the accuracy and reliability of measurements made from scans; it also must include a knowledge of the way a machine compares to its designed specification,

both in the short term and in the longer term, and a knowledge of the optimum conditions of use. Thus, there was a need for complete assessment of the various scanners and techniques, and a need for routine checking of calibrations, control settings and other characteristics. These requirements became especially important when new research methods were being considered, when alternative procedures and equipment became available, and as routine clinical and research interests expanded. Experience obtained within the first few weeks of clinical appraisal of these systems led naturally to the distinguishing of two types of imperfection in real scanners. There are often present 'remediable errors' which are errors of calibration or setting up of the scanner. These errors can be caused by faulty equipment, improper usage or incorrect manufacture or installation; they may also occur as components age or be due to human error in calibration of settings. This general class of errors includes such faults as registration errors, incorrect system velocity settings, incorrect swept gain and amplifier calibrations, and incorrect caliper calibrations. These faults may occur regularly, intermittently or completely at random, and must therefore be looked for periodically in a routine assessment of system performance. They are not, however, permanent limitations on system capability, and can be rectified by proper calibration of the system, at least to within the tolerances of the components and design. Thus, for example, a registration error may occur due to incorrect setting of the system velocity, but the error can be made as

small as the tolerance of the relevant adjustment. There are, however, always present some errors of a second class that are limitations on performance inherent in the basic design of a scanner. This class of 'fault' includes all those characteristics which can only be altered by changing the system or part of the system in a fundamental way, and are therefore more basic parameters with which to compare systems and with which to evaluate them. They are a limitation on the amount of information obtainable and remain even when a system is set up correctly and all remediable errors are removed. In this class are included such characteristics as axial resolution, lateral resolution, amplifier bandwidth and sensitivity, processor dynamic range, etc. In many cases, errors of both classes, whilst being distinguishable in origin and nature, are interactive or even additive in their effect. For example, range accuracy is determined partly be the pulse length and axial resolution (both basic parameters of the system, and therefore limitations of the second type) and partly by the velocity setting, a system variable that should be set at a particular value determined by the medium. It is therefore important to assess those parameters which will completely describe the system's ultimate limitation, in the absence of remediable faults. The assessment of system performance therefore must be a two stage process, in order to evaluate the two classes of errors separately. Thus, it is necessary, in a clinical or practical situation, to be able to measure the ultimate capability of a system and to check performance routinely.

Some of the previously mentioned attempts at scanner evaluation partially satisfy the routine requirement for regular checking for remediable faults. The performance of an NE4102 has been assessed by these and similar methods described below. The use of these conventional tests is also illustrated in the assessment of Multiscan equipment, where the limitation of such tests in the elucidation and description of basic parameters is easily illustrated. Routine checks may have to be varied slightly to suit each particular system, but there are several kinds of fault which are common to all systems. The errors illustrated in the next section for a NE4102 may be considered typical.

3.4 An assessment of a NE4102 Diasonograph

The NE4102 is representative of the present generation of ultrasonic B scanners found in routine clinical use. It differs from some other scanners in certain respects, most of which are not major deviations from the general design. The scanning gantry uses an x - y movement of the transducer and holder, whereas most scanners use an r,θ anglepoise arrangement; the NE4102 uses a signal processing for the B mode which utilises a pulse height to width conversion after echo peak detection that is designed to enhance resolution and maintain some amplitude information, and this is not a common feature of current systems. A more complete description of the design and construction of the 4102 is contained in Appendix A.

Many faults in scanners develop sufficiently to affect the quality of scans obtained when in clinical use. It is obviously preferable to detect such malfunctions before this occurs. The following programme of evaluation includes measurements to assess those performance errors or changes which may be identified as affecting scan quality.

(a) Registration errors

As noted by Hall and Fleming, Blackwell, and others, registration errors are common faults which drastically affect scan quality but which fortunately are easily identified by a simple procedure. Registration errors can be caused by incorrect settings of the system velocity, by incorrect adjustment of the delay between the start of the time base voltage ramps and the transmitter excitation, or by misalignment of

the display timebase vector and the transducer direction. When registration errors occur, point reflectors are not placed in the same position in the display when imaged from different places, which is equivalent to a variation of range accuracy with angle or position. Scanning points from different directions produces several arcs in a B scan, each arc caused by the non-zero beamwidth sweeping across the reflector. The presence of registration errors is indicated when these arcs do not meet at a point but form an enclosed area whose size is a measure of the severity of misregistration. A simple phantom to check registration is therefore a single wire that can be scanned from different directions in a water bath, and Figure 3.1 shows the effect of having incorrect system velocity. To detect other causes of registration error, the system velocity must be the same as the sound velocity in the water bath, which should be the same as the sound velocity in tissue. This requires maintaining a water bath at an elevated temperature or with an accurately known composition.

A more satisfactory method has been described by Hall (1974) which uses an accurately manufactured echo simulator to produce echoes and which checks the mechanical registration without requiring a water bath. This device is now commercially available from Diagnostic Sonar Ltd.

(b) Velocity calibrations

System velocity, the ratio of the display time base velocity to distance in tissue, may be checked by comparing distances measured by echo sounding in a medium in which the sound velocity is known with real distances measured in that

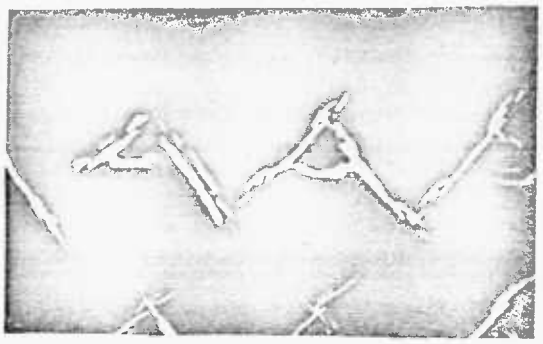
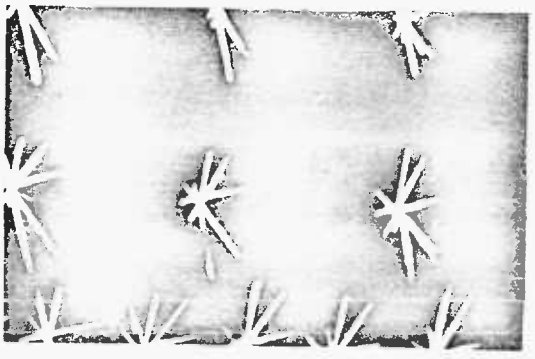


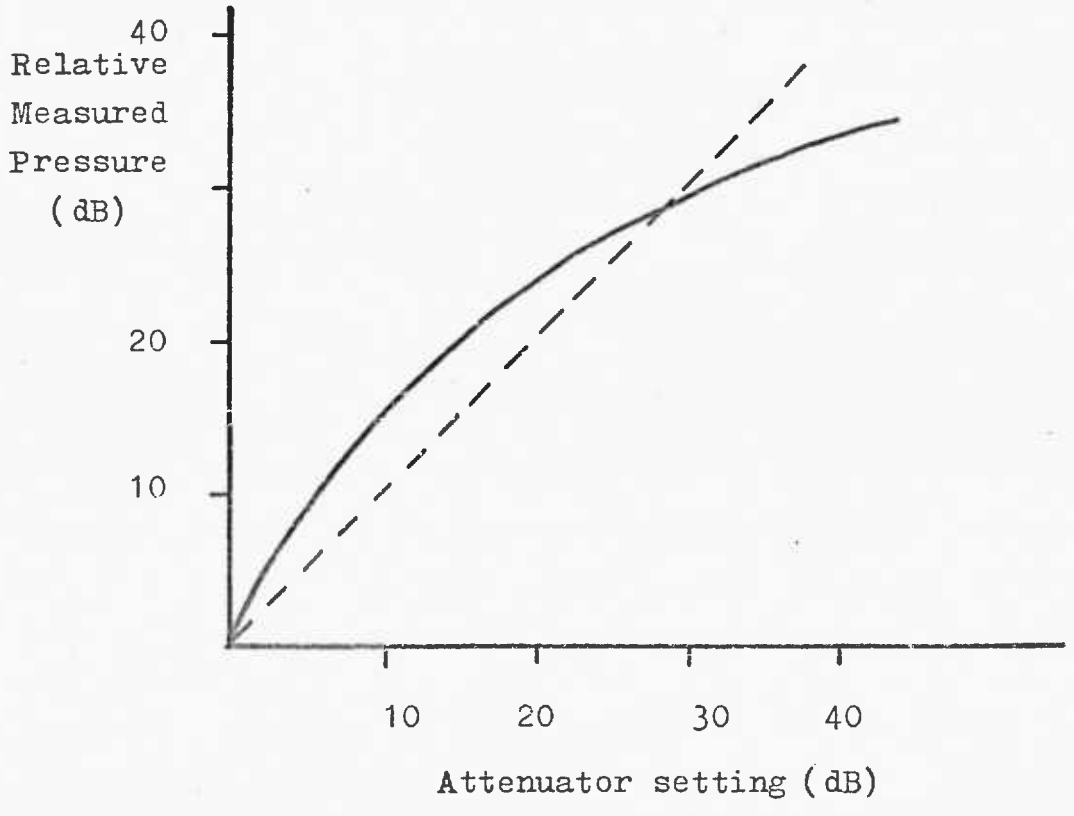
Figure 3.1

Wires scanned in water bath with wrong sytem velocity



... with correct system velocity

Figure 3.2 Calibration of output attenuator in terms of measured emitted pressures.



medium. The linearity and accuracy of a system velocity calibration can be assessed by plotting the A scan separation of the echoes from two wires whose separation in water may be varied and measured. If water is used as the medium, then its temperature should be monitored and the velocity obtained from tables or data published elsewhere (e.g. Montogomery, 1972). The ratio $\frac{\text{measured distance}}{\text{actual distance}}$ will equal $\frac{\text{system velocity}}{\text{medium velocity}}$. The calibration of the electronic calipers (the caliper velocity) can be obtained in a similar way. In general, the method requires a standard velocity against which the velocity being measured may be compared and this standard can be water of known purity and temperature, or it can be perspex or a similar material. However, the accuracy of such measurements is only of the order of a few per cent, and it requires considerable precision of measurement to improve this. Errors occur in the estimate of the medium velocity, and in the measurement of the wire or interface separation, and these are often of the same order as the miscalibrations that occur. A very much simpler technique uses an accurately known electronic delay. A convenient device is the Mullard DL50 television component which uses an ultrasonic delay line to delay an electrical signal by an accurately known time. The delay line is arranged so that the transmitter output is attenuated and delayed and input to the receiver so that it simulates echoes on the display. These 'echoes' are sharp and regularly spaced. The separation between echoes is the time delay of the delay line which is 64 μsecs. The separation on the A scan may be measured and the system or caliper velocity obtained by division. The NE4102 system velocity is usually

set at 1540 $m.sec^{-1}$ whilst the caliper velocity is 1600 m,sec^{-1}.

(c) Transmitter characteristics and output calibrations

The transmitter characteristics are important only as they affect the emitted acoustic power, though transmitters which are damaged or malfunctioning to a severe degree may affect the transmitted pulse shape. The transmitter must produce a fast voltage edge to the transducer of sufficient magnitude that the emitted pulse allows the receiver amplifier to be used at moderate gains and so that the swept gain facility has maximum flexibility. Too little emitted power means the amplifier is used at its highest gain settings leading to non linearity and poor signal to noise ratio, and limiting the range of variation of gain with time. Transmitter ageing causes loss of output power and is commonly due to an increase in the time constant of the transmitting voltage spike (usually the switching time of a thyristor). The state of the transmitter can easily be determined by using a wide band oscilloscope to display the output voltage spike. The PRF can also be measured directly from an oscilloscope; for the NE4102 the PRF was measured as 670 $\pm$ 10, although it was labelled by the manufacturer as 300. An accurate measurement can prove useful when estimating doses to patients.

The pressure-voltage transfer functions of plane piezoelectric transducers are considered in Chapter 4 and Appendix B, where the wave equation for a piezoelectric material which shows a linear coupling of electric and mechanical variables is solved for a variety of boundary conditions. They are

important in determining scanner performance because the shape of the transducer impulse response affects the emitted pressure pulse shape and the displayed signal shapes, whilst the validity of the calibrations of transmitter attenuator and receiver gain rely critically on the relation between acoustic and electrical parameters. The electric field and transducer displacement field are linearly coupled for an ideal transducer so that the acoustic pressure in front of a transducer depends directly upon the time derivative of the voltage applied to it, although the precise relationship is complicated by transducer loading effects. A properly functioning transmitter must switch a supply voltage rapidly into the transducer load. The switching time must, in the case of half wavelength transducer thicknesses, be less than $\frac{1}{2f}$, where f = the resonant frequency of the transducer, which is the transit time of a wave through the transducer element. The switching time may be measured with an oscilloscope with the transducer in the circuit to ensure that the impedance of the transducer affects the result in a realistic manner. The falling edge of the voltage spike must not contain sharp discontinuities as these are effectively differentiated and give rise to secondary emitted pulses in the wake of the primary burst.

The calibrations of signal strengths are generally derived electrically i.e. they relate to voltage amplitude ratios and in general are correct only for a limited range of source and load impedances. The accuracy of any of the signal amplitude calibrations may be checked by measurement of the displayed A scan echo from a reflector (e.g. plane perspex surface in water)

for various settings, which includes the behaviour of the receiver amplifier, but the output attenuator may also be checked by measuring the emitted pressure pulses using a piezoelectric probe whose characteristics are known. Figure 3.2 shows the results obtained for the NE4102, and obviously there is some discrepancy between the measured values and the calibration.

The 4102 transmitter uses a thyristor which is fed via a 100 ohm matched attenuator to the transducer, and the electrical impedance of the transducer at resonance must be 100 ohm for the attenuator calibrations to be exact. Considerable care must be taken in manufacture and design to provide a properly matched and terminated impedance network, both in output attenuator and input attenuator, if the machine calibrations are to be useful in quantitative work. The pressure at a point in the field of a transducer can be calculated using the Kirchoff integral of velocity distribution across the transducer face. (Appendix C.) The output electrical attenuator is required to alter $v(x,y)$, the distribution of velocity normal to the transducer surface which may generally be considered radially symmetric for circular transducers. In practice there may be an effect introduced by changing not only the magnitude but also the pattern of velocity distribution with different excitations. An ideal transducer is a plane piston which vibrates uniformly so that $v(x,y)$ = a constant. A real transducer may bend as a flexible membrane, and it will certainly couple energy into other modes; radial modes of vibration are easily observed with

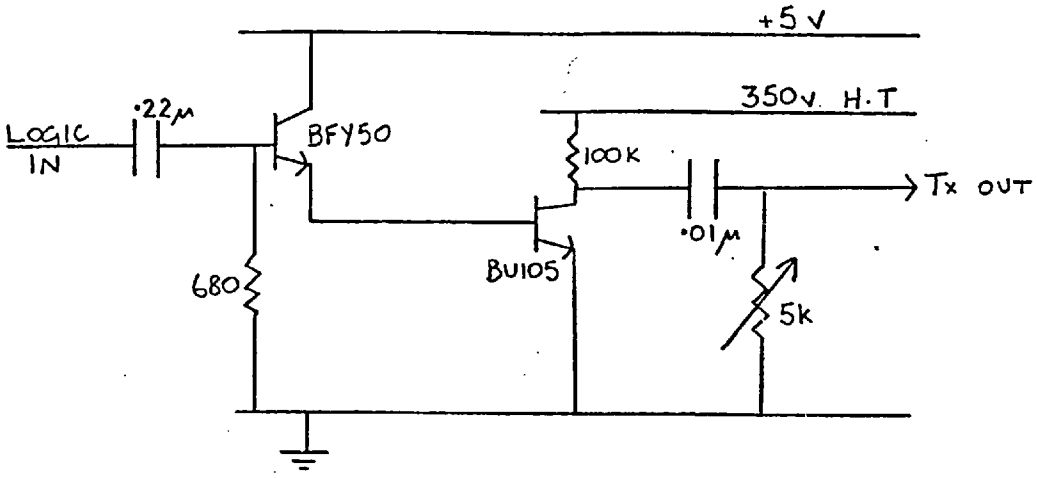
circular damped transducers. It is possible that the coupling of energy into other modes and other vibration configurations may itself be a function of vibration amplitude, and this will affect the pressure-voltage relationship.

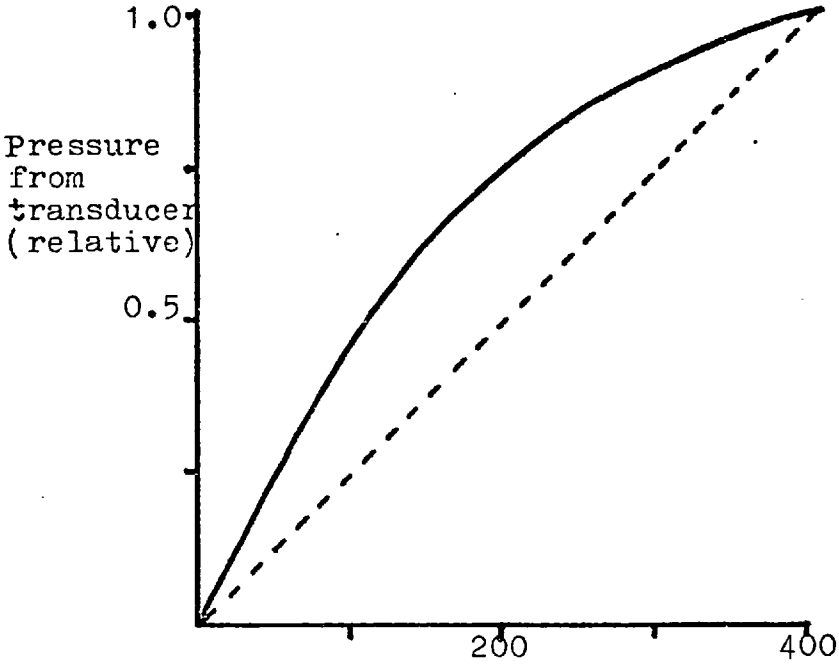
Transmitter loading effects may also alter the pressure-voltage relationship. Figure 3.3 shows an inexpensive switching transistor transmitter with high output impedance used for experimental purposes at Hammersmith Hospital. (Willson, 1974). The output from the transducer is affected by the current limitation imposed by the transistor. Figure 3.3 shows the resultant p_{out}-V characteristic. The 4102 transmitter is not subject to this limitation under normal conditions.

(d) Receiver Frequency Response

The receiver frequency response characteristics are important because they affect both the displayed pulse shape and axial resolution and the lateral resolution. Since axial resolution is a function of total system bandwidth, then the combined effect of transducer and receiver must be measured and this essentially is the basis of the criteria for resolution proposed later in this thesis. For system comparisons, however, it is useful to measure the frequency response curves of the RF amplifier. Figure 3.4 shows the normalised responses of the RF amplifiers of two 4102 scanners measured with the apparatus arranged as shown. The bandwidth has an important effect on signal to noise ratios and on the supression of low frequency oscillations of the transducer.

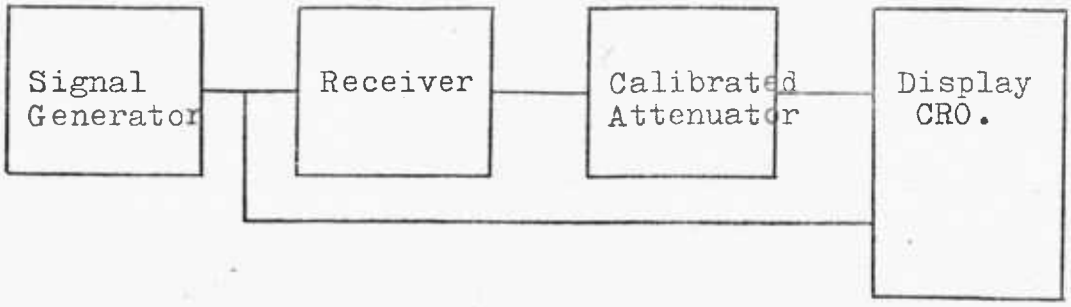
Fig. 3.3(a). Simple transmitter circuit (Willson 1974).

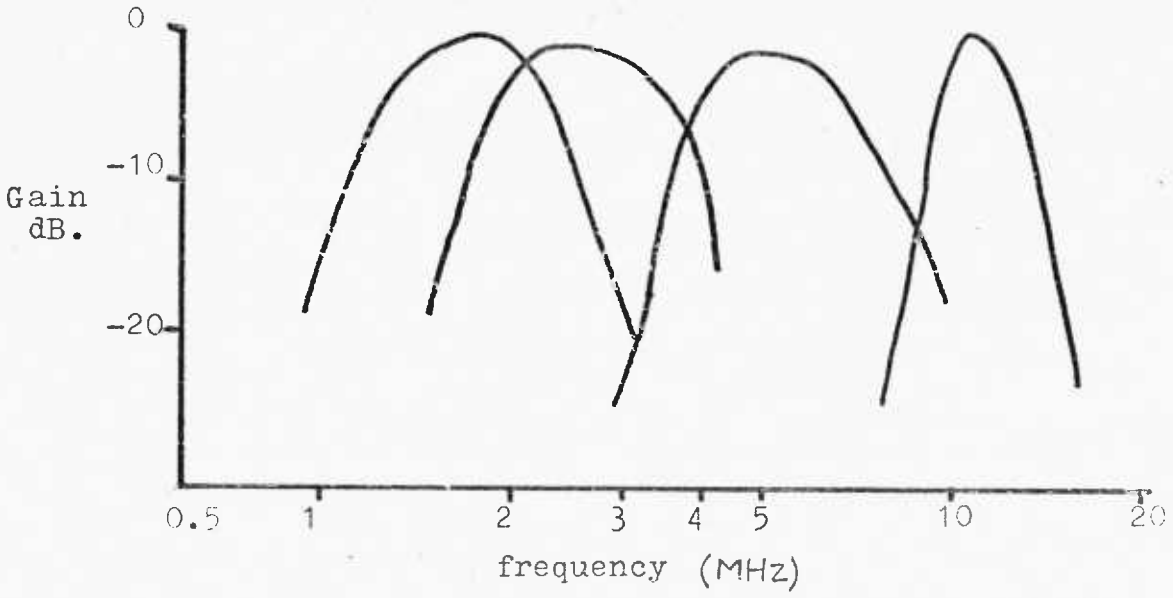




3.3(b) Performance characteristic of transmitter.

Fig. 3.4 Measurement of frequency responses of receiver.





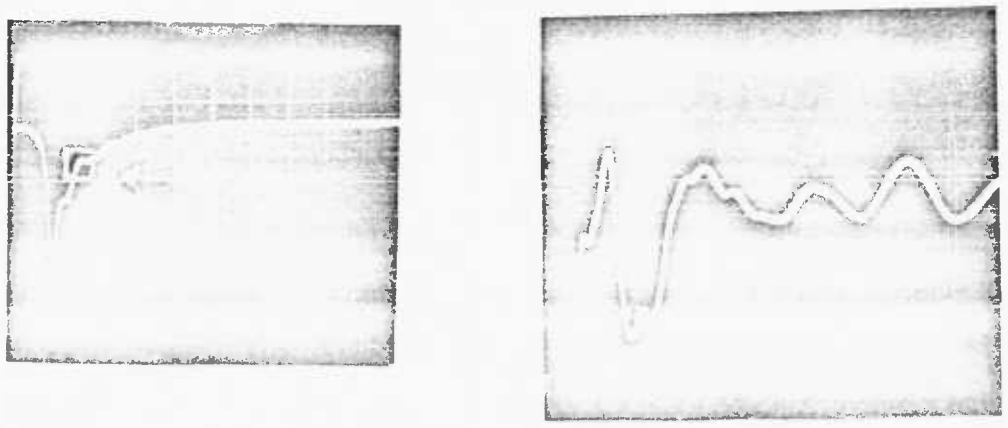


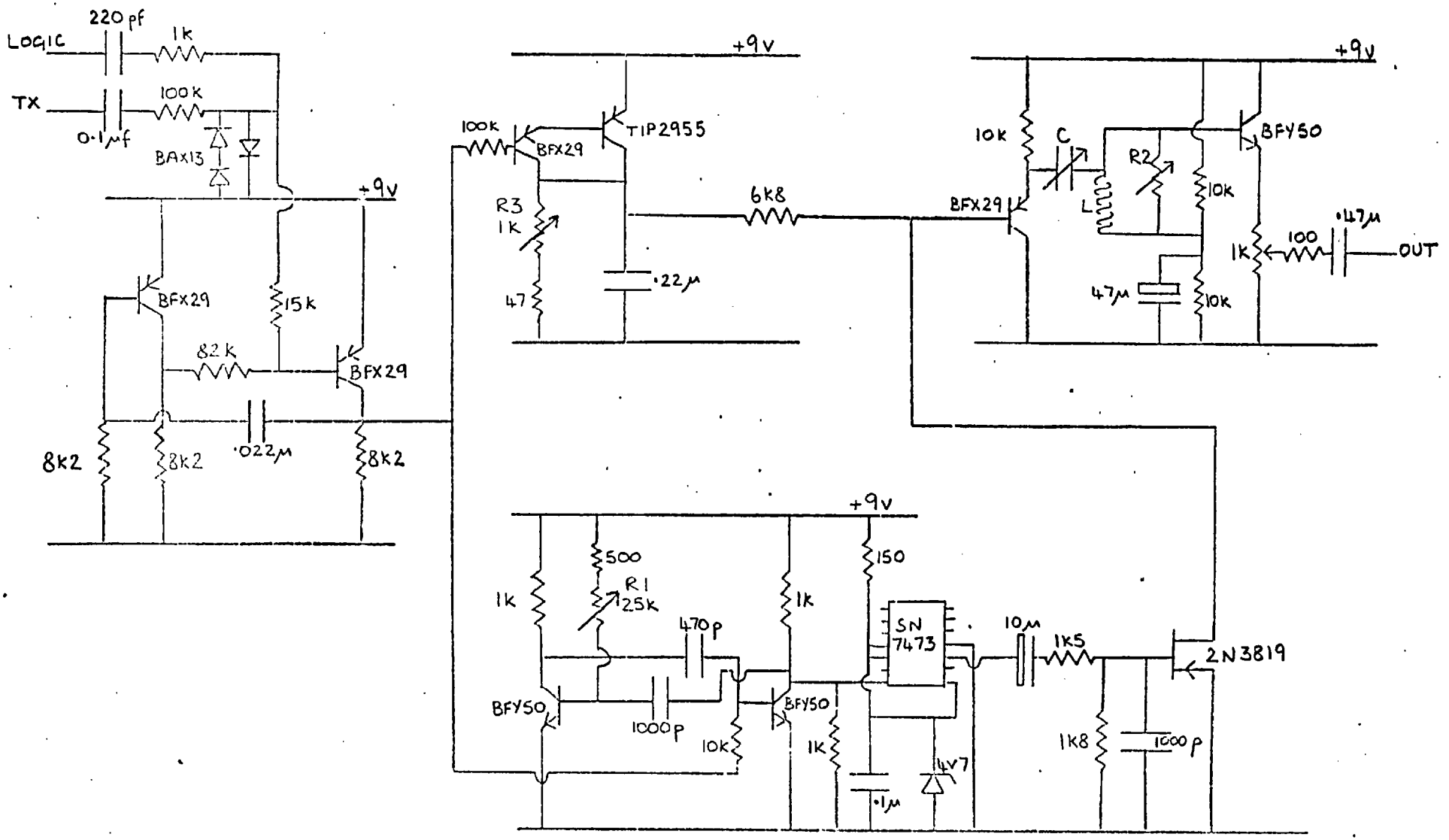
Fig.3.5 Low frequency signals at transducer before bandpass amplification.

In Figure 3.5 is the voltage across the transducer measured before the RF amplifier. Note that the initial burst input voltage contains large amplitude oscillations of frequency 100 kHz which are the radial oscillations of the crystal element and which are filtered out by the amplifier bandpass: this filtering will obviously determine the size of the opening burst on the A scan display. The importance of frequency response in determining transducer directivity is assessed in Chapter 5.

(e) Swept Gain and dynamic range measurements

The flexibility of the variation of amplifier gain with distance, and the accuracy of its calibration, can be assessed in several ways. Kossoff's phantom uses a wire cage in water and requires the measurement of the extra gain introduced by the Time Gain Control at all distances. A more versatile and convenient method uses an electronic echo simulator. For investigating the 4102 a versatile echo simulator was constructed on the basis of an original idea by Whittingham (private communication). This is capable of producing a train of signals like echoes that have equal amplitudes or which decay exponentially. The circuit is shown in Figure 3.6. The transmitter output is clipped and triggers a monostable whose output is at logic level 1 (+9 volts) for about 130 μsecs. The monostable itself gates a multivibrator that produces a train of logic pulses whose spacing is determined by the timimg resistor (R1); when this resistor is at 10 kohm then the simulator 'echoes' will be at 1 cm. intervals on a display whose velocity assumes a system velocity of 1540 $m.sec^{-1}$.

Fig. 3.6 Echo simulator (based on an original design by Whittingham)



In a later version of the simulator a further integrated circuit is included to divide the multivibrator frequency by 2, a necessary modification when long pulses are being generated. The train of logic pulses is then double differentiated to produce sharp edges that induce a damped oscillation in a tuned circuit - the LCR circuit used has a fixed inductance but the capacitance may be selected to produce different frequency pulses, and these may be chosen for any scanner to suit the bandpass of the input stage. The Q of the tuned circuit determines the damping of the pulses and this may be varied by changing the damping resistance (R2). The output is fed via a 100 ohm series resistance and the output voltage level is variable between 0 and 1.5 volts: thus the transmitter triggers a train of pulses whose frequency is determined by selecting the correct frequency of the LCR circuit and which appear the same as echoes to the scanner input.

The echo simulator built and used for the 4102 tests includes a further facility that was not used for the tests considered here but which enables a realistic train of echoes to be produced for the testing of exponential swept gain profiles. The monostable turns off a transistor that is normally saturated and whose collector is earthed via a capacitor that is normally held at supply voltage. When the transistor switches off, the charge on the capacitor is allowed to decay with a time constant that is determined by the parallel resistance (R3). This exponential decay is then chopped with the gated multivibrator output to produce an echo train that

shows an exponential amplitude decay. If the time constant is calibrated then the swept gain necessary to restore the decaying profile so that all the displayed echoes are equal can be equated to the time constant being generated. In practice it has been found more straightforward to calibrate the swept gain against the input attenuators and distance calipers of the 4102, correcting these where necessary with correction factors derived from an earlier comparison of input attenuator with a standard attenuator. The swept gain of the Diasonograph can in general be described by the equation

$$G(x) = G_o + k(x - D) \text{ if } x > D, = G_o \text{ if } x < D$$

$G(x)$ = amplifier gain at distance x in dB

G_o = gain of amplifier at x = 0

= Initial gain = Maximum gain - Initial attenuation

= 80 - I dB

D = Delay before gain increase, in cm.

k = rate of gain increase, called the Slope on the 4102, in dB/cm.

For two identical inputs to show the same displayed A scan height, if D = 0, then,

$$I_2 - I_1 = k(x_2 - x_1)$$

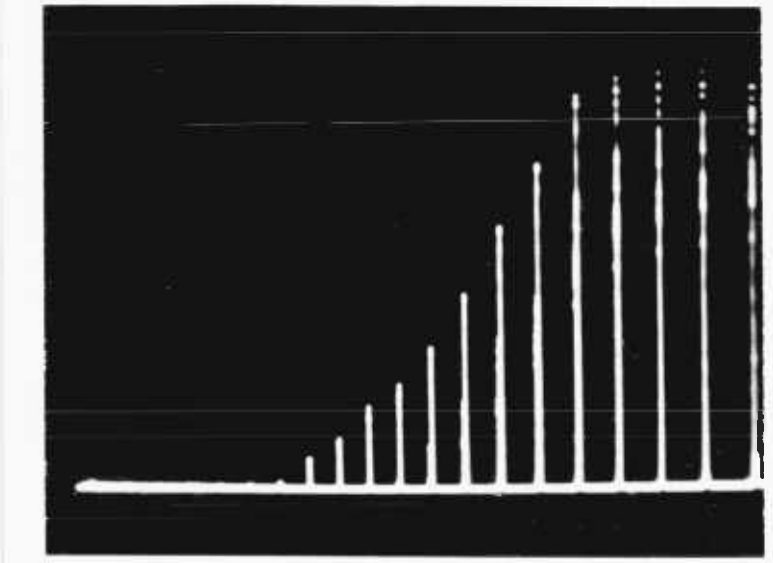
where I_2 and I_1 are the respective input attenuations and x_2 and x_1 are the positions of two equal echoes. Thus, to calibrate the swept gain rate, an echo from the simulator is displayed at a level that is easily recognised on the A scan, and the caliper is set on this echo and the input attenuation noted. The input attenuation is then increased and the

caliper moved (or, for the 4102, the calipers separated) until it is set on an echo that is at the same level as the first echo (which is now attenuated below this level). The caliper separation multiplied by the swept gain slope should equal the difference in initial attenuations. A series of such measurements can be made to determine the real slope of the swept gain. The gain time profile is displayed on the A scan and examples of this display are shown in Figure 3.7. In later versions of the 4102, a swept gain profile display is incorporated in the design, so the simulator can show up discrepancies between the display and the real swept gain functions. The results of measurements made on the 4102 are summarised in Table 3.2. The difference between the measured values and the manufacturers calibrations varies from 20 to 40 per cent.

(f) Amplitude transfer functions and dynamic ranges.

The same echo simulator can be used to measure transfer characteristics of the amplifier, processor and display. The simulator provides echo like signals whose amplitudes may be measured and varied over a wide range. The output of the RF amplifier, the displayed A scan echo height, and the width of the B mode processed pulse can be measured from the display or from the signals to the display. The 4102 height to width conversion is designed to produce an intensity modulation of the image in which the display cathode emission current is gated with pulses whose width varies 0 - 400 nanoseconds. The relationship of output amplitudes to input signals is of importance for using amplitude information and for image

Fig. 3.7 Examples of the A scan display of uniform trains of simulated echoes showing variations of scanner gain with time.



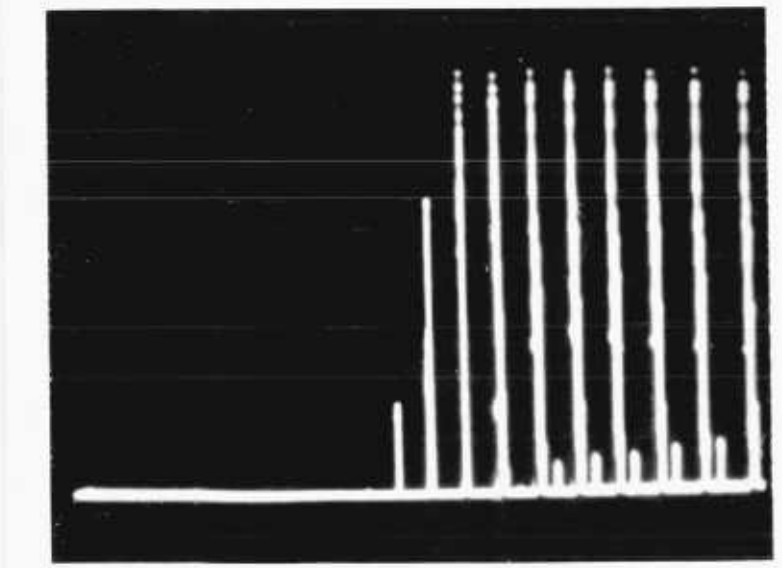


Table 3.2

Comparison of measured swept gain characteristics with those specified by the manufacturer.

Specified slope k_s	Measured slope k_m	$100. \frac{k_m - k_s}{k_m}$
2.0	1.7	- 17
4.0	3.2	- 20
7.0	4.8	- 46
10.0	7.0	- 30

contrast. The B-mode processing is intended to relate the echo peak amplitude directly to the charge emitted by the cathode of the display oscilloscope and the operation of this processing is summarised in Appendix A. The fidelity of this conversion is shown in Figure 3.8 from which the useful dynamic range of the processing can be measured. The relationship between input amplitude and B-mode ('output') intensity on the display was measured using a photomultiplier tube attached to the B scan tube - the measurements may be easily performed by using the TP display at constant slow sweep speed and a photomultiplier tube type EMI-9635 operating in the region where output current is directly proportional to input luminance. The useful dynamic range of the tube display is often determined by the tube phosphor in the storage mode. Figure 3.9 summarises the results obtained with the NE4102 in which the curves are normalised to the point where saturation occurs first. The useful dynamic range of the B scan is severely limited (= 17.4 dB) not by the inability of the displays, both storage and non storage, to portray intensities (the 'grey scale') but by the designed limitation of the signal processing which can only convert echoes of this dynamic range. The use of alternative displays e.g. computer displays, scan converter tubes, will be subject to the same limitation unless a modified signal processing is used. Further measurements of the structure of B-mode signals are given in Chapter 4, where the tube properties are shown to affect resolution.

An alternative method of measuring these transfer characteristics, using a calibrated attenuator to reduce the signal from a standard echo (e.g. a glass block in water) can

Fig. 3.8 Amplitude transfer function of B mode processing.

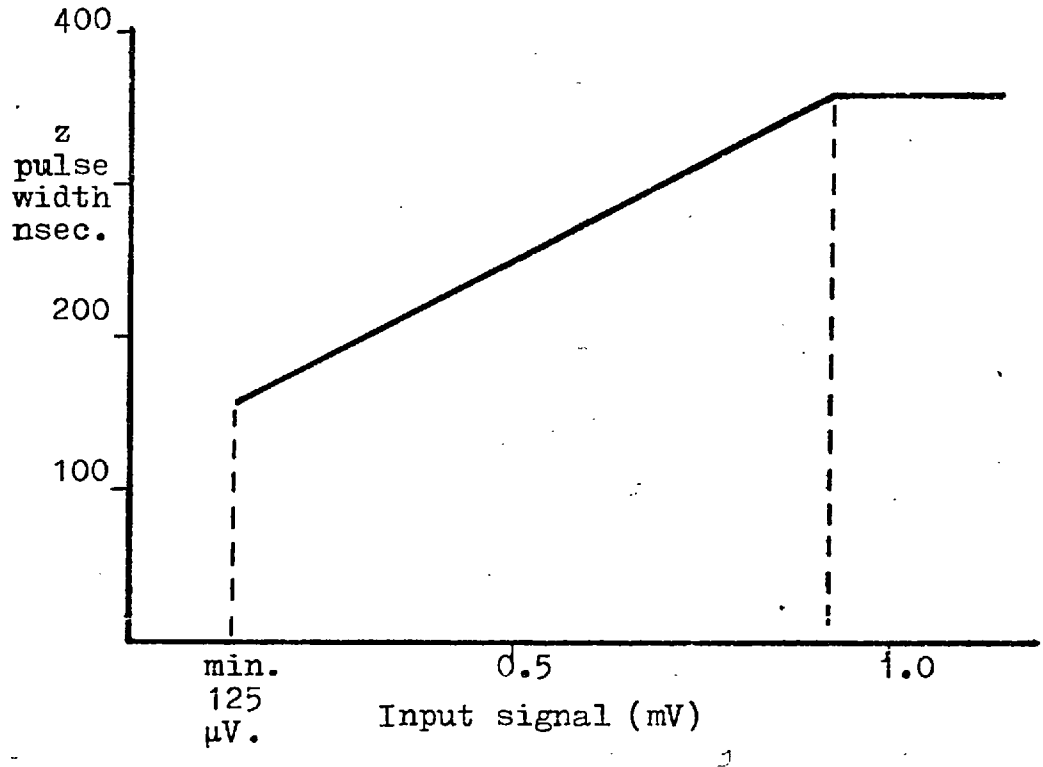
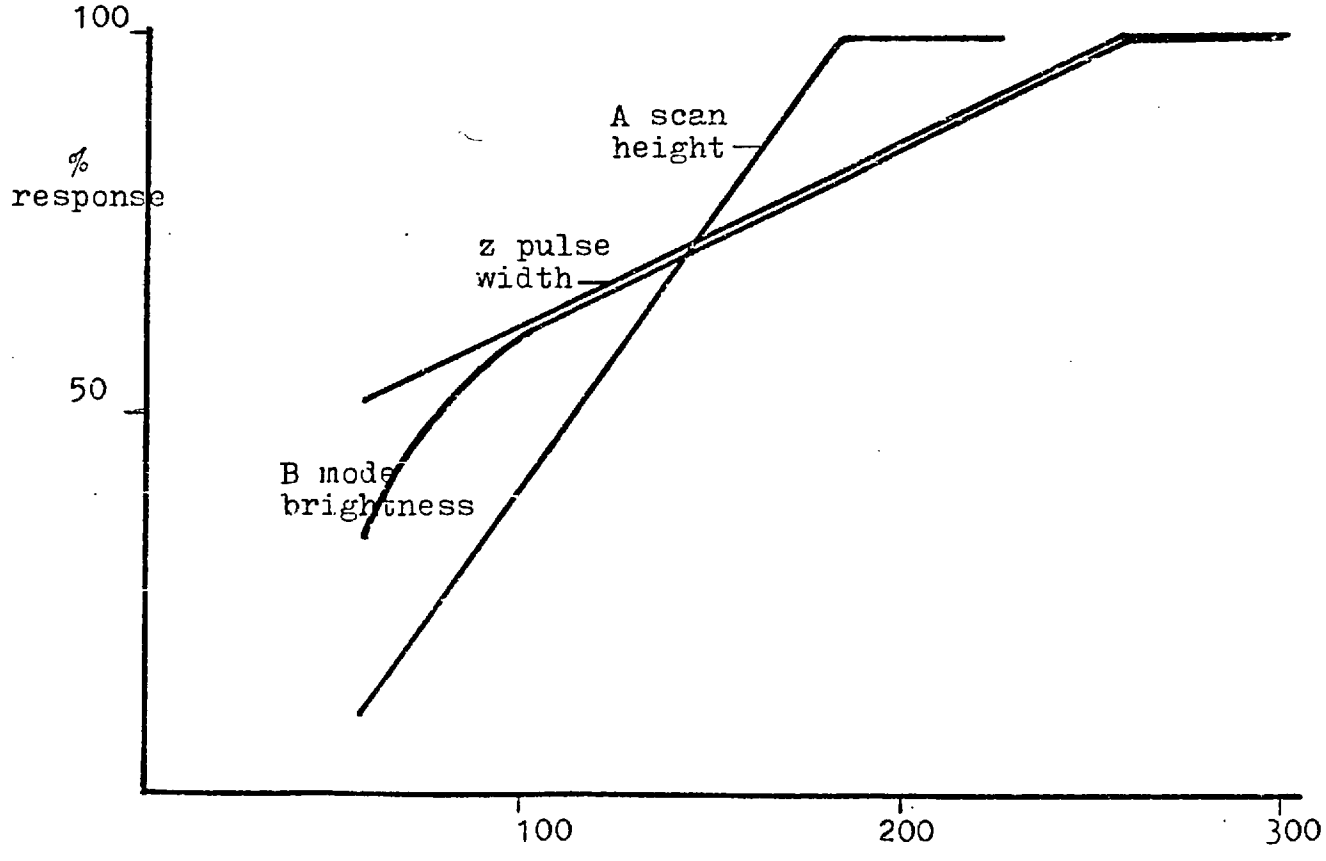


Fig. 3.9 Amplitude transfer functions of different stages (normalised to saturation level).



also be used. However, it is perhaps more informative to describe the response of the receiver to absolute voltage levels rather than relative acoustic levels, as it enables receivers to be evaluated and compared in the absence of other components in the system.

The dynamic range of the Suppressor control (in some other machines called the Reject) can be measured by comparing the input signals that just register on the A scan or the B scan for the two cases of no suppression and full suppression. The 4102 suppressor range was measured to be 14 $\pm$ 1 dB.

The overall system sensitivity can be determined in various ways. Kossoff suggests a glass-water interface as a standard echo, and the attenuation needed to reduce such an echo so that it is just displayed is a measure of system sensitivity. Overall sensitivity is the ability to detect very weakly deflecting interfaces and is determined by the acoustic output power, by the efficiency of the transducer in reception, and by the sensitivity of the receiver electronics. The acoustic output can be measured, for example, by measuring the radiation pressure incident on a perfect reflector (Wells, 1969). The absolute sensitivity of the receiver and display is that voltage that will register as an echo, and this is obtainable with the simulator by extrapolating the response-input curves to zero response. Thus, the minimum levels for the NE4102 A and B modes are 100 and 125 microvolts respectively.

However, Kossoff's method is useful as a simple check on the overall system, and it does measure the limit of

interface detectability relative to a standard reflector, but this is not the same for different regions of the sound field, particularly for focussed transducers that show a strong axial variation of pressure. Thus, Kossoff's measurement must be made at a fixed distance, which should be the position of the last axial maximum for measurement of maximum sensitivity. This measurement does not, as Kossoff states, enable a clinician to measure the absolute reflectivity of an object. In Chapter 6, the factors determining echo amplitude are considered and such a statement is shown to be meaningful only for very simple shapes of reflectors.

(g) Measurement of Lateral Resolution

The performance checks considered so far form the basis of a programme sufficient to assess all the characteristics mentioned in Table 3.1 except axial and lateral resolutions. A proper consideration of resolution is the subject of Chapters 4 and 5 but here the resolution of a B scanner is assessed using the methods suggested by previous workers.

According to Kossoff (1972) the lateral resolution is a measure of the ability of a scanner to distinguish two objects that are at the same distance from the transducer, and depends only on the width of the transducer beam. If this were true, then it would be sufficient to measure the width of the beam from the transducer, though it is not precisely clear what is meant by width of beam. The transverse acoustic pressure profiles emitted from a typical transducer are shown in Figure 3.10 for various distances from the transducer face. These profiles were obtained by measuring the peak excursion of the

radio frequency voltage from a piezoelectric needle probe that was scanned across the beam. The peak voltage was taken as it is the important parameter for the NE4102 signal processing. Figure 3.11 shows the variation in signal obtained at the input to the receiver as a steel ball bearing reflector was scanned across the beam; Figure 3.12 is the receiver signal for different shapes of reflector. These curves show the same general shape but different reflectors give curves with different widths. It is apparent that the variation of echo amplitude with reflector displacement from the central axis is related in some way to the emitted pressure profile at that distance from the transducer, but that it depends on the size and shape of the reflector as well, and it is also a function of the distance from the transducer. The normalised emitted pressure profile is the near field analogue of the Directivity Function used in sonar to describe the Far Zone variation of pressure with angle from continuously excited transducers; the echo from a ball is correspondingly related to the Product Directivity Curve, but because the conditions are not suited to the use of these curves, it will be more accurate in this context to refer to the Emitted Pressure Profile, EPP, and the Reflected Pressure Profile, RPP. The EPP is that variation in pressure measured by a point receiver at a fixed distance from the transducer. The RPP is that variation of received echo amplitude measured by the transducer when a reflector is scanned across the beam. The measurements described here were performed with a 6 mm diameter steel ball bearing, but it is shown in Chapter 5 that the reflector size is not critical.

In Figure 3.11 the RPP from various distances are shown for the 1.5 MHz transducer supplied with the Diasonograph. This transducer has an araldite lens on its face which is conically machined to focus the beam over much of its useful range. It is apparent that the beam shape changes with distance. The beamwidth may be measured in any of several ways, each equally valid. The width at any distance can be measured at some fraction of the central axis pressure at that distance, or at a fraction of the overall maximum pressure in the sound field. The value of the fraction may be chosen arbitrarily. Furthermore, the profile that is measured may be the acoustic pressure profile (which is the transducer voltage signal) or it can be the 'effective' profile of the signal at some other stage of the processing such as the B-mode intensity. For non-linear processing these profiles will be different. In Table 3.3 are the values of the beamwidth measured in various ways at 10 cms distance for five transducers. The criteria used for the definitions of beamwidth are closely related to those of the authors noted in Table 3.1. The ratios of the beamwidths of different transducers depend on the criterion chosen. This is discussed again in Chapter 4 but here the figures illustrate that a simple definition of beamwidth is insufficient to quantitatively compare the resolution of different scanners.

Instead of directly measuring beam profiles and widths, some workers have chosen to measure that beamwidth which actually produces and registers echoes on the B-mode display when a phantom is scanned. Kossoff (1972) used a wire grid

Fig. 3.10 Emitted Pressure Profiles from 1.5MHz transducer

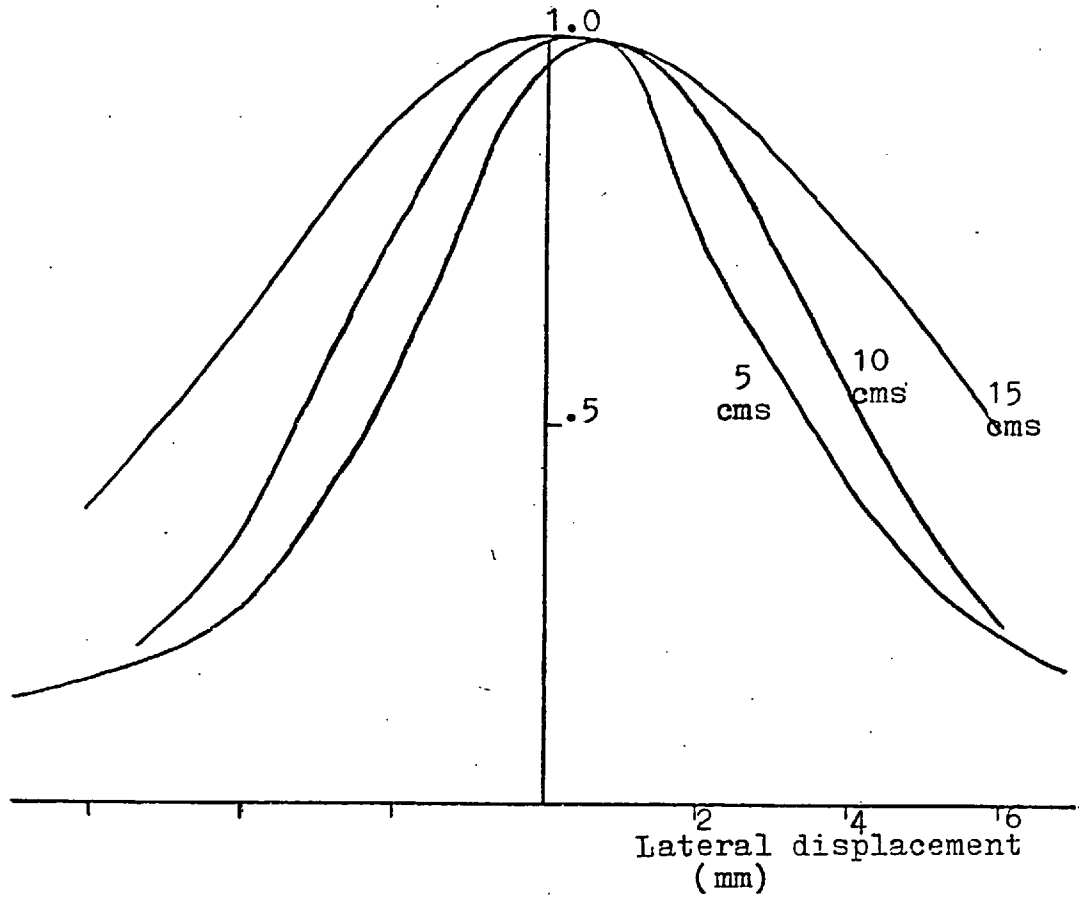


Fig. 3.11 Reflected Pressure Profiles of 1.5MHz transducer (measured with 5mm steel ball)

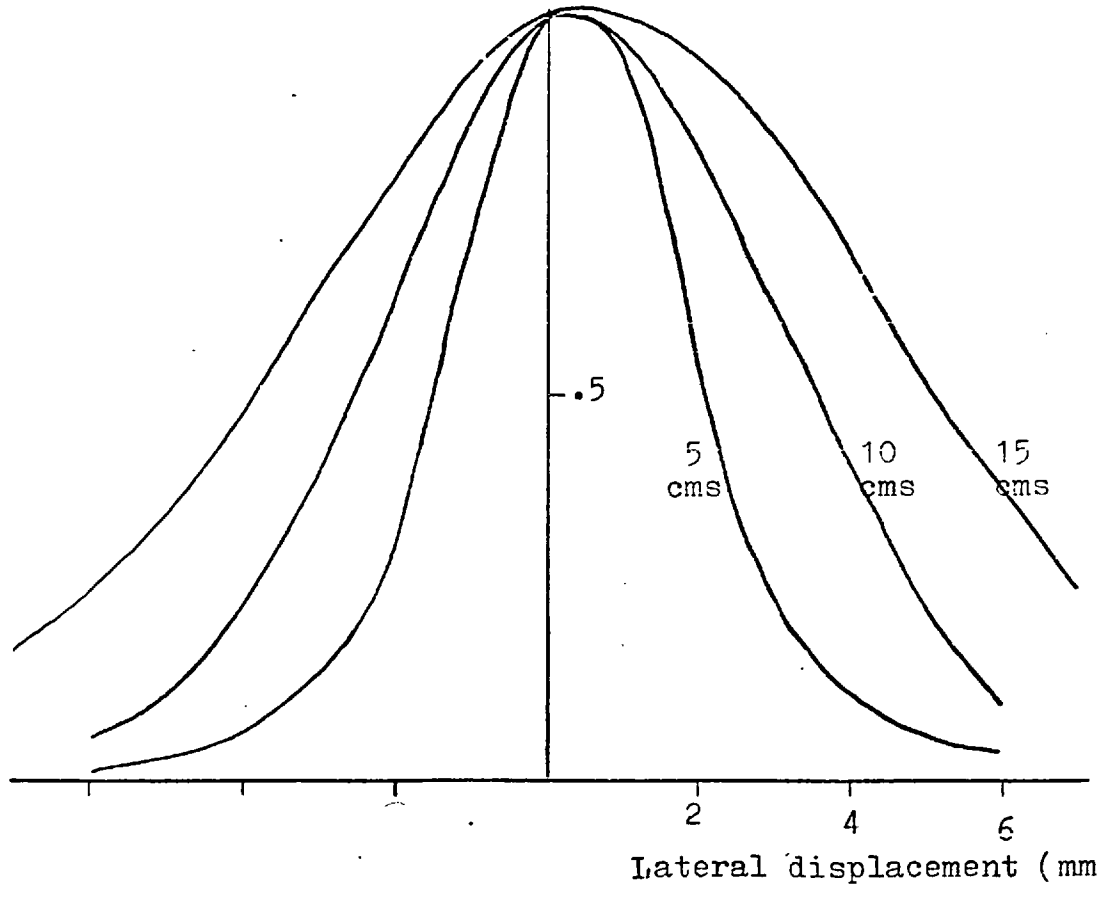


Table 3.3

Measurements of the beamwidths of five transducers using various criteria for defining beamwidth (all measured at 10 cms from the transducer ; each set is normalised to give beamwidth relative to a standard transducer).

Transducer frequency	1.5	1.5	1.5	1.5*	2.5*	MHz
Transducer radius	20	15	10	20	15	mm
Beamwidth at 70% signal level	1.22	1.10	1.00	0.98	0.82	
.. .. 50%	1.56	1.18	1.00	0.95	0.77	
.. .. 10%	1.33	1.31	1.00	0.75	0.63	

* indicates weakly focussed transducer

in which two 0.2 mm diameter steel wires were placed to form an acute angle of 10 degrees. By moving the scanning plane along the wires, the spacing between those sections of wire contributing to the echo could be changed. In the scanning plane the wires each produce an echo and the display shows two equal peaks separated by a trough. Adjusting the scanning plane along the wires until the trough level equals 0.7 of the peak amplitudes, or until the B-mode shows a dark line between two spots, corresponds to a measureable separation of the wires which is Kossoff's definition of lateral resolution. Such a phantom is useful only with sound fields that are rotationally symmetrical about the transducer axis, and where the field lacks such symmetry the phantom may give quite misleading results.

A similar phantom, in which a line of nylon sutures were arranged vertically in a test cage in water, was scanned with the Diasonograph. The separation of the wires varied from 20 mm down to 2 mm. The RPP from a single suture, shown in Figure 3.12, depends upon the variation of pressure across the sound beam, upon the shape of the reflected sound wavefronts at the transducer, and upon the averaging effects of the transducer in reception. When two sutures are in the beam then the reflected sound waves add and the transducer signal depends upon the pressure in the resultant wavefront. The shape of the wavefront at the transducer face is determined by the manner in which the waves from the sutures diffract. The resultant RPP from two wires does not correspond exactly to a simple addition of two single wire profiles because of

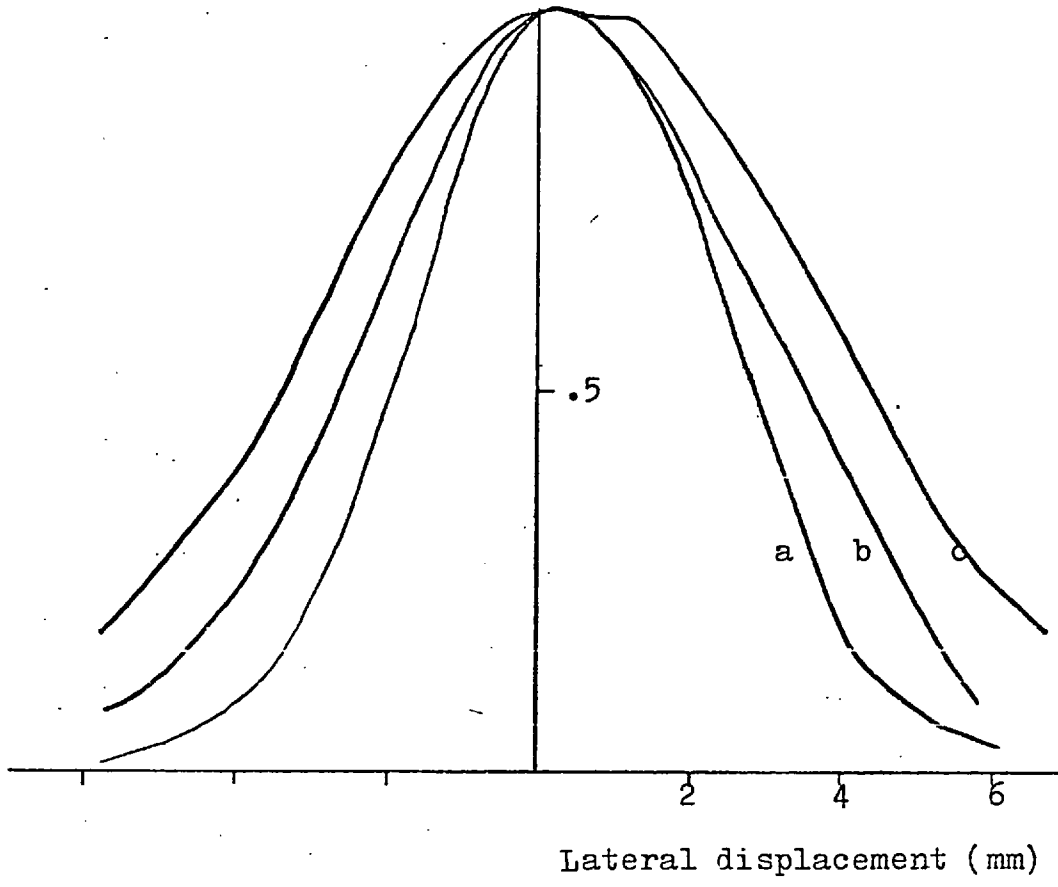


Fig. 3.12 Reflected Pressure Profiles of 1.5MHz transducer measured at 10 cms with different relectors.

a measured with nylon suture
b measured with 5 mm steel ball
c measured with 4 mm nylon disc

the varying path differences from the reflectors to points on the transducer face - such path differences are not recorded in the single RPP's which show only the pulse peak amplitudes and contain no phase information. However, when the sutures are far from the transducer the received waves are almost plane, so that the RPP from two sutures is the same as the sum of two separate profiles, and in practice this appears to be a good approximation for large regions of pulsed fields. Kossoff's criterion corresponds to that separation of wires, d, such that wires placed at $d/2$ from both sides of the transducer axis will reflect an echo equal to 0.7 of the signal reflected when one wire is on the axis and the other is at d from the axis. If the pressures of the waves reflected from wires at constant depth may be added in scalar fashion then the single wire RPP must satisfy the equation

$$0.7(E(o) + E(d)) = 2E(d/2)$$

where $E(d)$ denotes the echo amplitude when one wire is at distance d from the axis.

If $E(d) \ll E(o)$, then $E(d/2) = 0.35\ E(o)$

i.e. the resolution distance corresponds to measuring the RPP beamwidth at the -9.1 dB level. If $E(d) = \frac{E(o)}{10}$, however, then the resolution distance corresponds to measuring at the -8.3 dB beamwidth, whilst if $E(d) = \frac{E(o)}{5}$ then the resolution distance is the -7.5 dB beamwidth. Thus, such a phantom measurement does not measure the same parameter in different beams but the beamwidth chosen as an indicator of resolution depends upon the shape of the beam at low echo levels. It is possible to obtain anomalous results because of this.

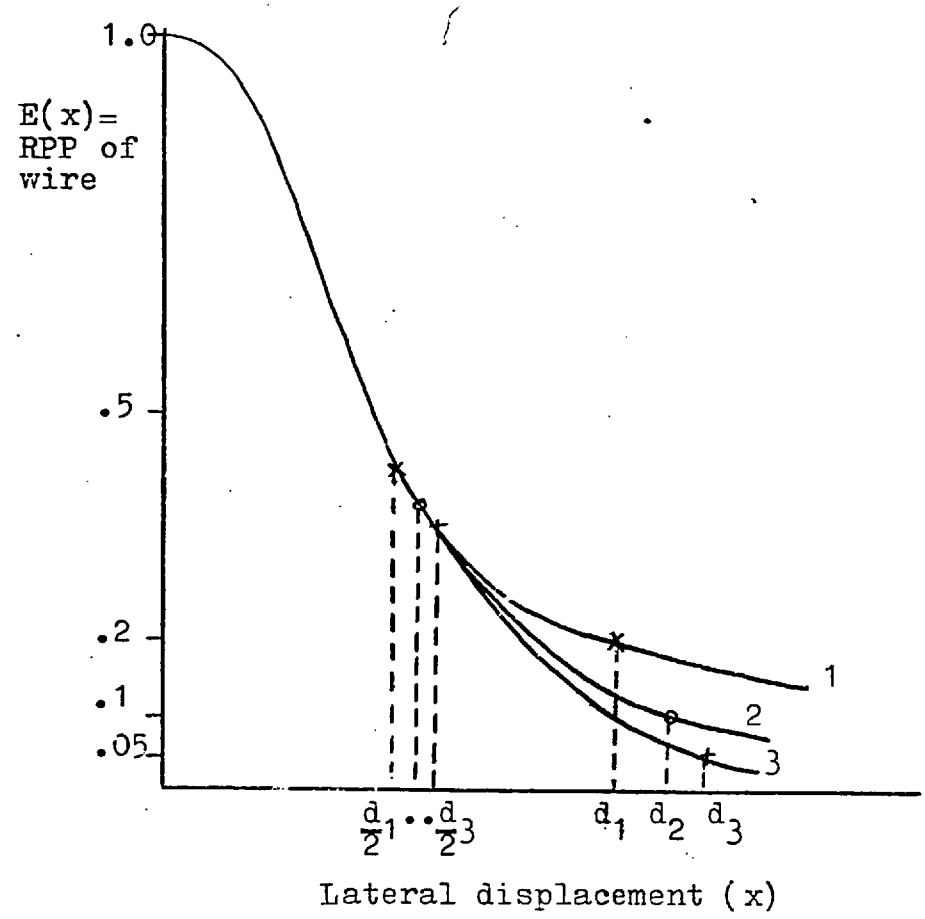


Fig. 3.13 Illustration of possible anomalous result obtainable with wire phantom measurement.

d_1, d_2, d_3 each obey equation

$$0.7(E(d) + E(0)) = 2E(\tfrac{d}{2})$$

$d_3 > d_2 > d_1$ yet 1 worse than 2 and 2 worse than 3

Figure 3.13 shows three profiles which are similar in shape down to the 10 dB level but which have different 'tails'. The beam which falls off least sharply with distance off axis has its beamwidth measured at the highest level (-7.5 dB level) so that the beam which intuitively is widest and has worst resolving power is deemed to be narrowest and to be capable of best resolutions. Such anomalies are accentuated if Kossoff's criterion is altered e.g. if the separation is measured when the central trough is 0.5 of the peak amplitude, in which case the beamwidths of interest are the 12.0, 11.2 and 10.5 dB levels. This method is therefore influenced by changes in the RPP and changes in the criterion chosen. It is also dependent upon the use of wires which scatter cylindrical waves, so that different quantitative results are expected if the method is used with balls which scatter spherical waves. Kossoff's alternative criterion requires a distinct separation of echoes on the B-mode. Figure 3.14 shows a line scan of a line of sutures as displayed on the NE4102 B scan. The sutures are just separable when they are 6 mm apart (when the A scan trough was 0.85 of the maximum signal, which means this criteria measures less than the 7.4 dB beamwidth). Figure 3.15 shows the effect of changing the receiver gain; the apparent resolution may be made better or worse. Similar changes in the resolution may be achieved by changing the transmitted power, the size of the reflector wire, the wire material, the attenuation of the medium, and the signal suppression. By adjusting the signal and suppressor levels two wires may still be resolved when separated by very small distances, the limit depending mainly upon the suppressor

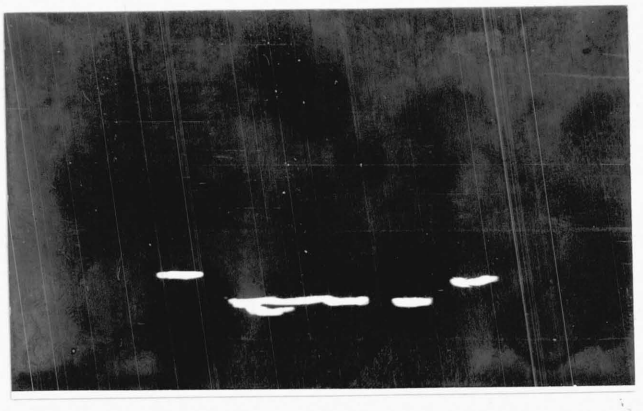
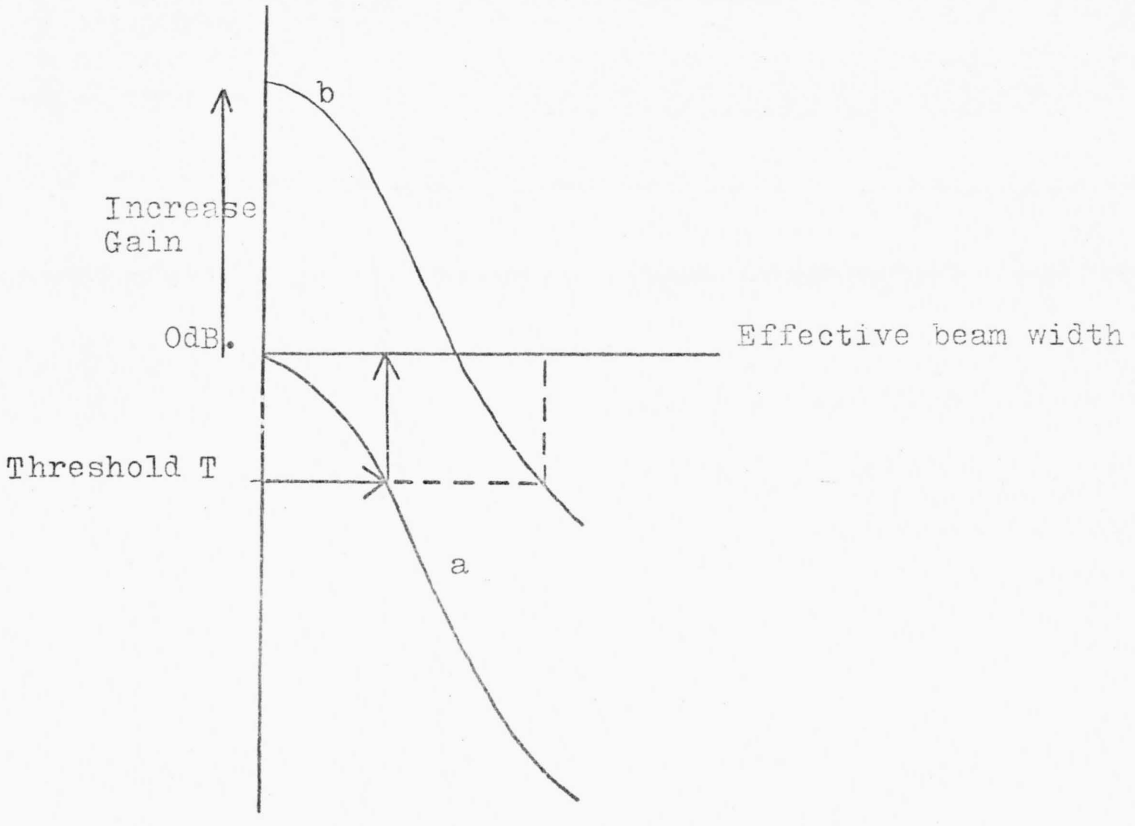


Fig. 3.14
Scan of nylon wires at gain G



Fig. 3.15
Scan of nylon wires at gain G - 10 dB

Fig. 3.16 Illustration of way that Effective Beam Width depends on Threshold and Gain.



dynamic range, and in spite of measured beamwidths which are an order of magnitude greater (typically, beamwidth ~ 1 - 2 cms, resolution limit ~ 2 mm).

The inadequacy of this measurement of resolution is thus demonstrated. The ability to separate two wires is not a fundamental characteristic of a scanner; it is a variable property that depends not only on the adjustment of the scanner controls but also on the object and medium scanned. In particular there is an interaction between receiver sensitivity, resolution and signal dynamic range, which is summarised by Figure 3.16. The echoes from a wire scanned across the beam are normalised to the axial maximum which then becomes the 0 dB level. There exists a minimum signal level beneath which the detector will not register a distinct echo. Smaller signals may be lost because of the presence of high noise levels, of low sensitivity or high input attenuation. Such a signal level constitutes a detection Threshold, which is the minimum acoustic signal that will register on the display, and it may be drawn as shown in Figure 3.16(a) so that the width of thecurve at the threshold level equals the length of the line displayed on the B-scan as the wire moves through the sound beam. If the receiver gain increases, then all signal amplitudes are increased and the curve when renormalised is unchanged except that, since the absolute value of the threshold level is unchanged, its value relative to all other signals decreases (as shown in Figure 3.16(b)), so that the displayed line increases in length. The resolution measured with the wires

is the length of the threshold line corresponding to the scanner settings used.

From these simple measurements it is apparent that resolution depends on beamwidth but that beamwidth measurements alone do not completely describe a scanner's resolving ability. It is necessary to distinguish between the emitted beam and the effective beam which is partly determined by the receiver sensitivity and threshold, and by the nature of the reflecting object. This last factor is a particularly undesirable feature of methods of comparing scanners using phantoms because it deviates from the objective of comparing properties of the scanners alone. The distinction between the resolution achieved in any situation and the inherent limitations of the scanner is again shown to be important in Chapter 4.

(h) Measurement of Axial Resolution

Axial resolution as defined by Montgomery and Kossoff has been measured using the device shown in Figure 3.17. The water filled space between two parallel perspex plates may be varied by a micrometer screw drive. The echoes from the two perspex-water interfaces are displayed on the A-scan. As the space is made narrower the two echoes close together and measurements of the plate separation can be made when the peak height to trough ratio on the display reaches some chosen value. Measurements were made with the three different transducers and receiver bandwidths of the Diasonograph for various selected ratios and the results, normalised to the 'worst' transducer, are shown in Table 3.4. Again a

quantitative comparison is impossible because the ratios vary with the criterion of resolution which is chosen arbitrarily. Furthermore, the resolution is again affected by the suppression and gain controls, and the measurements require specification of these variables. For example, if the peak (P) to valley (V) ratio is initially $R_1 = \frac{P}{V}$, then introduction of a suppression T alters this ratio to R_2, where $R_2 = \frac{P - T}{V - T} = R_1 + \frac{T(P - V)}{V(V - T)}$. Since R_2 is always greater than R_1, the plates must be moved together to reduce the ratio to R_1 i.e. the resolution is increased. In practice such measurements are quite difficult to perform accurately, and require a well engineered phantom. They cannot measure the axial resolution of the B mode and make no allowance for signal processing enhancement of resolution for the B mode.

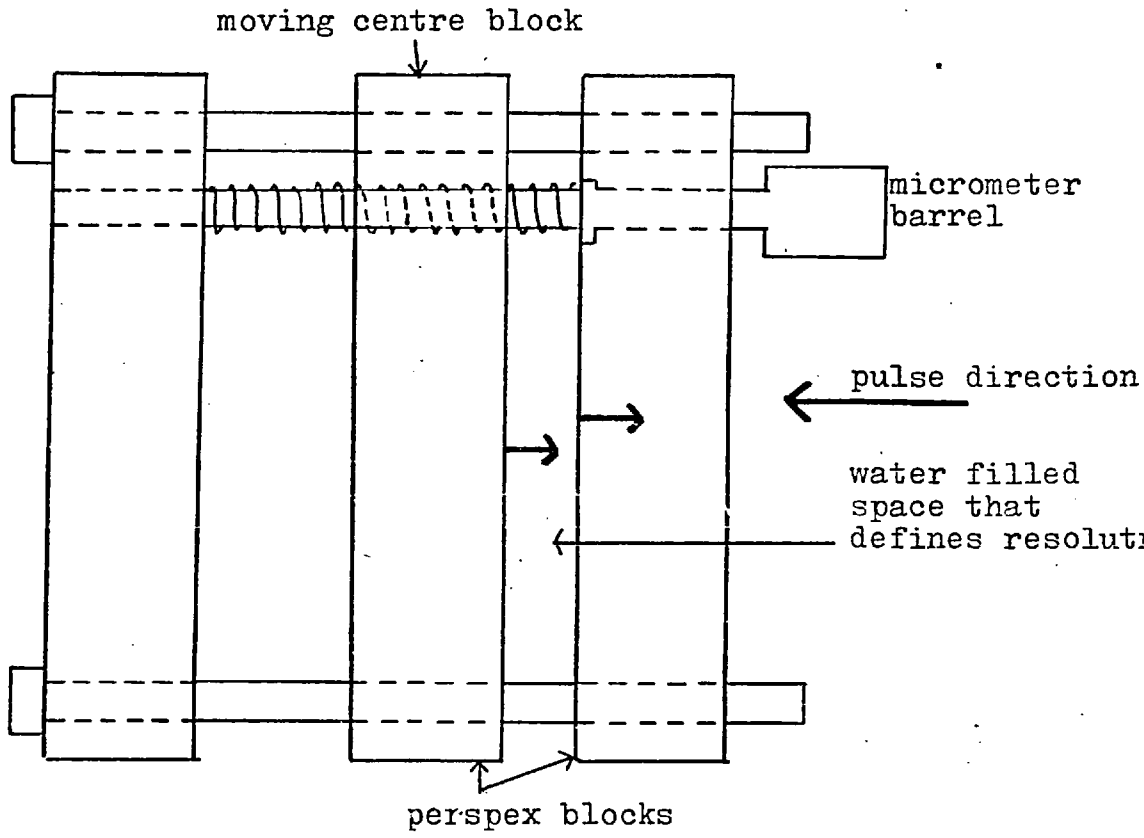


Fig. 3.17 Apparatus for measurement of axial resolution.

Table 3.4

Comparison of the axial resolutions of four transducers using different criteria of resolution obtained by measuring the width of a water layer and the corresponding A scan echo height to inter-echo trough ratio.

Transducer	A	B	C	D
Frequency (MHz)	1.5	2.5	5.0	1.5
$1/d_1$, where d_1 = the separation such that peak to trough ratio = 5 (normalised to transducer A).	1.0	1.5	2.0	1.2
$1/d_2$, wher d_2 = separation such that peak to trough ratio = 10 (normalised to transducer A).	1.0	1.9	2.4	1.1
$1/d_o$, wher d_o = separation such that two echoes completely separated (normalised to transducer A).	1.0	1.1	1.8	1.0

3.5 An assessment of a Multiscan

The Multiscan is a device designed to produce real-time images of cardiac cross sections and has been described by Bom (1972). The original system was first used clinically in 1971, but since then several versions have been developed. The Bom device is now commercially available from Organon Technica Ltd (Holland) whilst similar devices have been described by other authors (e.g. Whittingham 1975) and are now made by other companies (e.g. Mediscan Ltd, Denmark). A prototype Multiscan was supplied by Bom to Hammersmith Hospital in 1973 for a clinical and physical assessment as part of a collaborative arrangement.

The following series of measurements was performed primarily to demonstrate the problems associated with this type of scanner and to evaluate any image distortions that can occur clinically, since these affect the usefulness of the system in quantitative measurement. The results illustrate further many of the behaviour characteristics shown by conventional scanners and lead to a formulation of the parameters that are important in determining image distortion.

(a) Technical Description

The Multiscan consisted of 20 piezoelectric elements in a line which were excited separately but sequentially to produce 20 parallel, intensity modulated A scans on a cathode ray tube. Each element in sequence transmitted a short acoustic pulse and received the returning echoes; the depth of structures was indicated on the horizontal axis of a 20 line display, while the vertical position of each line

corresponded to the position of an element in the transducer. Rapid electronic switching enabled the entire array to be excited to produce 150 complete cross sections, each the height of the array itself, every second. In later versions, two successive frames were interlaced to give the appearance of a 40 line display at 75 frames per second.

The echoes were displayed as intensity modulated dots and although the signal processing of later versions provides a more versatile video processor, the prototype 'direct mode' processing simply displayed a bright line equal in length to the echo envelope above a threshold level. In Figure 3.20a the other signal processing modes are illustrated; all gave a displayed length which was dependent upon the echo length above a threshold. The Multiscan amplifier gave 80 dB maximum gain, but this could be varied with distance - there was a separate gain control for different regions of tissue, 5 controls independently determined the gain for the regions 0-1, 1-2, 2-4, 4-8, 8-16 cms respectively. The transmitter produced a gated sine wave of 250 volts, 1 μsec duration, at the transducer resonant frequency, 2.25 MHz. The transducers were damped P1-60 crystals, each 4 mm x 8 mm, on an araldite-tungsten (18%, 82%) backing with a quarter wavelength araldite faceplate (designed for matching the mechanical impedances of the crystal and medium). Details of the transducer design, and particular problems that had to be considered, have been given by Lancée (1973).

The receiver contained a linear RF amplifier with a maximum gain of 80 dB. The receiver gain determines the dynamic range of the echoes displayed - other constraints include the reflectivity of the target and the attenuating properties of the propagation medium, but for lossless media (water) and good reflectors (e.g. steel needles) the major variable constraint is the amplifier. A contrast control also affected the range of echoes seen in the image, but was only effective over about a third of its range. This third was subdivided into three regions (designated α, β, γ) for qualitative reference.

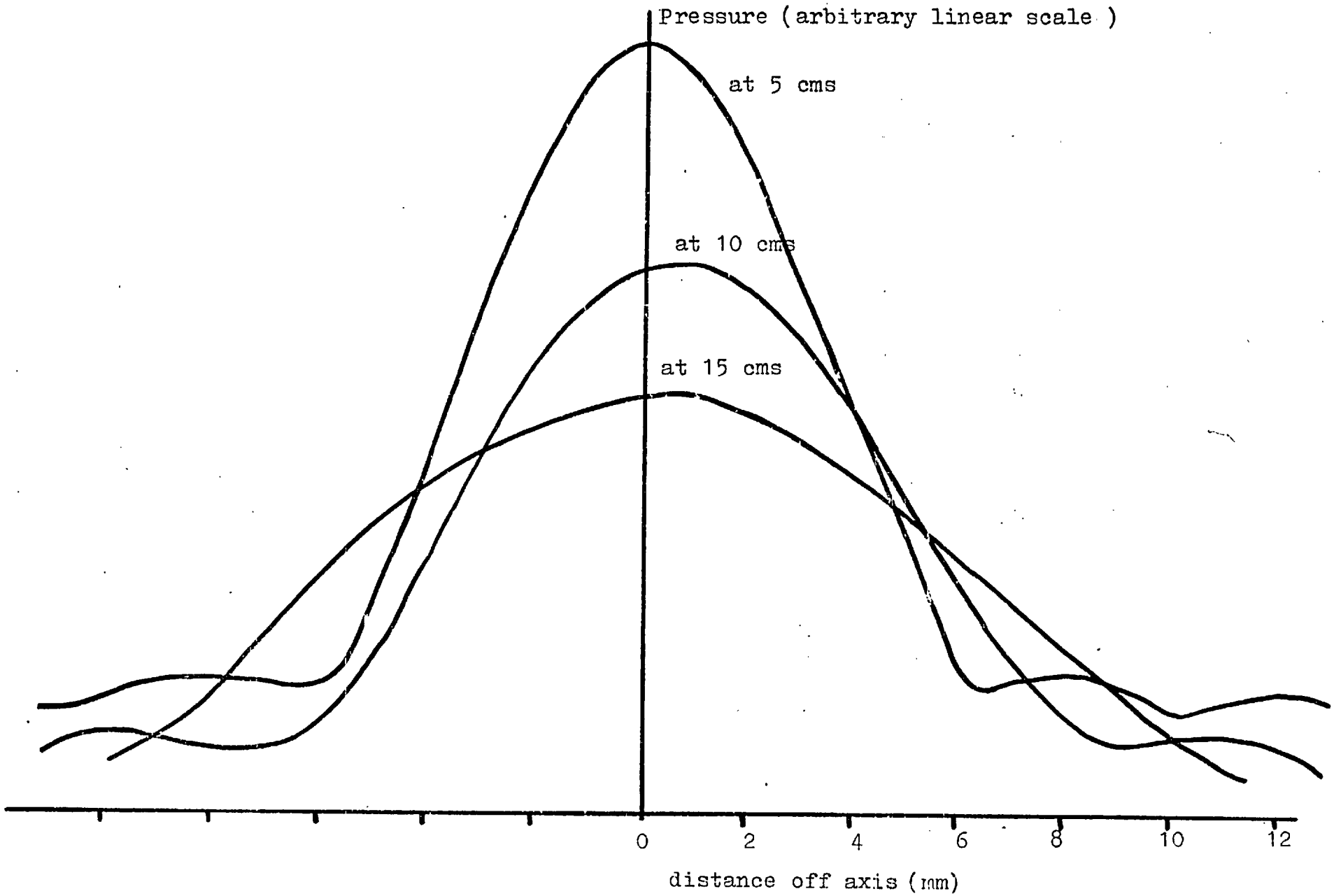
The system velocity was measured to be 1580 ($\pm$ 10) metres sec^{-1}. The PRF of the 20 elements combined was 3000 Hz; the active transmitter frequency 4350 Hz with inactive periods used after each 20 excitations to generate characters for the display.

(b) Measurements of Lateral Resolution

The emitted Pressure Profiles at various distances were plotted using a small piezoelectric probe. These are shown in Figure 3.18 and in the plane of the transducer array there is considerable divergence of the sound beam. This is not unexpected since the elements are only 4 mm (6 wavelengths) wide.

The element size was determined by compromising between the conflicting requirements of good lateral resolution, high line density on the display, good penetration (determined by dispersive attenuation in tissue) and overall size of the transducer. For a length of transducer of 80 mms (maximum

Fig. 3.18 Emitted Pressure Profiles from Multiscan 2.25 MHz transducer at various distances.



size for good contact on chest) and 2.25 MHz frequency, 20 elements was chosen as the best compromise (Lancee, 1973). Initial studies of simple phantoms showed that although the elements were excited separately, so that the echoes from one element's sound emission were not recorded by any other element in reception, it was possible for a reflector to be displayed on more than one line. For example, a metal needle in a water bath, arranged perpendicular to the line of elements, was displayed on more than one line of the display. For such a needle the display showed a series of short streaks which tapered as shown in Figure 3.19; the longest was in the centre of the group, which corresponded to the element directly in front of the needle.

The signal processing of the Multiscan amplified the RF electrical pulse from the transducer in reception, which is shown schematically in Figure 3.20. The pulse was then full wave rectified and demodulated, and the length of envelope above the detection threshold level defined the displayed pulse length on the intensity modulated monitor. The displayed length therefore was related to the intensity of the echo for pulses that were singly peaked. Cylindrical or spherical targets presented a reflecting area to some of the sound field from elements adjacent to that element in line with the target. The echoes back to these elements however, were derived from regions of the sound field of low intensity and were therefore displayed as shorter streaks. For a needle a line of echoes was produced as in Figure 3.19 and the lateral intensity distribution of each element was

Figure 3.19 Image of a cross section through a 2 mm diameter cylindrical steel needle in a water bath at high amplification

anterior posterior

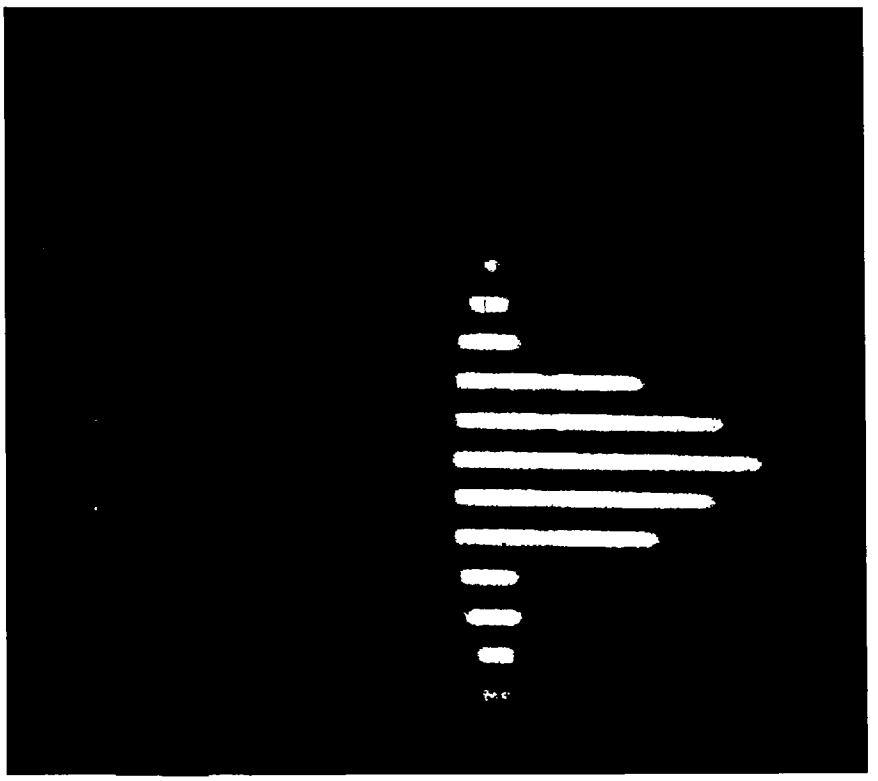
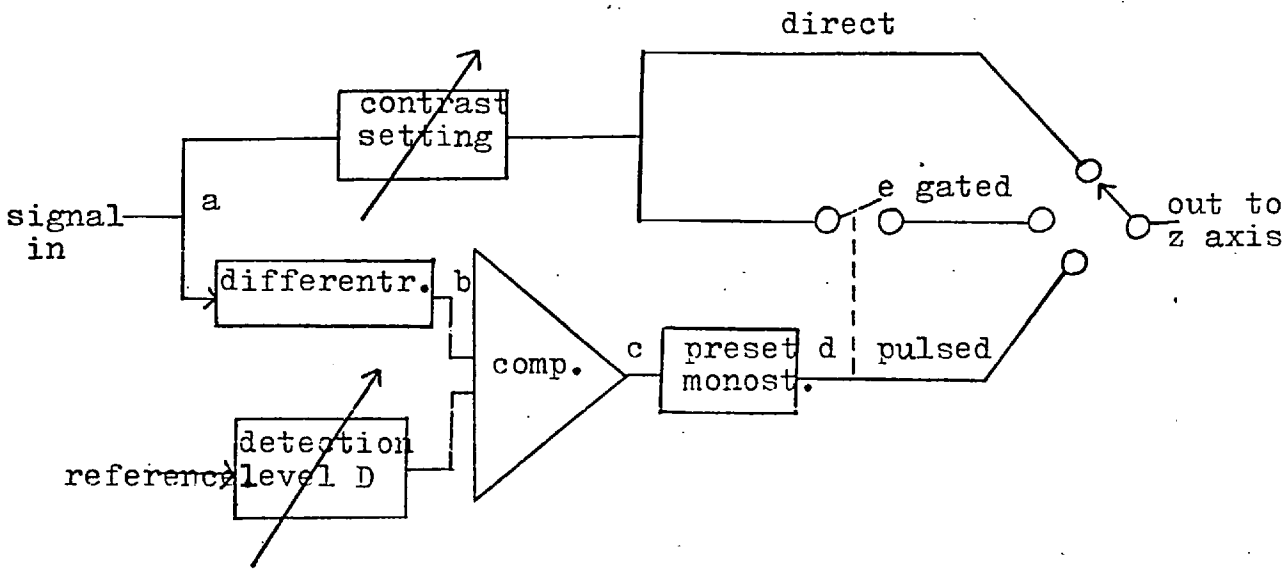


Fig. 3.20 Signal processing of Multiscan, and signals at various positions in the processing chain.



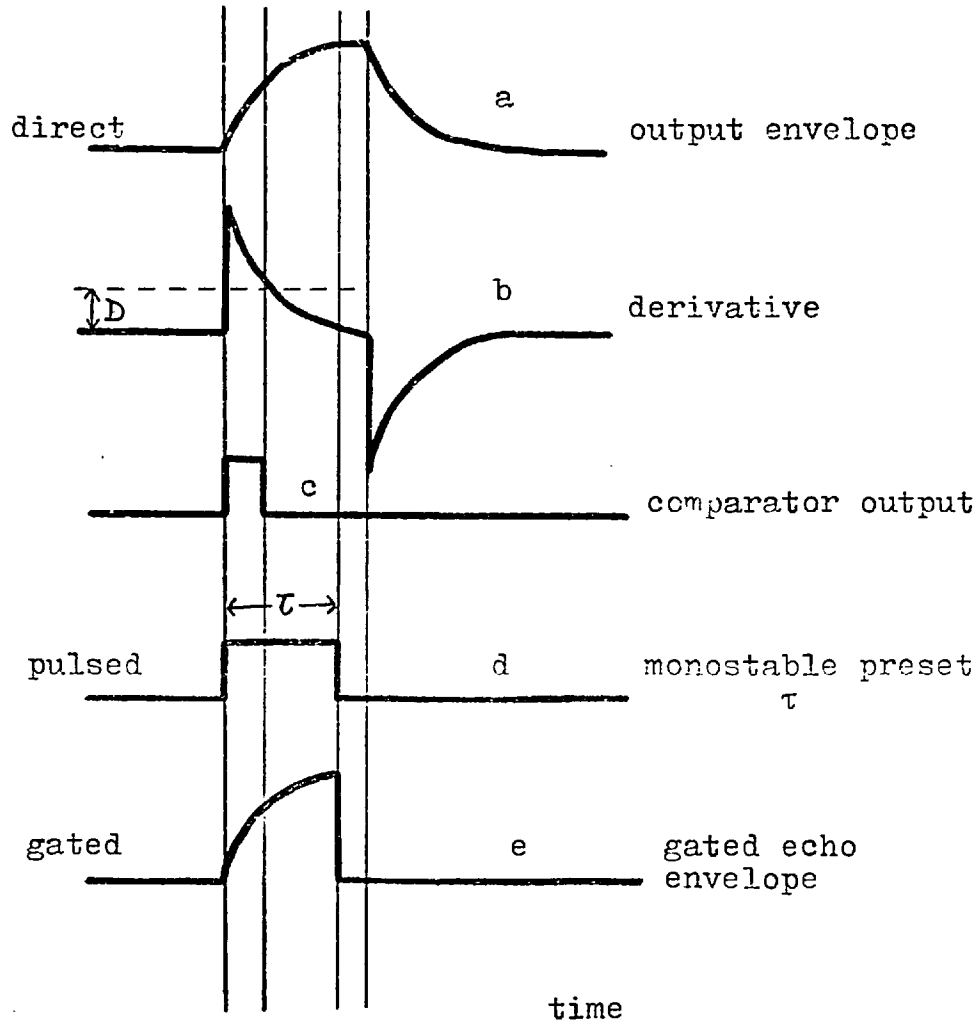


Fig. 3.20 Signal processing of Multiscan

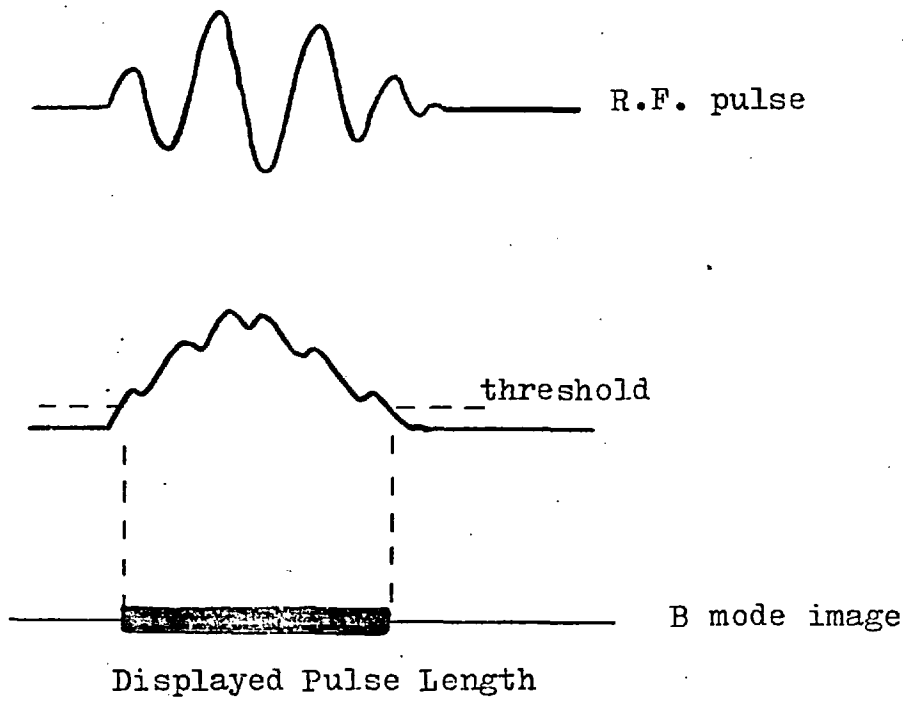
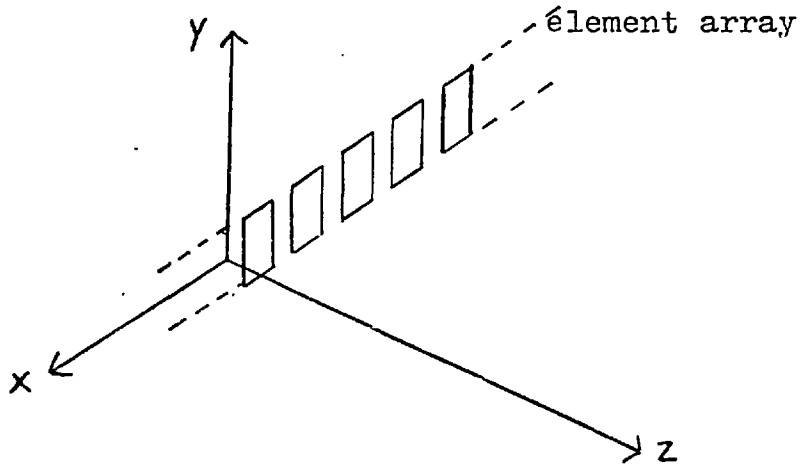


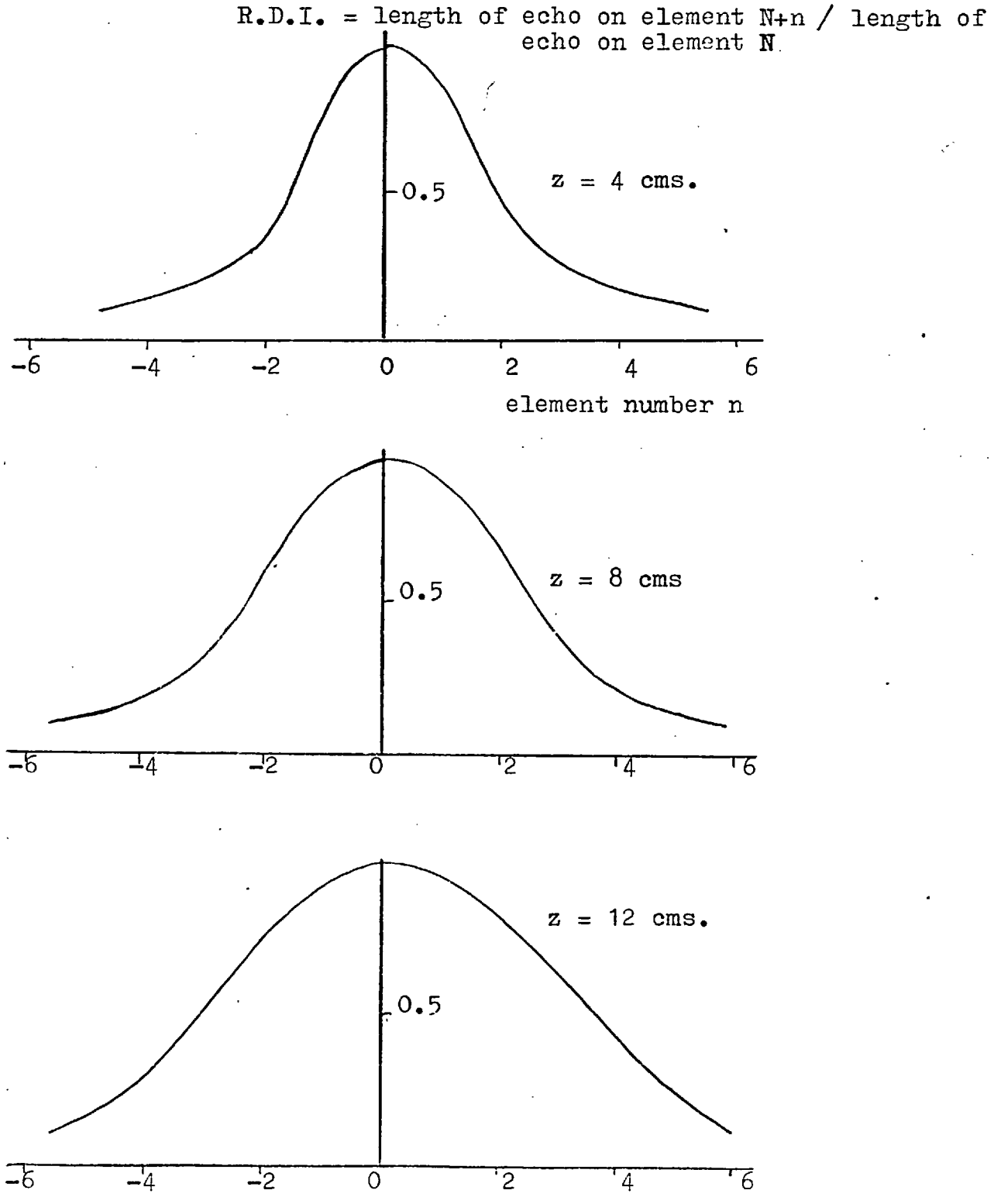
Fig. 3.21 Definition of coordinate system used.



inferred by inspecting the display. Consider the arrangement defined by the coordinate system of Figure 3.21. If all the elements are assumed identical then the echo intensity displayed by an element nd away from the axial element (where d = distance between element centre lines = 4 mm, and n = 1,2,3,...) is the same as the echo intensity that would be shown on the axial element's display line if the needle were moved nd in the x-direction: the intensity distribution on the display is directly related to the intensity distribution caused by any one element in the xy plane. The length of echo displayed on the monitor was taken as a measure of displayed intensity and Figure 3.22 shows the crude representation of Reflected pressure profile obtained by plotting the Relative Displayed Intensity. (= Length of echo on line n ÷ length of echo on central element) against lateral distance (= element number, n). This curve represents the effective RPP for the needle measured in this way.

The lateral intensity distribution might, in circumstances where the nature of the target reflector is known, be used to give an accurate indication of target position: thus, in Figure 3.19 the position of the needle was known from the position of the maximum echo in the line of echoes displayed. In attempting to obtain a quantitative description of the system's lateral resolution it was assumed that no such 'resolution enhancement' could be derived from consideration of the intensity distribution. For most situation this is more realistic.

Fig. 3.22 Estimation of the Received Pressure Profile from needle reflector by measurement of the Displayed Pulse Length.



Consider one element of the transducer, of width h and height d.

If the sound field from each element consisted at all distances of a plane, uniform distribution of pressure of area hd, then a point reflector anywhere inside the area hd in front of an element would either show on 1 line, the 'correct line' (= line corresponding to the element at the foot of the perpendicular from the point onto the array), or not at all, depending on its reflectivity. This hypothetical non-deviating sound beam would therefore show a positional uncertainty equal to the area hd = the uncertainty inherent in specifying the position of the point reflector in the xy plane. This positional uncertainty can never be improved with the Multiscan, however we choose to idealise the beam and processing, if no amplitude information is used, unless there are regions of the medium from which we obtain no information at all. If the beam is made narrow to any desired degree, a perfect reflector will still either be displayed on 1 line or not at all. A reflector such as a needle moving in the x-direction at constant z will not be 'lost' at any point in the medium if it is always displayed on a line, but the displayed movement will not be a smooth movement, but a series of steps from line to line, separated by periods of no apparent motion. For the sound field measured, the peak acoustic pressure varies by less than 1 dB over the area hd at any distance for most of the field, so in general there are no regions of the field in which conditions exist such that a point will show in some parts of the area hd and not others.

In order to be identified on the display, an echo has to be greater than a minimum level, the Minimum Display Level, of the system. The absolute value of this MDL, which is an acoustic intensity, depends on the sensitivity of the system - on transducer efficiency, amplifier gain, monitor tube sensitivity and contrast, and on observer acuity. The echo amplitude depends on the emitted power, target reflecting power, and medium properties. At a distance z from the transducer, movement of a metal needle in a water bath (as shown in Figure 3.21) along the line of elements (x axis) measures a width, Δx, in which the intensity is such that the needle is displayed all the time on a given element i.e. Δx defines the width of the single element beam which gives echoes above the MDL, with a needle reflector at that particular setting of the receiver and at that distance. Δx varies with receiver gain, since the absolute value of the MDL decreases with increasing sensitivity of the receiver/display. Similarly, a needle parallel to the x axis and perpendicular to y and z, when moved along the y axis, gives a width Δy. Needles are especially useful for this system, as they separate out variations in the x and y directions, yet provide a scattering body that reflects isotropically in the plane of interest. Δx and Δy are both positional uncertainties - the reflector is shown on a line and by looking at the display we cannot specify the reflector position more accurately than the area $\Delta x \, \Delta y$, unless we use information from adjacent lines and assume a known target geometry. $\Delta x \, \Delta y$ is the lateral 'area of uncertainty'. It is a function of the relative values of several Multiscan parameters, expressed as the MDL, for a

particular class of objects (generally only object reflectivity needs to be specified if water is the medium since transducer efficiency, the other important factor, is constant for all objects). The ratio $\frac{\Delta x \Delta y}{hd}$ is a dimensionless expression of the system's achieved performance compared with the 'best' performance obtainable. Figure 3.23 illustrates the effect of changes in the amplifier gain upon this parameter for different distances from the transducer. The gain may be re-expressed, after allowing for variations in the axial emitted pressures, as the dynamic range of echoes displayed on the monitor so that the curve (Figure 3.24) becomes a variation of positional uncertainty against echo strength relative to the MDL. Such curves are useful for predicting the effects of changing the reflector if the reflector strength is approximately known. Figure 3.25 illustrates similar effects but plots the single dimension uncertainties, $\frac{\Delta x}{h}$ and $\frac{\Delta y}{d}$. Figure 3.26 illustrates the importance of the monitor contrast control, which was not adjusted for the measurements above. The contrast changes the response of the display tube and appears to act in the same way as a non-linear amplifier. It could therefore be important in optimising the scanner performance but in practice was always fixed at the same value.

Δx and Δy are variables that are functions themselves of several parameters. They are the Effective Beam Widths and as such they define the resolution of the system in these conditions. Two equally reflecting targets at the same distance and separated by 1 EBW or less cannot be distinguished on the display since their reflection images overlap. In Figure 3.27, two needle images just overlap on the display

Fig.3.23 Effect of receiver gain on positional uncertainty of needle.

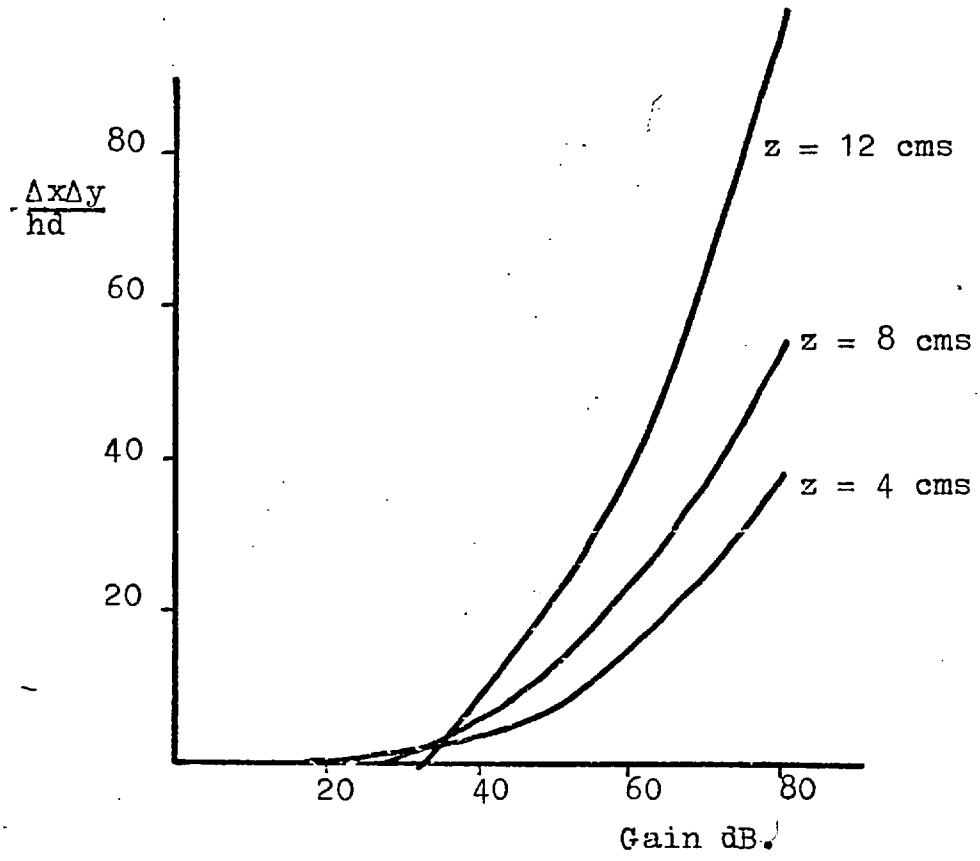
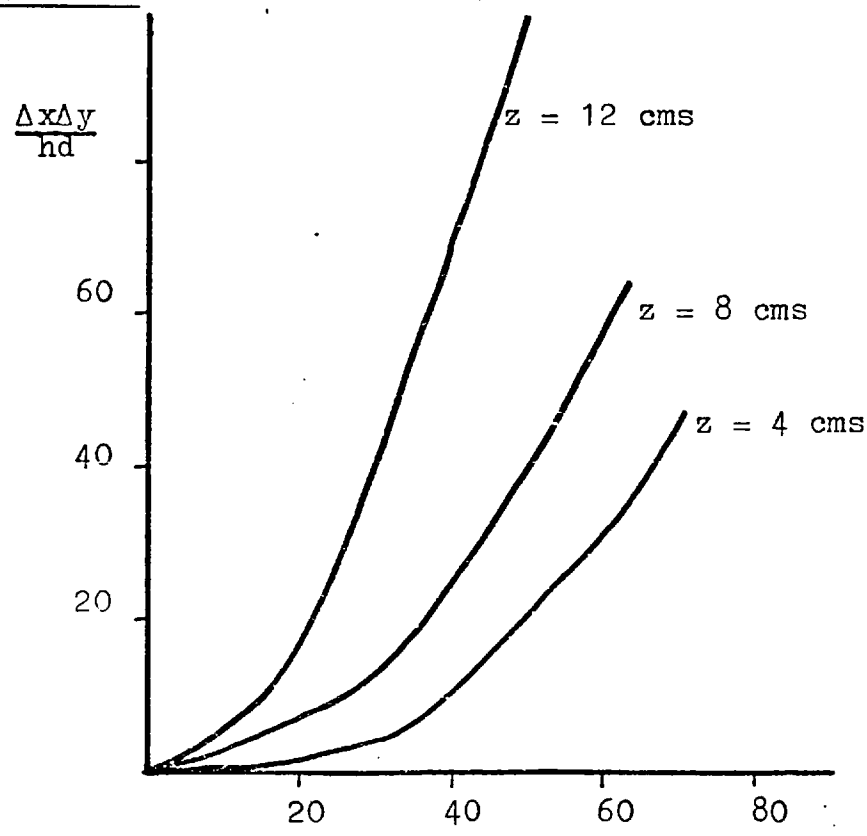
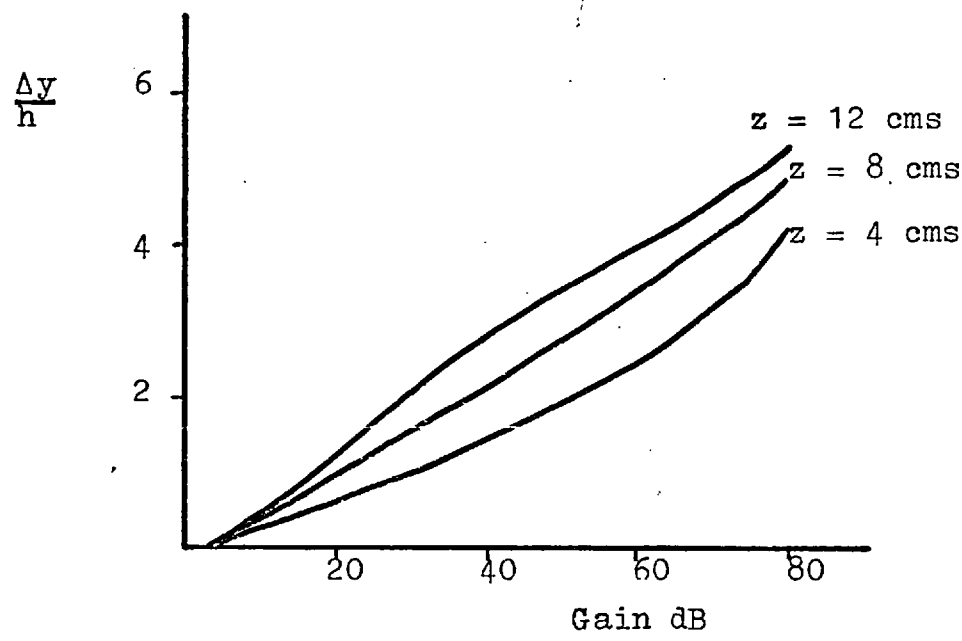


Fig. 3.24



Displayed dynamic range of echoes relative to MDL (dB).

Fig. 3.25 Effect of gain of receiver on one dimensional positional uncertainties.



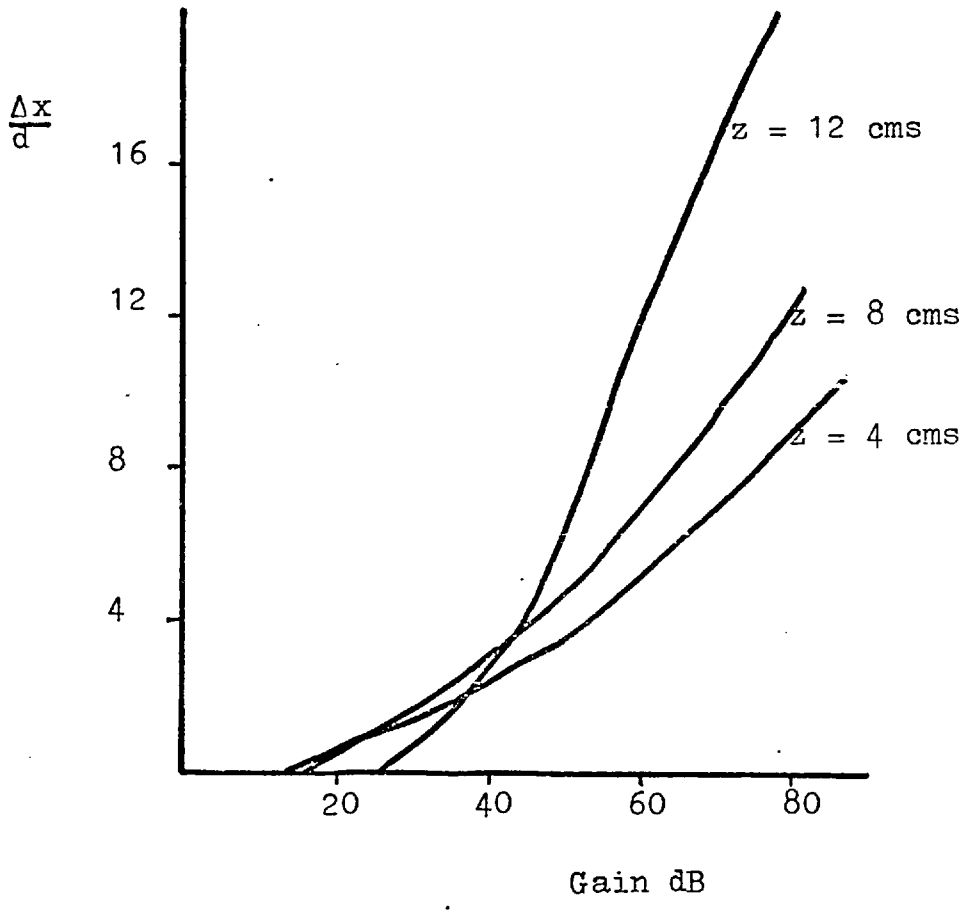


Fig.3.26 Effect of monitor tube contrast on image.

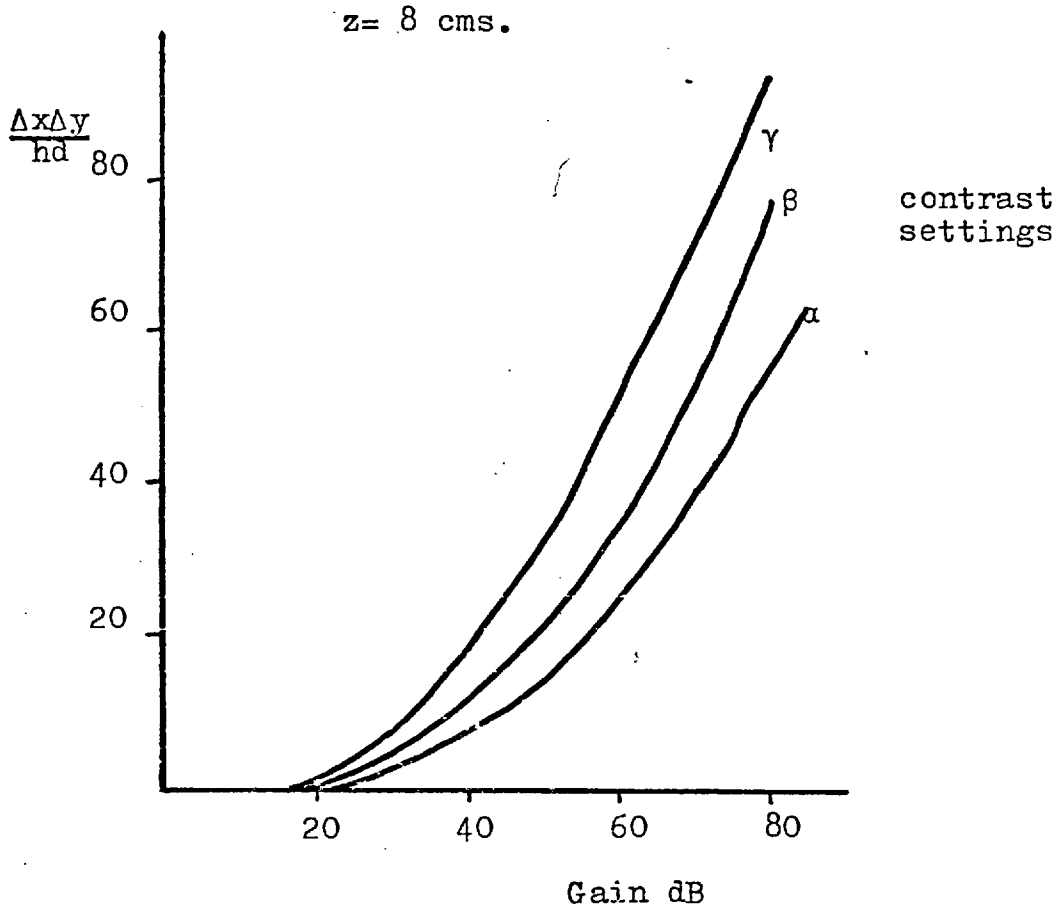
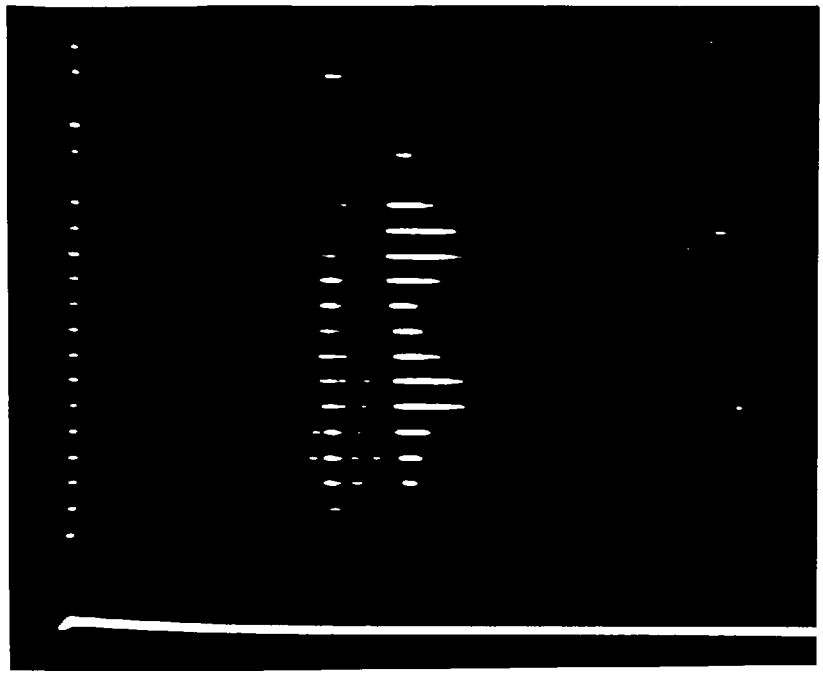
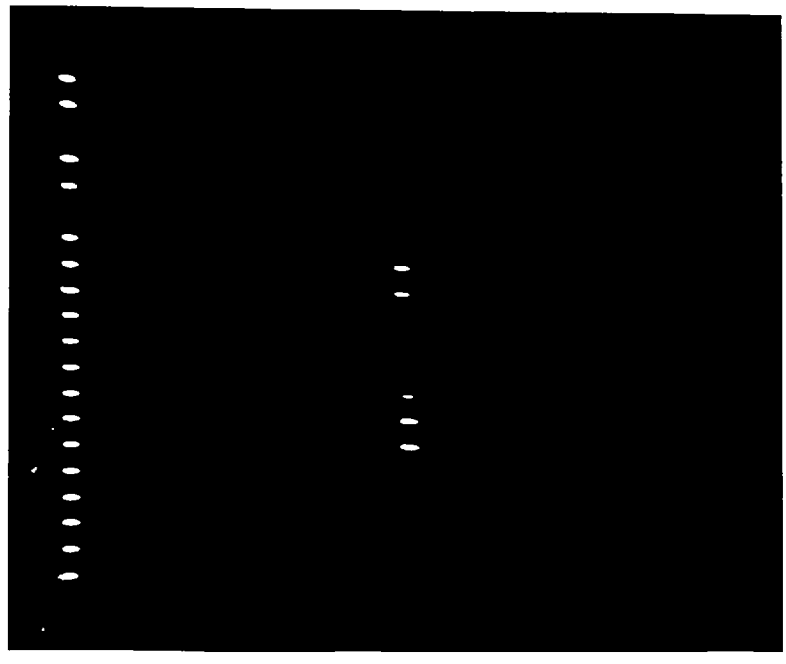


Figure 3.27 Multiscan images of two needles in a water bath at the same distance from the element array (a) at high gain (b) at reduced gain so that they are resolved.





until the receiver gain is reduced and the EBW made narrower.

Figure 3.28 shows how this may be interpreted in terms of the emitted sound beam. In (a) the regions of a single element field defined by the 5, 10 and 20 dB levels (measured relative to the axis) are shown; the areas inside these levels increase as the levels decrease. In (b) the fields from several elements are shown overlapping, and the number overlapping at any point is a function of the level chosen to define the field. The dB level that defines the effective field is determined by the target reflectivity and the overall system sensitivity and dynamic range, i.e. by the MDL for that target. The total emitted sound beam is 'filtered' by the receiver, the extent of the sample after filtering is the effective beam area and the exact nature of the filter is determined by the receiver settings. The MDL determines the limit of the effective sound field.

In Figure 3.29 the effect of echo dynamic range on lateral resolution is summarised. When the echo from a needle is just visible at 0 dB dynamic range, it will no longer be visible if moved laterally over any distance as the emitted pressure falls off axis. If the echo strength is increased by 10 dB, a reflector may be moved 5 mm in either direction at 8 cms and still be visible, or 9 mm at 12 cms. Similarly, the echo from a needle 8 cm in front of element N is just visible when the displayed range is 0 dB (Figure 3.30), but if this increases to 8 dB the needle is just visible at elements (N-1) and (N+1) whilst if it is increased by 14 dB it becomes visible on (N-2),(N+2), and so forth.

Fig. 3.28 (a) Sound field from a single element.

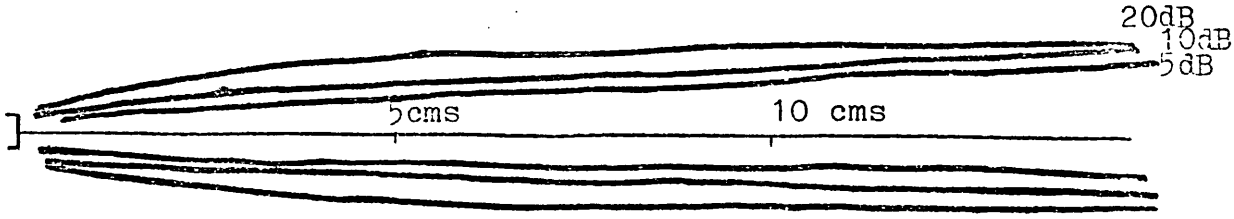
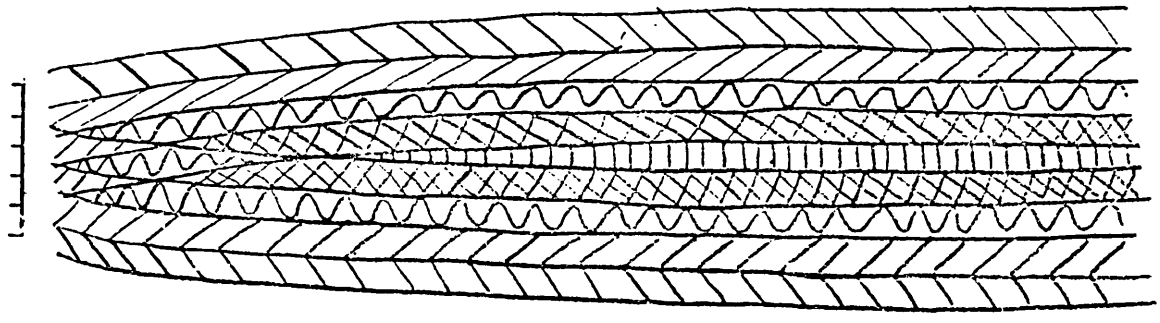


Fig. 3.28 (b) The sound fields from 5 elements at the 20dB level overlap so that different regions of the field are irradiated by different numbers of elements.



III in the field of all 5 elements

XX in the field of 4 elements

∿∿ in the field of 3 elements

/// in the field of 2 elements

\\\ only seen by one of these elements

Comparing (b) to (a), there will obviously be less overlap at the 5 or 10 dB level, but more at lower levels.

Fig. 3.29 Effect of sensitivity on lateral resolution.

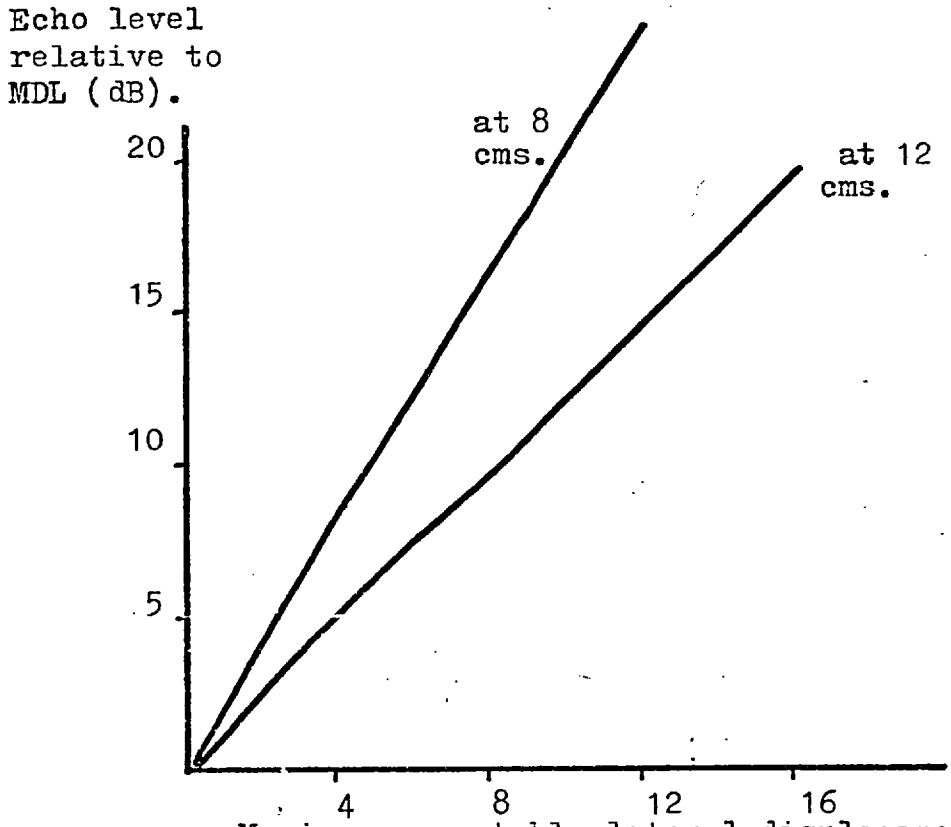
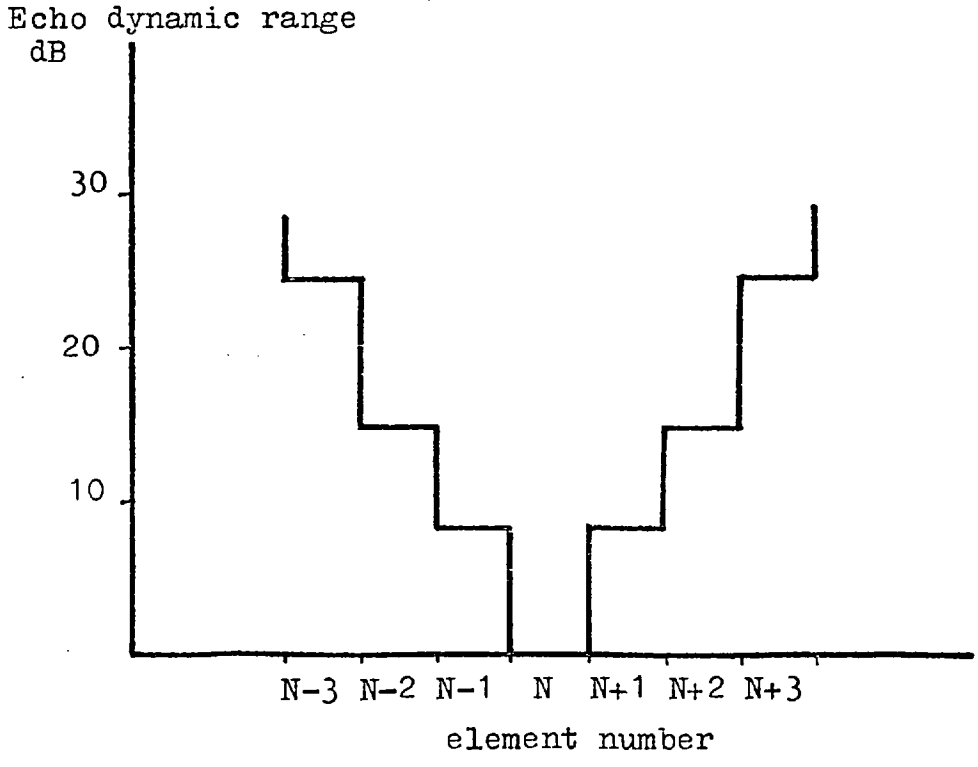


Fig. 3.30. Artefactual displays of echo from needle on adjacent elements when placed in front of element N as a function of dynamic range.



The resolution generally varies with distance but the dynamic range of echoes displayed may be varied to obtain uniform lateral resolution throughout the medium. If uniform lateral resolution is desired then the MDL must be made to vary with distance which could be accomplished by incorporating a suppression - time variation ('swept threshold').

(c) Range Precision and Resolution

The range precision determines the accuracy of measurements of distance along the transducer axis, either from transducer to interface of between two interfaces. Range resolution determines the ability to separate interfaces separated in range only. These working definitions suffice for a description of Multiscan performance.

An echo returning from an interface is a radio frequency signal, and the Multiscan displays an echo when its amplitude is greater than the MDL. Even in the gated and pulsed modes of processing the echoes, the MDL determines displayed pulse length though the MDL is a function of other variables. In Figure 3.31, T_1 denotes the acoustic MDL at some setting and the system displays a line equal to the echo length between A and D: if the threshold is T_2 ($>T_1$), the displayed pulse length is only B to C.

When the measurement of interest is from transducer to interface, then measurements from the display are made from the time base origin to the front of the displayed echo, and obviously this distance is a function of the relative size of echo to MDL. If the signal is amplified, or if the threshold is changed, the front of the displayed echo may shift (from A to B in Figure 3.31). The degree of shifting depends on

Fig. 3.31. Effect of changing detection threshold on range precision of Multiscan.

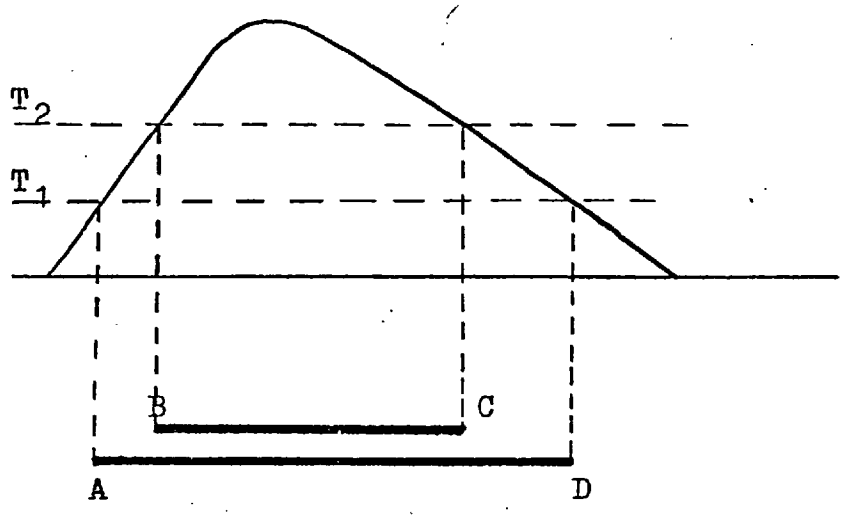
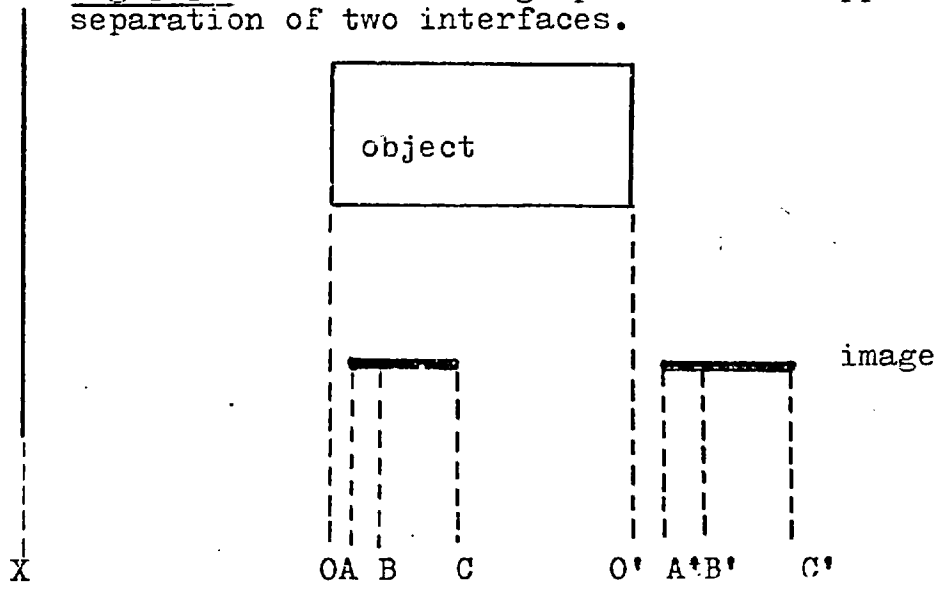


Fig.3.32. Effect of range precision on apparent separation of two interfaces.



A,A' are the apparent fonts of the echoes
B,B' are the positions of the peaks.

the pulse shape particularly the tail decay (damping). If the dimension of interest is the separation between two interfaces, then there are several measurements that might be made, as shown in Figure 3.32. The true dimension is OO', but OA and O'A' are shift errors that depend on the MDL: OA and O'A' are range errors, but may be approximately equal so that AA' = XA' - XA

$$= (XO' + O'A') - (XO + OA)$$

$$= (XO' - XO) + (O'A' - OA)$$

Thus, AA' = OO' + a second order term.

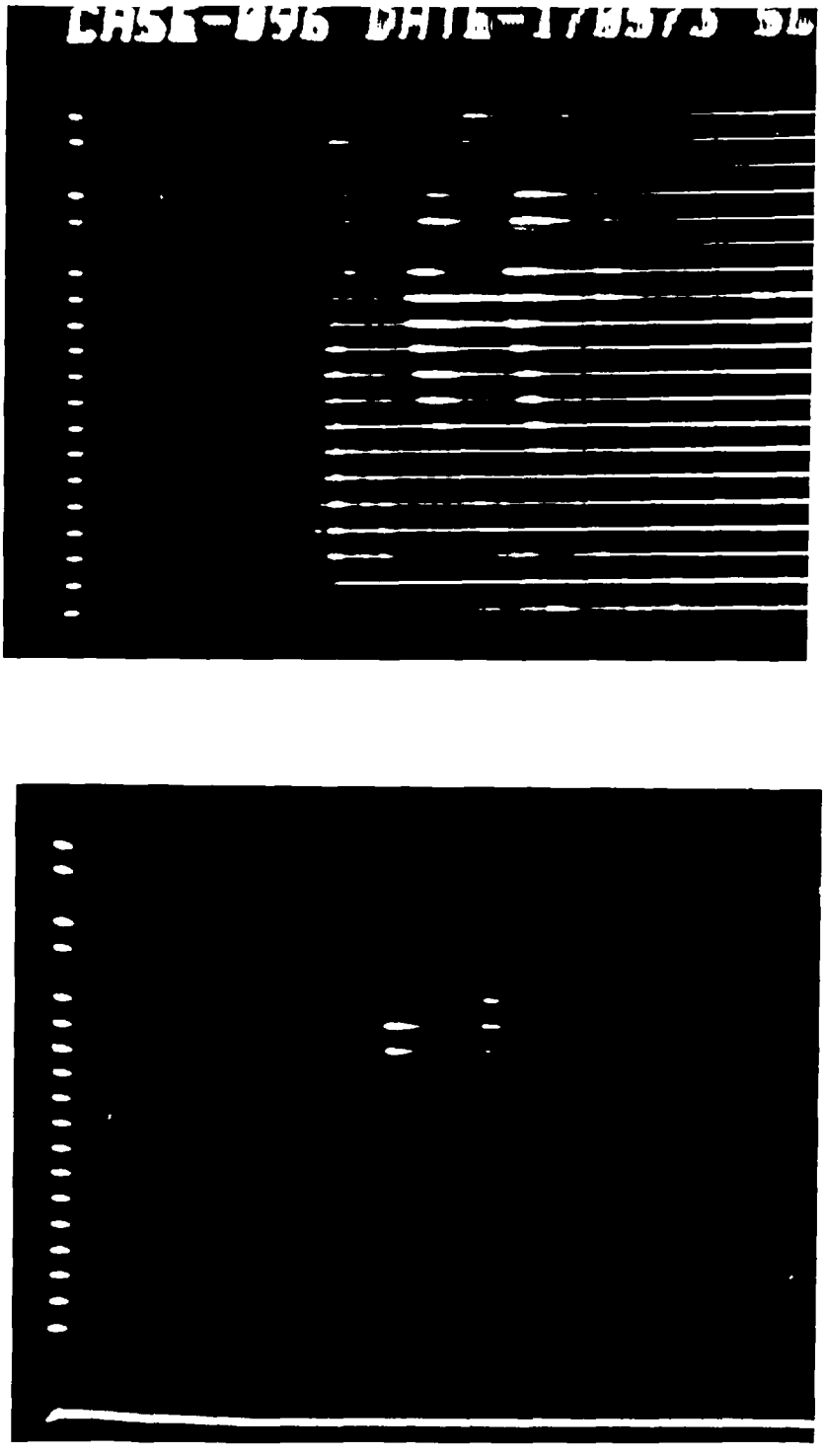
BB', the distance between peak intensities, is a good representation of OO' since the peak of the pulse will not move along the pulse for most real situations; but B and B' are not easily identified in an intensity modulated display. CA' is clearly not a good indication of separation though it is the dimension of the echo free region displayed. The optimum estimate of OO' is given above for O'A' = OA = 0 i.e. A and A' should be as near the front of the pulse as possible, which requires a low threshold relative to the echo size. The range precision of a pulse is therefore better if it is highly amplified, or if the MDL is low.

The Displayed Pulse Length, DPL, may be used as a criterion of range resolution: the DPL is the length of a pulse at the level of the MDL. When two interfaces are separated in range so that the echo from the second interface just overlaps with the tail of the echo from the first, then the echoes may appear as one continuous line on the display and the interfaces cannot be said to be resolved. The criterion for echo overlap is not simply a function of the relation between

the peaks of the pulses and the amplitudes in the region of overlap (i.e. not simply described by the peak - valley ratio of A-scan displays): the displayed line will be continuous if the sum of the two acoustic pressures remains above the MDL, so that there is no discernible break in the line. Figure 3.33 shows how two needles may have axially continuous pulses displayed so that the needles are not resolved, and how decreasing the gain resolves the needles. The MDL is increased and is now greater than the tail of the front echo, so range resolution is enhanced.

The requirements for range precision are different to those for range resolution, and the criterion used to describe range resolution does not allow for variations in achieved resolution between different classes of objects or for changes in the displayed dynamic range. The range precision requires a very low MDL to pick up the start of a pulse, whilst range resolution requires a high MDL relative to the echo peaks: the peak follower signal processing of the NE4102 may be considered as a means of obtaining the highest possible MDL for each pulse (see Appendix A) thereby providing optimal range resolution at the expense of range precision.

Figure 3.33 Illustration of the effect of receiver gain on the axial resolution of the Multiscan.
Two needles shown in the upper image cannot be resolved axially until the gain is reduced (lower image)



3.6 An assessment of distortions in Multiscan images.

The investigation of range precision, range resolution and lateral resolution, and their variations with other parameters, is relevant to a study of image distortions that occur with the Multiscan. Lateral resolution and lateral positional uncertainty have been shown to be closely related, they are measurable in the same units and are functions of the same variables. Range precision and range resolution are also related but in an inverse manner. However, in a typical scan, the range uncertainty of an interface must be taken as the entire length of a displayed echo, since the nature and positions of echo producing interfaces are not generally known, and no decision can therefore be made as to whether a line is produced by one or several closely spaced unresolved interfaces. Thus, there is also a practically important correspondence between range positional uncertainty and range resolution.

Distortion occurs when an image does not record the features of an object with their correct spatial relationships. On simple objects, the nature of the distortion may be discernible and the correct image interpreted by eye: for more typical scans, the distortion cannot generally be removed by the observer's interpretation. For the Multiscan, the object and image relationships are affected by the resolution of the system since this determines the positional uncertainty and error in the image: the ability to place an interface in its correct position in the image is further diminished by the lateral coordinate quantisation introduced by the discrete line appearance of the image.

Interpretation of the overall image depends on the perception of the images produced by individual elements. The way in which each single element irradiates the object determines, for example, how a small interface is spread on the display onto more than one line: the way in which the lines superimpose in the image determines the observer's interpretation and recognition of larger structures, and may, for example, determine how a series of discrete points become interpreted as a continuous structure. Spatial distortion occurs when objects are shown on the wrong line (lateral error) or at the wrong range (range error). In the examples that follow, the degree of distortion, which is a qualitative concept but which determines the ability of the Multiscan to make quantitative measurements, is shown to be determined by the positional uncertainties discussed earlier, and hence a function of the achieved resolution, the effective beam width and displayed pulse length.

An apparent shape distortion occurs for an echo free region whose boundaries are wrongly defined in the image because of the intrusion of long echoes from anterior structures into the region: an example of this is shown in Figure 3.34 for a perspex cylinder in water. The echoes from the front fill in the region even at moderate gain, changing the horizontal dimension of the echo free region and hence its cross sectional area. This error increases with increasing DPL, and thus with gain, and was one of the sources of discrepancy between Multiscan and angiographic cross sectional areas of the human left verticle cited by Pridie (1973).

In cardiac images of the type shown in Figure 3.35, the error in estimating the left ventricular short axis may be as much as 10%. Measurements from the fronts of the anterior echoes would be satisfactory but the fronts are poorly defined because the echoes are continuous with those from other anterior structures such as pericardium. Poor range resolution therefore introduces a range uncertainty and error.

Image distortions also occur because beam divergence affects range precision. The Multiscan necessarily contrains all reflectors within the field of a single element to be displayed along the same line in the image. When the effective beam width is large, two interfaces that are laterally separated but at the same range may be displayed as two echoes that have the same lateral coordinate but which are separated in range. Such a distortion represents a rotation by 90 degrees of the coordinate axes of small regions of the object. If an interface is displaced from its correct position in the image then the displacement may be described by the change in lateral position, Δx, and the change in range, Δz, from object to image. The root mean square displacement of the echoes, D, is a measure of the distortion. For the simple case shown in Figure 3.36, which represents two needles side by side,

$$D^2 = (\Delta x)^2 + (\Delta z)^2$$

$$= L^2 + ((R^2 + L^2)^{\frac{1}{2}} - R)^2$$

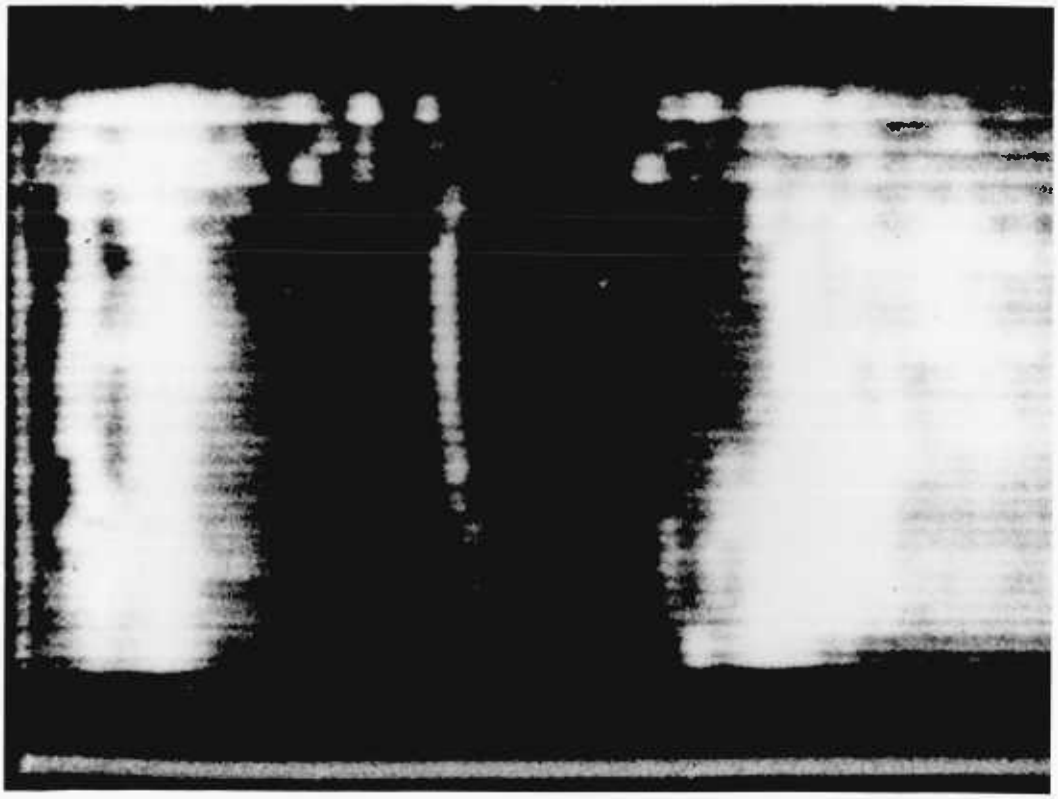
If $R \gg L$. then $D \doteq L\left(1 + \frac{L^2}{8R^2}\right)$

The range error is here small compared to the lateral error.

Figure 3.34 Multiscan image of a thin walled perspex cylinder



Figure 3,35 Multiscan image of a cross section through the heart along the long axis of the Left Ventricle showing some of the distortions discussed in Section 3.6



The distortion is dependent on L, and is worst when $L = L_{max}$, the maximum value of L that still registers an echo on the screen. For a needle, L_{max} is $\frac{\Delta x}{2}$, where Δx is the effective beam width described earlier. The ability of the Multiscan to display echoes from targets off axis, when the targets are non-specularly scattering areas irradiated by the less intense regions of the sound field, varies with the MDL of the system. The degree of distortion will depend upon the echo strengths relative to the MDL, and may be reduced by lowering the scanner's sensitivity. A particular consequence of this distortion is apparent in the images of surfaces where the displayed curvature differs from the object curvature. In cardiac images, in which the curved interface may be a chamber wall or valve leaflet, this produces a distortion not only of the shape and size of the heart but also of its apparent motion, and this may be illustrated by analysing the displayed image of a circular cross section.

Consider the cylinder shown in Figure 3.37 which has a radius R and which is imaged by the Multiscan. Ideally the Multiscan elements would record only the positions of those points which are the intersections of the circle with the element axes. These points would still lie on a true circle in the image. Some of the points however correspond to interfaces which do not have a favourable inclination towards the transducer to give an echo above the MDL. Nonetheless, the distance between such "ideal" image points and that element which is nw from the central origin (where w = an element width and n = 1, 2, 3, ...) would be

Fig. 3.36. A simple misrepresentation of two needles.

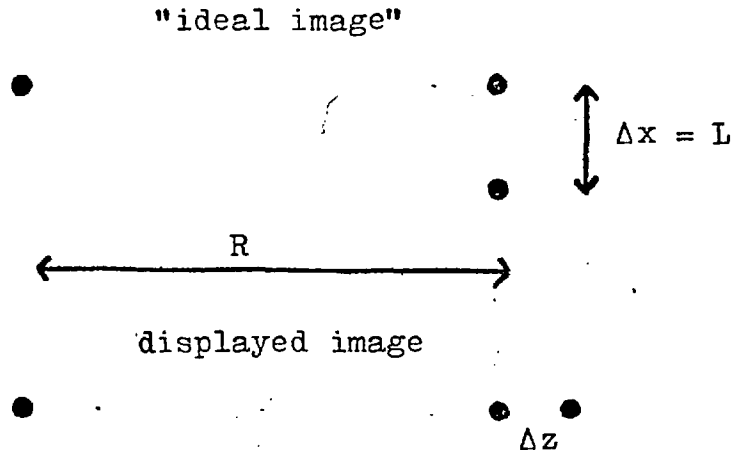
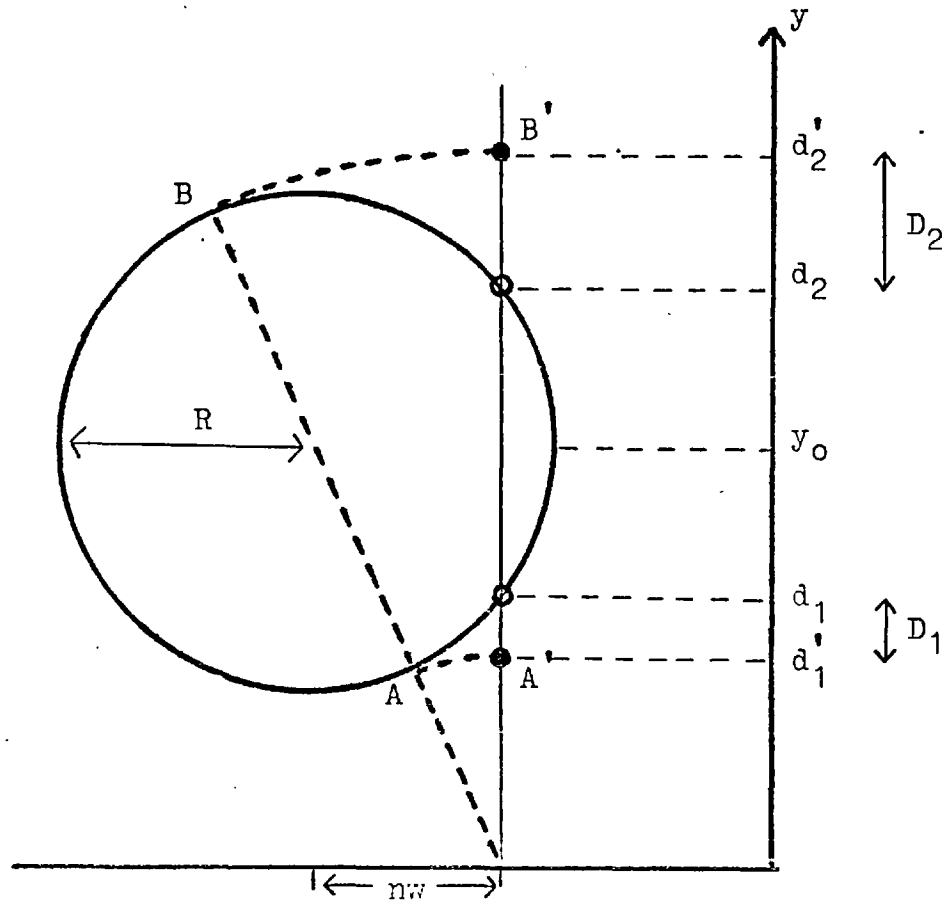


Fig. 3.37. Distortion of a circular object.



Echoes produced at A,B are displayed at A',B'
o denotes positions of echoes in "ideal" image
● denotes positions of echoes in real display.

$$d_1 = y_o - (R^2 - n^2w^2)^{\frac{1}{2}} \quad \text{(see Figure 3.37)}$$

for the point on the anterior surface and

$$d_2 = y_o + (R^2 - n^2w^2)^{\frac{1}{2}}$$

for the point on the posterior surface.

However, because the sound beam diverges, echoes are produced from points on the cylinder which are nearer to the element than the "true" points of the anterior surface, or farther than those of the posterior surface. The most anterior image points are produced by echoes originating from the points on the circle which are nearest to the element concerned, and these points lie on the intersection of the circle with the lines joining the circle centre to the transducer. (Figure 3.37). The echo producing interface is then normal to the sound field, and the distances of echoes from the element will be displayed as

$$d_1' = (y_o^2 + n^2w^2)^{\frac{1}{2}} - R$$

and $$d_2' = (y_o^2 + n^2w^2)^{\frac{1}{2}} + R$$

The resultant image has an increased radius of curvature of the front surface, and the back surface is parallel to the front and is completely inverted relative to the object. The displacements in range of the echoes from the "ideal" image are measurements of the distortion.

$$D_1 = d_1' - d_1 = (y_o^2 + n^2w^2)^{\frac{1}{2}} - R - y_o + (R^2 - n^2w^2)^{\frac{1}{2}}$$

$$D_2 = d_2' - d_2 = (y_o^2 + n^2w^2)^{\frac{1}{2}} + R - y_o - (R^2 - n^2w^2)^{\frac{1}{2}}$$

If $nw \ll R$, then

$$D_1 \simeq \frac{n^2w^2}{2} \left(\frac{1}{R} - \frac{1}{y_o}\right)$$

$$D_2 \simeq \frac{n^2w^2}{2}\left(\frac{1}{R} + \frac{1}{y_o}\right)$$

A "total" displacement error can therefore be measured for each line.

$$T_n = D_1 + D_2 = \frac{n^2w^2}{R}$$

Such a parameter is important when the Multiscan is used to measure cross sectional dimensions. The fractional error in estimating the range dimension of the cylinder is

$$E_n = \frac{\text{True dimension - Image dimension}}{\text{True dimension}}$$

$$= 1 - \left(1 - \frac{n^2w^2}{R^2}\right)^{-\frac{1}{2}}$$

$$\simeq -\frac{n^2w^2}{2R^2} = \frac{T_n}{2R}$$

The approximate fractional error is estimating the cross sectional area is given as

$$\text{Area Error} = \sum_n E_n = \frac{1}{2}\,\frac{w^2}{R^2}\,\sum_1^N n^2$$

where n is determined by the number of elements contributing to the distorted image, which depends upon the way in which the sound field intensity falls off with angle. Thus N is dependent on the sound pressure profile and the MDL. Table 3.5 summarises the calculated displacements of echoes from a 3 cm radius cylinder and the estimated fractional errors in Area for various values of N. The predicted image is shown in Figure 3.38 with an actual image of a perspex cylinder at high gain in which this distortion is very obvious.

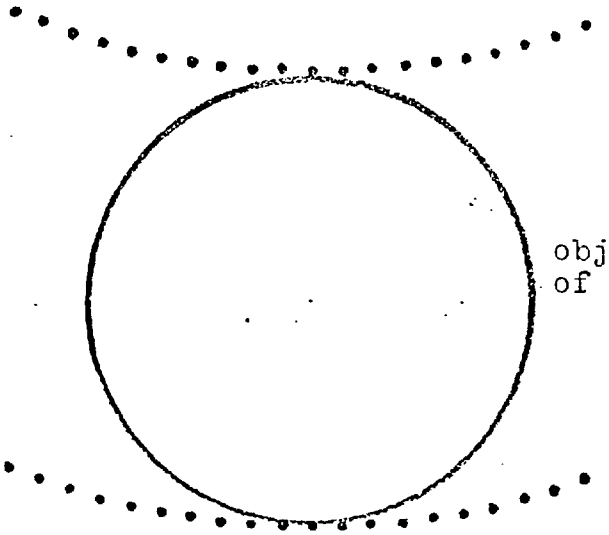
Table 3.5

Errors calculated for the distorted Multiscan image of a circular cross section (Figure 3.38) assuming the display contains only those echoes produced by normal reflections.

Element no., n	D_1 (cm)	D_2 (cm)	$\|D_1\| + \|D_2\|$ (cm)	E_n	Area Error, $\sum E_n$
1	-.020	.034	.054	.009	.009
2	-.078	.140	.218	.038	.047
3	-.180	.322	.502	.091	.138
4	-.335	.589	.924	.182	.320
5	-.566	.962	1.528	.342	.662
6	-.917	1.483	2.400	.667	1.329
7	-1.539	2.307	3.846	1.783	3.112

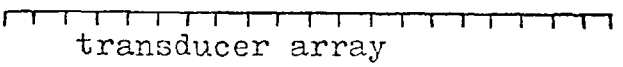
These errors were calculated for a 3 cm radius cylinder whose anterior surface was 7 cm from the element array.

Fig. 3.38 Distortions of circles produced by a Multiscan.



object = a circle of radius 3 cms.

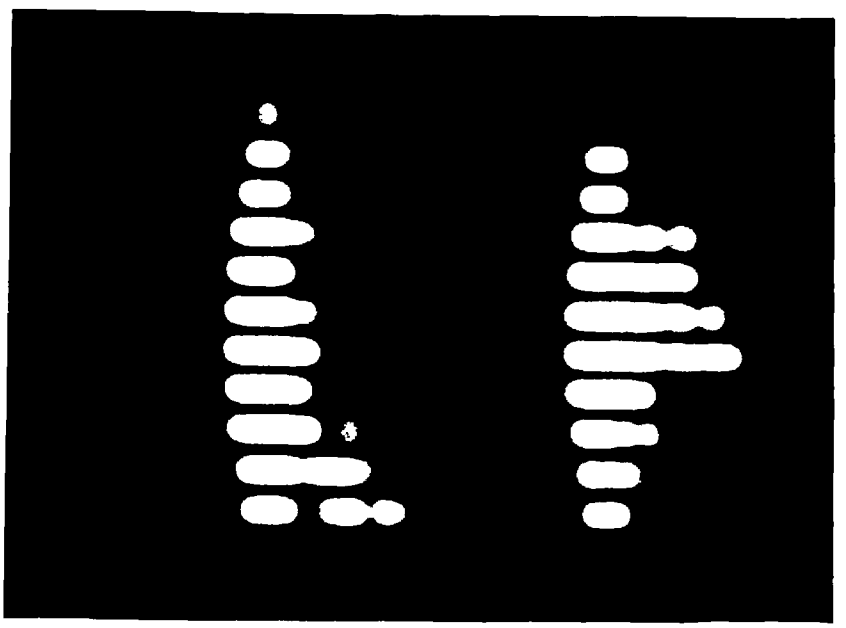
front of circle is 7 cms from transducer.



transducer array

The echoes produced off axis will be displayed as shown (◦).

ant.



post.

An example of the distortion calculated above is this image of a perspex cylinder.

This analysis has assumed that the echo from the points of the circle that are nearest to the elements is above the MDL of the scanner. Although the relevant sound field intensities fall off as n increases, the cylinder always forms a normally reflecting surface to the beam. When these points do not give strong enough echoes, the distance of the nearest registered interface depends upon the variation of emitted sound across the field and upon the manner in which the reflectivity of the cylinder wall changes with angle. The image will still however show changed curvatures of the circle.

An extreme case of distortion occurs if the sound fields have distinct side lobes or secondary maxima. The echoes are then produced at the points of intersection of the circle with lines that form an angle θ with the element axes where θ is the same for all elements (see Figure 3.39). The point P (x,y) is imaged by the element whose centre C is the point (d,o) as a reflector at P' (x'y') in the image. The image coordinates are related to x and y.

$$y = y' \cos \theta$$

$$x = x' - y' \sin \theta$$

The equation of the circle is

$$x^2 + (y - y_o)^2 = R^2$$

and the locus of points in the image is therefore

$$(x' - y' \sin \theta)^2 + (y' \cos \theta - y_o)^2 = R^2$$

The coordinates (x', y') may be transformed into new coordinates (X, Y), by rotation of the axes by $\frac{\pi}{4}$ and by shifting the origin by y_o. This gives the locus as

$$\frac{X^2}{R^2/(1-\sin\theta)} + \frac{Y^2}{R^2/(1+\sin\theta)} = 1$$

(where $x' = \frac{(X - Y)}{2}$, $y' = \frac{(X + Y)}{2}$)

This is the equation of an ellipse whose eccentricity e is given from

$$e^2 = \frac{2 \sin\theta}{1 + \sin\theta} \quad (\simeq 2\theta \text{ for small } \theta)$$

Thus, if artefactual echoes are produced by regions of the sound fields that are at the same angle θ to each of the element axes, then a true ellipse is superimposed on the image of the circle at 45° to the transducer. In general, however, the image is not a true ellipse.

The exact nature of the distortion depends on

(a) the shape of the object, whose curvature determines the lateral extent of the area that can give favourable reflections towards an element.

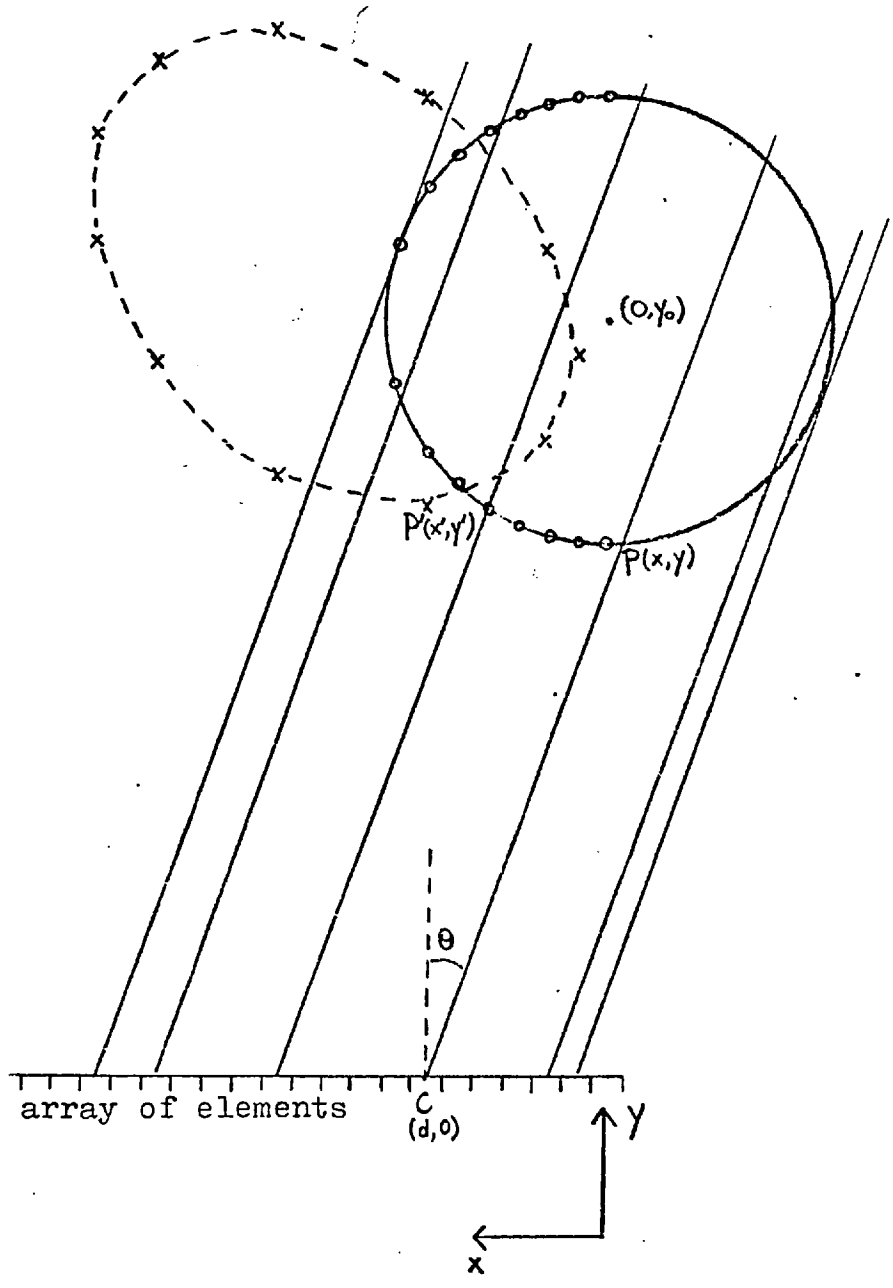
(b) the nature of the object surface, particularly the manner in which the echo amplitude changes with angle.

(c) the divergence and lateral profile of the emitted beams.

(d) the MDL of the receiver.

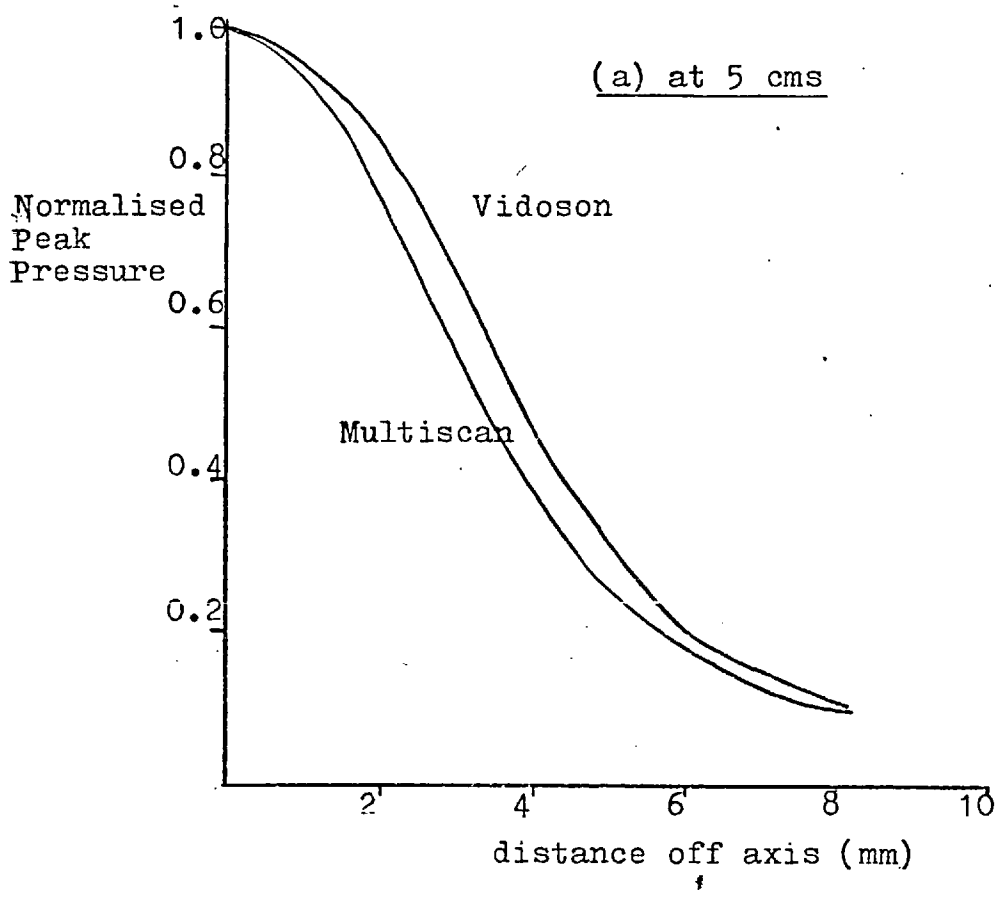
Multiscan distortions are caused when echoes that are produced from off the element axis are placed on the line of the axis and at the wrong range. The important feature of the scanner which determines the nature of the distortion is the effective beam width. However, the Multiscan is simply a special case of a B scanner that moves in a straight line, and therefore any linear scan may produce similar distortions

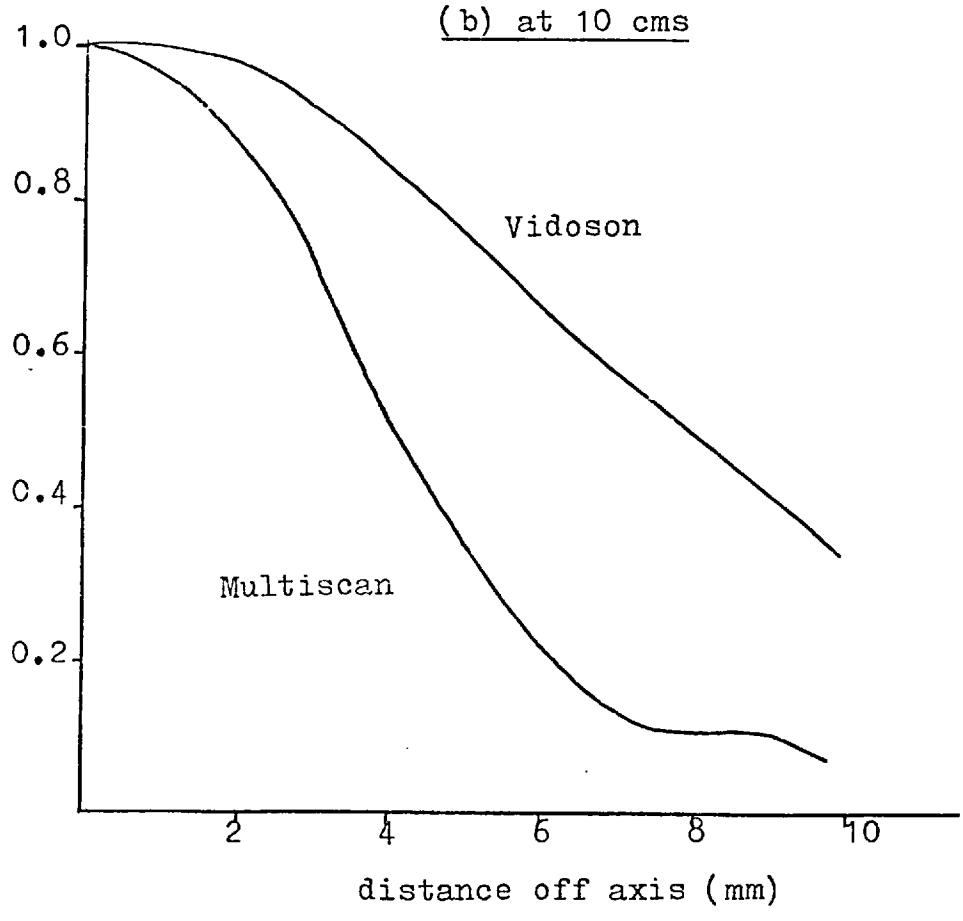
Fig.3.39 Construction of an ellipse in the image of a circle by side lobes.



The echoes produced at the points denoted ○ correspond to the true image of the circle, whereas those denoted × correspond to artefacts produced by the side lobes at angle θ to the axis of each element.

Fig. 3.40 Comparison of Emitted Pressure Profiles from Multiscan with Siemens Vidoson.





on circular objects when the EBW is large. In particular, the mechanically swept line scanner, the Siemens Vidoson, produces similar distortions of curved surfaces. The Vidoson produces an identical mode of scanning to the Multiscan, except that it moves a single beam mechanically in a line, and Figure 3.40 shows a comparison of the normalised beam profiles of these devices, from which it can be deduced that the resolution and distortions of the Vidoson are significantly worse than those of the Multiscan. The relatively small beamwidths of conventional scanners means that such distortions are not usually apparent.

Conclusions

In the study of both the Diasonograph and the Multiscan, the difficulty of defining and measuring resolution has been demonstrated. In both systems, the intuitive concept of the ability to separate two interfaces has been shown to be an inadequate criterion. This ability is not an inherent property of the scanner but it depends on various settings of the scanner controls, on the object and on the medium. It is directly related to the Effective Beam Width for any class of objects but the EBW is itself determined by the object and the Minimum Display Level of the scanner.

The Multiscan studies have also illustrated the relationship between positional uncertainty and resolution and between distortions and beamwidth, and a proper specification of one of these may well suffice to describe the rest.

Chapter 4: The Resolution of Ultrasonic A-scanners

4.1 Introduction

The methods of measuring resolution described in the last chapter were designed to enable routine comparisons and checks to be carried out on equipments. The grid of wires has found widespread acceptance as a method of assessing resolution particularly since its adoption by the American Institute of Ultrasound in Medicine as a standard test object. Measurements of the separation of interfaces, and of beam-width and pulse length, continue to be used to specify resolution even though it has been shown that they depend on arbitrary criteria or subjective decisions. The principal objections against such methods are summarised below.

It was demonstrated in Chapter 3 that pulse length and beamwidth may be measured in various ways. The relative capabilities of two scanners may vary considerably with the particular method adopted, so that assessments of resolution that are based upon single measurements of beamwidth or pulse length cannot completely describe resolution. Measurements of resolution which involve phantoms such as the wire grid measure a performance characteristic that depends on several variables in the total system, including the object and medium. The phantom and the conditions for its use must be specified exactly. In particular, the size and material of the wires of such a phantom must be specified since these determine the strengths of the echoes returned from the wires; the echo strengths should show a known relationship to those system

variables which have been demonstrated to affect the resolution i.e. to transmitted power, receiver sensitivity and threshold detection level. Thus, the use of the wire phantom for measuring resolution requires a specification of 'standard operating conditions' which may not always be objectively quantified (particularly detection threshold levels which involve the observer's perception of the display). The choice of these standard conditions may be made to simulate realistic (i.e. tissue-like) echoes, but the number of combinations of possible conditions is very large and no one is more relevant than any other. Having obtained a measure of resolution under specified conditions, it is not then possible to predict the performance under changed conditions, whether the change is due to alterations in system settings or in the type of object to be imaged. This underlines the inability of single, or indeed several, phantom measurements to indicate the scanner performance for an arbitrary object. It is not possible tc predict quantitatively the influence of changes in the overall system, nor is it possible to re-compose the information obtained from phantom measurements to describe quantitatively the images of other objects. This is a severe limitation when the object of interest bears no apparent similarity to the phantom grid; tissue interfaces do not look like wires in a test grid and no theoretical connection has been attempted between analytic phantoms and realistic objects.

A satisfactory method of assessing resolution must aim to overcome these objections. It is obviously desirable to measure some property of the scanner which can be objectively determined, independent of measuring method and materials and of the settings of the equipment. Such a property must enable the influences of changes of the conditions of the scanner and of the class of object to be quantitatively predicted, and the most general property would enable the image of any object to be predicted. This ability to predict images (or outputs) from objects (inputs) requires a knowledge of the transfer function which describes the imaging ability of the scanner. The property of interest in comparing scanners may be called the INTRINSIC RESOLUTION: the ACHIEVED RESOLUTION is then the resolving ability of the scanner under specified conditions, which may be better or worse than the intrinsic resolution, but which is predictable from it. Achieved resolution is related to the separability of interfaces determined by phantom measurements but it is only meaningful if all the relevant parameters of the system and the object are specified.

Thus, to adequately evaluate an ultrasound system, it is necessary to determine the intrinsic resolution of the system, and this chapter describes how such a property may be measured and used with an A-scanner. The reward for obtaining such a description will be a proper description of the ultimate limitations of a scanner, a prediction of the effect of design changes (and hence an insight into system design and improvement) and a measure of the influence of various compartments of the overall system.

4.2 Formulation of the Problem

The value of any criterion of resolution is dependent on the relevance of that criterion to the formation of real images. It is therefore essential to begin with a proper description of the image forming process and derive parameters such as resolution from this basic description so that they relate directly to the fundamental process.

Several interpretations of the meaning of resolution are possible and some of these have already been illustrated. It is intuitively understood that resolution describes the ability of a system to separate interfaces. However, resolution phantoms which give a single measurement of separation under fixed conditions only recognise the states 'separated' and 'unseparated'. They require a binary decision and give no measure of the degree of separation of surfaces, which is essentially determined by the contrast in the image between echoes from adjacent interfaces and which is related to the system's ability to image fine detail in an object (since fine detail will only be recorded when the system is able to discriminate the small signal fluctuations produced by structural details of interest). A third interpretation of resolution has been derived in Chapter 3 when considering the Multiscan, where the resolution and positional uncertainty in the display were shown to be related. This interpretation may be extended to the concept of resolution as the area which a point in the object appears to occupy (or which it can be made to occupy) in the image. An example of this is the way in which a needle is 'spread' by the Multiscan onto several lines.

These areas of resolution, the smoothing of detail, and the separation of discrete interfaces are each but single aspects of the overall imaging process, they all comply with our intuitive ideas of resolution, but none can be satisfactorily used by itself as a description of imaging performance.

In defining resolution in terms of some intrinsic ability of the scanner to form an image, it would be convenient if criteria could be derived which would enable scanner performance to be measured from the quality of images. Image quality encompasses a multitude of factors, it is difficult to quantify because quality in its most general sense relies heavily on subjective observer assessments of visual impressions. It may however be objectively described in terms of the deviations of the real image from an ideal image, where the ideal image can be defined for any object.

The formation of an image is an imperfect process in which the scanning system produces a representation of the object which is related to the object but which differs from it. Although in some instances these object-image differences enhance the subjective impression of an image, they cannot in general be considered desirable. An ideal scanner may therefore be defined as a scanner which, in the absence of specific knowledge as to what particular features of an object are useful diagnostically, reproduces the features of an object exactly. This definition of ideal disregards any subjective influences on the interpretation of images, and is the basis for all criteria of system performance derived below. The ideal image (as determined by the ideal system defined here)

may not be the most diagnostically useful image but such considerations need not enter a quantitative analysis of resolution, and are not therefore mentioned below. It will always be assumed that the ideal image is a faithful reproduction of the object. It is then a simple extension of this definition to describe imaging performance criteria in terms of the fidelity of the image compared to the object: poor performance will reveal no correspondence between object and image, ideal performance will reveal an identical correspondence, and in between these extremes will be a degree of correspondence which can be used as a figure of merit of the system.

It has not been necessary so far to consider the behaviour of an ultrasonic scanner in any but the most general terms, and what has been said has been quite generally applicable to all imaging processes. The definitions of ideal image and fidelity of reproduction require no detailed consideration of the imaging process. It is necessary however, before proceeding further, to establish more exactly the nature of the imaging problem and this requires a description of the object in an ultrasonic system.

4.3 Description of the Object

The acoustic properties of human tissue show wide variations. It was mentioned in Chapter 1 that the simplest description of echo formation (based on solving the one dimensional wave equation for plane monochromatic waves in a homogeneous medium) relates the reflected wave to a change in the acoustic impedance of the medium. Echo formation in tissues is complicated by the nature of the medium and by the use of acoustic fields generated by short pulses, and this simple model is not adequate to describe the general situation. Tissues are a complex, three dimensional arrangement of impedances; the impedance of any region may show small fluctuations over small distances and will change drastically at a tissue boundary. The boundaries of tissues do not form smooth, planar surfaces but instead show complex geometries. Several classes of scattering behaviour may be identified depending upon the nature of the surfaces and on the ratio of scattering body size to wavelength.

The echo pattern from a region of tissue may be predicted exactly if the diffraction integral for all the scattering surfaces in the sound field may be solved. The calculation of the secondary, reflected fields is difficult except for simple cases, such as those considered in Chapter 6. For the purpose of image analysis, the tissue may be depicted as a distribution of acoustic impedances: echoes are produced by changes in the acoustic properties of the medium and the effective object (i.e. that which is the input for the ultrasonic imaging system) is related to the spatial derivative of

the impedance field, which is a vector field. This field may be considered as a distribution of echo generators, the precise properties of which vary with the orientation and the nature of the incident sound field (in a more formal description these both modify the diffraction integral). This concept is extended later by the introduction of a mechanism of scattering that quantifies the distribution of echo generators. The echo generators of the derivative field are the object elements from which the ideal image must be constructed. Even without a quantitative analysis of the distribution of echo generators, the imaging problem may be clarified.

When any region of tissue is irradiated, the returned sound consists of the superposition of the echoes from a multitude of scattering centres. By analysing the echo shape, any object may be decomposed into an equivalent set of point scatterers which would produce the same echo. In general, an exact reproduction of the echo may require an infinite number of such point scatterers, but a close approximation may be obtained by considering a finite number of points, and the adequacy of this number will be partly determined by the presence of other system imperfections. A mechanism of scattering is described later which occurs with the sound fields considered here which reduces the equivalent set so that it contains very few points, and this forms the basis of using the point scatterer as the echo generating object element. The distribution of echo generators then becomes the arrangement of the point scatterers of the equivalent set, which depends upon the shapes of the object's boundaries. Where multiple reflections, or secondary fields due to surface wave

energy being radiated at delayed intervals, occur, these disturb the correspondence between the equivalent set of points and the object shape but otherwise the shape fully determines the set distribution. The limitations of this approach may already be deduced for a distributed target (such as a tissue interior) whose scattering behaviour may change with aspect. Scattering centres may disappear and new ones become effective, patterns of multiple reflections and surface waves may change, so that the same target at different aspects has not the same equivalent set. This limitation is further described later.

An ultrasonic scanner displays the variation with position and time of the received signals produced by reflections at these echo generators (changes in the acoustic properties of the medium along the path of the sound beam). The displayed signal at any time is therefore a superposition of contributions from all the echo generators on the surface all points of which are at constant ultrasound travel time from the transducer. The shape of this surface depends on the composition of the propagation medium as well as on the precise spatial and temporal distribution of emitted sound. An A-scan is used to distinguish between such <u>isochronal surfaces</u>, and the ability to make such a distinction is related to the axial (range) resolution. More complex scanning techniques are needed to observe the structure on any isochronal surface: the ability to image detail on an isochronal surface is described by the lateral resolution.

For plane transducers coupled to homogeneous media, the regions of the isochronal surface involved in echo formation approximate closely to planes parallel to the transducer face. The validity of this is considered later but it provides now a simplified model for image analysis. Under these conditions, a C-scan is a map of the echo generators on one isochronal plane ('constant depth scanning') whilst linear, sector and compound B-scans provide various techniques for imaging different sections through many isochronal surfaces.

The use of the distribution of echo generators, or derivative field, to describe the object is particularly valid when considering a scanner mapping a surface and such an object is useful for quantifying that geometrical information which is dependent upon the scanner's resolving ability. However, the mechanism of echo formation involved in surface mapping assumes a macroscopic variation of impedance and therefore does not relate to the small-scale tissue changes which give rise to backscattered small signals and which are depicted by the grey-scaling techniques developed by Kossoff. This discussion is therefore restricted to a consideration of the fidelity with which a scanner maps a surface, but the analysis of tissue interiors is shown to be a related problem in Chapter 7.

The analysis of images produced by pulse-echo systems which is described below relies upon a proper identification of the nature of individual echo generators, particularly for describing the imaging process of a B-scanner. However, the A-scan behaviour can be described now by recourse only to conventional theory.

4.4 Description of the A-scan as a Linear Filter

The formation of an A-scan image may be considered as an imperfect operation which produces a representation of an object on the display; an ideal scanner would produce an ideal image, so the real image is analogous to the output of a system which has as its input the ideal image. Physically, this input 'signal' cannot be monitored in a real sense, as might the real inputs to any component in the A-scanner. However, the concept of the ideal image may be introduced as the effective input signal to the A-scanner which then operates upon the input to produce the output (image).

Since the A-scan image is required to represent isochronal planes, the simplest object to be looked at is a single isochronal plane, which can be well approximated by an infinite, plane reflector normal to the sound beam in a non-absorbing medium. The impedance profile is a step-function along the distance (x) axis and is shown in Figure 4.1. The 'ideal' image for either of the step-functions shown would be an impulse of amplitude

$$\left|\frac{Z_2 - Z_1}{Z_2 + Z_1}\right|,$$

the modulus of the derivative of Z with respect to x, $\left|\frac{dZ}{dx}\right|$.

If $u(x - x_o)$ denotes a unit step function at x_o, then the ideal image would be $\delta(x - x_o)$: in practice, the system produces not an infinitely narrow spike on the display but some finite width function, $g(x)$, (see Figure 4.1). It is the width of this function, essentially a measurement of total system bandwidth which limits the axial resolution.

Figure 4.1 A representation of the A scan

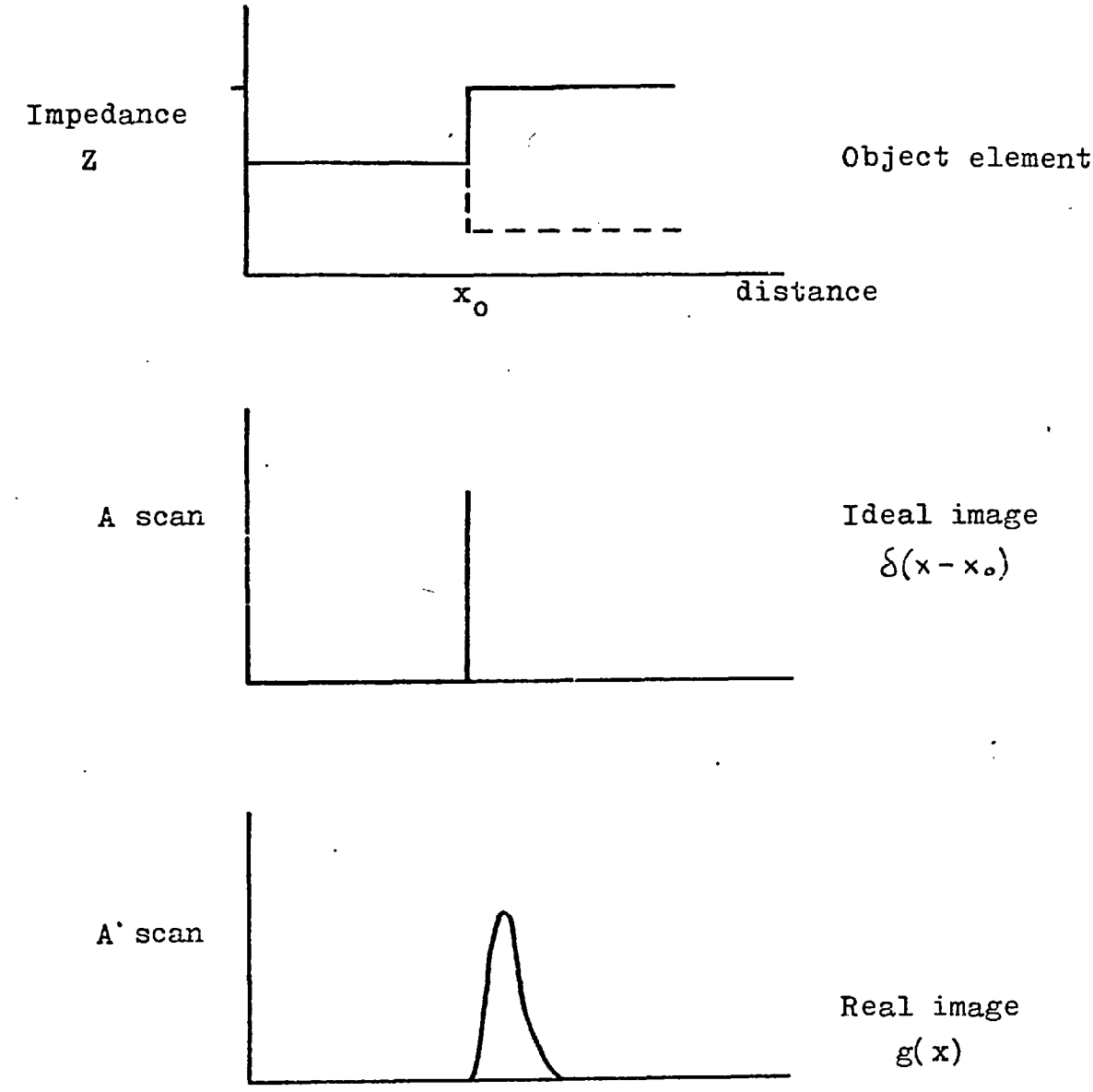
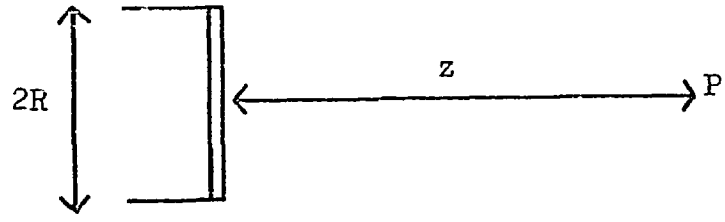


Figure 4.2 Coordinate system of the transducer



The formation of the real image is suggestive of a filtering process, and before proceeding further the principal results of the relevant linear analysis are summarised.

A linear filter associates a response, $g(t)$, with a signal $f(t)$. The correspondence satisfies two properties:

(i) it is linear

i.e. if $f_1(t) \longrightarrow g_1(t)$ and $f_2(t) \longrightarrow g_2(t)$

then $af_1(t) + bf_2(t) \longrightarrow ag_1(t) + bg_2(t)$

(ii) it is shift-invariant (it commutes with translations)

i.e. if $f(t) \longrightarrow g(t)$

then $f(t-t_o) \longrightarrow g(t-t_o)$

These two conditions lead to the requirement that a harmonic input gives a harmonic output at the same frequency.

Thus, if $f(t) = e^{iw_ot} \longrightarrow g(t)$

then linearity requires $e^{iw_ot_o}\, e^{iw_ot} \longrightarrow e^{iw_ot_o} g(t)$

Shift-invariance requires $e^{iw_o(t+t_o)} \longrightarrow g(t+t_o)$

and so $g(t+t_o) = e^{iw_ot_o} g(t)$

This can only be satisfied if $g(t)$ is proportional to e^{iw_ot}. Thus a signal which is harmonic generates a response which is modified only in amplitude and phase, but not in frequency. Any input may be considered as a superposition of elementary sinusoids by a Fourier Transform.

Thus, $f(t) = \int_{-\infty}^{\infty} F(w) e^{iwt} dw$ = the signal

$g(t) = \int_{-\infty}^{\infty} G(w) e^{iwt} dw$ = the response

where $G(w) = F(w).H(w)$ (1)

H(w) is a characteristic operator of the system. The inverse transform of (1) gives a convolution integral: if the inverse transform of H(w) is h(t),

$$g(t) = \int_{-\infty}^{\infty} f(t')\, h(t-t')\, dt' \qquad (2)$$

(denoted as $g(t) = f(t) * h(t)$)

When f(t) is a unit impulse applied at t = 0, then $f(t) = \delta(t)$ and the output g(t) is

$$g(t) = \int_{-\infty}^{\infty} \delta(t-t')h(t')\, dt' = h(t)$$

Thus, the response for a δ- function input is equal to the characteristic operator h(t), which is the transfer function of the filter.

It is apparent therefore that if an ultrasonic A-scanner may be considered as a linear, shift invariant filter then the ideal image, f(t), convolutes with the transfer function, h(t), of the system to produce a display, g(t), and that for an object which is a unit impedance step, the display is equal to the transfer function h(t). The A-scan records times of echo arrival, so that t is really a time. The Fourier Transform introduces a change of domain which physically corresponds to the temporal frequency spectrum of the signal, but this corresponds in the object to spatial frequencies along the axis. Let $k = \frac{w}{c}$ denote spatial frequencies where w = temporal frequency of the A-scan signal and c = velocity of sound.

H(k), the appropriately normalised Fourier Transform of h(ct), measures the response of the system to various spatial frequencies k and therefore describes the ability of the system to image different spatial frequencies in the object.

$$H(k) = \frac{\int_{-\infty}^{\infty} h(x)\ e^{ikx} dx}{\int_{-\infty}^{\infty} h(x)\ dx}$$

which is in general complex.

Let

$$|H(k)| = (H(k)\ H^*(k))^{\frac{1}{2}} = \text{the Impulse Response Function.}$$

H(k) may be determined by calculating the Fourier Transform of the A-scan display from a step impedance object. In general, $|H(k)|$ will decrease as k increases, and it is the manner in which $|H(k)|$ decreases which limits the imaging ability of the system.

Spatial frequency analyses of spatial arrays have proved to be valuable in other imaging fields, including medical scintigraphic and radiological imaging. The spatial frequency bandpass is a limiting factor on performance, and the necessary conditions for its measurement are described below. However, the utility of the analysis relies upon the conditions of linearity and stationarity invoked in the use of the convolution integral and these must first be established.

4.5 Discussion of Linearity and Stationarity

Linearity requires that changes in the amplitude of an impedance step be accompanied by corresponding changes in the amplitude of the A-scan display. For many systems, the linearity condition is easily fulfilled over a wide range of operating conditions. The piezoelectric characteristics of transducers are linear for the small mechanical deformations involved at these acoustic intensities, and properly matched systems will reliably relate voltages to pressure, whilst the behaviour of the amplitude transfer characteristics of the radio frequency amplifiers encountered in commercial systems is well described by a linear region with a well defined saturation level: the response curve for the NE4102 is depicted in Figure 3.9 . The measurement of the intrinsic transfer function should be made in the region where linearity holds. Where non-linear effects are important, such as in receivers which employ compression amplifiers, then the analysis may still be made valid by suitably amending the input or output variables. The general procedure may be described in terms of a succession of operations corresponding to a compartmental model of the imaging system, in which the input or output variables to the intrinsic transfer function are modified to enable linear filter theory to be applied. For example, the non-linearity introduced by a logarithmic amplification stage is removed when the output variable is considered as the antilogarithm of the A-scan display. Correction for known amplitude-transfer non-linearities may be made to produce a truly linear system in which the intrinsic

resolution is rigorously defined. Even when linearity does not hold, useful information is still obtainable from a linear analysis, and even systems which are non-linear by design (such as logarithmic systems) may be considered linear over a limited range of amplitudes. Most commercial systems at present fulfil the linearity condition (for which it is sufficient that input signals of frequency k generate only outputs of frequency k) so that only the harmonics introduced by saturation effects need be considered important. If $h(x)$ is to be shift-invariant then it must be measured as the reflection from a plane in a non-attenuating, non-dispersive medium with no swept gain applied. Shift invariance can be checked by observing the shape of the displayed echo from a plane reflector at different distances, and has been established for the Diasonograph's A-scan. The shapes of pulses reflected from a nylon plane in degassed, distilled water showed little discernible variation with distance. Theoretically, the pulse shape should vary slightly with distance, and whilst a detailed description of the structure of a pulsed acoustic field is not offered until Chapter 5, a simple description of the pulse arriving at points along the transducer axis is relevant here.

Figure 4.2 shows a plane transducer of radius R, and P is a point on the transducer axis at Z from the transducer face. If the transducer is step excited at time $t = 0$ then the first disturbance to reach P arrives at time t_1

$$ct_1 = Z$$

From t_1 on the acoustic disturbance at P is due to an annular

region of the transducer whose radius increases until a time t_2, after which the initial disturbance will have completely passed P.

$$ct_2 = (R^2 + Z^2)^{\frac{1}{2}}$$

During the interval $(t_2 - t_1)$, transient conditions prevail at P and this is the time interval which determines the way in which the emitted pulse varies with distance.

$$t_2 - t_1 \doteq \frac{R^2}{2Zc} \quad (\text{since usually } R^2 \ll Z^2)$$

If $R = n\lambda$, $Z = N\lambda$ then the transient interval is equivalent to $\frac{n^2\lambda}{2N}$ which is of the order of λ or less. Changes in $(t_2 - t_1)$ are therefore of little importance if the pulse emitted contains several wavelengths.

This description indicates that the pulse length on the axis depends on the distance, but the pulse length differences involved are small over most of the region of interest, and the bandwidth of real pulse systems will reduce the significance of such differences further. Thus, this theoretical non-stationarity can be ignored in nearly all cases. However, near regions of strong focus there may be observable changes in the reflected echo shape, although this depends on the receiver bandwidth. We are usually interested in describing the image from interfaces which are close together, and the linear filter analysis requires only that shift invariance exists over the narrow region of separation. The echo shape or amplitude may change slowly along the axis without invalidating the linear approach. The amplitude variation is indeed a slowly varying function for pulsed transducers (except in

some cases near foci and Fresnel zone nodes). The analysis could be made exact by considering the ideal image (and therefore the input variable) to be

$$\delta'(x - x_o) = \frac{\delta(x - x_o)}{p(x_o)}$$

where $p(x_o)$ = an area averaged pressure at distance x_o. This makes $h(x)$ truly shift invariant. The function $p(x_o)$ can be considered as a multiplying factor in the spatial domain so its Fourier spectrum convolutes with the intrinsic transfer function in the frequency domain. However, the description of intrinsic resolution below relies only on the shape of the pulse showing no observable changes over the regions of interest in A-scanning. Should transducers be used which show significant changes in echo shape at different distances, then the analysis must be performed separately for those regions in which the pulse shape is reasonably constant: such a variation would highlight not so much a deficiency in the linear analysis, but more a genuine dependence of axial resolution upon axial distance.

Having established that the conditions for the applicability of the linear filter analysis exist, a simple measurement procedure may be outlined. A plane reflector, perpendicular to the sound beam, is positioned in degassed water (in which attenuation is negligible) and the gain of the receiver or the output power is adjusted to give a large echo which does not saturate the amplifier. For most systems this is sufficient to completely describe the A-scan resolution provided the threshold is at a minimum (i.e. minimal small

signal suppressions) and there is no swept gain. Corrections may be made for amplitude transfer non-linearities which can be measured as described in Chapter 3. The A-scan displays $h(x)$ (which for these conditions is denoted $h_o(x)$, the Intrinsic Transfer Function). Fourier transformation of this gives $H_o(k)$, the Intrinsic Impulse Response Function. $H_o(k)$ describes the imaging ability under idealised conditions. In normal use, the conditions are changed so that in real situations of interest the imaging ability is not adequately described by $H_o(k)$. The resolution is then determined both by the intrinsic properties of the A-scan defined here and by external perturbations which may include influences of the nature of the medium, alterations in the system settings and design modifications. Each of these conditions may be described by its own transfer characteristic so that the overall effective transfer function for a given situation is then described in terms of a cascade of mathematical operators which includes the intrinsic properties. The δ-function ideal image is a convenient mathematical device to use as the input to predict overall effective A-scan resolution in real conditions. The usefulness of this kind of analysis is that it enables exact predictions to be made of changes in the resolving ability of the scanner in a variety of situations. Often, however, particularly when considering changes in the design of equipment, it is convenient to use reasonable approximations to $h_o(x)$ which are easy to use analytically in order to obtain an understanding of the importance of any modification, and several examples of this type of analysis are given below.

4.6 Single Index of Resolution

The function $H(k)$ describes the imaging ability for all spatial frequencies and in general it is desirable to know $H(k)$ at all values of k up to the frequencies where it vanishes. Conventional resolution measurements are equivalent to knowing the value of $H(k)$ at a particular k. For example, the value of k such that two pulses are only just separable on the A-scan indicates $|H(k)| \sim 0$. Single measurements of this type are unsatisfactory, but it would be convenient for quantitative comparisons to use a single numerical index of imaging ability. Caution is necessary in the use of such indices since the shape of $H(k)$ may vary from system to system. However, most physically realisable systems possess an IRF which falls away quite smoothly with increasing k, and whose support is bounded so that beyond a frequency k_{max}, $|H(k)| = 0$. For such systems a single index may be carefully chosen and used reasonably safely. Obviously an expression of the average ability of the system over all $k < k_{max}$ involves a measurement of the width of $H(k)$, and there are several measurements of width that may be used.

A straightforward measurement of width would be the Full Width at Half Maximum (FWHM), defined by

$$\text{FWHM} = 2k_1, \text{ where } \frac{|H(k_1)|}{|H(o)|} = \frac{1}{2}$$

This width gives no description of the distribution of $H(k)$ over the range of spatial frequencies.

A width which has been found useful for calculations of resolution is the variance or dispersion of $|H(k)|^2$. Other moments of $|H(k)|$ may be taken and the ultimate choice is arbitrary, but this second moment has significant advantages. The resolution R is defined from

$$R^2 = \frac{\int_{-\infty}^{\infty} k^2 \, |H(k)|^2 \, dk}{\int_{-\infty}^{\infty} |H(k)|^2 \, dk}$$

Since $|H(k)|^2$ represents the energy spectral density, then R is the r.m.s. bandwidth, and good resolution corresponds to large R. This width weights high spatial frequencies and therefore attaches significance to the 'tails' of Impulse Response Functions which approach zero slowly. This may lead to anomalous results for an H(k) which falls sharply for small k and is asymptotic to the k axis for high frequencies, but such systems are not of real importance and such behaviour would in any case be detectable by inspection. R^2 as defined above has an important physical interpretation which can be derived from the Bandwidth Principle (or Uncertainty Principle). This states (Champeney 1973) that for a function f(x) whose Fourier Transform is F(k), then

$$\frac{\int_{-\infty}^{\infty} x^2 \, |f(x)|^2 \, dx}{\int_{-\infty}^{\infty} |f(x)|^2 \, dx} \cdot \frac{\int_{-\infty}^{\infty} k^2 \, |F(k)|^2 \, dk}{\int_{-\infty}^{\infty} |F(k)|^2 \, dk} \geqslant \frac{1}{4}$$

This result is considered further in discussing Range Accuracy. The system will smear out details separated by distances of the order of $\frac{1}{R}$ consistent with the Bandwidth Principle inequality. A further significant advantage of this definition of R

is that it can be measured in a straightforward manner from the A-scan without recourse to a Fourier Transform, if $h(x)$ obeys certain conditions.

Since

$$h(x) = \int_{-\infty}^{\infty} H(k)\, e^{-ikx}\, dk$$

then

$$h'(x) = \frac{dh(x)}{dx} = -i \int_{-\infty}^{\infty} kH(k)\, e^{-ikx}\, dk$$

$$h^{*\prime}(x) = +i \int_{-\infty}^{\infty} kH^{*}(k)\, e^{+ikx}\, dk$$

(where * denotes the complex conjugate)

$$\int_{-\infty}^{\infty} h'(x)\, h^{*\prime}(x)\, dx = \iiint_{-\infty}^{\infty} kk_1 H(k) H^{*}(k_1)\, e^{-ix(k-k_1)}\, dk dk_1 dx$$

Since $h(x)$ is real, then

$$\int_{-\infty}^{\infty} (h'(x))^2\, dx = \int_{-\infty}^{\infty} k^2 H(k) H^{*}(k)\, dk$$

However, by Parseval's Theorem (Champeney 1973)

$$\int_{-\infty}^{\infty} |H(k)|^2\, dk = \int_{-\infty}^{\infty} |h(x)|^2\, dx$$

Thus,

$$R^2 = \frac{\int_{-\infty}^{\infty} k^2 |H(k)|^2\, dk}{\int_{-\infty}^{\infty} |H(k)|^2\, dk} = \frac{\int_{-\infty}^{\infty} (h'(x))^2\, dx}{\int_{-\infty}^{\infty} (h(x))^2\, dx}$$

R may be found by measuring only $h(x)$ and its derivative. However, this equation is only valid if $h(x)$ is zero and $h'(x)$ is continuous at $x = 0$. For any realistic $h(x)$ this is not an important limitation but it restricts the number of functions that may be chosen as approximations to $h(x)$.

An estimation of R^2 may be obtained if the A scan pulse shape is sampled at constant intervals, Δx , so that $h(x)$ is represented as a series of discrete steps, h_i . Various numerical approximations to the derivative may then be used, the simplest of which produces

$$R^2 = \frac{1}{(\Delta x)^2} \frac{\sum_{i=1}^{n+1} (h_i - h_{i-1})^2}{\sum_{i=1}^{n} h_i^2}$$

where $h_{n+1} = h_o = 0$, which is adequate if Δx is small enough.

A discrete Fourier Transform may be used to calculate $H(k)$ completely if $h(x)$ is sampled at a frequency which is twice that of the maximum k of interest. If N such values of h_i are available then a reasonable approximation to $H(k)$ can be obtained using

$$H(k) = (A_k^2 + B_k^2)^{\frac{1}{2}}$$

where

$$A_k = \sum_{i=1}^{N} h_i \cos\left(\frac{2\pi ik}{N}\right)$$

$$B_k = \sum_{i=1}^{N} h_i \sin\left(\frac{2\pi ik}{N}\right)$$

Discrete transforms may contain some error introduced by the finite size of the sample interval and by truncation of the transform but they are especially useful where computing facilities are readily available. Fast Fourier Transform programmes are commonly available (e.g. HARM in IBM's catalogue) but are not essential if computing time is not critical and the numbers of data points small.

4.7 Approximations for Real Transfer Functions

Before attempting to utilise the Impulse Response Function to describe the resolution under non ideal conditions, some experimentally measured transfer functions are considered here in order to be able to use realistic analytical approximations later. In Figure 4.3 are shown the echoes from plane sheets for three transducers (from the NE4102 Diasonograph). Since the emitted sound pulse from a transducer is the damped transient response of an elastic mechanical vibrator, it is reasonable to attempt to approximate the emitted pulse by a damped exponential.

If $h(x) = e^{-\alpha x}$ for $x > 0$

$= 0$ for $x < 0$

then $H(k) = \frac{1}{ik-\alpha}$ and $|H(k)|^2 = \frac{1}{\alpha^2+k^2}$

The discontinuity at the origin prevents the calculation of R but the HWHM is $3^{\frac{1}{2}}\alpha$. Figure 4.4 shows a plot of log $h(x)$ against x for pulses measured from the Diasonograph: the approximation is reasonable except for small x.

A more realistic approximation is obtained by considering the transducer action in transmission and reception. If the impulse response in both directions is an exponentially damped ringing then the resultant signal at the receiver from a plane reflector will be a convolution of two exponentials.

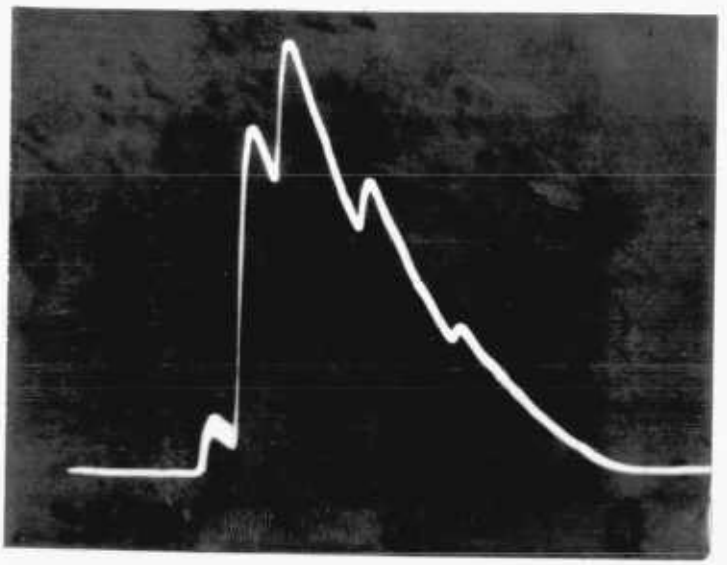
Let the impulse response of the transducer in transmission

$= ae^{-\alpha x}$ $(x > 0)$

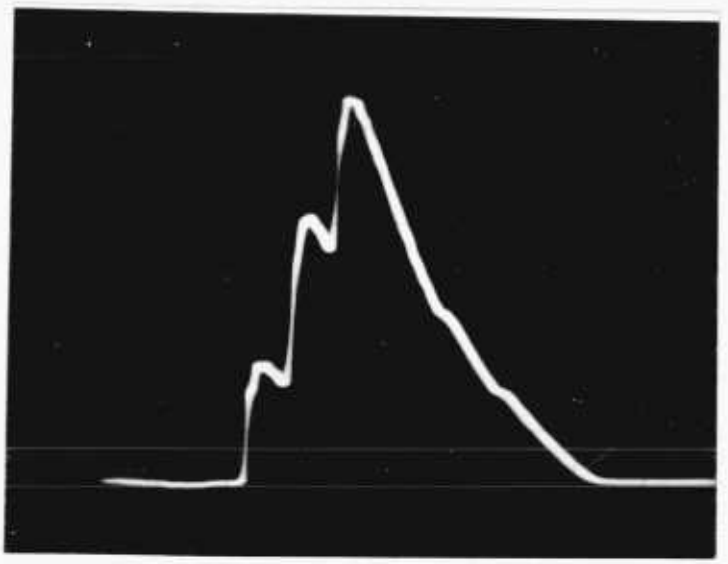
and the impulse response in reception

$= be^{-\beta x}$.

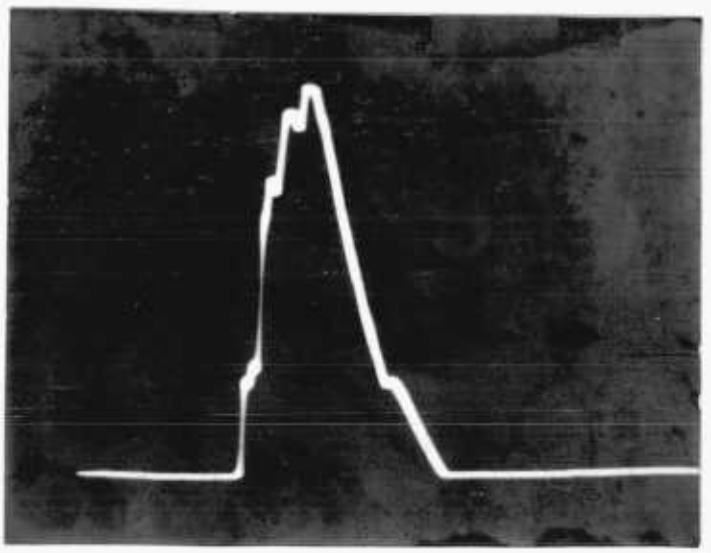
Figure 4.3 A scan representations of echoes from a plane reflector in a water bath obtained with the NE4102 and three transducers of frequency 1.5, 2.5, 5.0 MHz .



1.5 MHz
x 10 scale



2.5 MHz
x 20 scale



5.0 MHz
x 20 scale

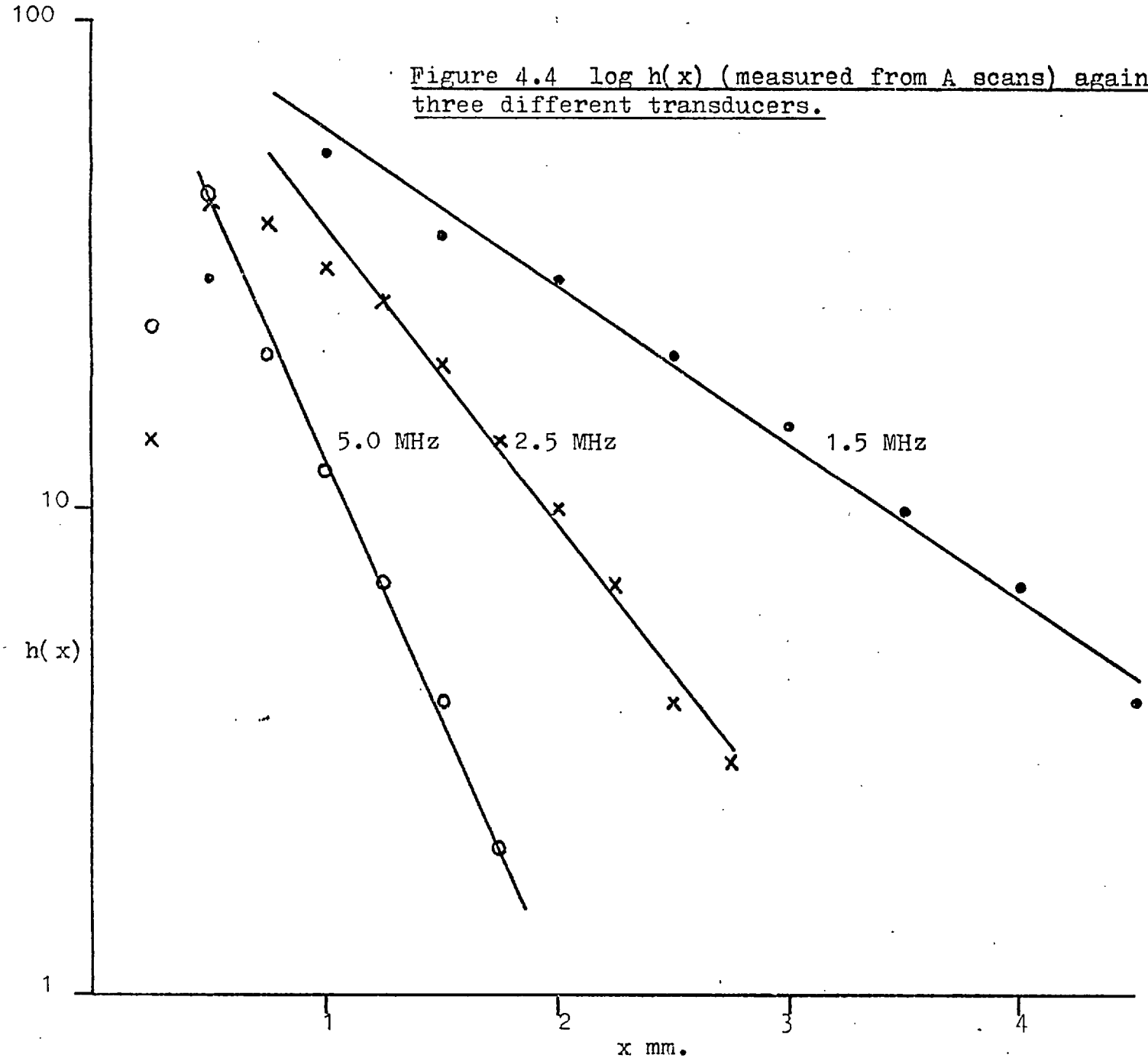


Figure 4.4 log h(x) (measured from A scans) against x for three different transducers.

The overall impulse response will be

$$h(x) = ae^{-\alpha x} * be^{-\beta x} \qquad \text{for } x > 0$$

$$= abe^{-\beta x} \int_0^x e^{(\beta-\alpha)u} du$$

$$\therefore \quad h(x) = ab \frac{(e^{-\alpha x} - e^{-\beta x})}{(\beta - \alpha)}$$

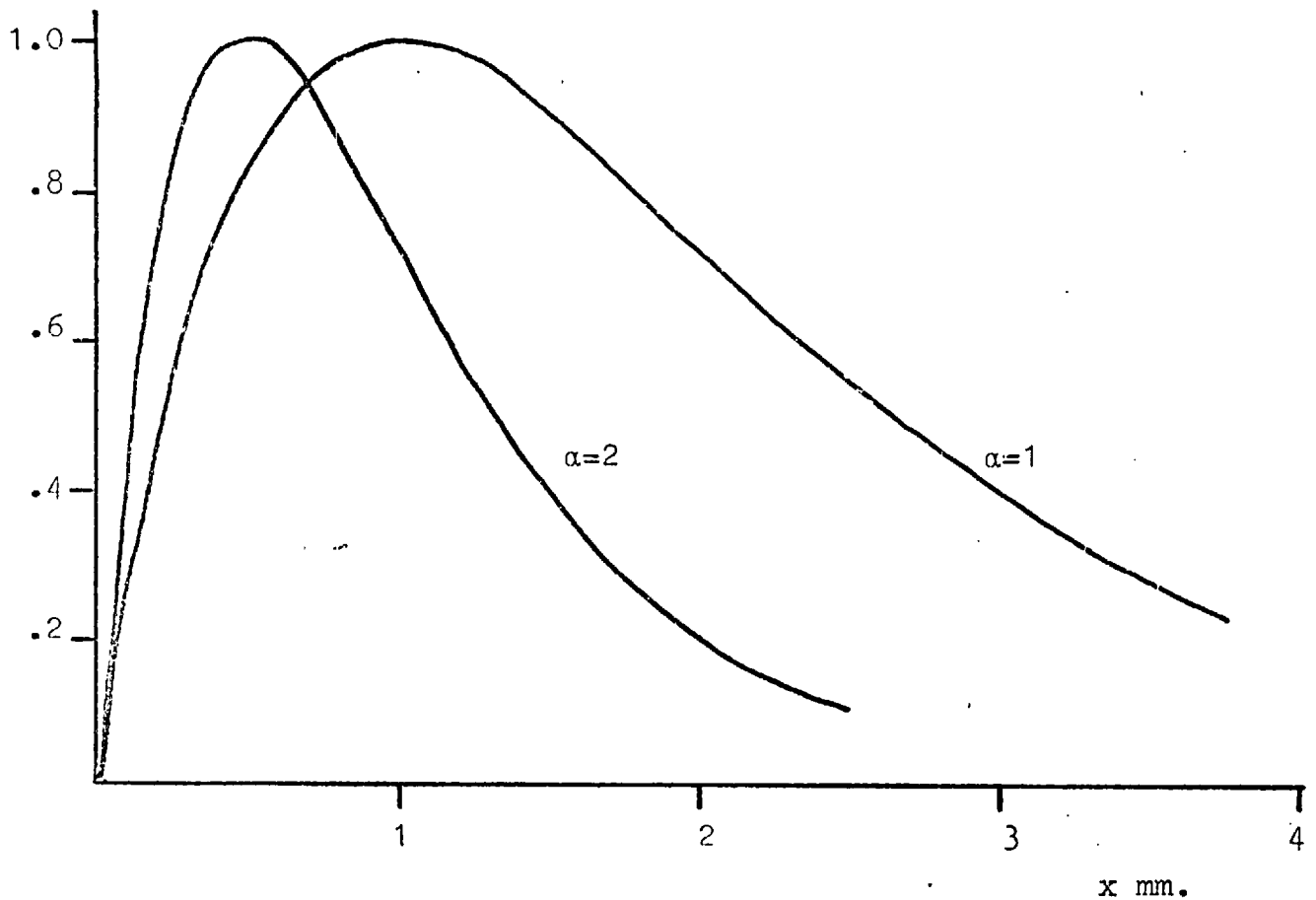
If $\alpha = \beta$, then $\beta - \alpha \longrightarrow 0$

$$h(x) = \lim_{\beta-\alpha \to 0} ab \frac{(e^{-\alpha x} - e^{-\beta x})}{(\beta - \alpha)}$$

$$\therefore \quad h(x) = ab. - \frac{\partial}{\partial \alpha} (e^{-\alpha x}) = abxe^{-\alpha x}$$

Thus, an approximation of the form $h(x) = Axe^{-\alpha x}$ is suggested by considering the physics of transducer action, and an example of such a function is shown in Figure 4.5. Figures 4.6 and 4.7 show a comparison of experimental data (from measurements of the 4102 A-scan) with approximations of this form. The function $\log \frac{h(x)}{x}$ is plotted against x and the fit is obviously good except near the peak of $h(x)$. Damping constants (α) can be measured from such curves, and values measured in this way were used to calculate the functions that are compared in Figure 4.7 to the measured transfer functions after normalising for equal areas. All values of x are expressed in terms of millimetres of tissue: little error is involved in assuming a sound velocity of 1500 m/sec, so that the units might equally be expressed in units of T, where $T \doteq 2/3\mu$sec.

Figure 4.5 Examples of the function $xe^{-\alpha x}$ for different values of α. This function closely resembles many A scan responses found in practice.



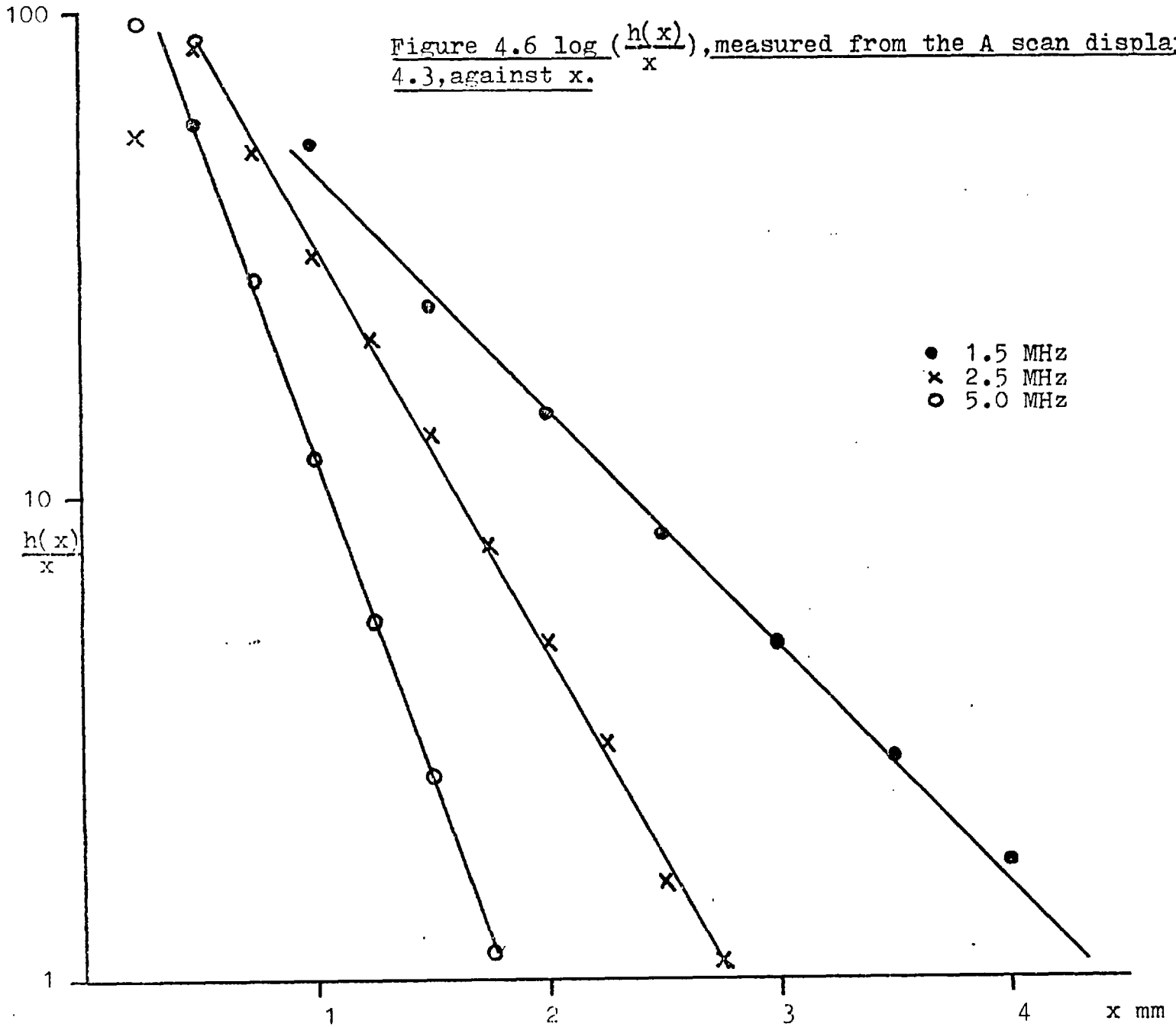


Figure 4.6 log $(\frac{h(x)}{x})$, measured from the A scan displays of Figure 4.3, against x.

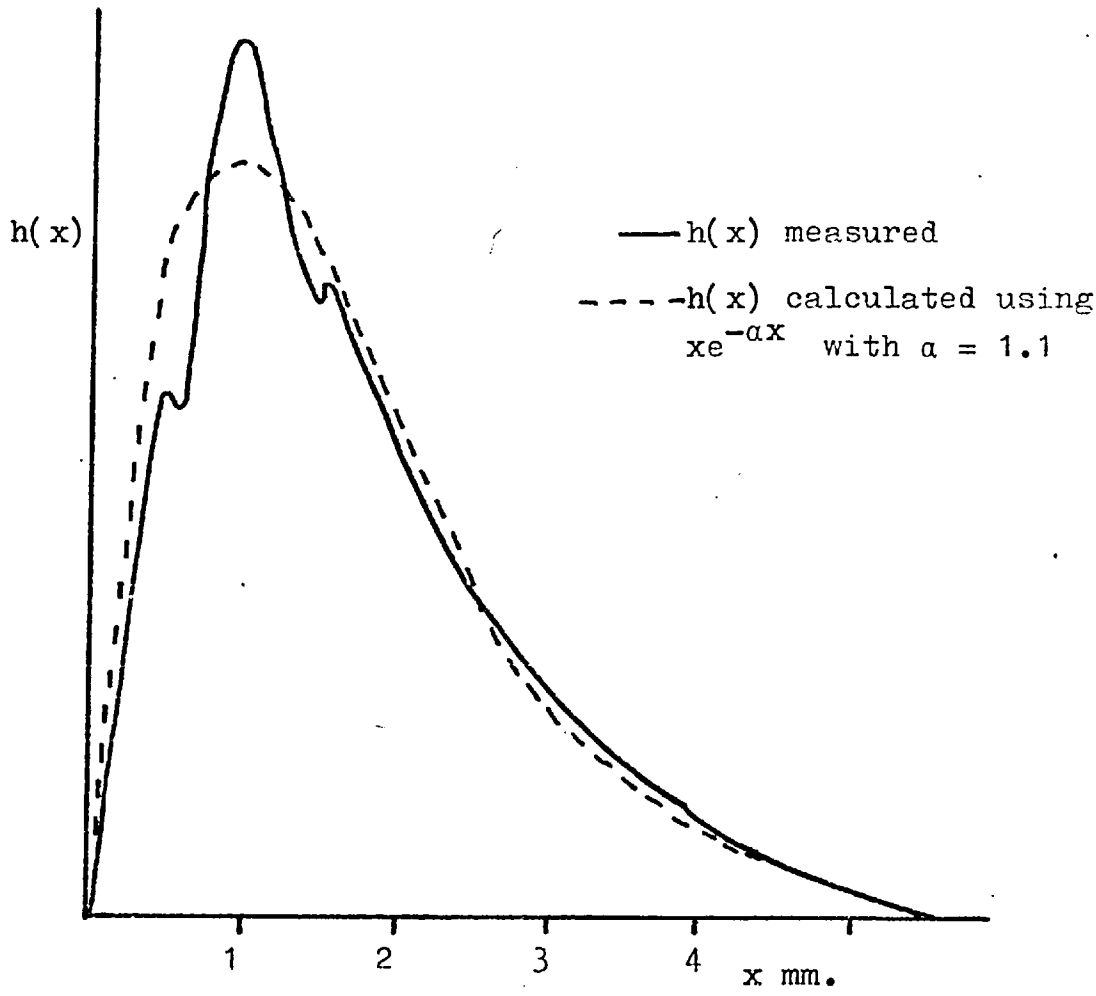


Figure 4.7 A comparison of experimental h(x) with a simple analytical approximation, normalised for equal areas.

Table 4.1
Values of α for three transducers , measured in three ways.

	1.5 MHz	2.5 MHz	5.0 MHz
(a) from slope of plot of log(h) against x.	1.13	1.93	3.12
(b) by measuring from origin to peak	1.11	1.67	2.83
(c) by measuring FWHM of calculated H(k).	1.0	2.2	2.8

The properties of this approximation are as follows.

If $h(x) = xe^{-\alpha x}$ for $x > 0$

$= 0$ for $x < 0$

then $H(k) = \frac{1}{(ik - \alpha)^2}$ and $|H(k)| = \frac{1}{k^2 + \alpha^2}$

The FWHM is 2α.

The resolution defined above is

$$R^2 = \frac{\int_0^\infty (1 - \alpha x)^2 e^{-2\alpha x} dx}{\int_0^\infty x^2 e^{-2\alpha x} dx} = \alpha^2, \text{ so that } R = \alpha$$

The resolution is determined by α, but other definitions of width of $|H(k)|$ may be more complicated functions of α. Furthermore, for systems which show a good fit to $xe^{-\alpha x}$ for small x, since

$$\frac{dh(x)}{dx} = (1 - \alpha x)e^{-\alpha x}$$

then the distance from $x = 0$ to the maximum value of $h(x)$ is simply $\frac{1}{\alpha}$.

Therefore R may be obtained either from the slope of $\log (\frac{h(x)}{x})$ vs x or from the distance from the start of the pulse to its maximum. Table 4.1 shows some results of these measurements for the pulses shown previously. Included are the results of computer calculations using the algorithm given in Section 4.6: $|H(k)|$ computed is shown in Figure 4.8 compared to

$$\frac{1}{k^2 + \alpha^2}.$$

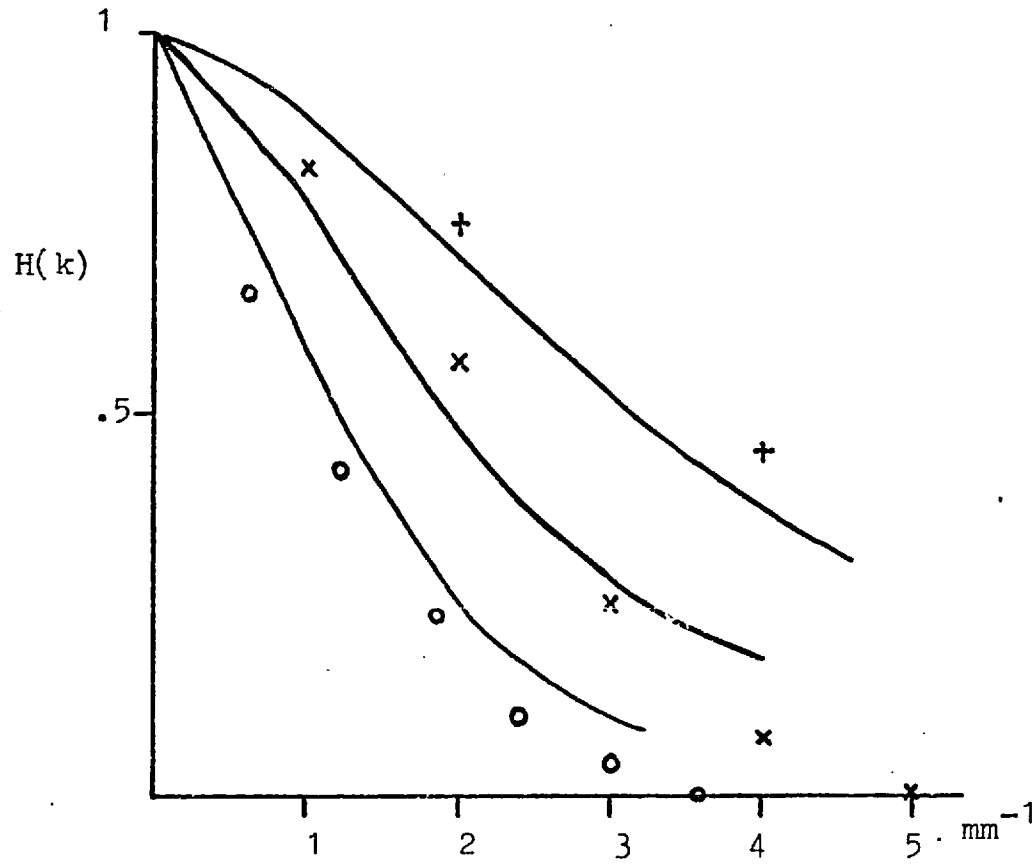


Figure 4.8 A comparison of experimentally determined responses with a simple approximation.
The curves represent the function $a^2(a^2 + k^2)^{-1}$ calculated with the values of a measured from Figure 4.6. The symbols are values of the frequency response calculated by Fourier transformation of the A scan pulses of Figure 4.3
o = 1.5 MHz x = 2.5MHz + = 5.0 MHz.

α is determined by the transducer frequency and damping, and essentially measures a pulse length but this pulse length is defined in terms of the overall spatial frequency response and includes an assessment of the imaging ability for all possible separations of interfaces.

The particular approximation chosen here proved valuable in calculating the effects of changes in the conditions of operating the scanner and gives a realistic expression of the intrinsic transfer function of systems whose principal limitation is transducer bandwidth. The achieved resolution under real conditions can be estimated using this approximation.

4.8 Estimates of Achieved Resolution

The intrinsic transfer properties of the system are denoted by subscript 0. Fourier Transform pairs are denoted by small and capital letters,

e.g. $f(x) = FT^{-1}(F(k))$ will denote effective inputs.

$g(x) = FT^{-1}(G(k))$ will denote outputs or images.

(a) Effect of attenuation or gain

Simple changes in the amplitudes of echoes should not affect resolution but by analysing such changes some of the concepts used later may be introduced. For a plane reflector normal to the axis at x_1 from the transducer, the effective input is $f_1(x)$.

$$f_1(x) = \delta(x - x_1)$$

so that $F_1(k) = e^{ikx_1}$

and $G_1(k) = H_0(k)e^{ikx_1}$

If the medium attenuates the signal then the reflections are reduced in amplitude: similarly, changing the gain of the receiver changes the displayed amplitude. The attenuation effectively multiplies the display by a factor that depends on the distance of the reflector. The input then is $f_2(x)$.

$$f_2(x) = f_1(x)a(x)$$

where $a(x)$ is the amplitude magnification.

The transform of $f_2(x)$ is $F_2(k) = F_1(k) * A(k)$,

where $A(k) = FT(a(x))$.

The object becomes $g_2(x) = f_2(x) * h_0(x)$

so that $G_2(k) = F_2(k)\ H_0(k) = H_0(k)\ \left[F_1(k) * A(k)\right]$

The effective transfer function for the scanner is defined as the function which convolutes with the original ideal object, $\delta(x - x_1)$ to produce the image. This is $h_{EFF}(x)$ defined by

$$g_2(x) = h_{EFF}(x) * f_1(x)$$

so that $G_2(k) = H_{EFF}(k)F_1(k)$

The effect of the amplitude change therefore is considered as a modification of the transfer function of the overall process, as shown in Figure 4.9

$$H_{EFF}(k)F_1(k) = H_o(k)\left[F_1(k) * A(k)\right]$$

When $F_1(k) = e^{ikx_1}$ then

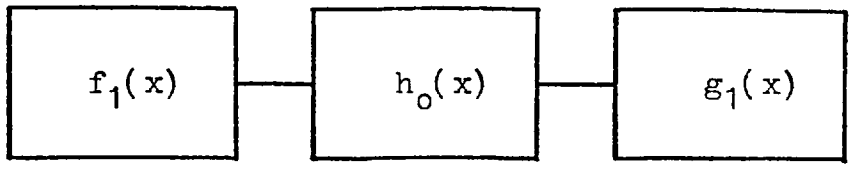
$$F_2(k) = F_1(k) * A(k) = \int_{-\infty}^{\infty} A(k')F_1(k-k')\,dk' = \int_{-\infty}^{\infty} A(k')e^{ix_1(k-k')}\,dk'$$

$$= a(x_1)e^{ikx_1}$$

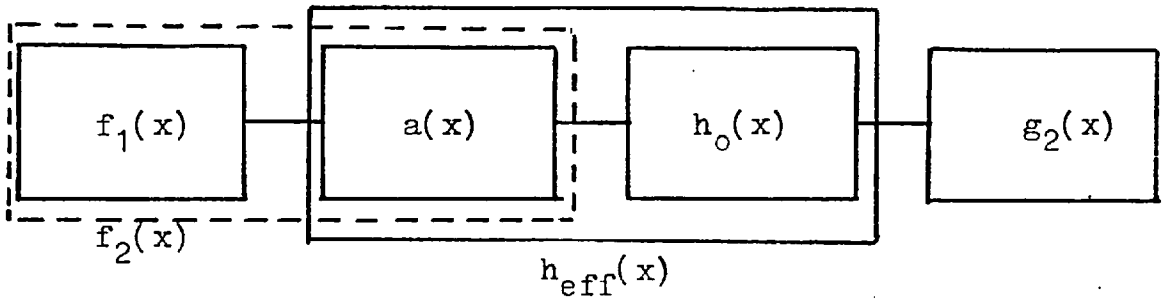
Thus, $G_2(k) = H_o(k)a(x_1)e^{ikx_1} = H_{EFF}(k)e^{ikx_1}$

so that $H_{EFF}(k) = a(x_1)H_o(k)$

$a(x_1)$ is a real constant so the shape and width of the Impulse Response are unchanged. Attenuation and gain applied as a multiplying factor in the spatial domain do not affect resolution. This somewhat obvious result was derived in the above way to introduce the concept of the effective response, H_{EFF}, which measures the achieved resolution under various conditions. It is also useful to distinguish this form of attenuation from those considered below.



(a) Initial state



(b) Modified state

Figure 4.9 Schematic representation of how modification of system (a change in attenuation or amplification) may be incorporated into an effective transfer function. The modified input is really $f_2(x)$ but the change is incorporated into a system function $h_{eff}(x)$ which has f_1 as input.

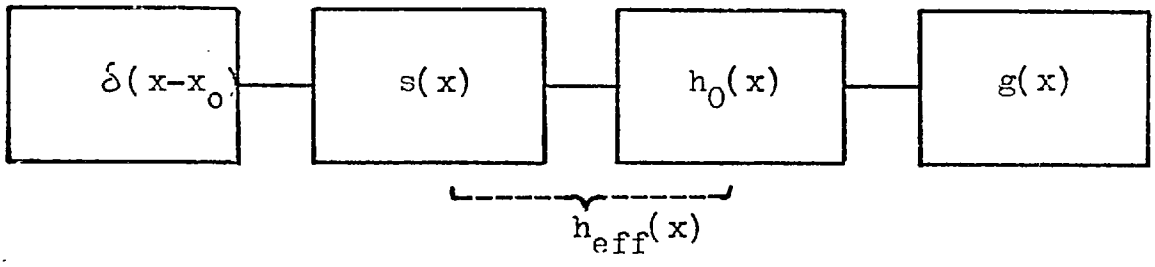


Figure 4.10 Effect of swept gain, $s(x)$

(b) Effect of Frequency Dependent Attenuation

When the attenuation of sound varies with frequency then the spectrum of the A-scan echo changes and the resolution may be affected. The significance of such dispersive attenuation (or similarly, of frequency dependent gain) depends on the signal bandwidth and the nature of the frequency dependence.

Consider a medium in which the attenuation α is a function of frequency so that the acoustic pulse spectrum changes with distance x. If the effective input is again a reflection from distance x_o, then whereas for no attenuation

$$\delta(x - x_o) \longrightarrow e^{ikx_o} H_o(k)$$

with dispersion

$$\delta(x - x_o) \longrightarrow e^{ikx_o} H_o(k) \; e^{-2x_o\alpha(k)}$$

so the effective response is

$$H_{EFFECTIVE}(k) = H_o(k) \; e^{-2x_o\alpha(k)}$$

An exact calculation requires a precise knowledge of the variation, $\alpha(k)$, of attenuation coefficient with frequency. Experimental data on such variations is available (Chivers, 1973), so it is possible to estimate the influence of such attenuation on resolution.

Attenuation mechanisms in biological materials have recently been reviewed by Wells (1975). Tissues may absorb energy from the sound beam by several processes some of which are not well understood. Elastic hysteresis losses are

directly proportional to frequency as the energy loss is constant in any cycle, but when the predominant loss mechanism is due to viscous and thermal effects ('classical absorption') the absorption is dependent on the frequency squared. Relaxation processes show an intermediate dependence on frequency. Here we consider a general case using approximations which are exact for classical or elastic absorption. It is more appropriate here to consider the Fourier spectrum of the radio frequency signal before demodulation, which is the video envelope spectrum shifted by the carrier frequency k_o. The attenuation coefficient can be expanded as a Taylor series about k_o, and most $\alpha(k)$ will possess small derivatives above second order. Thus,

$$\alpha(k) \doteq \alpha_o + \left(\frac{d\alpha}{dk}\right)_{ko} (k - k_o) + \tfrac{1}{2}\left(\frac{d^2\alpha}{dk^2}\right)_{ko} (k - k_o)^2$$

whence

$$H_{EFF}(k) = e^{-Ax_o} H_o(k - k_o)\, e^{-2x_o b(k - k_o + \frac{a}{2b})^2}$$

where

$$A = \frac{4b\alpha_o - a^2}{2b}$$

$$a = \left(\frac{d\alpha}{dk}\right)_{k_o}, \quad b = \tfrac{1}{2}\left(\frac{d^2\alpha}{dk^2}\right)_{k_o}$$

Thus, H_o is modified by a Gaussian term which depends on x_o and $\alpha(k)$. The Impulse Response Function is no longer symmetrical about k_o and the resolution depends on the depth in tissue. Consider the case of classical absorption when a is zero and b is a

constant so that the spectrum is still centred around k_o. In this case, Suppose the half width at $\frac{1}{f}$ of the maximum is k_1

i.e. $H_o(k_1 - k_o) = \frac{1}{f} H_o(0)$

The new half width at the same fraction f of H_o is k_1'. It can be seen that, for any such fraction f,

$$e^{-2xb(k_1' - k_o)^2} \left|H_o(k_1' - k_o)\right| = \left|H_o(k_1 - k_o)\right|$$

Since the Gaussian term is always less than or equal to 1, then this implies that

$$\left|k_1' - k_o\right| < \left|k_1 - k_o\right|$$

Thus, all the widths of the normalised modified Impulse Response Function are less than those of the intrinsic function, so that the resolution is always worse with classical absorption. A particularly illustrative example of the effects of attenuation may be derived by considering a signal which is a radio frequency pulse with Gaussian envelope. In this case,

$$h_o(x - x_o) = A\, e^{\frac{\beta}{2}(x - x_o)^2}\, e^{-ik_o(x - x_o)}$$

The resolution R_o is $(\frac{\beta}{2})^{\frac{1}{2}}$ (from the definition of R above). The Impulse Response is

$$H_o(k - k_o) = A(\frac{2\pi}{\beta})^{\frac{1}{2}}\, e^{-\frac{(k - k_o)^2}{2\beta}}$$

Attenuation produces a response

$$H_{EFF}(k) = B\, e^{-(\frac{1 + 4b\beta x_o}{2\beta})(k - k_o + \frac{2a\beta x_o}{(1 + 4b\beta x_o)})^2}$$

The response is still Gaussian but is now peaked around $k_o - \Delta k$, where

$$\Delta k = \frac{2a\beta x_o}{1 + 4b\beta x_o}$$

The new resolution R_E is related to R_o as

$$\left(\frac{R_E}{R_o}\right)^2 = \frac{1}{1 + 4b\beta x_o}$$

The resolution is degraded to a degree that depends on the relative sizes of b, β and x_o. The length of the Gaussian time domain pulse is determined by the value of $\left(\frac{1 + 4b\beta x_o}{\beta}\right)$, which increases linearly with depth into tissue, and this may produce a serious limitation upon axial resolution in deep tissues.

When the attenuation is caused by elastic hysteresis then b = 0 but a is positive and not necessarily small. For such a medium, the resolution is unaffected by the attenuation, the pulse envelope is unchanged in shape but the carrier frequency is shifted to a lower value.

$$\Delta k = 2a\beta x_o$$

$$R_E = R_o$$

When the expansion of $\alpha(k)$ has only a quadratic term then the absorption is classical and a = 0 but b is positive. For such a medium, there is no shift of dominant frequency, the envelope broadens as the distance x_o increases but the pulse remains symmetrical about k_o.

$$\Delta k = 0$$

$$R_E = R_o(1 + 4b\beta x_o)^{-\frac{1}{2}}$$

It is worthwhile estimating the practical importance of such attenuation in a real situation. The response of the NE4102 is not Gaussian but its shape is not dissimilar in many respects. The width at half height of the 1.5 MHz response considered earlier is 1.9 mm, so that if $h(x) \simeq Ae^{-\beta\frac{x^2}{2}}$ then $\beta \simeq 1.54$. If a reflector lies at a depth of 10 cms in a tissue for which the attenuation is 1 dB/cm/MHz, which is a typical value for many biological materials (Wells, 1969), then x_o = 10cms, and

$b \simeq .006\ mm^{-1}\ MHx^{-2}$. In this case

$R_E \simeq 0.46\ R_o$.

The resolution is approximately halved.

Real materials will probably possess a frequency dependence intermediate between the elastic linear dependence and the classical quadratic. In general therefore the impulse response will be changed in shape and shifted in frequency. Although real pulses are not precisely Gaussian in shape, it is interesting to note that all pulses tend to a Gaussian shape when they travel in a medium in which there is classical absorption. The rela tionship between wave number and frequency is then of the form

$$k = \frac{w}{c} + i\gamma w^2$$

and whereas with no absorption the pressure pulse obeys

$$\frac{\partial p}{\partial x} = \frac{-1}{c}\frac{\partial p}{\partial t} ,$$

for a travelling pulse solution with k as above, p must obey

$$\frac{\partial p}{\partial x} = \frac{-1}{c}\frac{\partial p}{\partial t} + \frac{\gamma\partial^2 p}{\partial t^2}$$ (Landau and Lifshitz, 1970).

If $t - \frac{x}{c} = \tau$, then

$$\frac{\partial p}{\partial x} = \gamma \frac{\partial^2 p}{\partial \tau^2}$$

i.e. with attenuation the wave equation reduces to a diffusion equation. This result is derived and solved by Morse and Feschbach (1953). The general solution is

$$p(x,\tau) = \frac{1}{2(\pi\gamma x)^{\frac{1}{2}}} \int p(0,\tau') \, e^{\frac{-(\tau' - \tau)^2}{4\gamma x}} \, d\tau'$$

in which the Gaussian term is derived from the appropriate Green's function. If

$$B = \int p(0,\tau') \, d\tau'$$

then B represents the area under the pressure pulse envelope. At sufficiently large distances from the transducer

$$p(x,\tau) = \frac{B}{2(\pi\gamma x)^{\frac{1}{2}}} \, e^{\frac{-\tau^2}{4\gamma x}}$$

which is a Gaussian pulse whose amplitude falls off as $x^{-\frac{1}{2}}$ and whose width increases as $(\gamma x)^{\frac{1}{2}}$.

(c) Effect of Time Dependent Gain

In any real system, swept gain is used to compensate for signal amplitude losses (due to attenuation, scattering and beam spreading). With simple gain or attenuation, all parts of each pulse are affected to the same degree, but with swept gain the pulse shape is changed because different parts of each pulse are amplified by different amounts. Swept gain may, however, be considered as a multiplying function that operates after convolution of the ideal image with the intrinsic transfer function of the system. Let $s(x)$ = the swept gain function. The overall system is depicted in Figure 4.10

If the input is $\delta(x - x_o)$, then

$$G(k) = H_{EFF}(k)e^{ikx_o} = \int_{-\infty}^{\infty} S(k - k_1)H_o(k_1)e^{ik_1x_o}\,dk_1$$

For a perfect system, $H_o(k_1)$ = a constant, c, for all k.

Then, $H_{EFF}(k) = c\,e^{-ikx_o}\int_{-\infty}^{\infty} S(k_1)e^{i(k - k_1)x_o}\,dk_1$

$$= c\,s(x_o), \text{ a constant}$$

Thus, a perfect system is not affected by swept gain. However, for a system for which

$$h_o(x) = xe^{-ax} \quad \text{for } x > o,$$

the resolution is degraded. Swept gain also introduces a form of non-stationarity, but this is not important as the variation of $s(x)$ will be relatively slow compared to $h(x)$, and perfect stationarity may be regained by renormalising the image variable in terms of the gain at the start of the pulse such that, for an input of the form

$$f(x) = \delta(x - x_o)$$

the output is considered to be

$$g(x) = \delta(x - x_o) * \frac{(h_o(x)s(x))}{s(x_o)}$$

This is not necessary when the analytic form of $s(x)$ (and therefore the pulse shape) does not change with x. The most useful swept gain to be considered is exponential in form, in which case

$$s(x) = e^{\beta x} \quad (\beta \text{ positive})$$

$$h_{EFF}(x) = xe^{(\beta - \alpha)x} \quad \text{for } x > 0.$$

Therefore, R, the resolution defined above, is now $(\alpha - \beta)$

The fractional decrease in resolution is $\frac{\beta}{\alpha}$, which corresponds to a pulse stretching caused by amplifying the echo tails more than the leading edges. The NE4102 utilises such an exponential swept gain and here the importance of such a gain variation is calculated numerically. The 4102 is calibrated in terms of the gain in dB/cm.

Let $s(x)$ be G dB/cm, corresponding to an exponential gain of form $Ae^{\beta x}$.

$$\beta(x_2 - x_1) = 2.3 \log_{10}\left(\frac{s(x_2)}{s(x_1)}\right)$$

In a distance of 10 mm, then

$$10\beta \cdot \frac{20}{2.3} = 20 \log_{10} \left(\frac{s(x_2)}{s(x_1)}\right) = G \quad \text{dB}$$

The fractional decrease in resolution $= \frac{G}{\alpha} \cdot \frac{2.3}{200}$

The 'worst case' for the 4102 is G = 10 dB/cm and α (for 1.5 MHz) $\doteq 1.13$

when $\frac{\beta}{\alpha} = \frac{2.3}{200} \cdot \frac{10}{1.13} \simeq \frac{1}{10}$

Thus, the Diasonograph swept gain may change the achieved resolution by up to 10 per cent.

(d) Effect of Threshold

In general, $h(x)$ approaches zero more rapidly than any of the approximate functions considered so far. There is always a lower limit on the system sensitivity caused by thresholds of signal detection and display. In practice, thresholds are deliberately introduced and varied to allow small signals to be suppressed (in the NE4102, this is the Suppression: in the Eskoline 20, the Reject control). If the threshold level is T, then the achieved resolution is determined by $h(x)$ where

$$h(x) = h_o(x) - T \qquad \text{for } x_2 \gg x \gg x_1$$

(where $h_o(x_2) = h_o(x_1) = T$)

$$= 0 \qquad \text{elsewhere}$$

Truncation of the transfer function in the x-domain limits the support of $h(x)$ so that its transform in changed in width. Figure 4.11 shows the A scans obtained with the NE4102 for two different threshold levels, whilst Figure 4.12 shows the corresponding frequency responses calculated using the computer programmes described in Section 4.6. Increasing the threshold level improves the resolution. The change caused by a truncation of the transfer function may be estimated. Suppose $h_o(x)$ is cut off at x_1 and x_2 as shown in Figure 4.13. A truncated function and a tail function can be defined

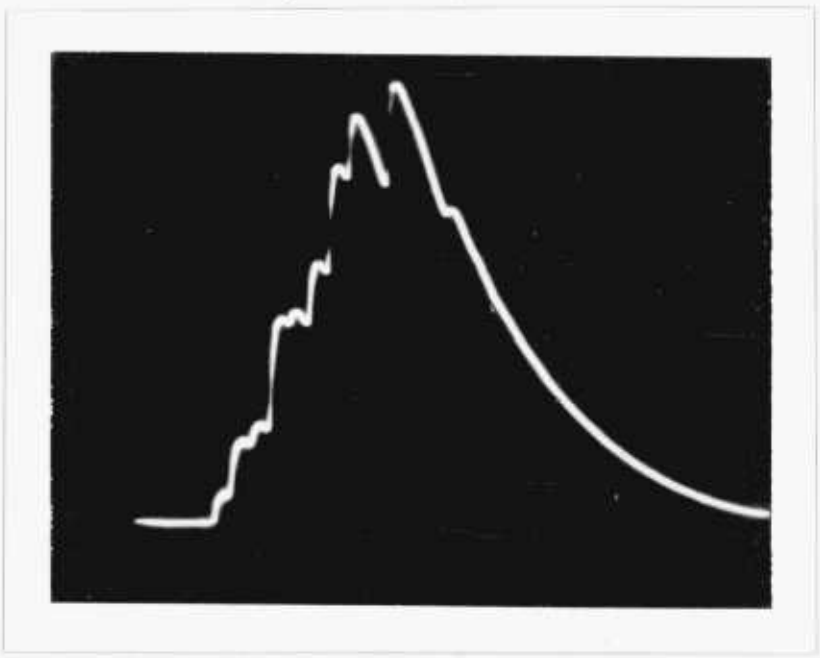
$$h_T(x) = h_o(x) - T \qquad x_1 \ll x \ll x_2$$

$$= 0 \qquad \text{elsewhere}$$

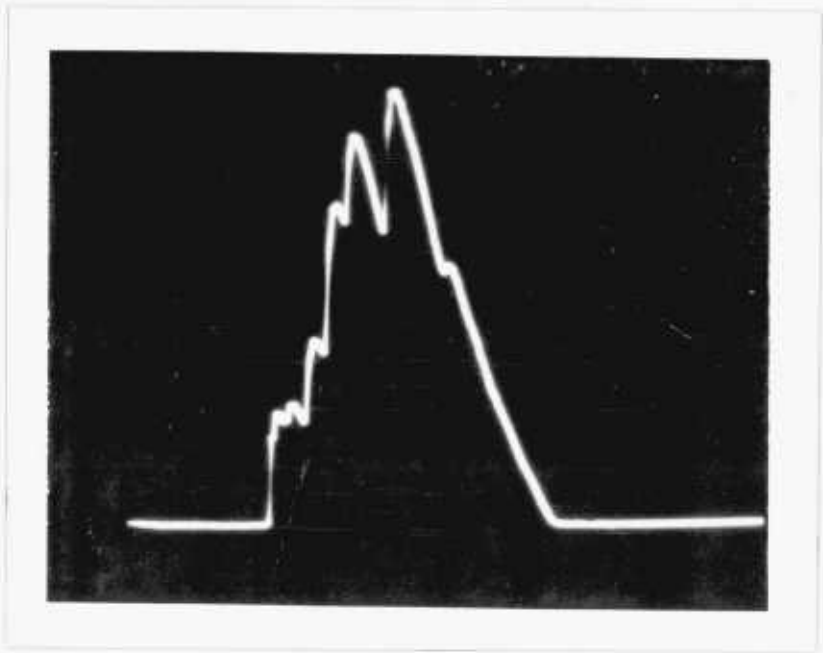
$$h_E(x) = h_o(x) \qquad x_1 \gg x,\ x \gg x_2$$

$$= T \qquad x_1 \ll x \ll x_2$$

Figure 4.11 A scan echoes (a) with minimal suppression and (b) with 10 dB suppression followed by a compensation in amplification.



(a)



(b)

The echo heights are the same but the achieved resolution would be different.

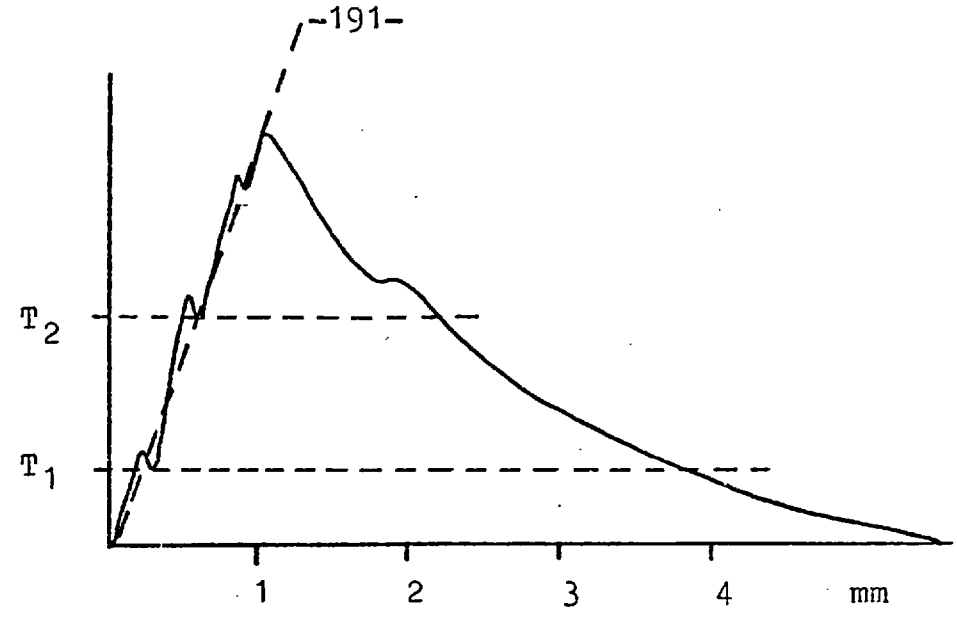


Figure 4.12a A-scan display of pulse that is truncated by increasing the threshold to T_1 and then T_2.

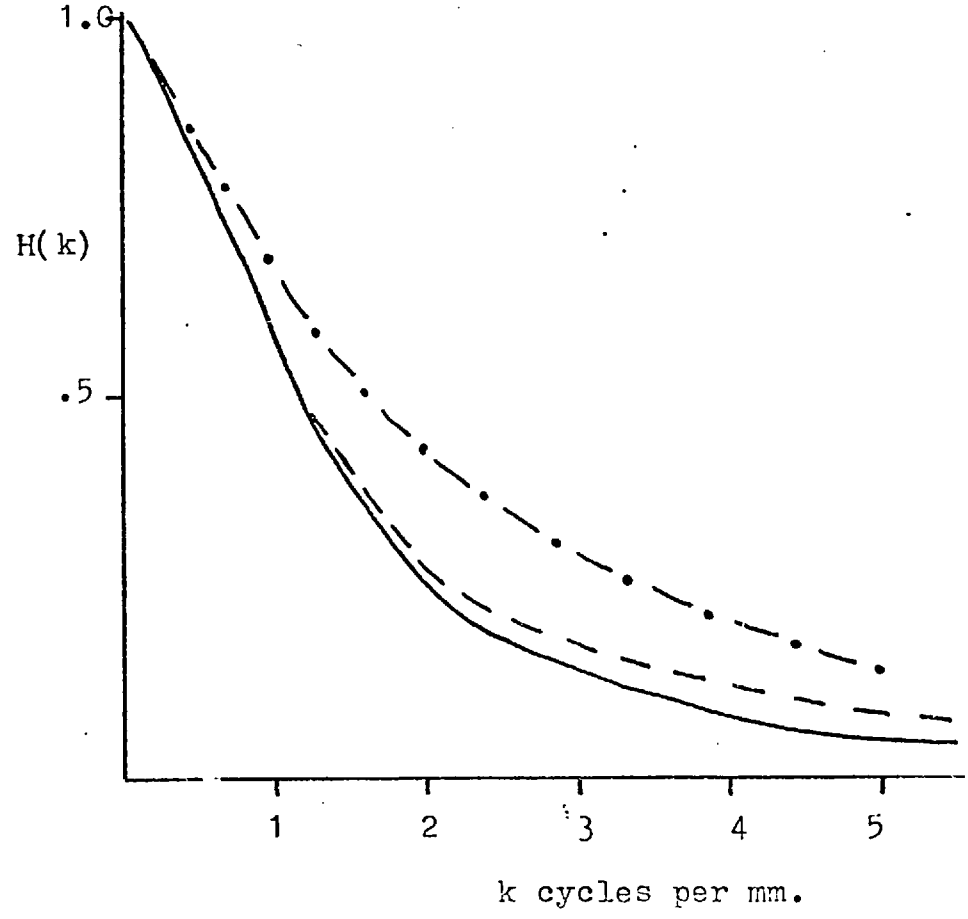


Figure 4.12b Effect of truncation of the time domain pulse on its frequency spectrum.

The A scan pulse was Fourier transformed and normalised to give the full curve. Introduction of a suppression that removed all the pulse below T_1 causes the spectrum to broaden (dashed line) whilst a further increase of threshold to T_2 gives the response shown • — • — •.

The calculated values of the resolution index R for these conditions were 0.9, 1.11, and 1.74 respectively.

Since $h_o(x) = h_T(x) + h_E(x)$

then $H_o(k) = H_T(k) + H_E(k)$

The change in the normalised IRF, ΔH, can be estimated using a method similar to that of Doi et al (1972).

$$\Delta H = \frac{H_T(k)}{H_T(0)} - \frac{H_o(k)}{H_o(0)}$$

$$= \frac{H_E(0)}{H_T(0)} \left[\frac{H_o(k)}{H_o(0)} - \frac{H_E(k)}{H_E(0)} \right]$$

But, $H_E(0) = \int_{-\infty}^{\infty} h_E(x)\, dx$

so $\Delta H = \dfrac{(\text{area of } h_o(x) \text{ under T})}{(\text{area of } h_o(x) \text{ above T})} \cdot \left[\dfrac{H_o(k)}{H_o(0)} - \dfrac{H_E(k)}{H_E(0)} \right]$

As T increases, so $\frac{H_E(k)}{H_E(0)}$ decreases, and the area under T increases. Therefore ΔH increases rapidly with increasing T. An upper bound on ΔH may be estimated since

$$\left| \frac{H_o(k)}{H_o(0)} \right| \leqslant 1, \left| \frac{H_E(k)}{H_E(0)} \right| \leqslant 1$$

then $\Delta H_{ub} \leqslant 2 \dfrac{H_E(0)}{H_T(0)}$

Improvements in the resolution due to threshold changes are dependent on the fractional change in the area under the transfer function introduced by the change.

Figure 4.13 Definition of parameters used to calculate the effect of truncation of pulses on the achieved resolution.

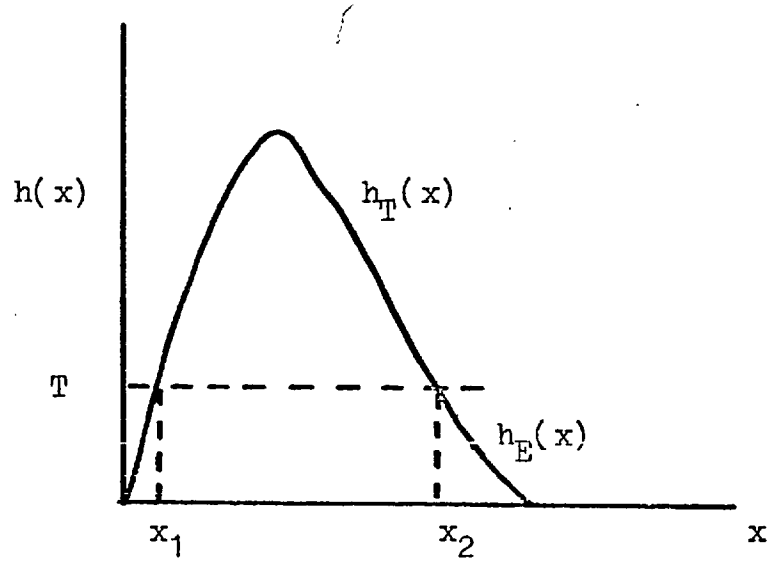
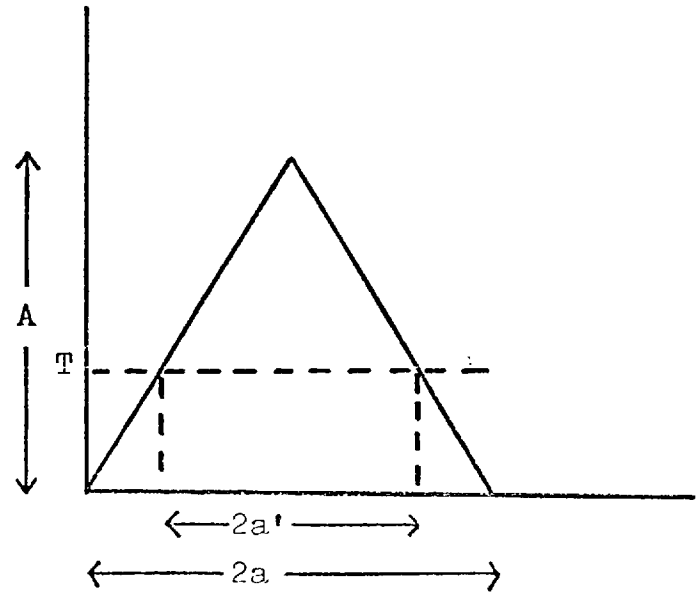


Figure 4.14 Definition of triangular approximation used to illustrate effect of truncation on achieved resolution.



The analysis of the effect of threshold is considerably simplified if h(x) is approximated by an isosceles triangle. Such an approximation preserves the essential features of the transfer function and is particularly easy to use in calculations.

Let $h_o(x) = \frac{A}{a} x \quad$ for $0 < x < a$

$= 2A - \frac{Ax}{a} \quad a < x < 2a$

$= 0$ elsewhere

Then $R^2 = \dfrac{\int_o^a dx}{\int_o^a x^2\, dx} = \dfrac{3}{a^2}$, so $R = \dfrac{3^{\frac{1}{2}}}{a}$

The resolution is independent of the height on the triangle and depends only on the base width, the x domain support. A threshold T changes the support limits, as shown in Figure 4.14. The height is reduced to (A - T), whilst the base is reduced to 2a', where $\frac{A}{A-T} = \frac{a}{a'}$.

The new resolution is therefore

$$R' = \frac{3^{\frac{1}{2}}}{a'} = R\left(\frac{A}{A-T}\right)$$

The fractional improvement in resolution is $\frac{T}{A-T}$ according to this criterion. The effect of threshold should not however be considered in isolation to the effect of amplification. If a gain G is applied before signal suppression then

$$h(x) = Gh_o(x) - T = G\left(h_o(x) - \frac{T}{G}\right)$$

If the amplification is applied after the small signal suppression, then

$$h(x) = G(h_o(x) - T) = G(h_o(x) - \frac{GT}{G})$$

i.e. gain applied before threshold lowers the effective threshold, and the increase in resolution is less marked. Therefore to obtain maximum resolution enhancement by signal suppression, the suppression should be introduced at an early stage of the processing. However, suppressing low level signal decreases the number of echoes displayed and the energy contained in each echo signal. It therefore is most useful for large echoes or with high gain, noiseless amplifiers. Theoretically, if there is no limit to the amplification available then any A-scan may be converted into a sequence of δ-functions of arbitrarily small width. In practice, the usefulness of this processing is limited by the signal energy and noise. In the Diasonograph, the suppressor can remove signals whose amplitude is 1/5 of the A-scan maximum height. Therefore the resolution can be enhanced by up to 25% if the echoes are strong, and even more improvement is obtained with smaller signals.

(e) Effect of differentiation

Several scanners use differentiation to increase their ability to detect small signals. Differentiating circuits are used in the hybrid processing circuits of some 'grey scaling' systems to expand the useful dynamic range of the system, but here only the effect of differentiation on resolution is considered.

If $h_o(x)$ is again taken to be xe^{-ax} for $x > o$, then

$$\frac{dh}{dx} = (1 - ax)e^{-ax}$$

and this function is not zero at $x = 0$, so that R cannot be calculated as before. The achieved imaging ability with differentiation is described by $H_{DIFF}(k)$:

$$H_{DIFF}(k) = ik\, H_o(k),$$

$$|H_{DIFF}(k)| = \frac{k}{a^2 + k^2}$$

The maximum of $|H_{DIFF}|$ is not at $k = 0$: the effect of differentiation is to enhance the higher frequency response which compensates for some of the effects of the narrow bandwidth of the intrinsic response. Quantitatively this is expressed by the multiplication of the intrinsic Impulse Response by a linearly increasing function in the frequency domain. The shapes of the resultant Impulse Response Functions are shown in Figure 4.15. The maximum of $|H_{DIFF}|$ occurs at k_o given by

$$\frac{d|H_{DIFF}|}{dk} = 0 \text{ at } k = k_o$$

i.e. $k_o = a$

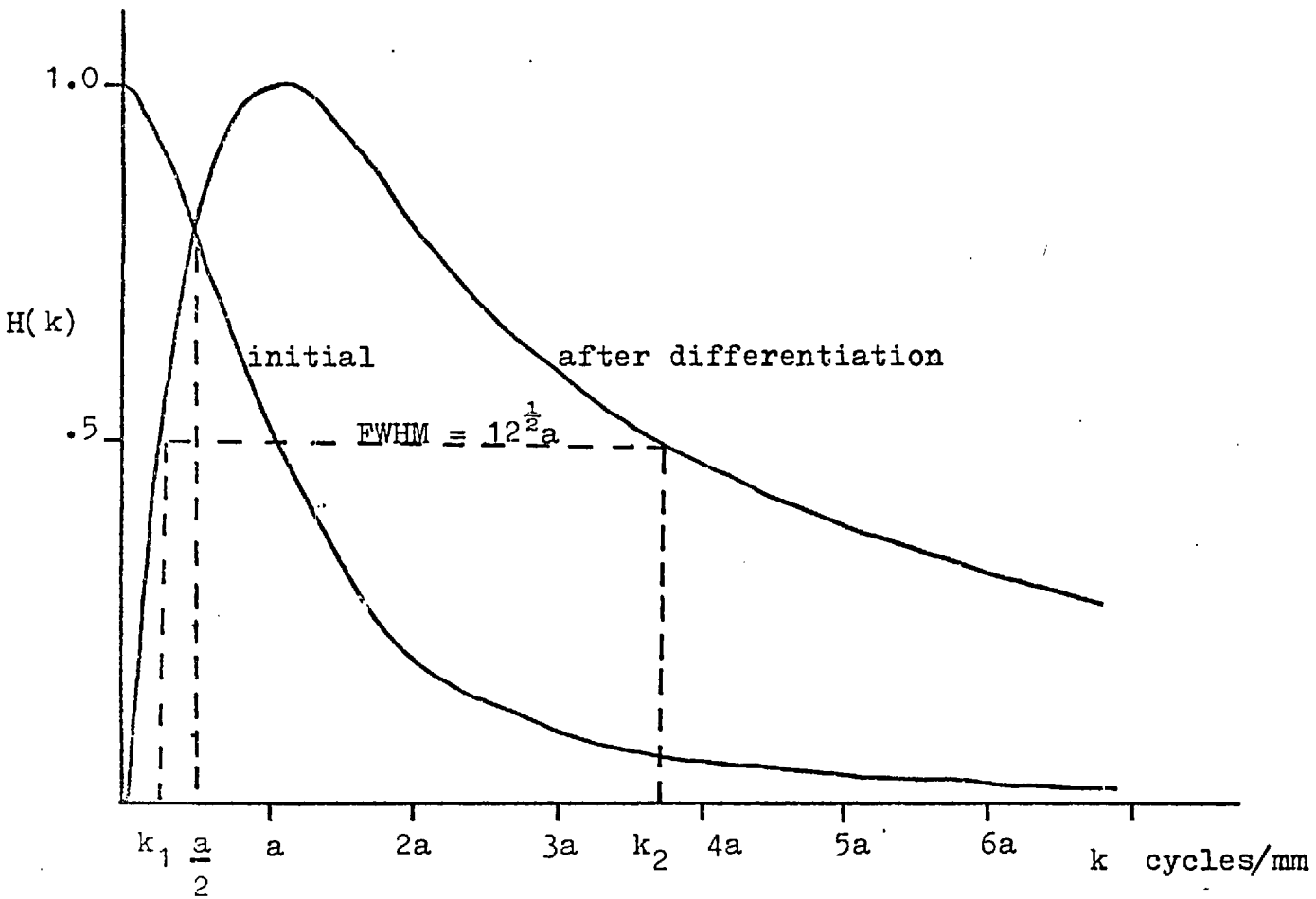
At $k = a$, $|H_{DIFF}| = \frac{1}{2a}$

A measure of the overall resolution enhancement is given by the FWHM, $(k_2 - k_1)$, where k_1 and k_2 satisfy

$$a^2 + k^2 = 4\, ak$$

Figure 4.15 Effect of differentiation on the achieved responses of an A scan.

The curves represent the calculated frequency responses of a scanner whose intrinsic time domain response is xe^{-ax} before and after a differentiation, normalised to the peak response in each case.



$$k_{1,2} = \frac{4a \pm a.12^{\frac{1}{2}}}{2}, \text{ so that FWHM} = 12^{\frac{1}{2}}a$$

For the non differentiated response, the FWHM is 2a. There is therefore an increase in this width by a factor $3^{\frac{1}{2}}$. If the curves are normalised to their maximum values, then the two curves intersect at k given by

$$\frac{|H(k)|}{|H(0)|} = \frac{a^2}{a^2 + k^2} = 2a. \frac{k}{a^2 + k^2}$$

i.e. at $k = \frac{a}{2}$. Beyond $k = \frac{a}{2}$, the scanner response is improved: below $k = \frac{a}{2}$ it is diminished.

It is of interest to consider the hybrid signal processing used by Kossoff and others to obtain good grey-scale echographs. Such a processing adds the normal video signal to the differentiated signal to obtain a waveform which is purported to contain more information. Thus, instead of

$$h_o(x) = xe^{-ax} \quad \text{for } x > 0,$$

the transfer function is of the form

$$h_E(x) = h_o(x) + b. \frac{d\, h_o(x)}{dx}$$

where b is a factor which determines the relative weightings of the two components.

We can define

$$H_E(k) = FT(h_E(x)) = (1 + ikb)H_o(k)$$

so that $|H_E(k)| = (1 + k^2b^2)^{\frac{1}{2}} |H_o(k)|$

For the approximation used earlier, then

$$H_E(k) = \frac{(1 + k^2b^2)^{\frac{1}{2}}}{(a^2 + k^2)}$$

If $bk \ll 1$ then there is no effect from the differentiation, whilst if $bk \gg 1$ ($\frac{1}{b} \rightarrow 0$) then the differentiated component is dominant. Thus, simply by varying b the achieved resolution may be altered and the relative imaging capabilities over a range of frequencies can be modified. The effect of varying b is depicted in Figure 4.16 where $|H_E(k)|$ is calculated for $|H_o(k)| = \frac{1}{k^2 + a^2}$, a = 1, and b is varied from 0 to 1. Kossoff uses a processing in which $b \doteq 0.3$.

The process of differentiation may be considered as a convolution of the intrinsic transfer function with a modifying function. It is possible to produce an equivalent function which has the property that, when convoluted with the intrinsic transfer function, produces the same output as the hybrid processing.

If $(1 + ikb)$ is denoted as $G(k)$, then

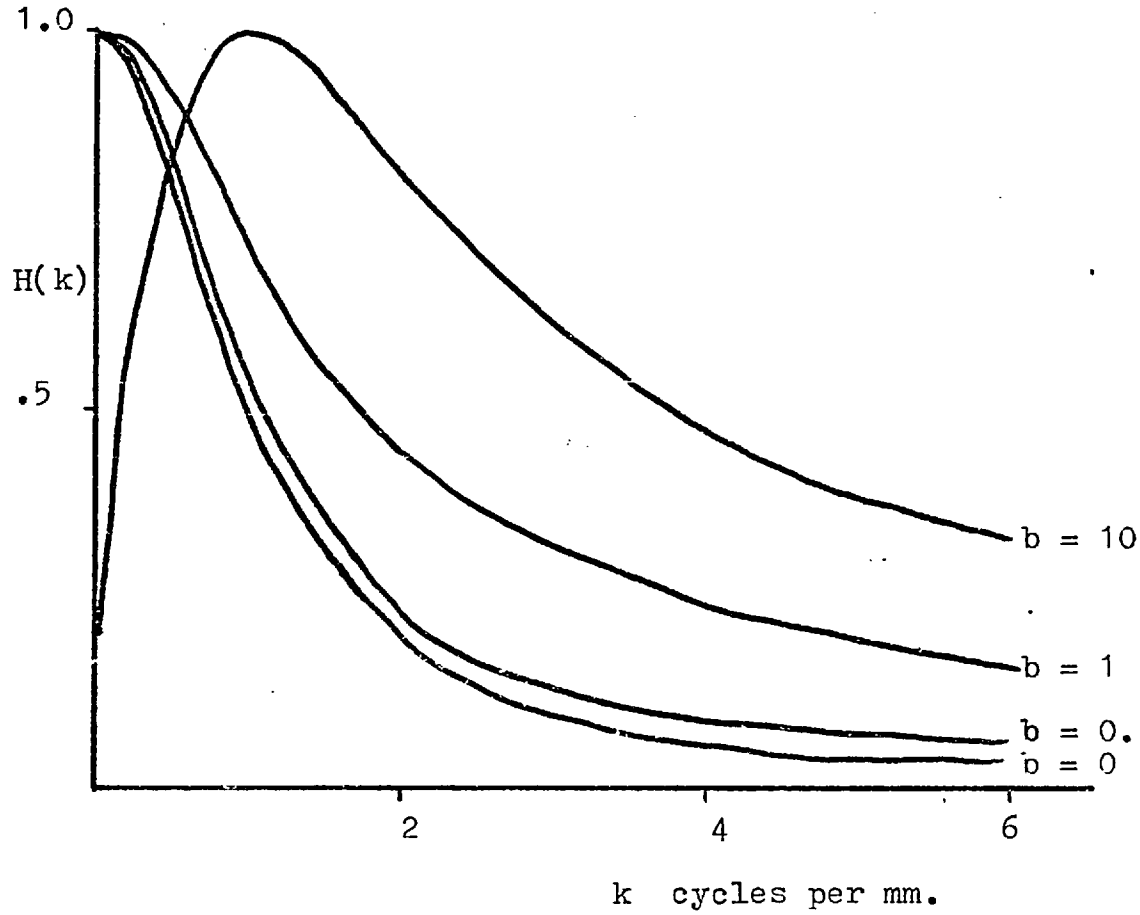
$$H_E(k) = G(k)H_o(k)$$

so that $h_E(x) = g(x) * h_o(x)$

where $g(x) = F.T^{-1}(G(k))$

In practice, $g(x)$ may not exist or may be wholly unrealistic, but some of these difficulties may be circumvented by considering only physically realisable $H_o(k)$. For any real scanner, $H_o(k)$ must be identically zero for all k above a frequency k_{max},

Figure 4.16 Effect of using hybrid (differentiate and add) signal processing on the achieved response of an A scan.



The curves show the calculated frequency responses of a system whose intrinsic time domain response is $x.\exp(-ax)$ which is modified by adding the derivative of the response to the A scan .The curves were calculated using different values for b and assuming $a = 1$ in the expression

$$H_{eff}(k) = \frac{(1 + k^2b^2)^{\frac{1}{2}}}{a^2 + k^2}$$

and there is no net effect produced by introducing the same limits on G(k), since extending the limits of G(k) beyond k_{max} has no effect on $h_E(x)$. The effective modifying function, $g_{eff}(x)$ can therefore be written as

$$g_{eff}(x) = \int_{-k_{max}}^{+k_{max}} (1 + ikb)e^{-ikx}\, dk$$

$$= 2\left(1 + \frac{b}{x} + 2ik_{max}b\right) \frac{\sin(k_{max}x)}{x}$$

If $2bk_{max} \ll 1$, then this function is real and physically realisable, but if not it is complex and therefore produces a phase shift of the output equal to θ where

$$\tan\theta = \frac{2\ x\ bk_{max}}{x + b}$$

Such a phase shift is shown to affect range accuracy in Section 4.10. Another estimate of the effect of differentiation may be obtained by calculating R as defined previously for a realistic function.

Suppose

$$h_o(x) = x^2\ e^{-ax} \qquad \text{for } x > 0$$

This approximation retains the essential features of the transfer function. A differentiation converts this response into

$$h_E(x) = (2x - ax^2)e^{-ax}$$

The intrinsic resolution is $R_o = 3^{-\frac{1}{2}}a$

The resolution after differentiation is $R_E = 3^{\frac{1}{2}}a$, so that

$$R_E = 3\ R_o$$

The fractional improvement in resolution by this criterion is independent of a, the parameter which characterises the response.

(g) Summary

In this section the concept of the effective transfer function has been utilised to predict the achieved resolution when various conditions are changed. The effective transfer function is produced by modifying the intrinsic transfer function and such a method of describing A-scan resolution has proved particularly useful when predicting the behaviour of a scanner in circumstances where measurements using phantoms may not be made. In considering the effects of changes in the signal processing, no significant new information on the design of scanners has been revealed, but the effects of these changes may be quantified and the consequences of further modifications can be predicted.

4.9 Axial Resolution of the B-mode: the TP scan

In this section, the resolution of a different mode of scanning is considered using the methods described above. The B-mode presentation of echoes is usually swept with time on a TP display or with angle on a B-scan, but here a single, intensity modulated line is considered fixed and defines the x-axis. The B-mode line can be described as an output luminance (intensity) distribution on the cathode ray tube, or as a photographic response (density) distribution. The intrinsic response of the B-mode processing and display may be analysed in isolation to the effect of scanning, and for TP scans it is only this intrinsic response which is important.

Each impedance step of the object gives rise to an image on the B-mode which should be a point whose intensity represents the size of the step. In fact, the image is extended in two dimensions for a variety of reasons, which include the signal processing, the non-zero cross section of the scanning electron beam of the CRT, and light diffusion in the phosphor and photographic emulsion, and this spreading of each image point is an intrinsic limitation on B-mode resolution. In order to use the kind of analysis used for the A-scan, the conditions of linearity and shift-invariance must be fulfilled.

Some components of the intensity modulation processing and B-mode display are non-linear in general but in Chapter 3 it was shown that the echo height to pulse width conversion of the NE4102 produces a linear relationship of input echo amplitude to output phosphor brightness over a limited region. Furthermore, non-linear relationships which produce a unique

output for any input, such as the exposure - density characteristic of photographic films, may be allowed for in the analysis. Shift invariance supposes that the individual intensity modulated image points are the same over all the image. In considering B-mode displays, there are two separable mechanisms which cause points to spread, one of these is always reasonably shift invariant whilst the other depends on the transducer direction. Shift invariance is satisfied by processes such as light diffusion and electron optical aberrations except for extreme effects such as curvature of the image field edges, but even then the image plane can be divided into smaller areas ('isoplanatic patches') in which it holds. However, there is also the spreading of the image points due to the deflection of the electron beam during the time of electron emission, and this deflection depends on the velocities of the x and y time base ramps. Since the time base velocities are themselves dependent on the transducer orientation, then the image point shape is determined by the orientation of the transducer. In a B-scan, therefore, where the transducer direction continually changes, the spread of the point in the image is not strictly shift-invariant, but in any case this effect is of little significance in B-scanning. Here the intrinsic transfer function for a fixed transducer orientation only is considered: for a TP scan, the spreading due to the beam deflection during emission is only along the x axis, for any other orientation there is an x and y deflection.

The NE4102 TP scan processing is described in Appendix A. The resolution of such a processing can be shown to depend on echo amplitude. The peak detection circuits produce an electron emission at the CRT cathode whose duration is dependent upon the height of the echo peak relative to the threshold level, and such an emission occurs at each maximum of the A-scan envelope. If it is assumed that the peak detector produces an electron emission which is directly proportional to each echo maximum, then the detector must act as a differentiator which triggers a response whenever the waveform derivative changes polarity from positive to negative. If the A-scan waveform is $h(x)$, then when $\frac{dh(x)}{dx}$ is 0 and $\frac{d^2h}{dx^2}$ is negative, a B-mode signal is generated. The ideal image would be a point of strength A, $A\delta(x)\,\delta(y)$. Such a point is spread on a TP scan in the following ways.

(a) Isotropically, because of the intrinsic point spread of the display. $\delta(x)\,\delta(y) \longrightarrow p(x,y)$

(b) Because of the deflection of the electron beam, a point on the x-axis becomes a line of uniform brightness whose length is a measure of the strength of the point. For an echo of height A above the threshold level the length of echo is $\alpha\beta A$ where α = a conversion factor of echo amplitude to pulse width in seconds and β = velocity of time base across the display in mm tissue/second.

For the TP scan, the spread in the y direction is of no significance. The x-direction transfer function, $h(x)$, which operates on the ideal image point, $A\,\delta(x)$, to produce the output, is

$$h(x) = \frac{1}{A}\,(u(x) - u(x - \alpha\beta A)) * \mathcal{L}(x)$$

where $u(x)$ = Heaviside's unit step function

and $\mathcal{L}(x) = p(x,0)$

Such a transfer function is not generally applicable for any input but it does describe the response to a simple peak in the A-scan. The spatial frequency response is then

$$H(k) = \frac{1}{A}\,L(k) \int_0^{\alpha\beta A} e^{ikx}\,dx$$

where $L(k) = FT(\mathcal{L}(x))$ = the relevant intrinsic spread function

$$|H(k)| = \frac{2}{k}\left|\sin\left(\frac{k\alpha\beta A}{2}\right)\right| .\ L(k)$$

The relative importance of the electron beam deflection compared with the intrinsic point spread depends on the size of $\alpha\beta A$ and the shape of $L(k)$. An approximate comparison may be made in terms of characteristic widths of

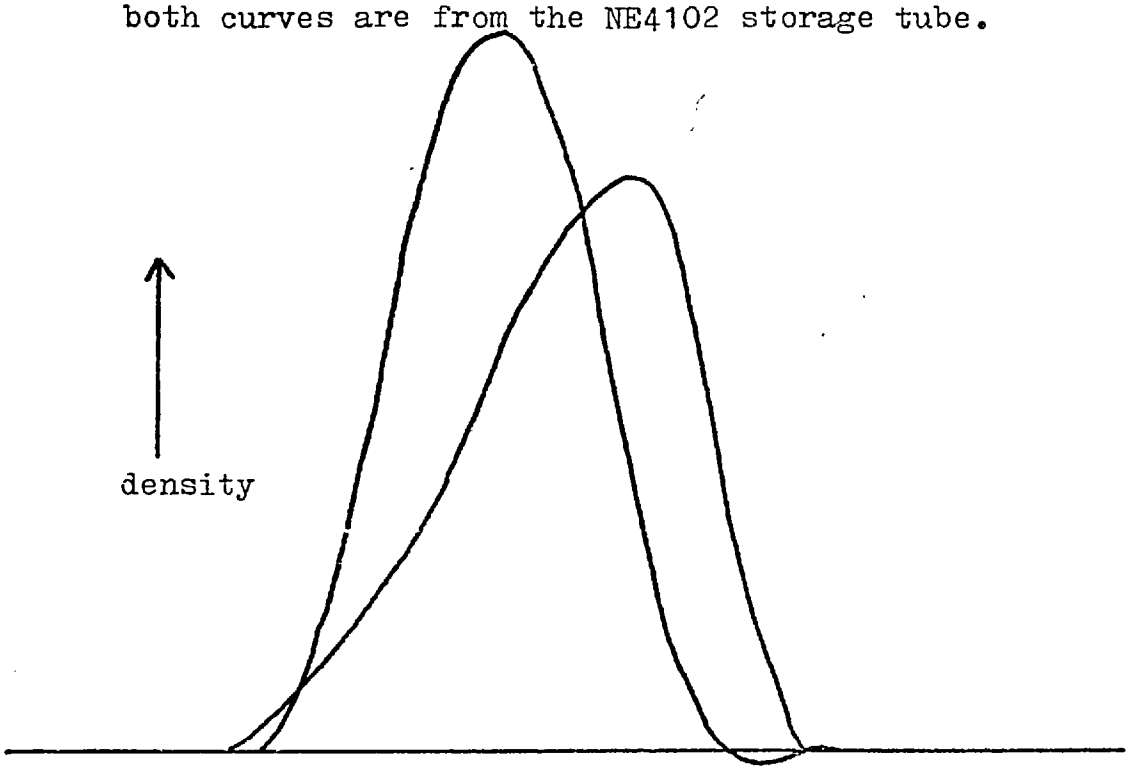
$\frac{\sin\left(\frac{k\alpha\beta A}{2}\right)}{k}$ and $L(k)$. The former function has a width determined by the angle $\frac{k\alpha\beta A}{2}$, so that a frequency that characterises the width is $k_c = \frac{\pi}{\alpha\beta A}$. If α increases, the pulses increase in length so k_c decreases (poorer resolution). If the gain of the receiver decreases, or the detection threshold increases, then A decreases and k_c is increased (better resolution).

L(k) may be obtained by Fourier Transformation of the Point Spread Function of the display or display and recorder, which were measured photographically from the Diasonograph B mode. A photographic film, operating in an approximately linear region of its exposure-density characteristic curve, was exposed to single image points of the CRT produced by single echoes. The resultant optical density profile was then scanned using a microdensitometer (scanning aperture 5 mm x 20 μm) and the traces obtained are shown in Figure 4.17. These traces are line spread functions ($L(x)$), but they completely describe the Point Spread Function when it is rotationally symmetric (see Chapter 5). The measured $L(x)$ could reasonably be approximated by a Gaussian of the form $c_1 e^{-a^2x^2}$, whose half width $\frac{1}{a}$ is 0.8 mm. The Fourier Transform of this curve is $c_2 e^{-\frac{k^2}{4a^2}}$ and it has a half width $2a = 2.5$ mm^{-1}. From the NE4102 data of Figure 3.9, αA can vary from 100 to 300 nanoseconds, whilst β is simply the velocity of sound in tissue multiplied by the TP display magnification factor, m.

$\beta = 1.5$ m mm/μsec.

If m = 1 then $\frac{\pi}{\alpha\beta A}$ varies from 7 to 21 mm^{-1}. At this scale, the width of the transform of the deflection spread function is greater than the display's intrinsic spatial frequency response, so a limitation on resolution is derived from the CRT spot size. However, when the TP range axis is magnified the deflection spread function limits resolution.

Figure 4.17 Microdensitometer traces of photographic recordings of single B mode points.
These curves are Line Spread Functions of the B mode and are approximately Gaussian in shape.The skew trace was obtained by a slight adjustment of the focus control, both curves are from the NE4102 storage tube.



Actual size x 50.

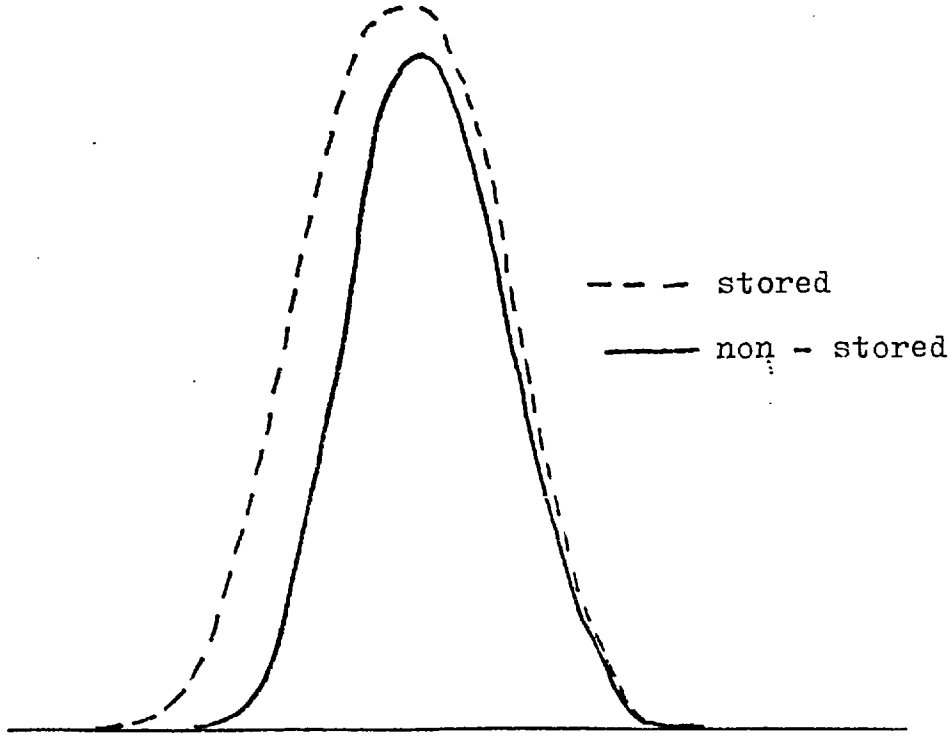
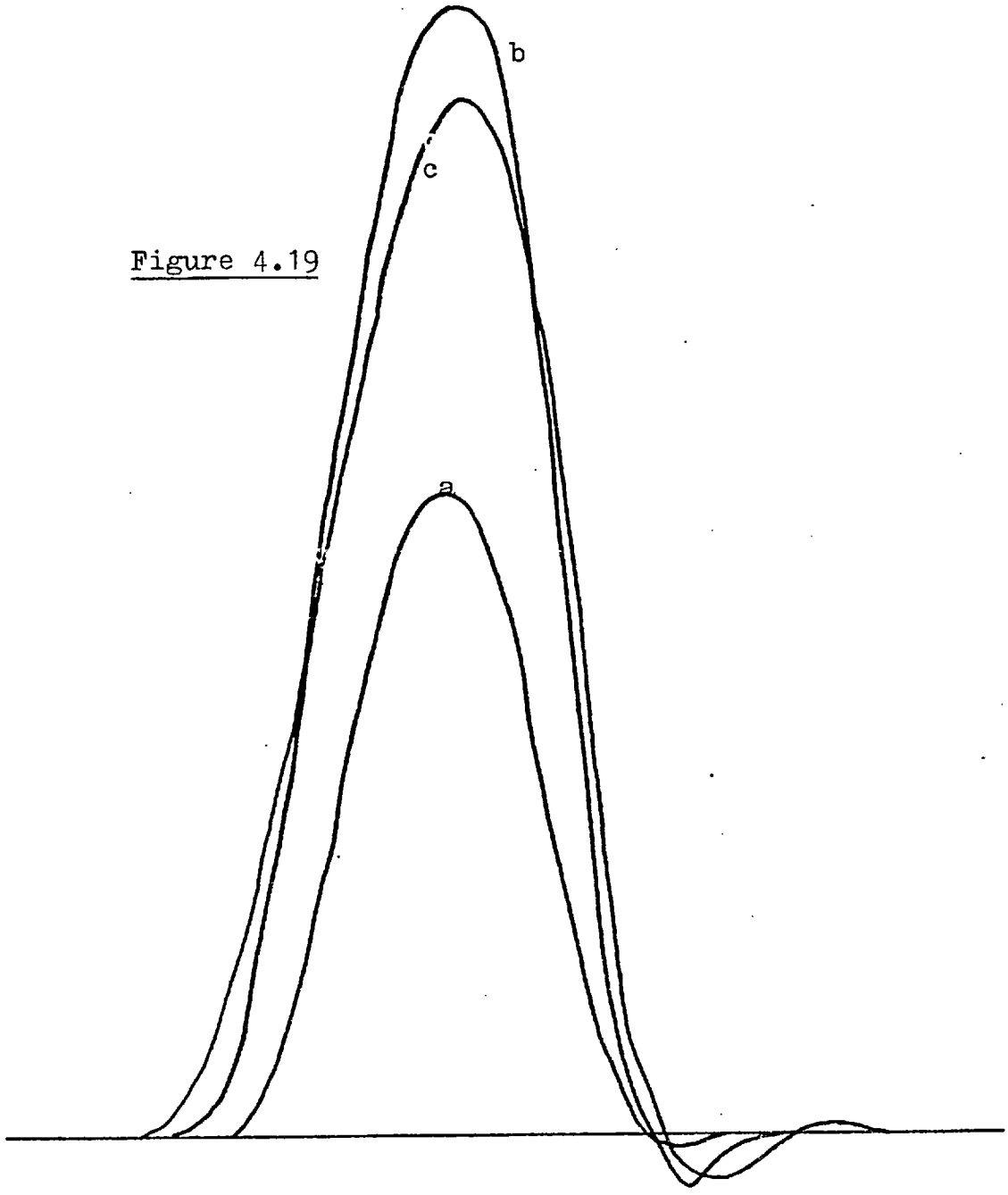


Figure 4.18 Line spread functions of the B mode in stored and non - stored modes.

Figures 4.18 - 4.20 show further measurements of such spread functions. The use of a storage phosphor significantly reduces the resolution of the display because the spot spread significantly broadens when used in a storage mode. The spot size, and therefore the resolution limit, depends also on the time the image is written onto the display and on the delay between writing and storage. Figure 4.19 shows the effect of spot blooming caused by charge leakage in the tube phosphor which is itself dependent on the tube operating conditions. Figure 4.20 shows a microdensitometer scan through a TP line produced by sweeping a single echo vertically. The magnification of the TP range is x10 and the two spread functions are of comparable importance.

In considering the resolution of the TP scan, some shortcomings of the linear transfer function analysis have been highlighted. The function $h(x)$ derived above depends on the input and is not therefore an intrinsic property of the system. Different inputs produce different resolving behaviour and only $\mathcal{L}(x)$ is an intrinsic property of the scanner. However, the analysis above shows the relative importance of the limitations imposed by the display and by the desire to maintain amplitude information in the B-mode. The Diasonograph TP processing is non-linear in that the output from two inputs is not the sum of the two outputs produced individually. Two echoes are not able to overlap along a B-mode line, so a linear theory is not exact. The simpler concept of the Z-modulation pulse length, which is unambiguously defined for any input echo is more useful here.

Figure 4.19



Actual size x 50

Line spread functions of the B mode, measured by scanning a photographic negative of a single point.
Curve a was measured in a non - store mode.
Curve b was measured in the stored mode after writing for 5 seconds the same point.
Curve c was measured 20 seconds after storing point image b

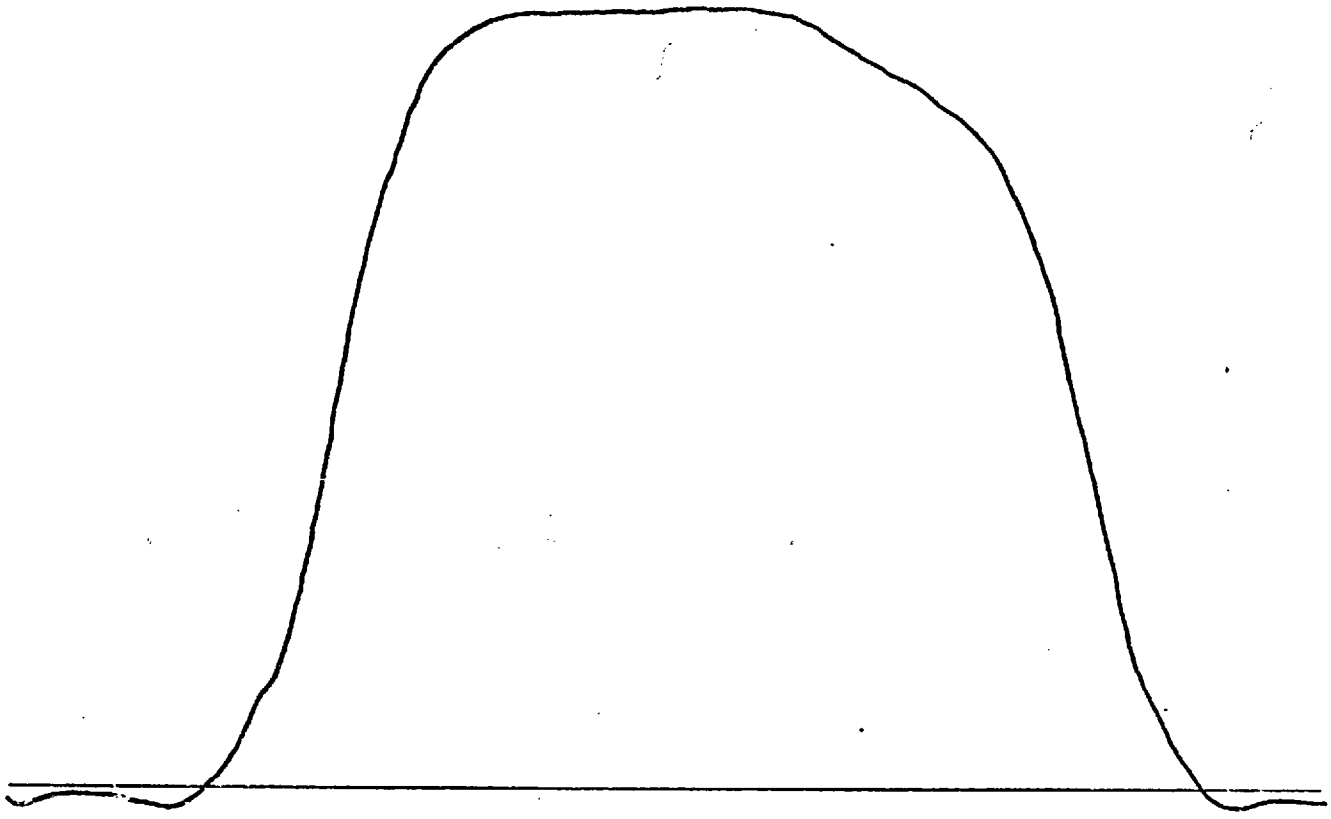


Figure 4.20 Microdensitometer trace through the image of a single TP line whose scale was x10 tissue distances. The densitometer trace magnification is x50. The edge unsharpness caused by the response of the tube is here of the same order of magnitude as the deflection of the spot in the TP mode.

4.10 Intrinsic Range Accuracy of the A-scan

Range accuracy is of importance in the evaluation of imaging performance because it describes the ability of an A-scan to place an echo at its correct position on the display, and when reflecting interfaces are placed at incorrect distances from the transducer then the image is distorted. The criterion used for describing A-scan resolution may also be extended to describe the intrinsic range accuracy of a scanner. Range errors may be caused in several ways, many of which (e.g. refraction) are determined by the medium and object, but these degradations are independent of the A-scan intrinsic limitations. Range errors may be introduced by the signal processing or miscalibration of an A-scan, but a particular form of distortion is introduced by the finite rise time of the A-scan display which is closely related to the A-scan resolution.

It was postulated in Chapter 3 that distortions may generally be regarded as differences between object and image, and that a numerical expression of these differences is a useful index of the magnitude of the distortion. When an isolated A-scan pulse is observed the position of the reflector is commonly considered to be the position of the peak of the signal since this is most readily identified and is not dependent on the choice of threshold or gain settings. If the object is a plane reflector then the ideal image would be $\delta(x - x_0)$, a Dirac impulse at the true position of the reflector x_0. If there are no other sources of range error, the system registers a real image $h(x - x_0)$ due to its finite

bandwidth, which is equivalent to a spreading of the ideal image along the x-axis. The degree of spreading is a measure of the range error, e_1, introduced by the finite resolution, and may be expressed as the moment of $h(x - x_o)$ about the true position of the reflector. Without loss of generality, let $x_o = 0$, so that

$$e_1 = \frac{\int_{-\infty}^{\infty} x\, h(x)\, dx}{\int_{-\infty}^{\infty} h(x)\, dx}$$

e.g. for the approximation used earlier,

$$e_1 = \frac{\int_{0}^{\infty} x^2\, e^{-\alpha x}\, dx}{\int_{0}^{\infty} x\, e^{-\alpha x}\, dx} = \frac{2}{\alpha}$$

Since R, the Resolution index, is α, then for this case

$$e_1 \cdot R = \text{constant.}$$

This relates the conditions for good resolution and good range accuracy.

This particular description of range error enables errors due to other factors to be simply added to give an overall range error. Thus, if L_1 and L_2 are respectively the range errors (= x axis displacements) due to incorrect calibration of the A-scan time base and to refraction, then the overall error is

$$e_T = \frac{\int_{-\infty}^{\infty} (x + L_1 + L_2) h(x)\, dx}{\int_{-\infty}^{\infty} h(x)\, dx}$$

$$= e_1 + L_1 + L_2$$

e_1 may be considered as a particular intrinsic error whilst L_1, L_2 are additional achieved errors. In Chapter 3 it was shown that range errors may be introduced instrumentally by use of the suppression control which changes the threshold of detection. Unlike the increase in resolution caused by threshold increases, signal suppression corresponds to a decrease in range accuracy and this is here expressed by the way that the normalised first moment of $h(x)$ about the true position of the reflector increases. This effect of the detection threshold expresses mathematically the behaviour of performance observed in Chapter 3. A more general relationship may be derived between R (as defined in section 4.6) and an index of range error. The range error is dependent upon the moments of $h(x)$ about its origin, but the precise choice of moment is not important and an error index E may be defined in terms of the second moment of $|h(x)|^2$.

$$E^2 = \frac{\int_{-\infty}^{\infty} x^2 \, |h(x)|^2 \, dx}{\int_{-\infty}^{\infty} |h(x)|^2 \, dx}$$

From the Uncertainty (Bandwidth) Principle

$$\frac{\int_{-\infty}^{\infty} x^2 \, |h(x)|^2 \, dx}{\int_{-\infty}^{\infty} |h(x)|^2 \, dx} \cdot \frac{\int_{-\infty}^{\infty} k^2 \, |H(k)|^2 \, dk}{\int_{-\infty}^{\infty} |H(k)|^2 \, dk} \geqslant \frac{1}{4}$$

$$E^2 R^2 \geqslant \frac{1}{4}, \quad \text{for any choice of } h(x)$$

$$E \geqslant \frac{1}{2R}.$$

This expression qualifies the dependence of positional error upon resolution. Such a dependence is not a peculiarity of the A-scan processing but is a general property of imaging processes which are expressable in terms of linear filters. Consider an object distribution $f(x)$ which produces an image $g(x)$. Any measurement of the object-image differences may be defined as a useful index of distortion. Such an index for example is the mean square difference between the object and image distributions when these are suitably normalised. Thus, if

$$\frac{f(x)}{\int_{-\infty}^{\infty} f(x)\,dx} \longrightarrow \frac{g(x)}{\int_{-\infty}^{\infty} g(x)\,dx}$$

(where the normalisation takes into consideration any changes of intensity).

then an index D may be defined as

$$D = \int_{-\infty}^{\infty} \left[\frac{g(x)}{\int_{-\infty}^{\infty} g(x)\,dx} - \frac{f(x)}{\int_{-\infty}^{\infty} f(x)\,dx} \right]^2 dx$$

where $f(x) * h(x) = g(x)$

$F(k) \cdot H(k) = G(k)$

and $\int_{-\infty}^{\infty} g(x)\,dx = G(o), \quad \int_{-\infty}^{\infty} f(x)\,dx = F(o)$.

Parseval's Theorem states that for any function $s(x)$ whose Fourier Transform is $S(k)$,

$$\int_{-\infty}^{\infty} s(x)s^*(x)\,dx = \int_{-\infty}^{\infty} S(k)S^*(k)\,dk$$

so that

$$D = \int_{-\infty}^{\infty} \left| \frac{G(k)}{G(o)} - \frac{F(k)}{F(o)} \right|^2 dk$$

$$= \int_{-\infty}^{\infty} \left| \frac{F(k)}{F(o)} \right|^2 \cdot \left| \frac{H(k)}{H(o)} - 1 \right|^2 dk$$

In any real system, $\frac{H(k)}{H(o)} \neq 1$ so that there always exists a difference between object and image. This distortion index expresses mathematically the effect of poor resolution upon the positional uncertainty of reflectors observed in Chapter 3.

In general $H(k) \longrightarrow 0$ beyond some $k = \pm k_{max}$.

Thus,

$$D = \int_{-k_{max}}^{+k_{max}} \left| \frac{F(k)}{F(o)} \right|^2 \left| \frac{H(k)}{H(o)} - 1 \right|^2 dk + \int_{|k| > k_m} \left| \frac{F(k)}{F(o)} \right|^2 dk$$

Even if the first integral may be made vanishingly small, it is a consequence of the limited support of $H(k)$ that there remains a minimum value for D which depends on the relationship of k_{max} to the highest spatial frequency in the object:

$$D_{min}(k_{max}) \gg \int_{|k| > k_{max}} \left| \frac{F(k)}{F(o)} \right|^2 dk$$

This minimum value becomes zero only when the object distribution, $F(k)$, is itself bounded.

A further source of range error may be derived from the intrinsic behaviour of the scanner when the phase of the Impulse Response Function varies with frequency. The response may be written as

$$H(k) = |H(k)| \; e^{i\phi_o}$$

when the phase, ϕ_o, is independent of frequency. If however, ϕ may be expanded by a Taylor expansion about a centre frequency k_o then, neglecting all but the first terms (weak dispersion)

$$\phi(k) \simeq \phi(k_o) + (k - k_o) \frac{\partial \phi(k_o)}{\partial k}$$

$$\Rightarrow \quad H(k) = |H(k)| \; e^{i(\phi(k_o) - k_o \frac{\partial \phi(k_o)}{\partial k})} \cdot e^{ik\frac{\partial \phi(k_o)}{\partial k}}$$

Therefore, the transfer function becomes

$$h'(x) = \int_{-\infty}^{\infty} |H(k)| \; e^{i(\phi(k_o) - k_o \frac{\partial \phi(k_o)}{\partial k})} \; e^{-ik(x - \frac{\partial \phi}{\partial k})} \; dk$$

$$= \text{constant} \times h(x - \frac{\partial \phi(k_o)}{\partial k})$$

A range error which depends on the variation of phase angle with frequency is introduced. Such a range error may be introduced by dispersive signal processing but its importance remains to be established.

4.11 A consideration of A-scan design

The resolution and accuracy of A-scans have been directly related to a single transfer function, $h(z)$, and here the factors in the design of a scanner which determine $h(z)$ are reviewed. If the processes of pulse transmission, reflection, reception and display are considered separately then each may be described by its individual transfer function. In general the overall transfer function of the scanner may be written as

$$h_o(t) = V(t) * h_T(t) * TF(t,\underline{r}) * RF(t,\underline{r}) * h_R(t) * G(t)$$

where $V(t)$ = the excitation voltage applied to the transducer

$h_T(t)$ = the transmission impulse transfer function which relates emitted sound pressure to the exciting voltage.

$TF(t,\underline{r})$ = a function which depends upon the shape of the transducer which governs the shape of the sound pulse at any field point. In Chapter 5, the exact form of TF is derived for plane transducers. For quasi-monochromatic pulses, TF is not a major influence on the pulse shape.

$h_R(t)$ = the receiver function that corresponds to $h_T(t)$.

RF = the receiver function that corresponds to TF.

$G(t)$ = the function which acts in convolution with the same effect as the frequency dependent gain of the receiver amplifiers.

The dominant influences upon $h_o(t)$ are h_T, h_R and $G(t)$, but the evaluation of TF and RF is left until Chapter 5. $G(t)$ is most easily measured in terms of the frequency response curve of the receiver alone, and is essentially chosen by the scanner

designer who compromises the scanner bandwidth to obtain low noise levels. The factors relevant to designing tuned amplifiers are well understood and G(t) may be changed when the noise levels are low. The principal interests here are the transient responses of the transducer in transmission and reception since these are least well understood and are usually the single most significant difference between different A-scanners.

4.12 Transfer Functions of Piezoelectric Transducers

The behaviour of a piezoelectric transducer is usually described either in terms of its behaviour at or near resonance (e.g. Tiersten, 1969) or in terms of an equivalent electrical circuit (e.g. Mason, 1964), and these two approaches have been related in several papers (e.g. Meeker, 1972). These techniques rely upon the solution of relevant differential equations and usually produce expressions for the impedance of a transducer at different frequencies. Whilst such techniques are useful for many purposes, they do not easily render the transfer function of interest here. A treatment which is more useful has been derived by Cook (1956) for weakly coupled transducers, and by Redwood (1961) for restricted boundary conditions. Both of these treatments produce a transient analysis of the thickness mode transducer. Redwood's equations are developed in Appendix B to produce a general solution in the form of a transfer function in the frequency domain which enables the output from the transducer to be calculated for any input. This general solution is independent of particular boundary conditions, but both Redwood's and Cook's solutions are obtainable if suitable approximations are made.

A completely general solution for the behaviour of transducers would involve couplings between complex modes of vibration so that the exact form of the transducer transfer function is determined by the particular choices of material constants and boundary conditions, but approximate solutions are obtainable for simple crystal geometries. If the transducer

area is large compared to the thickness and if the material is strongly polarised in the thickness direction, then most of the electrical energy applied will be coupled directly to a thickness expansion mode of vibration. Cross coupling to other modes may be significant when the crystal is anisotropic in several directions or when the mounting of the crystal imposes mechanical boundary conditions which are suitable for motions other than planar piston movements. In particular, the circumferential clamping of transducer elements may enhance the formation of surface waves by promoting flexural movements of the crystal (cf. elastic membranes), whilst piezoelectric coupling to transverse or radial modes may result in the conversion of energy into oscillations whose frequencies are determined by the transducer diameter rather than the element thickness. In the analysis of Appendix B these effects are neglected (although radial modes are observable in transmission as shown in Section 3.4).

The derivation of the wave equation for a piezoelectric medium and details of its solution are given in Appendix B, but the principal results are summarised here.

(a) Solutions for transducers in transmission

(i) General solution

The Laplace Transforms of output pressure and input voltage are related as equation B.12.

$$\bar{T} = \frac{-\bar{V}hC_o\frac{Z_F}{Z+Z_F}\left(1 + k_Be^{-2\gamma L} - \frac{2Z}{Z+Z_B}e^{-\gamma L}\right)}{1 - k_Fk_Be^{-2\gamma L} - \frac{h^2C_o}{p}\left(\frac{(k_Be^{-\gamma L}-1)(e^{-\gamma L}-1)}{Z+Z_F} + \frac{(k_Fe^{-\gamma L}-1)(e^{-\gamma L}-1)}{Z+Z_B}\right)}$$

(ii) Solution for weakly coupled transducers in transmission.

In the time domain, $T(t) = V(t) * h_T(t)$, where

$$h_T(t) = \frac{-hC_o t_{TF}}{2}\left(\delta(t) - \sum_{n=1}^{\infty} (\alpha_{TB}\alpha_{TF})^{n-1}\left(t_{BT}\delta\left(t + \frac{L}{v} - \frac{2nL}{v}\right) + t_{FT}\alpha_{TB}\delta\left(t - \frac{2nL}{v}\right)\right)\right)$$

(Equation B.14)

(iii) Solution for rigidly backed transducers in transmission.

$$h_T(t) = \frac{-hC_o t_{TF}}{2}\left(\delta(t) - \sum_{n=1}^{\infty} \alpha_{TF}^{\,n-1}\, t_{FT}\, \delta\left(t - \frac{2nL}{v}\right) - \sum_{n=o}^{\infty}\sum_{m=o}^{n} A_{mn} e^{-a\left(t - \frac{2nL}{v}\right)}\left(t - \frac{2nL}{v}\right)^m\right)$$

A_{mn} depends upon Z, Z_F, h and C_o (Equation B.16).

The series form of the solutions indicates that a single applied voltage impulse will produce several pressure impulses separated in time and with amplitudes determined by the mechanical boundary conditions. If equation B.14 is compared with B.16 it can be seen that the assumption of rigid backing predicts no change in the output at times that are odd integrals of the transit time of a mechanical disturbance through the transducer, $\frac{L}{v}$. The fundamental frequency of the output stress wave is determined by the spacing of the terms in the series, and it is clear that a rigidly backed transducer acts as though its fundamental frequency is half that of a transducer backed

by a lower impedance. If $Z_B = \infty$ in B.14, then we obtain the transfer function for weak coupling and rigid backing.

$$h_T(t) = \frac{-hC_o t_{TF}}{2} \left(\delta(t) - \sum_{n=1}^{\infty} \alpha_{TF}^{n-1} \, t_{FT} \, \delta\left(t - \frac{2nL}{v}\right) \right)$$

Comparing this with B.16, it is apparent that the assumption of weak coupling in Cook's analysis is equivalent to putting all the A_{mn} of B.16 equal to zero. Furthermore, comparison of the frequency domain responses shows that Cook's approximation is exactly equivalent to assuming that

$$\frac{a}{p+a} \ll 1$$

in the expression for $\bar{T}$ (equation B.15). Both p and a are frequencies, and Cook's approximation is only valid when a is much smaller than the frequencies of interest. Redwood (1961) calculated a for quartz transducers. Table 4.2 shows comparative values of the relevant material constants for quartz and PZT5 obtained from manufacturers' data. The frequencies of interest (p) are of the order of a Megaherz so that

$$\frac{a}{p+a} \simeq \frac{1}{25} \quad \text{for quartz}$$

and $$\frac{a}{p+a} \simeq \frac{1}{2} \quad \text{for PZT}$$

Thus, Cook's approximation is valid for quartz but is not valid for PZT because of its high permittivity, so that a real ceramic transducer will produce not only a sequence of Dirac impulses when excited with a voltage impulse but also a sequence of exponentially decaying stress impulses. Cook's

Table 4.2

Material constants of quartz and PZT5 transducers

	Q	PZT5
h (volt. metre^{-1})	4.5×10^{9}	1.3×10^{9}
σ (Farad. metre^{-1})	4×10^{-11}	1500×10^{-11}
v (metre. sec^{-1})	5740	3780
Z_T (kgm. sec^{-1})	1520	2930
C_o (Farad) *	6.6×10^{-12}	3.7×10^{-9}
a (MHz) **	.044	1.08

* C_o calculated assuming radius r = 1 cm. and thickness = $\frac{\lambda}{2}$ when frequency f = 1.5 MHz

** $a = \frac{h^2 C_o}{Z_T + Z_F} = \frac{\pi h^2 r^2 \sigma f}{c Z_F}$ (when $Z_T = Z_F$)

solution predicts that a voltage impulse generates four acoustic impulses, two at each face of the transducer element whose magnitudes depend on the front, medium and back impedances, and one impulse from each face moves through the element itself until some of its energy is reflected at the element face. Redwood's solution shows that rigid backing removes the impulses generated at the back face whilst strong coupling decreases the bandwidth of the individual impulses so that they have an exponential tail. If the exciting voltage is itself a Dirac function, a series of similar impulses is produced, whereas if the voltage has any other form each individual term in the series produces a wavefrom similar to the excitation but delayed in time and with varying amplitude. The resultant stress pulse shape depends on the way these individual waveforms overlap. Indeed, if the transmitter rise time is greater than $\frac{\lambda}{2v}$ then the individual stress impulses will overlap in a rigidly backed transducer. The series solution may however be used to calculate how the output stress may be reduced to a single impulse by exciting the transducer with a sequence of impulses designed to produce a cancellation of all terms except the first.

Equation B.16 shows how a voltage impulse is modified by convolution with a Dirac function and an exponential term. As α_{TF} decreases, so the exponential terms dominate, and the exact form of the stress pulse then depends upon the value of

$$a = \frac{h^2 C_o}{Z+Z_F}$$

since this is the time constant of each term. The logarithmic decrement of each term is inversely proportional to C_o, and

therefore to the transducer area. Thus, the shape of the emitted stress pulse depends not only upon the choice of thickness and impedance, but also upon the transducer area.

The overall pulse length depends principally upon the reflection coefficients at the front and back of the transducer. This is illustrated in Figure 4.21 where the calculated responses of weakly coupled transducers are shown for various combinations of Z_F, Z_B and Z. Similar results were given by Cook. The effects of changes in Z_F and Z_B may be predicted from equations B.14 and B.16. If $Z = Z_B$, the backing is matched to the transducer and only two components of the series are not zero as all reflections from the back are removed. The separation between the terms is $\frac{L}{v}$. If $Z = Z_F$ and $Z_B = \infty$, two terms remain but the separation is $\frac{2L}{v}$. The criteria for choosing Z_F and Z_B for high efficiency and wide bandwidth have been extensively dealt with in the literature but the analysis of Appendix B enables the effects of changes in the impedance upon emitted pulse lengths to be evaluated.

(b) Solutions for transducers in reception

(i) Open circuit response

The receiver transfer function $h_R(t)$ is given by equation B.19.

$$h_R(t) = h \sum_{n=0}^{\infty} A_n \, u(t - \frac{2nL}{v}) - B_n \, u(t - \frac{L}{v} - \frac{2nL}{v})$$

where $u(t)$ is Heaviside's unit step function and the A_n, B_n coefficients depend on Z_F, Z_B and Z.

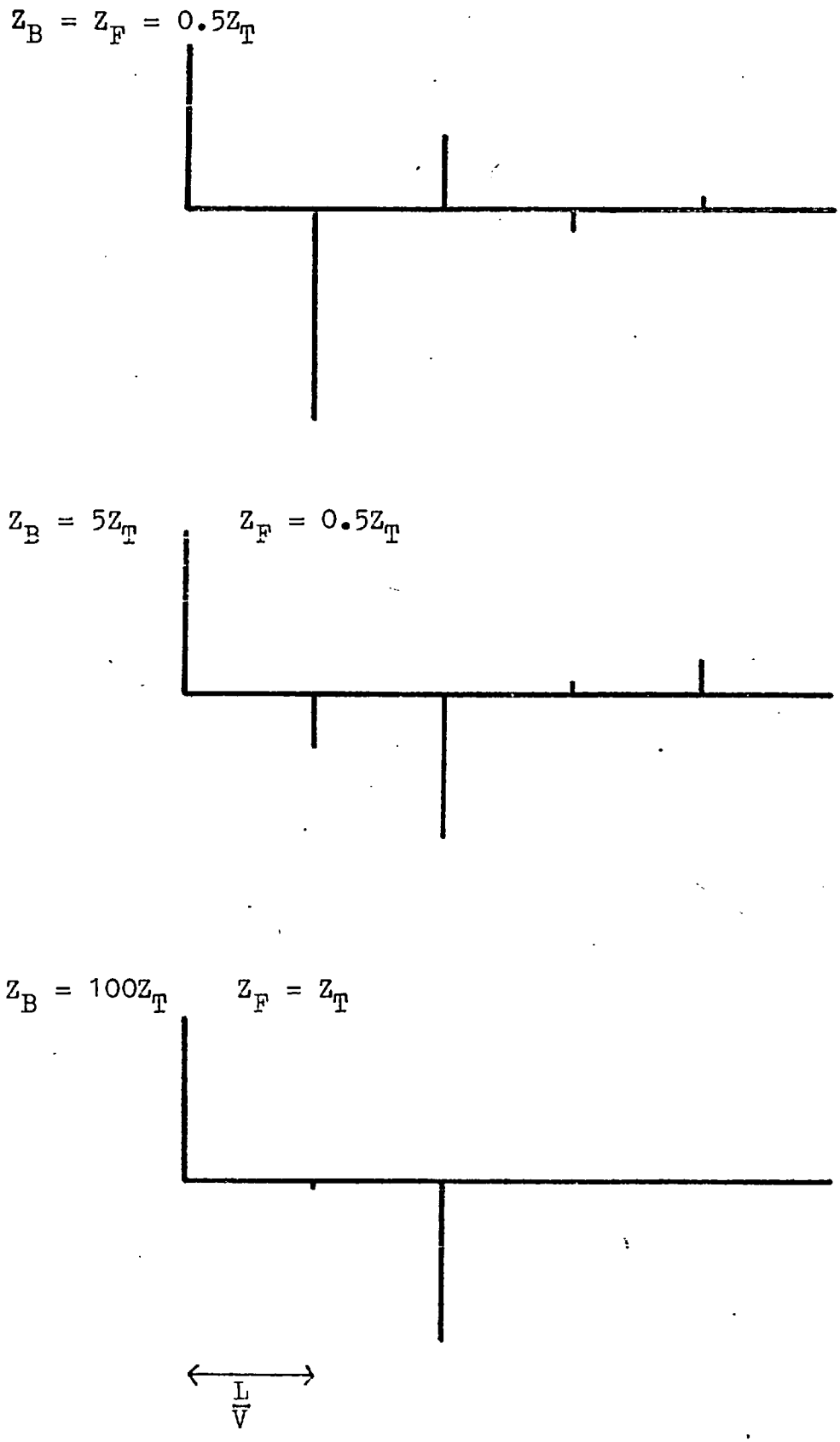


Figure 4.21 Examples of calculated responses of transducers in transmission using the assumption of weak coupling with a Dirac impulse excitation.

(ii) Response for rigidly backed transducer with finite load.

$$h_R(t) = LT^{-1}\ (\ H\ (p)),\ \text{where}$$

$$H(p) = \frac{-2h}{Z+Z_F}\ p \sum_{n=o}^{\infty} \frac{(p^2k_F+\tau(pk_F+a))^n}{(p^2+\tau(p+a))^{n+1}}\ (e^{-2n\gamma L} - e^{-2(n+1)\gamma L})$$

(Equation B.20).

Redwood (1961) analysed the response of a transducer to a step function of force of height F_o. The voltage across an infinite load would be

$$V = \frac{-2hF_o}{Z+Z_F}\ (t - (1+k_B)(t-\tau) + k_B(1+k_F)(t-2\tau).....)$$

which is a summation of voltage ramps displaced in time but with slopes dependent on the reflection coefficients k_F and k_B. If the acoustic input is some other function, F(t) then the response would be

$$V(t) = F(t) * h_R(t)$$

so that

$$\frac{dV}{dt} = F(t) * h \sum_n A_n\, \delta(t - 2n\tfrac{L}{v}) - B_n\, \delta(t - \tfrac{L}{v} - \tfrac{2nL}{v})$$

$$= \sum_n C_n F(t - n\tfrac{L}{v})$$

which shows that the voltage is effectively the integral of the incident pressure. The stress pulse produces a deformation and the spatial integral of the strain determines the transducer voltage. This effect may be important in the

interpretation of echo amplitudes and is reconsidered in Chapter 6.

In reception, as in transmission, reflections from the back face may be eliminated if $Z_T = Z_B$ (a_{TB}, k_B both zero). Similarly, if k_F is zero, reflections from the front are removed and the transducer is mechanically matched to the medium. If the force has a duration greater than $\frac{L}{v}$, the output voltage may be a complex superposition of terms, and since k_F and k_B lie between +1 and -1, many combinations of amplitudes are possible. The output voltage waveform is also dependent on the load resistance whose importance can be estimated by observing that B.20 reduces to B.21 when $\tau = 0$ and that the ability of B.21 to describe the transducer action decreases as $\frac{p}{\tau}$ decreases. Thus, the load impedance effect is not important if $pRC_o \gg 1$. Using the data of Table 4.2, this implies that R must be much greater than 250 ohms for PZT (but 10^5 ohms for quartz). Usually the impedance of the transducer is matched to its load so that $R \simeq \frac{1}{2\pi f C_o}$, which is not large enough to make loading time constants negligible. However, when τ is relatively large (low load impedances) then B.20 reduces to

$$H(p) = \frac{c}{\tau}\, p \sum_{n=o}^{\infty} \frac{(pk_F + a)^n}{(p+a)^{n+1}} \left(e^{-2n\gamma L} - e^{-2(n+1)\gamma L}\right)$$

and the first terms of the time domain transfer function will be

$$h_R(t) = \frac{c}{\tau}\left(\delta(t) - ae^{-at} - \delta\left(t - \frac{2L}{v}\right) - ae^{-a\left(t - \frac{2L}{v}\right)} \ldots.\right)$$

When the transducer permittivity is high, the exponential terms decay rapidly and the series reduces to a sequence of impulses each of which is only a slight distortion of the force waveform. With small electrical loads the voltage produced is like the force itself and is not the integral of the force. Thus, with any receiving transducer, the electrical loading and transducer time constants may have important effects on the linearity of response. The transducer voltage can resemble the force itself or the force integrated temporally between limits determined by the transducer thickness. The transducer time constants depend not only upon the material chosen for the device, but also upon the area of the transducer.

Chapter 5: The resolution of Ultrasonic B-scanners

5.1 The Formation of B-scan Images

The formation of a B-scan image may be analysed using some of the ideas introduced into the description of the A-scan. The identification of the impedance step as the object element of the A-scan resulted in the construction of a transfer function that could be used to predict the system's representation of any object. The B-scan may similarly be analysed by first identifying the object elements from which an ideal image can be constructed. The use of point scatterers as the object elements from which the equivalent set of points for any object may be derived, was outlined in Chapter 4 but further justification is offered here.

The spatial distribution of scattered radiation from sound waves incident on an object has been investigated by many workers. In particular, there has been much interest in the investigation of scattering mechanisms and their relationship to body shape, and a good review of this work has been given by Freedman (1962). Additionally, much work has been done on the scattering of sound from rough surfaces and from non-rigid, elastic bodies (e.g. Hickling 1962). A collation of references for much of this work has been given by Skudryzk (1971) and more recently by Chivers (1973), who himself was concerned with a study of scattering from human tissues. The particular treatment of acoustic scattering used below is due originally to Freedman (1962), but the important aspects of the present analysis do not rely critically on any of Freedman's

own assumptions. Here the Freedman analysis is utilised to describe qualitatively the mechanisms of scattering, later it is again involved in describing the sound field of transducers. Before considering the Freedman analysis in full however, its important features are introduced using the following simplified argument, which illustrates those aspects of the approach of interest here.

Consider an object which has dimensions and radii of curvature large compared to the wavelength whose surface is a rigid reflecting interface. Figure 5.1 shows such a body irradiated by a small fixed sound source. All points on the surface element of area dS, which lies between ranges r and r + dr, are at equal acoustic travel time from the transducer. Such a surface has been called an isochronal surface and for a uniform medium and small source it forms part of a spherical shell. If this surface reflects sound with uniform phase change then the acoustic pressure at the transducer location at time t is composed of contributions from all parts of dS. Accordingly, if the Kirchoff approximation may be used,

$$p(t) = \iint_{r,l} g\left(t - \frac{r}{c}, l\right) \cdot \frac{1}{r} \, ds$$

t = the time from the outset of the emitted sound pulse.

l = an angle variable which designates location on the isochronal strip between r and r + dr.

g = a time varying "source strength" of the surface dS.

For a rigid boundary, the source strength g is proportional $\frac{\partial v_n}{\partial t}$ where v_n is the normal component of the particle velocity of the incident field at the surface. If the incident

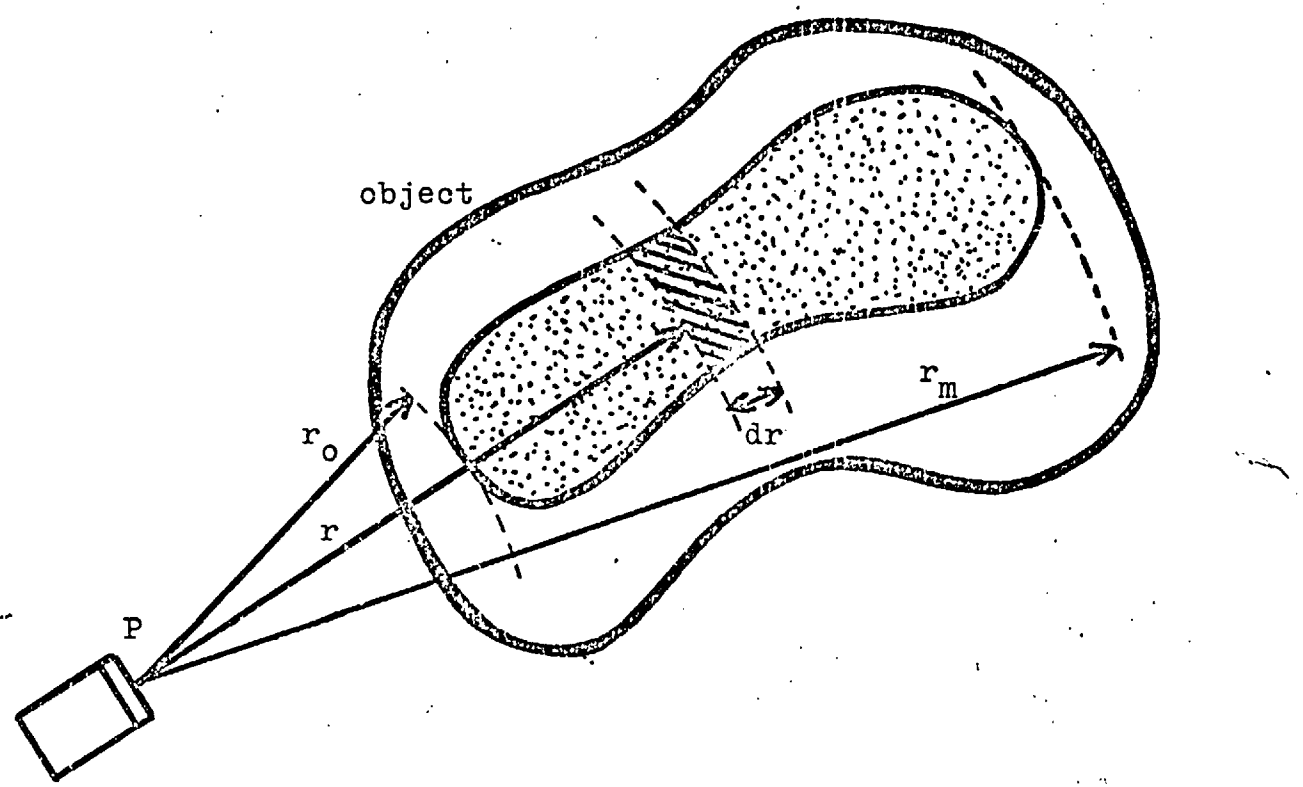


Figure 5.1 Large irregular object seen by small transducer at P.
r_o and r_m are the minimum and maximum ranges of that region (stippled) of the objects surface which is irradiated as the emitted pulse traverses it. The hatched region denotes an isochronal surface between ranges r and r + dr such that all points on it are to first approximation at equal acoustic travel time from the transducer. Location of elements of area on such an isochronal strip is given by a set of variables l.

pressure pulse normalised shape=P(t) over the whole region irradiated then

$$V_n = P(t - \frac{r}{c}) \cdot f(r,l)$$

Where f = a geometrical factor which takes into account both changes in the incident pressure produced by scattering, and spreading as well as variations in the angle between incident wave vector and normal to the boundary at the location (r,l). These geometrical variables need not be defined explicitly here because they may be removed by integration over the surface. The pressure at the transducer becomes

$$p(t) = \int_{r_o}^{r_m} A(r) \frac{\partial P}{\partial r} (t - \frac{2r}{c}) \, dr$$

where the identity

$$\frac{\partial P}{\partial t}(t - \frac{2r}{c}) = -\frac{c}{2} \frac{\partial P}{\partial r}(t - \frac{2r}{c})$$

has been utilised.

r_o, r_m are the minimum and maximum ranges of the irradiated region of the object.

A(r) = a range function which changes with the aspect of the object projected towards the transducer.

That the echo strength should be critically dependent on the object shape is not surprising, but a particularly interesting solution of the integral is the echo field produced by an object whose range function A(r) varies slowly and smoothly in the range r_o to r_m. p(t) is obtained by partial integration;

$$p(t) = A(r_m)\,P(t-\frac{2r_m}{c}) - A(r_o)\,P(t-\frac{2r_o}{c}) - \int_{r_o}^{r_m} \frac{dA}{dr}(r)\,P(t-\frac{2r}{c})\,dr$$

Since A(r) is slowly varying, the dominant contributions to the echo come from the first two terms. These represent delayed pulses of the same shape as the emitted pulse but scaled by geometrical factors A(r). The total echo is therefore a sum of these two echoes, each a replica of the original sound pulse and originating at the near and far points of the object. The partial integration is only valid over regions in which the integral and its derivatives are continuous, but at discontinuities in A(r) the integral may be split into sub-integrals with intermediate limits so that the partial integration produces replica pulses at the ranges of the discontinuities. The formation of replica pulses in scattering was analysed in detail by Freedman (1962) and some experimental evidence for their existence is given in Chapter 6.

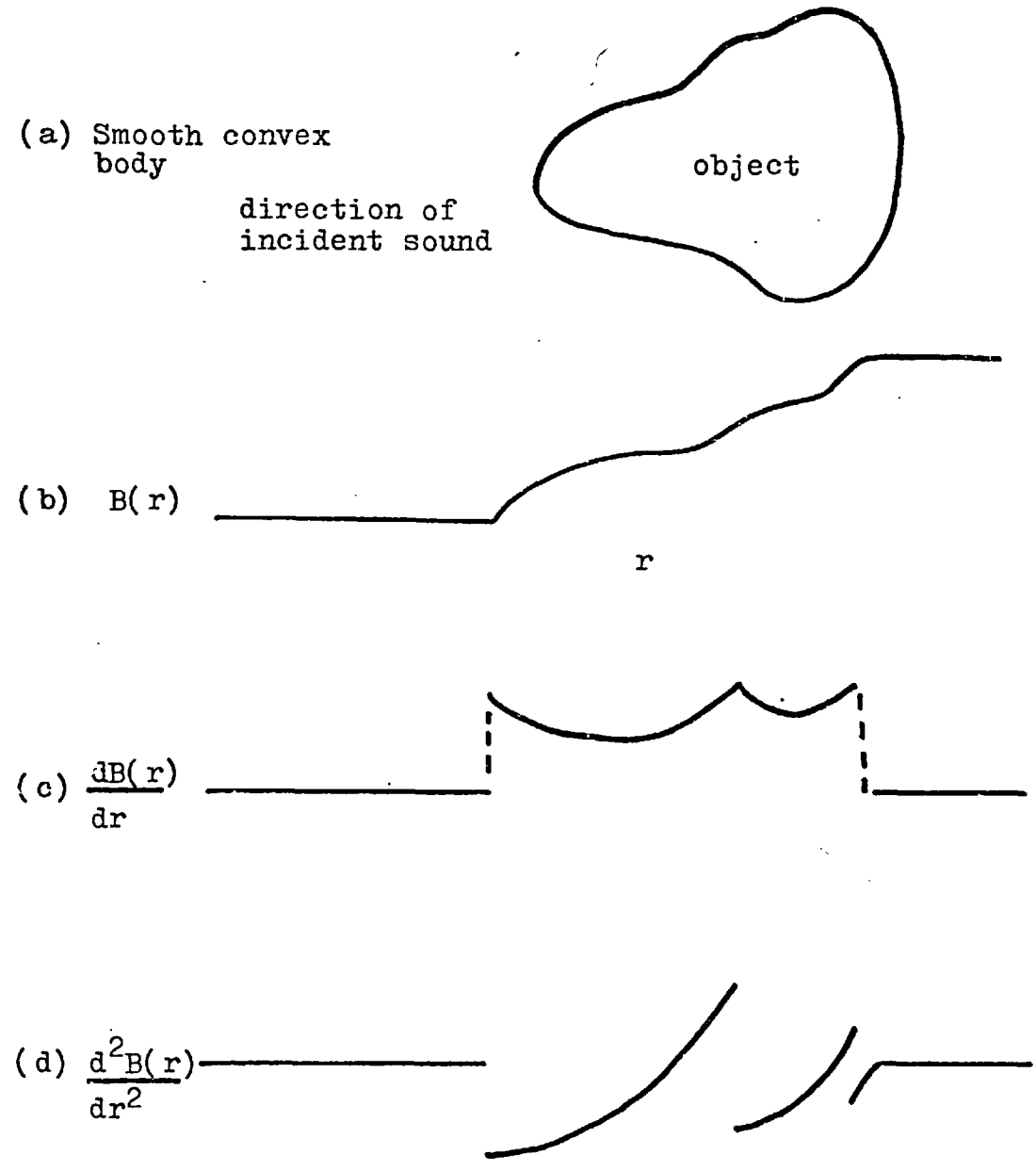
In Freedman's analysis, the scattering body is again assumed rigid and immersed in an unbounded, non-dissipative fluid. Rigidity imposes the condition whereby no radiation penetrates the body so that the fluid motion at the surface simply undergoes a phase change and the acoustic velocity is proportional to the pressure. By confining the analysis to bodies which are large and smooth compared with a wavelength, only direct scattering need be considered, and the Kirchoff approximation for the sound radiated by an elementary area is valid. The total echo depends only on the shape of the body directly irradiated, and the shape within the geometrical shadow region is not important.

In Figure 5.2a is shown a smooth, convex, rigid body, and at some distance from this is the transmitter-receiver. Figure 5.2b shows a plot of $B(r)$, the projection towards the transmitter of all those parts of the body which are visible and within total travel path r. $B(r)$ increases with r until all directly visible area is encompassed. In Figure 5.2c is shown a plot of $\frac{dB(r)}{dr}$, and this exhibits a number of discontinuities corresponding to sudden changes in $B(r)$. Similarly,

$$\frac{d^2B}{dr^2}, \ldots\ldots \frac{d^nB}{dr^n},$$

may show discontinuities at ranges which correspond to 'highlight features'. In his analysis, Freedman interprets these discontinuities in a particular way which helps suggest a choice of object element for image analysis. If a pulse is transmitted towards the object, each discontinuity in $\frac{d^nB(r)}{dr^n}$ $(n = 0, 1, \ldots.)$ generates a component towards the scattered signal, and on the assumption of certain bandwidth limitations, each component has the same envelope shape as the radiated pulse. The scattering therefore may be described in terms of a number of image pulses produced at discontinuities in any of the derivatives of $B(r)$. The amplitude of each scattering component is proportional to the magnitude of the generating discontinuity. The foregoing example may be extended to the case where the transducer has non-uniform directivity. The contributions of different elements of surface are weighted then by appropriate directivity functions, so that $B(r)$ is

Figure 5.2 Illustration of Freedman discontinuities



Replica echoes are produced at the ranges corresponding to the discontinuities in any of the derivatives of B(r).

replaced by $B_W(r)$. If the directivities are themselves continuous, then the discontinuities remain at the same positions but are altered in magnitude.

Freedman adopts the following notation for the echo signal produced by a scattering body whose nearest point is at r_o ($kr_o \gg 1$)

$$E = \sum_{g=1}^{m} E_g$$

where E_g is an image pulse.

$$E_g = \frac{iM_g}{\lambda} \exp(-i2k(r_g - r_o)) \sum_{n=o}^{\infty} \frac{D(W_W, g, n)}{(i2k)^n}$$

in which $M_g = P(t - \frac{2r_g}{c})$ VH.exp $(i(wt - 2kr_o))$.

$P(t - \frac{2r_g}{c})$ = envelope of transmission pulse (on delayed scale).

V,H are transmitter and receiver sensitivities.

$$c = \frac{w}{K} = \text{velocity} = \frac{\text{mean frequency}}{\text{mean wave number}}$$

r_g = a range at which finite discontinuities occur in one or more values of

$$\frac{d^n W_W(r)}{dr^n}$$

$W_W(r)$ = value of $W(r)$, the solid angle subtended by the body within range r, when each element is weighted by the product transceiver directivities.

$D(W_W, g, n)$ = notation of a discontinuity in $\frac{d^n W_W(r)}{dr^n}$ at range r_g.

r_m = furthest range of irradiated part of body.

For a range extent $(r_m - r_o)$ much less than the mean range $\bar{r}$, this reduces to

$$E_g = \frac{iM_g}{\lambda \bar{r}^2} \exp(-2k(r_g - r_o)) \sum_{n=o}^{\infty} \frac{D(B_w, g, n)}{(2ik)^n}$$

where $B_w(r)$ = directivity weighted area of projection considered earlier.

The formal derivation of these equations was obtained by Freedman by expanding the Kirchoff integral after formulating the integral in a convenient coordinate system. No new physical ideas were involved in obtaining these expressions for the scattered sound.

The various assumptions involved in the derivation of the series solution are not always rigorously satisfied and this leads to a loss of quantitative accuracy. For the purposes considered here, the quantitative validity is unimportant, but Freedman's method is also inapplicable when used to analyse scattering from surfaces which exhibit non-finite mathematical discontinuities. However, the essential features of the mechanism - that the echo is primarily generated at discrete discontinuities in the object's projection - remain the same (Freedman, 1962) and the theory has been shown to give useful results even when the conditions imposed are seriously violated.

The Freedman approximation predicts a series of replica pulses identical to the interrogating pulse only when the pulse bandwidth is restricted, but Freedman has indicated that the bandwidth restriction is not severe (a bandwidth of $\frac{1}{2}$ of

centre frequency gives good correspondence to theory) and is normally met by pulses used in diagnosis. When the restriction is not met, the replica pulses are distorted but they are still produced at discontinuities in the object area function. It is however possible to obtain pulse distortions due to scattering from some bodies. Robinson et al. (1974) has discussed the bandwidth restriction in detail, and his conclusions are introduced later in this chapter.

Each term of the series solution has the same dimensions, and because the denominator is $(2ik)^n$, then successive terms differ by $\frac{\lambda}{4i\pi}$. Each differentiation must therefore drop by a power of a length where the length involved will depend on the body radii, the distance from the transducer, and the size of the body, all of which are much greater than λ. Thus, successive terms differ by factors that decrease very rapidly with n so that the series converges quickly and only the first few terms are significant. It is this convergence which makes the Freedman analysis particularly useful in this context because it means that the equivalent set of point scatterers which can be used to represent the body completely can itself be well approximated by a small number of points each of which corresponds to a term in the series of Freedman discontinuities. This allows the object and the process of image formation to be properly described.

The 'field of echo generators' considered in Chapter 4 can now be reduced to the distribution of Freedman discontinuities, at least for certain classes of object. The extension of a Freedman type analysis to less ideal objects has been attempted with some success (e.g. Hickling 1962) and it

is reasonable to suppose that the qualitative features of the mechanism of replica pulse formation will be valid for several classes of scatterer found in the body, especially in considering the mapping of organ outlines and well defined surfaces. The equivalent set of point scatterers can be reduced, for any given transducer position, to a few points which correspond to the geometrical 'highlights' - those dominant features of objects at which the surface changes rapidly. The introduction of finite impedances into the object and medium properties suggests that the Freedman highlights will change to points at which the object's impedance changes rapidly. It is possible therefore to introduce an image Generating Function (GF) to describe the object even when an exact quantitative description is not available. The echo consists of a number of sequentially arriving pulses, each a scaled (and sometimes distorted) replica of each other. The number, relative spacings and magnitudes of the pulses are determined by the precise geometry considered, which is mathematically described by the Generating Function, so that the echo is a convolution of the transmitted pulse with the GF.

When replica pulses overlap, they do so vectorially and may produce complex pulse shapes. The significance of this and the extension of Freedman's analysis to describe the overall scanning procedure are discussed in Chapter 6. A simple model however is available to produce criteria for resolution. When the Freedman points are at different ranges from a transducer position then their separability is the problem of range resolution: when the Freedman points are on the same isochronal surface then they can only be separated by moving the transducer, which is the problem of lateral resolution.

5.2 Scanner Transfer Functions

The use of Freedman's analysis has suggested the use of point scatterers as object elements but it also illustrates a fundamental difficulty of evaluating images produced by pulse echo techniques which is that the object is not uniquely defined for all transducer positions. The image Generating Function depends on the aspect from which the object is viewed so that when an object is scanned the discontinuities which dominate the scattering change position in the object. This seriously limits the applicability of simple transfer function analysis.

Consider an object which consists of a number of discrete, fixed point scatterers which are scanned by a pencil beam of sound. The point scatterers are then the object field, $O(x,y,z)$

$$O(x,y,z) = \sum_n a_n \delta(x - x_n)\delta(y - y_n)\delta(z - z_n)$$

so that the sound arriving at the receiver (ignoring multiple scattering) at any instant is in this case produced at a single point. If the beam direction defines the z-axis, then for an impulse response $h(z)$ the A-scan becomes

$$A(z : x_o, y_o) = \sum_n a_n \delta(x_n - x_o)\delta(y_n - y_o)h(z - z_n)$$

where $(x_o, y_o, 0)$ is the beam origin. If a simple line scan is performed, the echo signal would be

$$L(x, z : y_o) = \sum_n a_n \delta(x - x_n)\delta(y_n - y_o)h(z - z_n)$$

In practice, the beam is not infinitely narrow but has a transverse intensity distribution. If $l(x)$ denotes the variation in received signal as a single point reflector is scanned in a simple line scan, then

$$L(x,z:y_o) = \sum_n a_n \delta(y_n - y_o)\, l(x - x_n)\, h(z - z_n)$$

$L(x)$ may vary with distance, z. An ideal C-scan can be described as a mapping of positions of the point reflectors which lie on a plane of constant $z = z_d$

$$C(x,y:z_d) = \sum_n a_n \delta(x - x_n)\, \delta(y - y_n)\, \delta(z_n - z_d)$$

For a real beam, C is approximately given by

$$C(x,y;z_d) = \sum_n a_n P(x - x_n, y - y_n\ ;\ z_d)\, \delta(z_n - Z_d)$$

where $P(x,y)$ = the variation of received echo signal from a point reflector as the transducer moves in the (x,y) plane. When a scanner completes many C-scans at different depths d, then the object is completely represented in three dimensions as

$$C(x,y,z) = \sum_n a_n P(x - x_n, y - y_n, z_n)\, h(z - z_n)$$

An object which consists of fixed point scatterers produces an image that depends on $P(x,y:z)$ and $h(z)$. Such an object is special in that it is the only object that can be chosen such that the Generating Function is uniquely defined and not dependent on the mode of scanning. Other objects, such as a

series of parallel lines which are scanned in a direction normal to the lines, possess this property for some scanning modes. For the fixed points only, the image may be described as a simple convolution of the Generating Function with the relevant scanner transfer function. The relevant scanner transfer function may itself be dependent on the mode of scanning e.g. the relevant beam profile for sector scans differs from that for line scans. Furthermore, as is shown in Appendix C, the transfer functions mentioned above, $P(x,y)$; $l(x)$, are themselves dependent on the choice of $h(z)$, so that the image can be written in the form

$$C(x,y,z) = GF(x,y,z) * h(z) * SF(x,y,z)$$

where SF = a transducer function determined by the shape of the transducer (and is related to TF of Appendix C). For any realistic object, such a simple equation is insufficient to describe the image. If the sound field scans then the viewpoint of the object relative to the transducer moves so that the Freedman points map a locus which is partly determined by the mode of scanning and partly by the nature of the object itself. Whereas the image, I, of a fixed point is described by an equation of the form

$$I(x) = \delta(x - x_0) * l(x)$$

a Freedman point on a real object moves so the image is

$$I(x) = \delta(x - x_0) * S(x)$$

where $S(x)$ describes the manner in which the highlight changes, which depends on $l(x)$, the intrinsic nature of the sound beam, on the mode of scanning and on the object curvature. For any except the simplest of objects, the process of image formation is not a simple linear convolution of generating function with

scanner filter function. However, Freedman's analysis enables a relationship to be made between simple fixed point scatterers and real objects, whilst it emphasises the importance of complex scanning procedures in determining the achieved resolution of a B-scan. For the purposes of evaluating different B scanners, and of deriving suitable criteria for resolution, the response of the scanner to a single fixed point reflector is sufficient to completely describe the intrinsic properties of the scanner. The Point Spread Function can be defined as the scanner response to a single point when scanned in all directions in a C-scan, and this will behave as a linear filtering function upon the ideal image of the point.

$P(x,y:z)$ = the normalised variation in signal amplitude received from a perfectly reflecting point moved in the (x,y) plane at distance z from and parallel to the transducer face.

This definition can be used with non planar transducers but the received signal amplitude must be clearly defined. As is shown later in this chapter, the emitted pulse shape varies throughout the sound field so that a single echo amplitude may not be readily defined. $P(x,y)$ could, for example, represent the integral of pressure with time, the average pressure or the peak pressure in the pulse, and the relevant choice depends upon the nature of the signal processing of the scanner. $P(x,y)$ can therefore be measured meaningfully for a total system only so that the effects of differentiation, integration or other operation are included in the measurement. However, if $P(x,y)$ is measured as an A-scan height or a B-mode intensity on present generation scanners, the important parameter is usually the peak pressure in the echo pulse, so

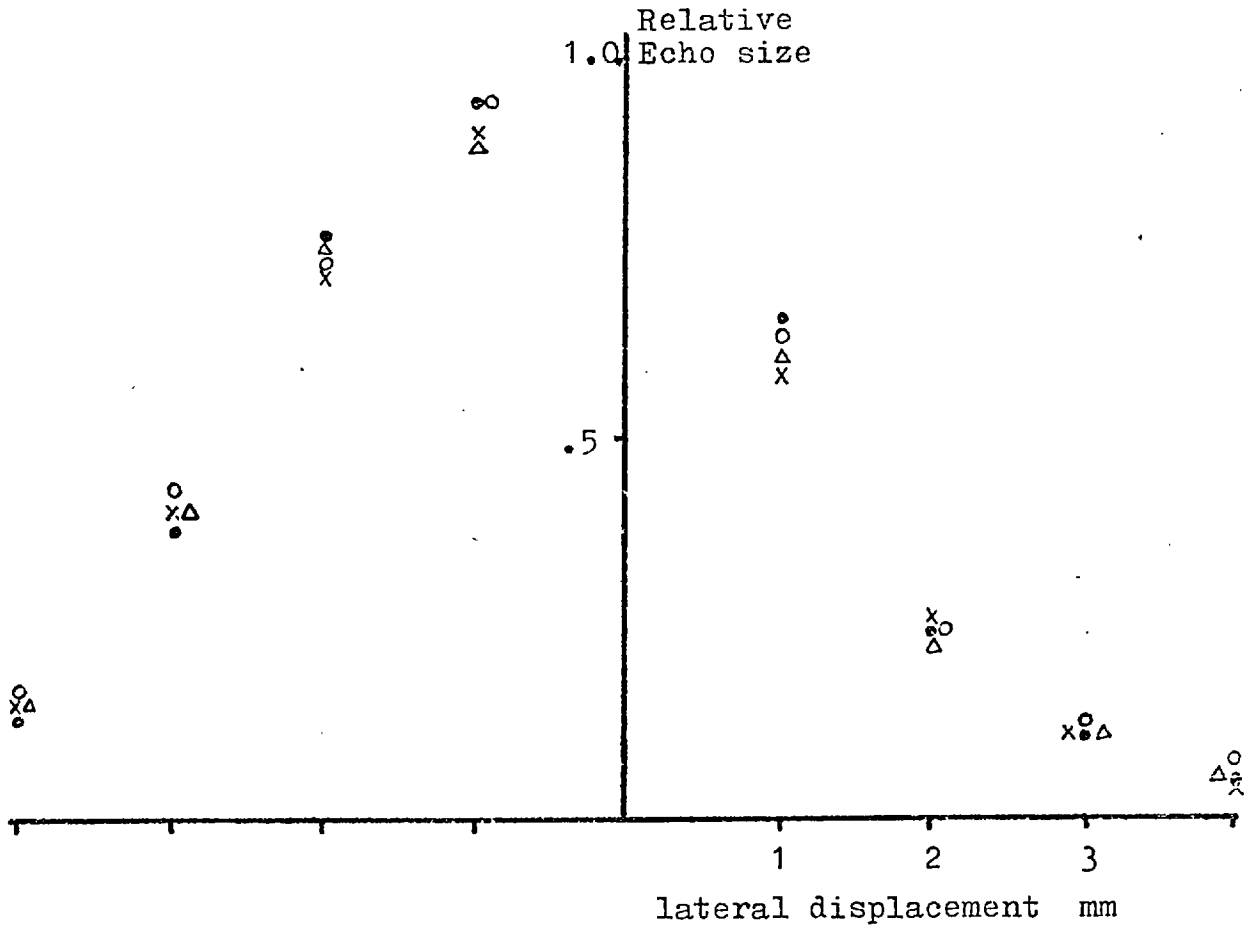
that P(x,y) is directly related to the maximum excursion from zero of the RF voltage induced at the transducer by the sound reflected from a point reflector.

The Point Spread Function defined and measured in this way is the Reflected Pressure Profile of Chapter 3 rotated about the transducer axis, if the sound field is cylindrically symmetric. Measurements of this function have often been used to compare scanners, but some experimental details remain undiscussed in the literature, and single indices of resolution have not been extracted satisfactorily.

5.3 The Point Spread Function

The reflector used to plot sound fields must be large enough to produce an echo of reasonable amplitude but small enough to act as a point reflector. Large spheres may possess directional scattering characteristics which can influence the apparent beam profile. The angular distribution of sound scattered from a sphere becomes omnidirectional as the radius to wavelength ratio decreases (Morse and Ingard 1968) but important directional characteristics are expected when the radius is greater than a few wavelengths. Since the spheres used in practice are a few millimetres in diameter, the importance of sphere diameter was checked experimentally. The lateral beam profiles of a transducer (centre frequency 1.5 MHz) were measured using spherical reflectors whose diameters varied from 0.8 mm to 12.7 mm. The normalised beam profiles are shown in Figure 5.3, from which it is seen that there was no discernible difference between these measurements. Furthermore, changing the material of the sphere from steel to plastic (nylon, perspex) made no difference. Hickling (1962) showed that a rigid, elastic sphere scatters a sound pulse in the same way as a point located on the sphere's surface, but his calculations of the variation of backscattered pressure with radius to wavelength ratio suggest that the sphere's material constants and diameter may be of considerable importance in selectively filtering the sound pulse frequency system, so that the echo spectrum is dependent on the choice of sphere. Such considerations do not appear to be important in practice, but they do suggest that the sphere must be chosen with caution.

Figure 5.3 Reflected Pressure Profiles for different sizes of spherical reflector. (1.5 MHz focussed transducer, at 6 cms)



Sphere diameter mm

• 12.7 ○ 6.3 × 2.4 △ 0.8

The Point Spread Function is a scanner transfer function which describes how a single fixed point is imaged on a C-scan. If it is measured with minimal small signal suppression and below amplifier saturation level by plotting with a sphere in degassed water then it may be called an intrinsic transfer function. Point Spread Functions vary in shape and it is this variation which makes a single beamwidth an unsatisfactory parameter to use as a measurement of resolution. In order to compare scanners in a quantitative fashion it is convenient to extract from $P(x,y)$ a single parameter which indicates the overall scanning ability. An integral transform of P includes the values of the Point Spread Function everywhere, and the widths and moments of such a transform may again be used as suitable indicators of the general shape of P. Whilst the selection of such parameters is arbitrary, some guidance may be derived from examining the shapes of real beam profiles.

Since $P(x,y:z)$ is a two dimensional amplitude distribution, it requires a two dimensional Fourier Transform to describe the distribution of spatial frequencies in the image of a point. However, when P is rotationally symmetric then the two dimensional transform may be simplified. In a polar coordinate system, if

$$x^2 + y^2 = r^2$$

then $P(x,y:z) = P(r,z)$.

An appropriate transform for such a function is the one dimensional Hankel Transform with zero order Bessel function as kernel. It is easily shown (Dainty and Shaw, 1975) that if $F(q,z)$ is defined from

$$F(q,z) = 2\pi \int_0^\infty P(r,z) J_0(2\pi qr) r \, dr$$

$$\text{then } P(r;z) = 2\pi \int_0^\infty F(q,z) J_0(2\pi qr) q \, dq$$

where $P(r,z)$ is normalised to $r = 0$.

$F(q,z)$ describes the spatial frequency response of the C-scan and it contains all the characteristics of the scanner which determine its intrinsic resolution. $F(q,z)$ is a surface which is rotationally symmetric and which in general is peaked at $q = 0$ and slopes down with increasing q, where q has dimensions of cycles per unit r. Such a surface is shown in Figure 5.4. The total volume under $F(q,z)$ is $V(z)$.

$$V(z) = 2\pi \int_0^\infty F(q,z) q \, dq$$

This volume is dependent on the overall imaging ability whilst the manner in which $F(q,z)$ decreases is determined by the relative ability of the scanner to detect and display different spatial frequencies. The width of $F(q,z)$ indicates this response and a useful width for describing the resolution is the Equivalent Frequency, which is the radius of the cylinder erected in q-space which has the same height as the maximum value of $F(q,z)$ and which encloses the same volume, $V(z)$. Such a cylinder is shown in Figure 5.4.

If the Equivalent Frequency is Q and if $F(q:z)$ is peaked at $q = 0$ (which is usually the case) then

$$V(z) = F(0,z)\pi Q^2(z)$$

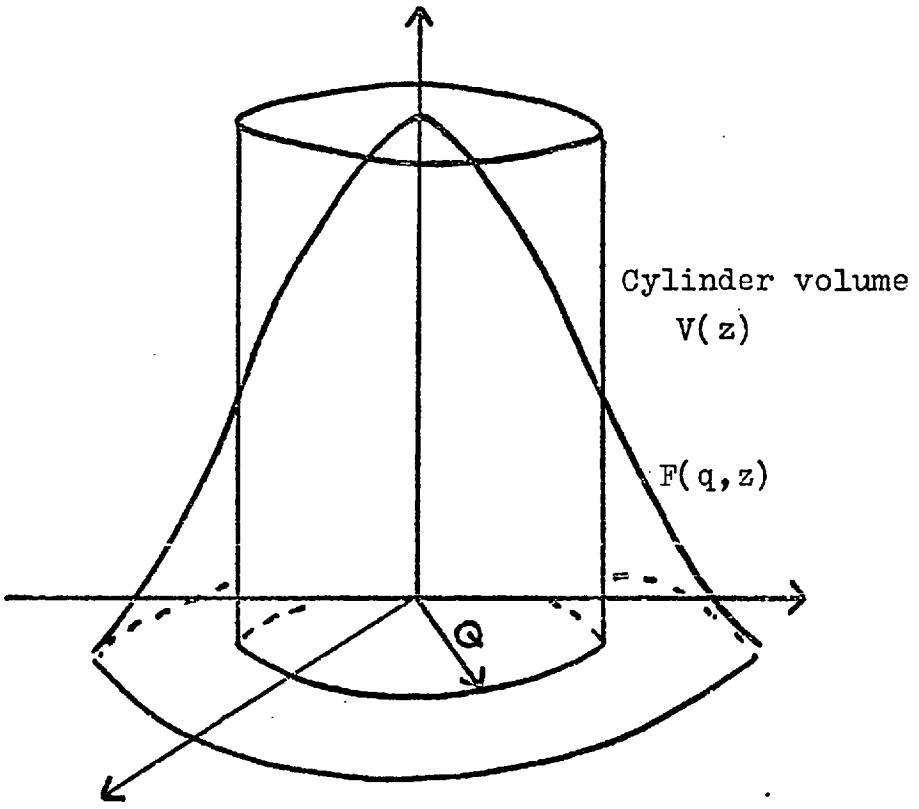


Figure 5.4 Illustration of definition of the Equivalent Frequency, Q , of a transducer response.

$$\pi Q^2(z) = \frac{2\pi \int_0^\infty F(q,z) q \, dq}{F(0,z)}$$

Q may be calculated from this equation after Hankel transformation of P(r), but this particular choice of width of F(q,z) has the advantage that it can be found by an alternative technique which avoids the integral transform. From the definition of F(q,z) it can be seen that

$$\pi Q^2(z) = (2\pi \int_0^\infty P(r,z) r \, dr)^{-1}$$

Thus, the Equivalent Frequency is inversely dependent on the volume under the Point Spread Function. This volume, in the spatial (image) domain, may similarly be replaced by an equivalent cylinder of the same height whose radius is R.

$$\text{i.e. } 2\pi \int_0^\infty P(r,z) r \, dr = \pi R^2(z)$$

$$\text{so that } Q(z) = \frac{1}{\pi R(z)}$$

Thus Q(z) can be calculated from the value of the first moment of P(r,z) which represents the volume of the Point Spread Function. From such a measurement, 2R(z) may be calculated, which is the beamwidth that corresponds to the diameter of the cylinder that has the same volume and height.

The volume under the Point Spread Function is the integral of the total signal recorded by the scanner for a point reflector. P(r,z) as defined above is normalised with its value at r = 0, but if the unnormalised profile is P'(r,z), where

P' is a signal on an absolute scale, then,

$$P'(r,z) = P'(0,z)P(r.z) .$$

Then, $2\pi \int_0^\infty P'(r,z)r\,dr$ = the volume under the unnormalised Point Spread Function, $S(z)$.

$S(z)$ is a measurement of the sensitivity of the scanner but it depends on the nature of the reflector. However, it can be made a useful standard for comparing different scanners by adopting a standard sphere reflecting in a water bath. Since the echo amplitude from a sphere is approximately proportional to the sphere radius (see Chapter 6) only the material of the sphere need be specified to allow quantitative comparisons of equipment, and steel spheres are suitable and readily available. For such a standard interface, therefore,

$$S(z) = \frac{P'(0,z)}{\pi Q^2(z)}$$

$P'(0,z)$ is the axial amplitude in absolute terms, and it varies with amplifier gain, transducer damping, z, etc. This equation relates a measurable scanner sensitivity to these variables and to a resolution area, πQ^2, in q-space.

Q may be interpreted in terms of the response of the scanner to simple objects other than spheres which are scanned in modes other than the ideal C-scan. If a straight edge is scanned by a linear scanner, the edge is not sharply defined in the image and such blurring may cause measurement errors or lead to a loss of image quality when boundaries are not clearly delineated. If the edge is scanned in a normal direction the resultant echo signal variation is $E(x)$, and such an Edge

Spread Function is shown in Figure 5.5. Similarly, the Line Spread Function, L(x), may be obtained by observing the variation in signal from a wire scanned in a direction perpendicular to its length (Figure 5.6). E(x), L(x) and P(r) are the intrinsic functions that determine the fidelity of B-scan images even though the exact form of an image depends on the pattern of scanning. These three functions are related for linear systems, and the experimental results depicted in Figure 5.7.suggest that these linear relationships are valid for ultrasonic scanners. In particular, the Line Spread Function is an Abel Transform of P(r,z)

$$L(x,z) = 2 \int_{x}^{\infty} P(r,z)\ (r^2 - x^2)^{-\frac{1}{2}}\ r\ dr$$

from which follows the Fourier Transform relationship

$$F(q,z) = \int_{-\infty}^{\infty} L(x,z)\ e^{-2\pi i q x}\ dx$$

The Edge and Line Spread Functions are related by

$$\frac{dE(x,z)}{dx} = L(x,z)$$

A commonly used quantity which is correlated to subjective impressions of the sharpness of an edge is the mean square gradient of the edge profile, which is the acutance, A (Wagner 1974)

$$A(z) = \int_{-\infty}^{\infty} \left| \frac{dE(x,z)}{dx} \right|^2 dx$$

$$= \int_{-\infty}^{\infty} |L(x,z)|^2\ dx$$

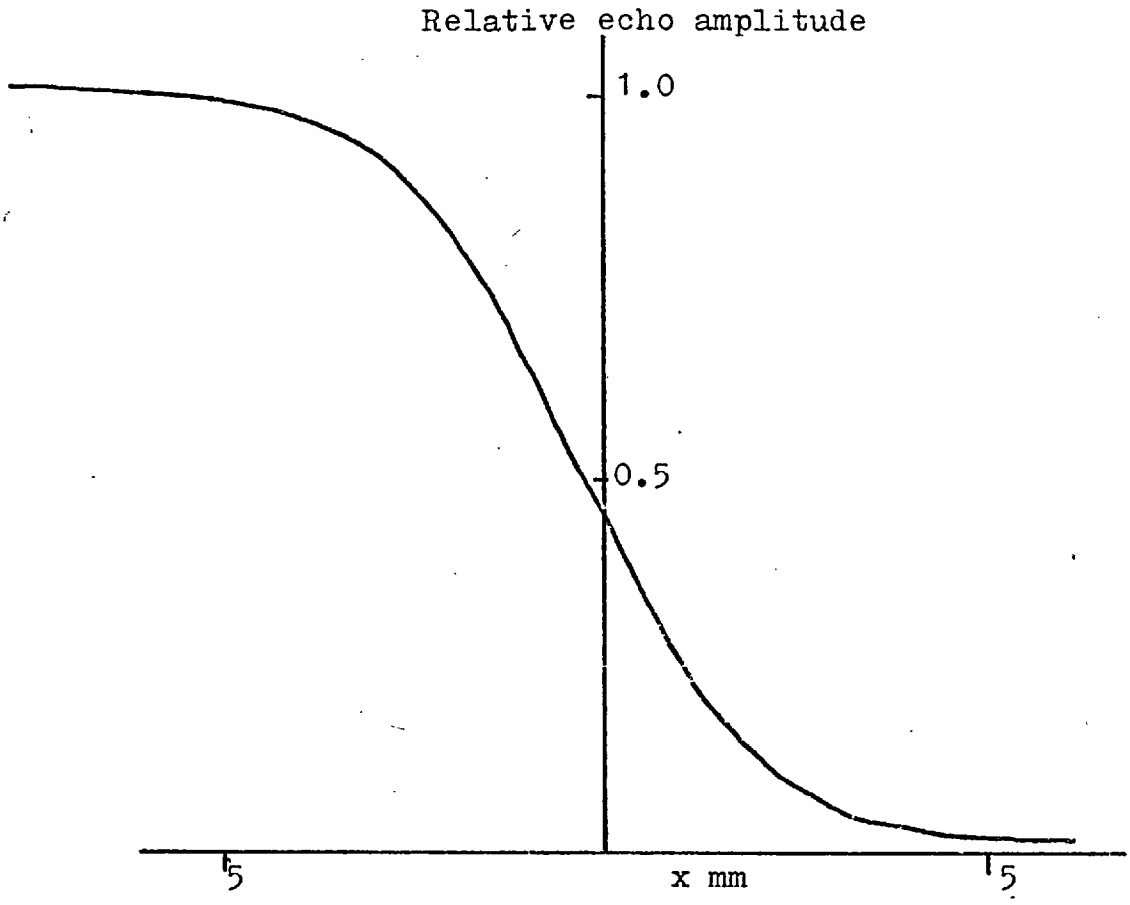
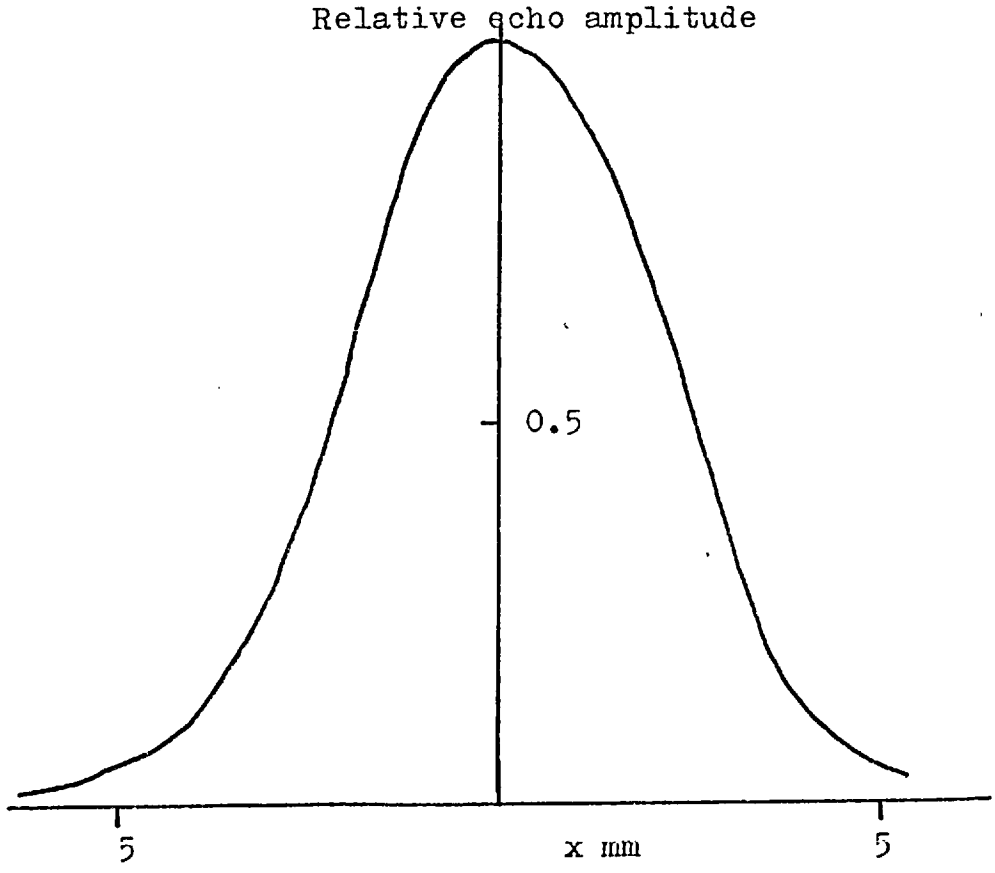


Figure 5.5 Measured Edge Spread Function, E(x)

Figure 5.6 Measured Line Spread Function, L(x)



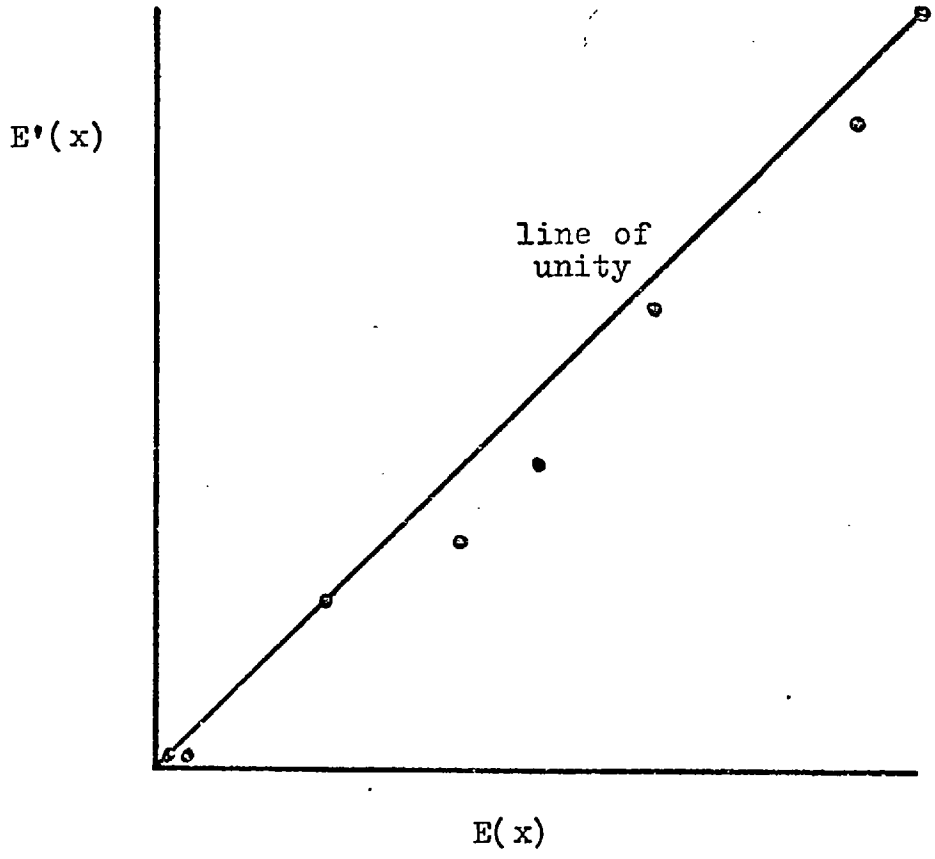


Figure 5.7 A comparison of the Edge Spread Function, E(x), measured experimentally, and E'(x), the Spread Function obtained by integrating a measured Line Spread Function.

$$E'(x) = \frac{\int_{-\infty}^{x} L(x)\ dx}{\int_{-\infty}^{\infty} L(x)\ dx}$$

which from Parseval's Theorem means that

$$A(z) = \int_{-\infty}^{\infty} |F(q,z)|^2 \, dq$$

The calculation of $F(q,z)$ from the Point Spread Function enables the acutance of an edge to be expressed simply. The Edge Spread Function represents the smearing out of an impedance step in the direction of the scan, and the acutance is a useful measure of the sharpness of the step. Furthermore, from the properties of the Abel Transform (Bracewell, 1965) it can be seen that

$$\int_{-\infty}^{\infty} L(x,z) \, dx = 2\pi \int_{0}^{\infty} P(r,z) r \, dr = \frac{1}{\pi Q^2(z)}$$

Thus, Q may be calculated by integrating the area under the normalised Line Spread Function. $L(x,z)$ may be measured by scanning a wire but the important quantity, its normalised area, is independent of gain settings, size and type of wire, etcetera.

Simple analytic expressions are not good fits to the beam profiles of most transducers. Some functions match the beam curvature near the axis (e.g. Gaussian curves) whilst others e.g. the exponential curve, fit well away from the transducer axis but are too sharp near the axis. However, for estimating the effects of changes on the Point Spread Function it is convenient to use simple approximations for which the Equivalent Frequencies may be easily calculated.

e.g. $P(r,z) = e^{-ar}$

This curve was found by Atkinson and Berry (1974) to be a good fit to their curves.

$$F(q,z) = \frac{2\pi a}{(4\pi^2 q^2 + a^2)^{\frac{3}{2}}}$$

$$R = \frac{2^{\frac{1}{2}}}{a}, \quad Q = \frac{a}{\pi 2^{\frac{1}{2}}}$$

R corresponds to the beamwidth at a level 12.3 dB below the maximum.

Similarly, suppose $P(r,z) = e^{-a^2 r^2}$

$$R = \frac{1}{a}, \quad Q = \frac{a}{\pi}$$

For this curve, R corresponds to the 8.7 dB beamwidth. Thus, the Resolution defined in this way is equivalent to measuring a single beamwidth but the value of the beamwidth level depends on the shape of the beam. This is an advantage of specifying the resolution in terms of a spatial frequency response.

A further useful interpretation of the Equivalent Frequency Q is that it can be used to construct an Equivalent Beam Profile, $P_E(r,z)$. This is the beam which is the exact Hankel inverse transform of the cylinder of radius Q. $P_E(r,z)$ has the same Equivalent Frequency, the same volume under $F(q,z)$ in the frequency domain, but it images perfectly up to frequency Q when its spatial frequency response cuts off sharply.

$$P_E(r,z) = \frac{2J_1(\frac{2r}{R})}{\frac{2r}{R}}$$

Such a function is a useful approximation to some beam profiles, and it provides a physical interpretation of the Equivalent Frequency.

5.4 Measurements of Point Spread Functions

The normalised profiles, $P(r,z)$, of a 1.5 MHz focussed transducer are shown in Figure 5.8 for various distances from the transducer. From these curves the volumes, $V(z)$, of the Point Spread Function were calculated, and the values of Q and R obtained are shown in Table 5.1. The axial signal variation, $P'(0,z)$ shown in Figure 5.9 was measured with a 6.3 mm radius steel ball. P' is the peak RF voltage at the output of the RF amplifier and Table 5.2 shows that the sensitivity, $S(z)$, measured as indicated above can be expressed in absolute terms for this reflector.

Figure 5.10 depicts the manner in which $Q(z)$ and $R(z)$ vary with z, and also shown are the values of the 10 dB beamwidths at various distances. The curve of $R(z)$ is almost identical to the locus of the 10 dB beamwidth, so that for the beam shapes of this transducer the 10 dB beamwidth is a parameter that has a well defined physical interpretation in terms of the spatial frequency response of the scanner.

Figure 5.8 Normalised profiles, P(r,z), measured for a 1.5 MHz focussed transducer at various distances z.

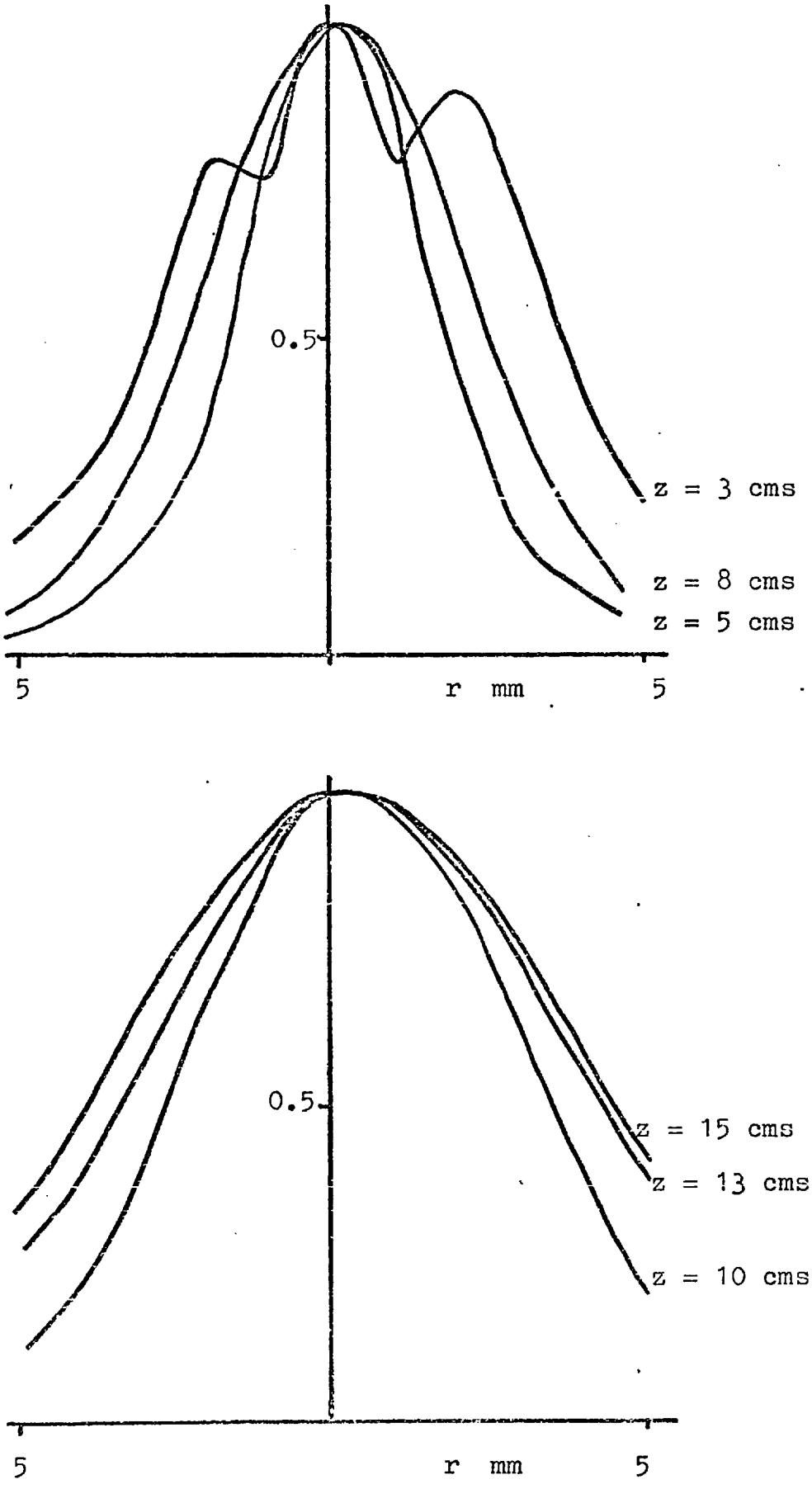


Figure 5.9 Axial signal variation P'(0,z) for 1.5 MHz focussed transducer

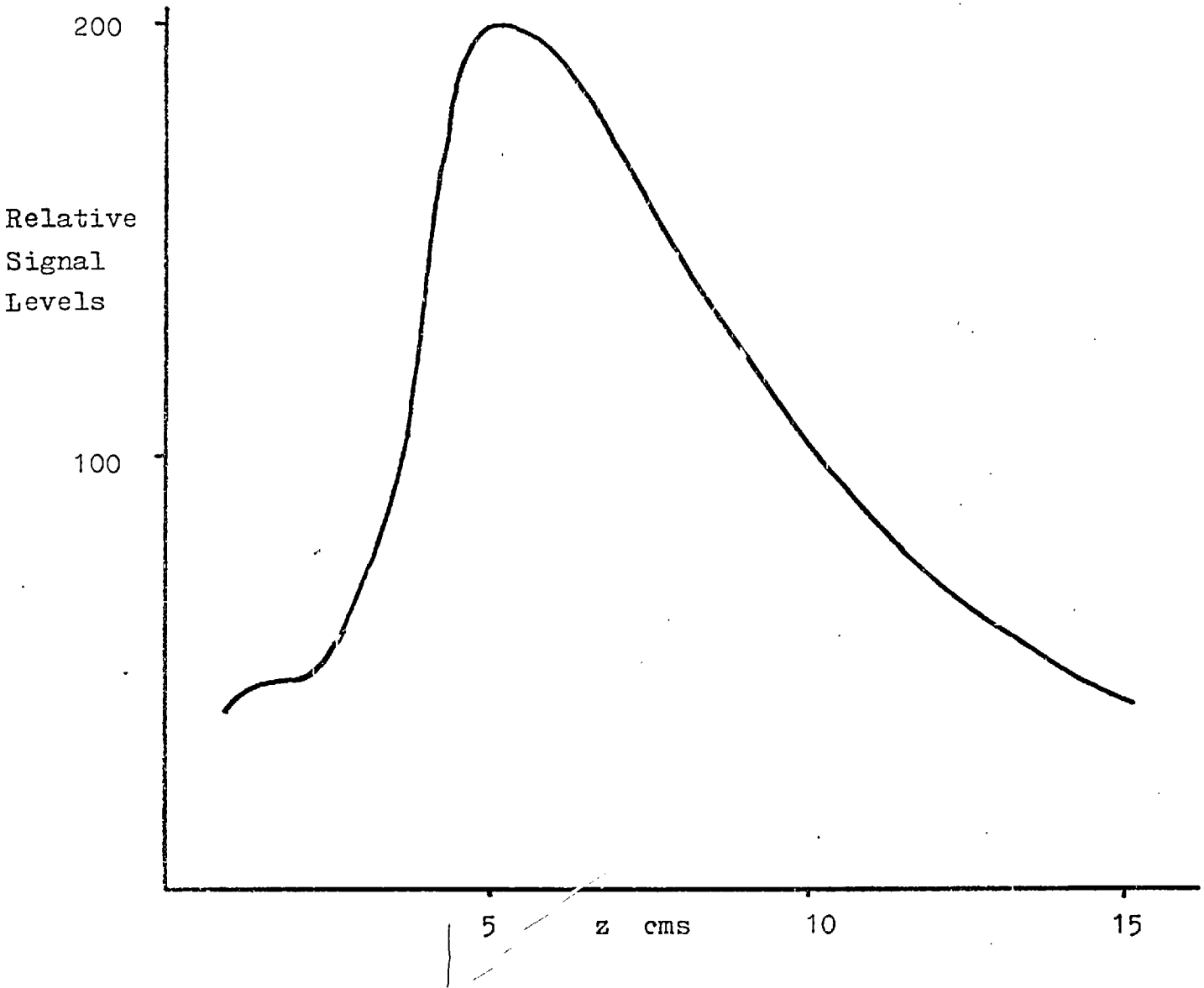


Table 5.1

Measurements of the Resolution of 1.5 MHz (focussed) transducer

z (cms)	V(z) (mm^2)	R(z) (mm)	Q(z) (cycles/mm)
3	53.5	4.13	0.77
5	17.6	2.37	1.34
8	31.6	3.17	1.00
10	45.1	3.79	0.84
13	69.2	4.69	0.68
15	93.0	5.44	0.59

Figure 5.10 Comparison of the functions Q(z) , R(z) , and the 10 dB beamwidth for a 1.5 MHz focussed transducer.

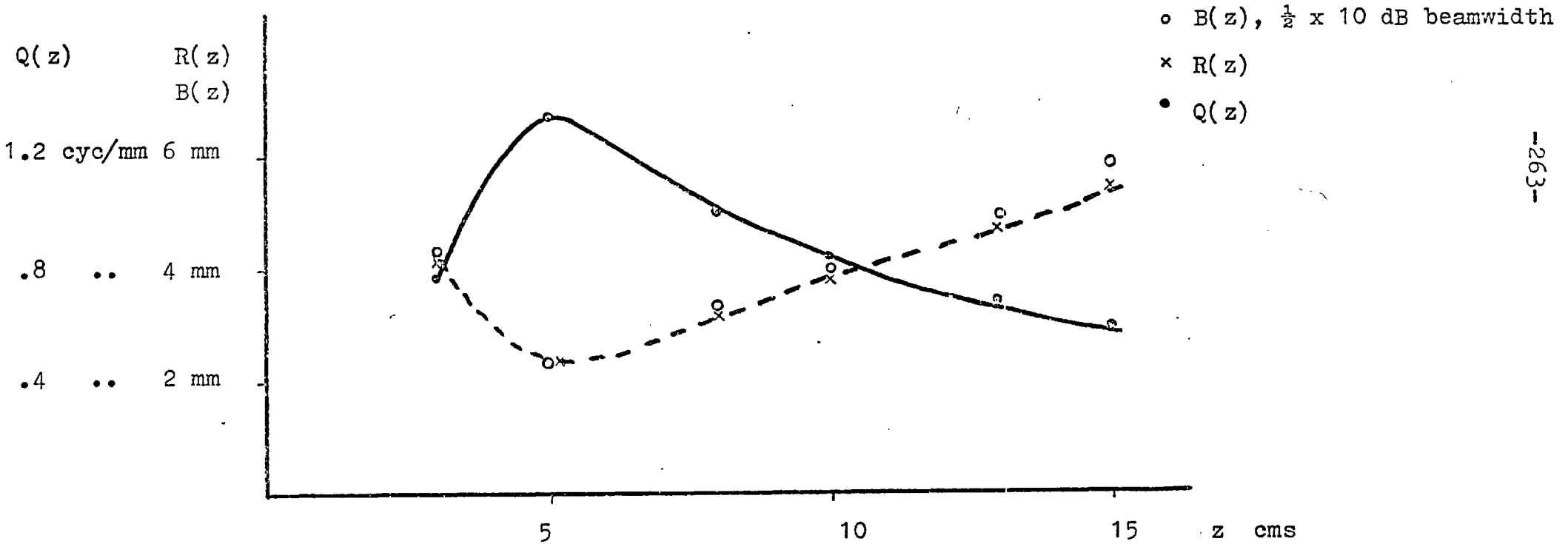


Table 5.2

Sensitivity of a 1.5 MHz transducer

z	P'(0,z) (volts	S(z) (volts.mm^2)
3	1.16	62
5	2.85	50
8	2.00	63
10	1.40	63
13	0.82	57
15	0.58	54

S(z) measured for 6.3 mm radius sphere of steel in water.

5.5 Some factors affecting the Equivalent Frequency

The achieved resolution must again be distinguished from the intrinsic resolution, but often the former may be estimated when the latter is known, and some examples of such calculations are given here.

(a) Effect of Threshold

A suppression control changes the detection threshold of a scanner by removing small signals, which subtracts the base of the Point Spread Function, thereby changing the volume under its surface as well as its maximum amplitude. Suppose the suppressor removes all amplitudes below a value T from the normalised Point Spread Function ($0 < T < 1$). With no suppression, P(r) cuts off at some radius r_1, so that the volume under P without suppression is

$$V_1 = 2\pi \int_0^{r_1} rP(r)\, dr = \pi R_1^2 ,$$

Introduction of a suppression of amplitudes below T means that the cut off radius is reduced from r_1 to r_2. The new Point Spread Function is

$$P_2(r) = \frac{1}{1-T} \quad (P(r) - T) \quad 0 < r < r_2$$

$$= 0 \qquad\qquad r \gg r_2$$

The volume is reduced to V_2

$$V_2 = 2\pi \int_0^{r_2} r\, P_2(r)\, dr = \pi R_2^2$$

Thus, $(1-T)\pi R_2^2 = \pi R_1^2 - V_{REM}$

where the volume removed by suppression is

$$V_{REM} = 2\pi \int_{r_2}^{r_1} rP(r)\,dr + T\pi r_2^2$$

If $R_2 = \alpha R_1$, then

$$\alpha^2 = \frac{1}{1-T}\left(1 - \frac{V_{REM}}{V_1}\right)$$

When $T = 0$, $\alpha = 1$, whilst α decreases to 0 as T tends towards unity. The change in resolution is quantitatively given by α. Furthermore, the new sensitivity can be described as

$$S_2 = \pi R_2^2 \; P_2'(0,z)$$

$$= \alpha^2 (1-T) S_1$$

so that the change in sensitivity may be estimated.

Similarly, altering the receiver gain increases the sensitivity, and the volume of the Point Spread Function above the detection threshold increases. The resultant decrease in resolution can be found.

(b) Effect of Non linear Amplification

A non-linear response e.g. a logarithmic amplifier, may amplify small signals more than large signals, thereby broadening the Point Spread Function and increasing its volume. If the signals into such an amplifier are $P_{in}(r)$ and the signals out are $P_{out}(r)$, then

$$P_{out}(r) = k_1 P_{in}(r) + k_2 P_{in}^2(r) + k_3 P_{in}^3(r) \ldots\ldots$$

The constants k_2, k_3.... describe the degree of signal compression, and are all zero for a linear amplifier. Thus, the volumes under the Point Spread Function for linear and non linear responses are related as

$$V_{\text{non-linear}} = V_{\text{linear}} + \sum_{n=2} k_n \int_0^{\infty} P_{in}^{n}(r) r \, dr$$

The last term represents the effect of the non-linear response on the resolution of the scanner.

(c) Effect of Bistable displays

A non-linearity of particular importance in the overall response is the echo amplitude-display brightness characteristic, which for bistable tubes is a discontinuous step function at some threshold amplitude T. The Point Spread Function for a bistable system is a cylinder whose radius, r_T, depends on the detection threshold level of the scanner.

$P(r) = 1 \qquad r < r_T$

$= 0 \qquad r > r_T$

The Equivalent Frequency is $Q = \frac{1}{\pi r_T}$. As the threshold increases so r_T decreases, and the resolution improves.

(d) Effect of Focussing

Focussed transducers are used to improve the lateral resolution over limited regions of the sound field. Kossoff (1963), following the ideas of O'Neill (1949) derived a dimensionless parameter from the dimensions of a spherical radiator to describe the degree of focussing of such a transducer. Such a parameter, however, is inapplicable to transducers

which radiate wide band pulses, it does not describe the degree of 'unfocussing' of the sound field away from the focal region, and it cannot be used with non-spherical radiators. Even plane transducers may be considered focussed in the Near Zone. Furthermore, such a dimensionless parameter does not give any indication of the absolute resolution of the beam. In order to compare two transducers quantitatively, two useful quantities may be extracted from the shape of $Q(z)$. Firstly, an overall impression of the average resolution of the scanner can be obtained from the volume of rotation of $Q(z)$ about the transducer axis. In calculating this volume, the limits of integration can be adjusted to include only that region of tissue of interest to the user. Thus, if an application involves only a region between distances z_1 and z_2, the volume of resolution is U.

$$U = \int_{z_1}^{z_2} \pi Q^2(z)\, dz$$

Secondly, an indication of the degree of focussing of the sound beam is given from the curvature of $Q(z)$, and the sharpness of the maximum of $Q(z)$. This can be denoted by f. The radius of curvature of $Q(z)$ is

$$\frac{(1+(\frac{dQ}{dz}))^{\frac{1}{2}}}{\frac{d^2Q}{dZ^2}}$$, so that at the maximum of $Q(z)$, $f = \frac{d^2Q}{dz^2}$.

f may be calculated for any transducer, and Figure 5.11 shows the results of measurements made on the 1.5 MHz transducer considered earlier.

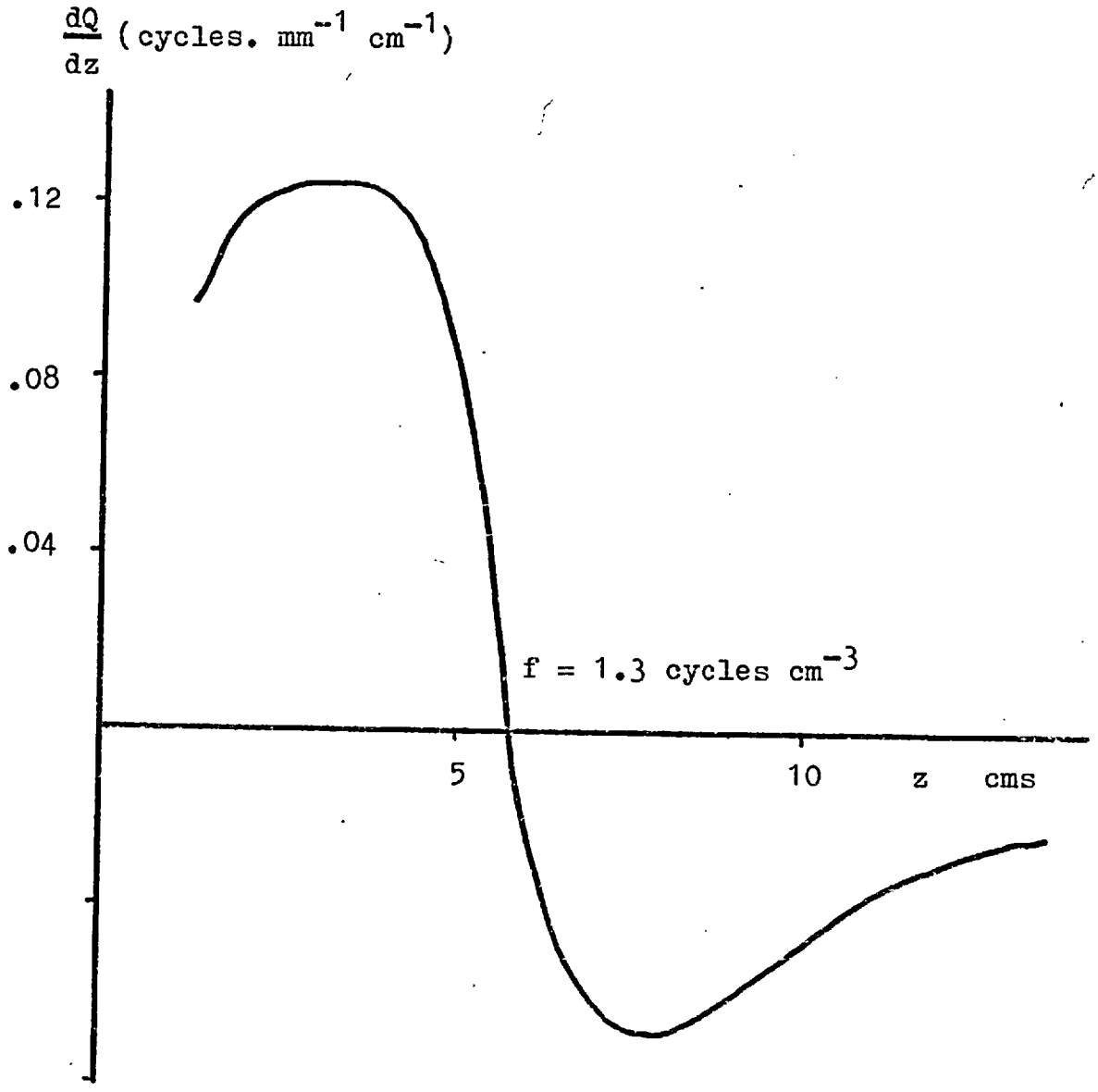


Figure 5.11 Measured values of the rate of change of the Equivalent Frequency with distance, $\frac{dQ(z)}{dz}$.

5.6 A consideration of factors that determine the intrinsic Point Spread Function

P(r,z) depends on the signal processing used in a scanner, and the achieved resolution varies with several independent factors. However, a prime influence on P is the variation in pressure incident on the sphere used to plot the sound field, and the factors that determine this emitted pressure profile are also fundamental to the resolution. These factors are considered here and the intrinsic transfer function of the transducer is derived. Whereas some features of transducer design are well understood, other are based on theories which are inapplicable to transient conditions and it is necessary to consider from first principles the formation of a pulsed sound field.

(a) The sound field from a pulsed transducer

The variation of pressure in the emitted sound field of a transducer is well understood for plane transducers radiating continuous monochromatic waves, but the behaviour of transient field patterns have not been documented so well. The diffraction patterns obtained with continuous excitations are not useful indications of the patterns obtained with wide bandwidth pulses since pulsed conditions do not allow the strong interference phenomena of the CW field to form. Usually, wave fields are calculated by superposing contributions from elementary sources with regard to phase and amplitude, and diffraction minima may then arise because wave phasors cancel destructively. A simple consideration of the effect of overlapping two identical pulses shows that a complete cancellation

is impossible even with a phase difference of π

When two pulses overlap the resultant acoustic signal may show a complex variation in shape and amplitude depending upon the degree of overlap, and this variation considerably confuses an exact calculation of the transient field. Furthermore, because the transducer is a relatively large aperture, the region of interest here usually lies in the 'Near Field' in which the Fraunhofer approximation is not valid, so this mathematical convenience is not valid. Several authors have discussed Near Field transient patterns e.g. Morse and Ingard (1968), Freedman (1970a), and several methods have been reviewed by Freedman (1970b). In Appendix C, the near field structure of a plane transducer is derived by extending the Kirchoff integral to polychromatic excitations from which the sound pressure at a point as a function of time may be derived by Robinson's method (1974). The pulse structure is determined by the way in which the area of radiator contributing to the sound varies with time. It is shown that both the near and far field pressures from a plane transducer may be written in the form

$$p(\bar{r},t) = TF(\bar{r},t) * h(t)$$

where $\bar{r}$ is a field coordinate defined in Appendix C and $h(t)$ is the velocity of the transducer face. The intrinsic transducer function in transmission is $TF(\bar{r},t)$, the pressure distribution when the velocity is a Dirac impulse, but it is often more convenient to consider the related function $\phi(\bar{r},t)$ that describes the velocity potential in the field. It may be deduced from the results derived in Appendix C that the field

for an impulsive motion shows the following characteristics.

(i) On the transducer axis, the velocity potential waveform is a rectangle of duration T

$$T = \frac{(z^2 + a^2)^{\frac{1}{2}} - z}{c}$$

The acoustic pressure on axis consists of two δ-functions of opposite sign, separated by an interval T. As z, the distance from the transducer, increases, so these two δ functions approach each other and for large distances

$$T \doteq \frac{a^2}{2cz}$$

The impulse amplitudes are the same for all z.

(ii) At a distance y off the axis but still inside the cylinder defined by the transducer, the velocity potential shows a discontinuous step up at a time $t_o = \frac{z}{c}$, which is followed by a period of duration

$$t_1 - t_o = \frac{1}{c}((a^2 + y^2 - 2ay + z^2)^{\frac{1}{2}} - z)$$

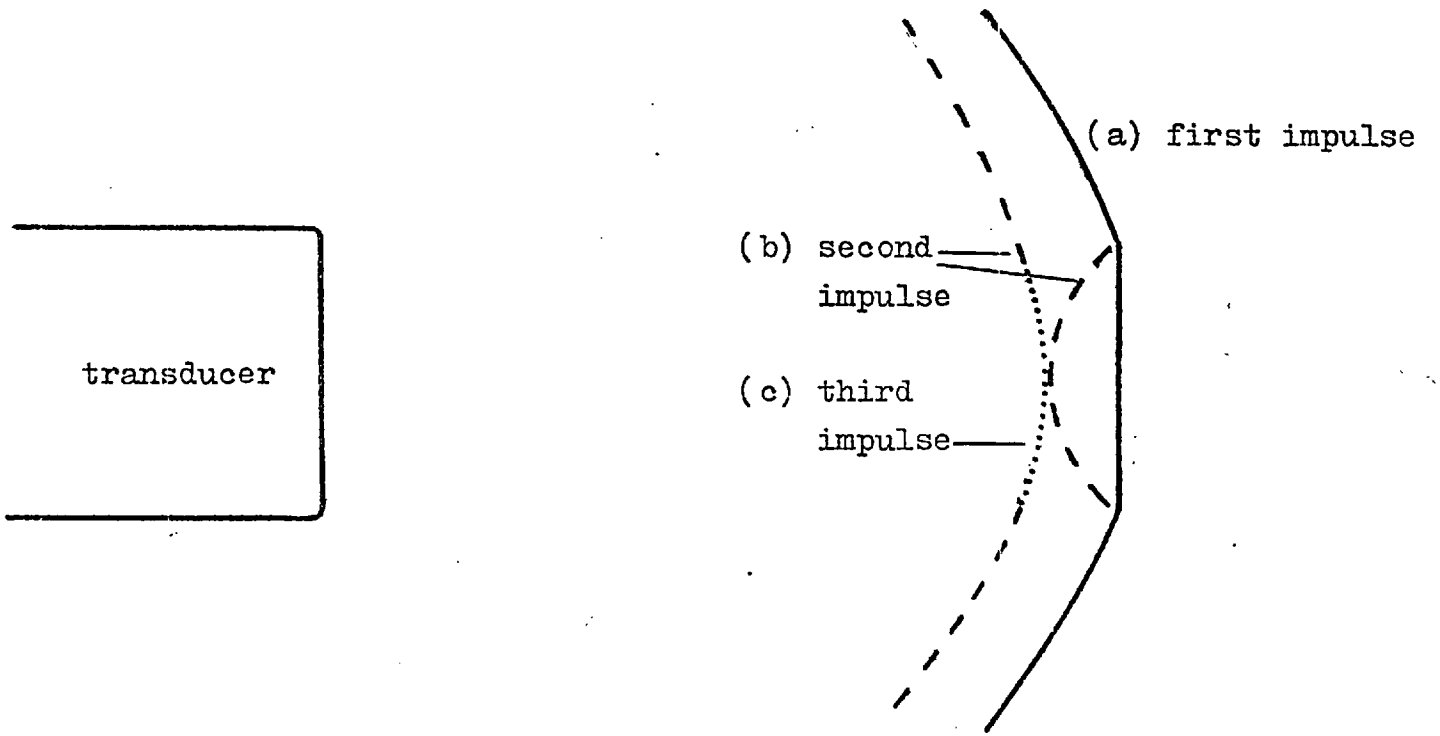
in which the velocity potential remains constant (this corresponds to the period in which the contributing annular elements are complete circles). This is followed by a period in which the velocity potential decays monotonically to zero. The pressure waveform is therefore an impulse at time $\frac{z}{c}$, followed by a period with no disturbance, followed by a transient of opposite sign which is not a delta function but has finite bandwidth. The amplitude of the initial impulse is constant for all values of y less than the transducer radius.

(iii) Outside the cylinder, the velocity potential rises and decays, but the waveform is never flat and it is always of smaller amplitude than the axial rectangle.

The initial impulse arrives at the same instant at all points in the circle of radius a in a plane parallel to the transducer face. Outside the cylinder defined by the transducer, the wavefront which is the locus of the initial impulses bends back towards the transducer. Inside the cylinder the disturbance forms a plane wavefront and the isochronal surface for the initial disturbance is as shown in Figure 5.12a. The secondary impulses, which mathematically can be seen to arrive from the near and far points of the transducer edge, correspond to Freedman's replica pulses. Robinson (1974) analysed the degree of distortion of these impulses when compared with Dirac impulses, and showed that this depends upon the position in the sound field. At points off the transducer axis, there are three impulses separated in time and some calculated shapes are given in Appendix C. Whilst the surface of Figure 5.12a is isochronal to the initial impulses, it cannot be isochronal to the second and third impulses. Figures 5.12b and c show the shapes of surfaces which are isochronal for these components. There is therefore no clearly defined single isochronal surface for a transducer excited with very short pulses.

Inside the cylinder of radius a, the maximum pressure at a point is reached at the instant the initial impulse arrives at the point (at $t = \frac{z}{c}$), so that a plot of maximum pressure amplitudes would show no variation throughout the cylinder. If the transducer face undergoes a step displacement, the sound

Figure 5.12 The shapes of isochronal surfaces for different components of the pulse from an impulsively excited plane transducer.



beam profiles are flat for a width 2a, beyond which they decay to zero. The analysis predicts no transverse peak pressure variations, nor any axial pressure oscillations as in the CW case. The beam shows no side lobes. The pulse shape at any point in the field is given by the transducer 'shape function', $TF(\bar{r},t)$, so that the production of very short pulses from a transducer is limited not merely by the crystal impulse response, but also by its shape and size. The implications of this for A scans are considered further in Section 5.6.

The transient field produced by a general excitation may be calculated by the convolution of transducer face velocity with $TF(r,t)$

$$p(\bar{r},t) = \rho\frac{c}{\pi} h(t) * \frac{\partial\theta(ct)}{\partial t}$$

(Appendix C, Equations 7 and 8).

(i) On axis, the total disturbance consists of a pair of pulses identical in shape to the velocity waveform, separated in time and with opposite sign. These replica pulses overlap when the pulses are longer than T, whilst shorter pulses are clearly separable. Since T depends on z, then the degree of overlap of the pulses varies with distance from the transducer, thereby resulting in a variation in axial pressure amplitudes. The severity of these axial pressure variations lies between the extremes of CW excitation and Dirac impulse excitations, and it depends on the transducer bandwidth. If the transducer impulse response is of short duration, the energy of the acoustic disturbance is distributed over a broad band of frequencies and at any position in the field some of these

frequencies may cancel when the replica components overlap, but others may interfere constructively. As the impulse response lengthens, its frequency spectrum narrows, so that destructive interference between the component impulses causes a cancellation of a much greater fraction of the total signal. The degree of variation of the axial peak pressures is therefore a measure of the transducer bandwidth for a shock excited transducer, and an axial beam plot may be used to infer the shape of the sound pulse.

If $h(t)$ is quasi-monochromatic e.g.

$$h(t) = a(t) \cos w_o t \quad , \quad w_o = \frac{2\pi c}{\lambda}$$

then axial pressure maxima or minima may be expected at values of T that correspond to path differences of $(2n+1)\frac{\lambda}{2}$ and $2n\frac{\lambda}{2}$ respectively, as long as the envelope, $a(t)$, does not vary rapidly over distances of order $\frac{\lambda}{2}$. As for a CW excitation, minima are expected at values of z given by

$$z = \frac{a^2 - n^2\lambda^2}{2n\lambda}$$

For n = 1, the minimum may be quite pronounced if the pulse is a few wavelengths long, but for larger values of n, the shape of the component impulses becomes increasingly important. When these components are separated to such an extent that the tail of the first interferes with the peak of the second, they can not cancel to a significant extent with the result that as n increases, the peak axial pressure tends to a constant value. The number of axial minima and the severity of the axial pressure oscillations are therefore inversely dependent upon the ratio of the spread of frequencies contained in the envelope

spectrum to the carrier frequency i.e. the transducer's bandwidth. Figure 5.13 shows axial pressure plots obtained with a 20 mm diameter, plane 1.5 MHz transducer. These curves confirm the changes in axial pressure oscillations which occur as the pulse length increases from the minimum obtainable (shock excitation) to the CW case. Variable pulse lengths were obtained using the transmitter of Figure 5.14 which produces a short oscillating voltage pulse.at the resonant frequency of the transducer. The excitation envelope, a(t), is determined by the damping of the LCR output circuit.

(ii) Off axis, but inside the cylinder of radius a, the first impulse produces an exact replica of the face velocity waveform whose amplitude is not dependent on y. The other components produce distorted pulses with narrower bandwidths. There is a variation of peak pressure amplitudes across the beam which depends on the pulse shapes and carrier frequency. The total pulse shape varies across the beam. The degree of variation depends on the manner in which the separation of the replica components changes across the beam, relative to the wavelength. The shape variation is unimportant when the condition

$((a-y)^2 + z^2)^{\frac{1}{2}} - z \ll \lambda$

is satisfied. Since $z \gg \lambda$ usually, then this becomes

$(a-y)^2 \ll 2z$.

The lateral beam profile is not flat inside the cylinder because the replica pulses overlap and interfere, and consequently the Point Spread Function is dependent on the shape of the replica components. The beam profile can be changed by using

Figure 5.13 Axial pressure variations from plane 1.5 MHz transducer for different excitations.

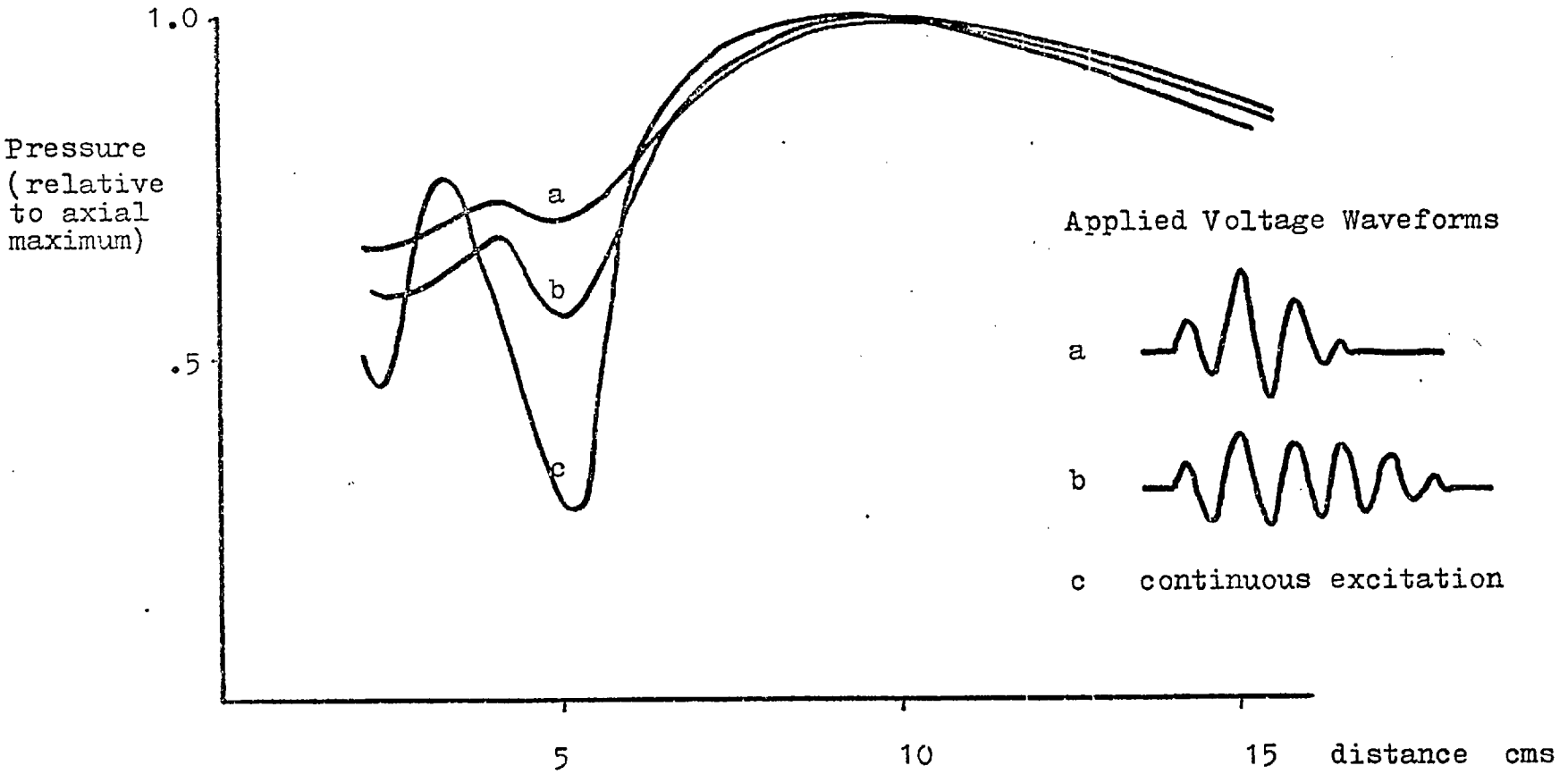
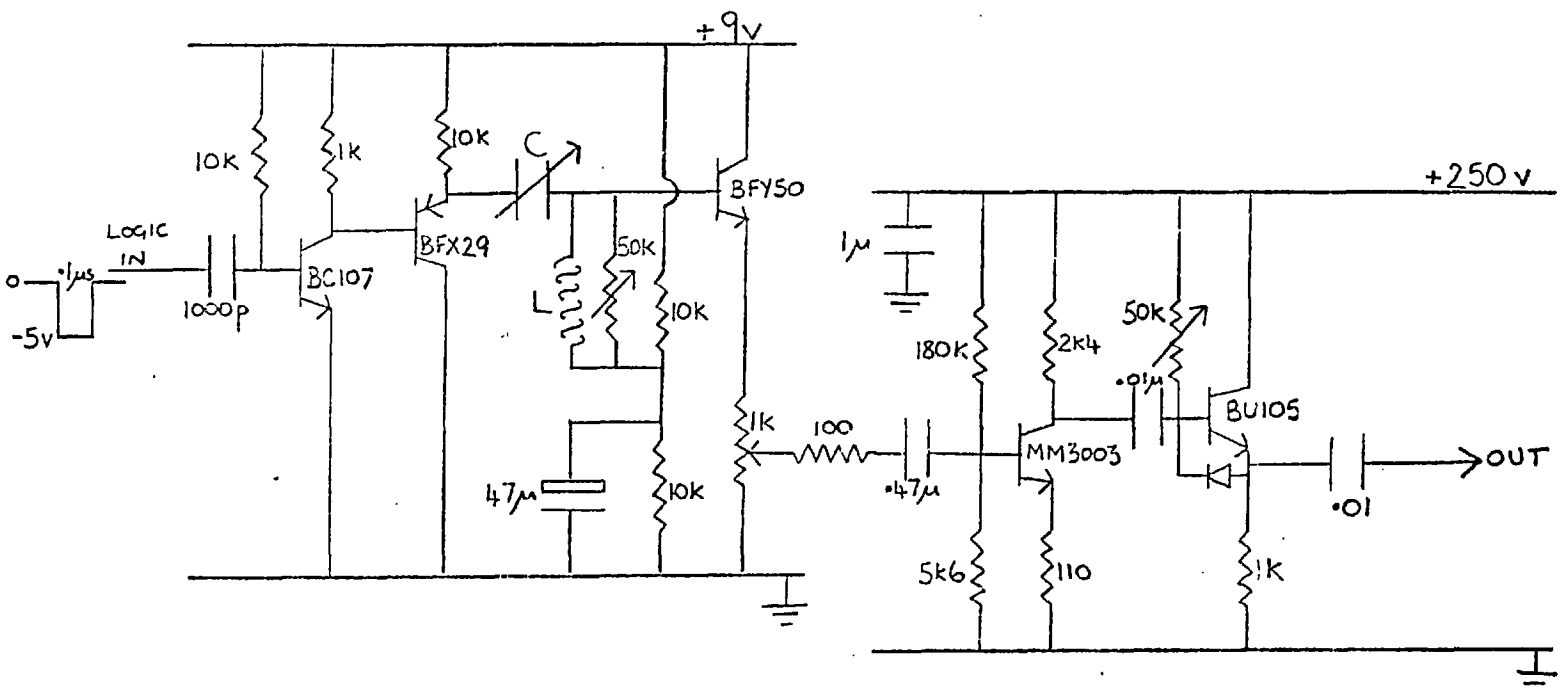


Figure 5.14 Circuit diagram of RF pulse generator used to vary excitation of transducer



different transducer excitations and the Point Spread Function can be changed by altering the bandwidth of the scanner receiver.

The beam profile should ideally be peaked on the transducer axis and it should fall rapidly away off axis, but this amplitude decay can only be achieved by destructive interference between replica components. The rate of decay, which is the sharpness of the lateral profile, depends upon the rapidity with which the separation of replica components decreases for a given displacement from the axis. In the coordinate system of Figure 5.15 the separation of the components is d.

$$d = h - z$$

$$\frac{dd}{dy} = -\frac{(a-y)}{h} = -\sin\theta$$

The path difference decreases most rapidly if θ is large so the beam is sharpest for large transducers. However, as θ decreases the profile curvature decreases whilst the third replica component moves away from the other two. Whereas the Near Field pattern of a continuously excited transducer shows secondary maxima across the beam, these will not be apparent in the pulsed field if the pulse is sharply peaked. Instead, the replica pulses separate and their amplitudes fall off slowly.

(b) Design considerations for pulsed fields

The analysis above illustrates the dependence of the emitted sound field, and therefore the Point Spread Function, on the size and velocity of a transducer face.

(i) The sound pulse shape varies throughout the sound field, and this implies that the usefulness of a transducer depends

Figure 5.15 Coordinate system used to calculate replica pulse separations (see text)

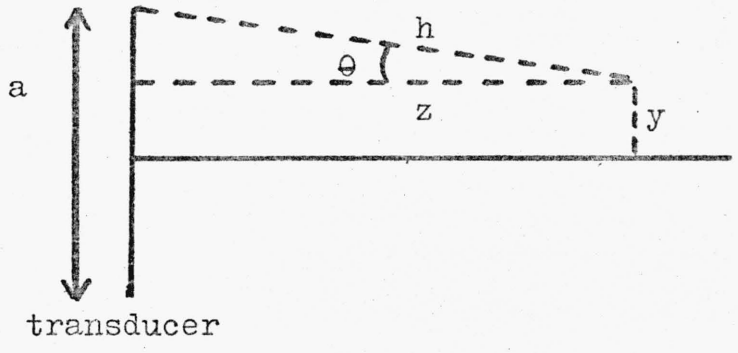
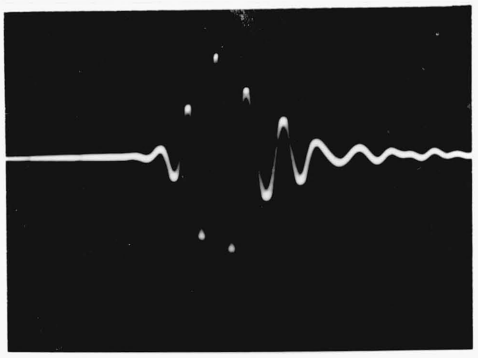
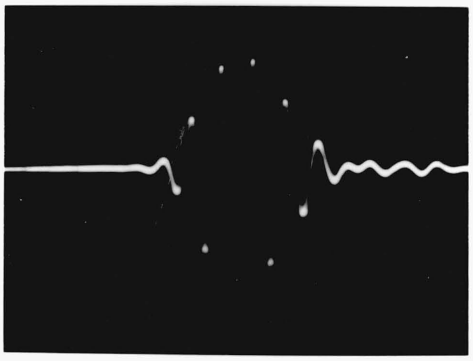


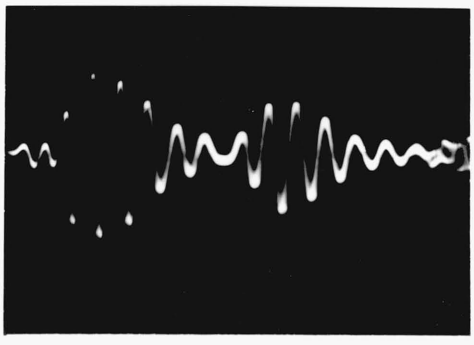
Figure 5.16 Observed replica pulses in the field of a plane 2.5 MHz transducer, radius $7\frac{1}{2}$ mm, at 3 cms depth of water



z = 3 cms
y = 0
x 1 gain



z = 3 cms
y = 3 mm
x 3 gain



z = 3 cms
y = 7 mm
x 10 gain

on the nature of the receiver signal processing - a transducer could have relatively good resolving ability if the peak pressure of the echo is recorded, whereas it could be relatively poor if the echo is integrated by the receiver. Although the Point Spread Function as defined earlier is a sufficient description of the overall system, a single pulse amplitude is not a sufficient description of the sound arriving at any field point.

(ii) The emitted beam shape depends on the size of the transducer which should be large to obtain sharp beams near the axis. However, it is not necessarily true that the beamwidth of a large transducer is smaller than that of a small transducer at all levels, and the converse is often found towards the edges of the sound field. Here the rates of change of the amplitudes of the individual replica components begin to influence the beam profile. At the edge of the cylinder defined by the transducer the lateral pressure variation is no longer solely dependent on interference effects because even the intrinsic function $TF(\bar{r},t)$ begins to decrease. This decay occurs nearer to the transducer axis when the transducer radius is small.

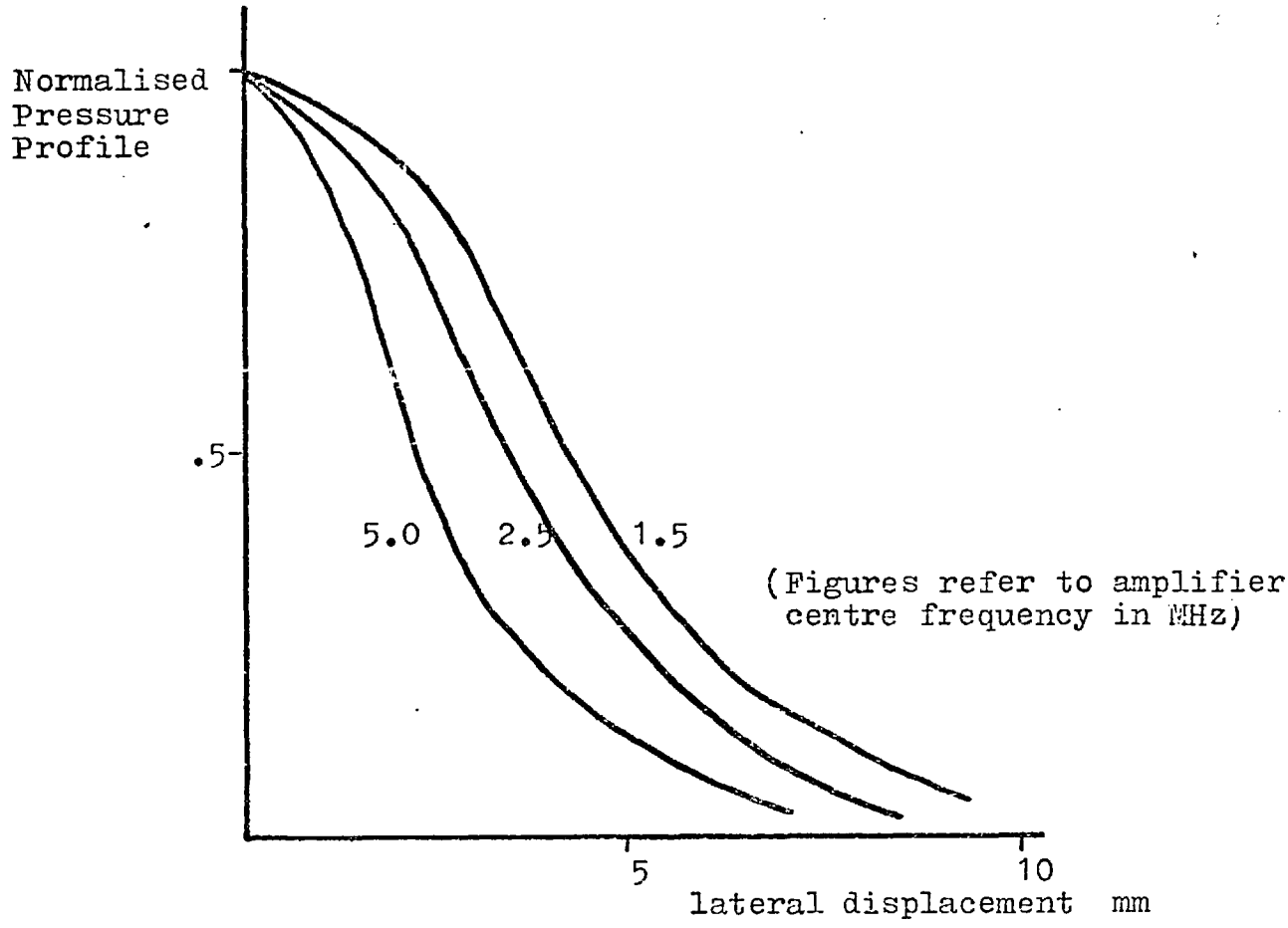
(iii) At some positions of the field the replica pulses separate to such an extent that two or more pulses are clearly distinguishable, and an example of this splitting is shown in Figure 5.16. To completely characterise a beam the variation of each of the replica components should be plotted separately. In particular, the intrinsic transfer function of the transducer could in principle be obtained by deconvoluting the

pulse at any position, $p(\bar{r},t)$, with $h(t)$, and three beam profiles would then be obtained corresponding to the three principal components of $TF(\bar{r},t)$. Furthermore, if two replica pulses are separable by the signal processing then the Point Spread Function will contain two surfaces displaced in distance from the transducer. Such artefacts are considered in the final section of this chapter.

(iv) When a beam profile is measured, either with a piezoelectric sensor or with a spherical reflector, the bandwidth of the signal amplifier affects the measured profile. In Figure 5.17 are shown the emitted pressure profiles from a transducer, measured with a piezoelectric needle probe from which the signals were amplified by the tuned RF receiver of the NE4102 (see Chapter 3). The effect of changing the receiver bandwidth is equivalent to changing $h(t)$ in the expression for $p(\underline{r},t)$. It is not therefore sufficient to describe a transducer by its centre frequency and size alone. The total system frequency response must also be specified. Furthermore, it is not satisfactory to measure transducer sound fields with equipment whose frequency response is not the same as the scanner with which the transducer is to be used, unless it is the intrinsic transfer function, $TF(\bar{r},t)$, which is to be determined.

(v) The analysis of the structure of the Near Field shows that two extreme situations can arise. The sound field produced by a Dirac impulse is uniform, the lateral beam profile is flat and resolution is poor. Severe artefacts can arise because of the separation of replica components. The field of

Figure 5.17 Effect of measuring system frequency response on pressure profiles obtained



a monochromatic radiator shows strong interference phenomena, and the resolution is degraded by the formation of secondary maxima off axis and side lobes, whilst no axial resolution is obtainable. The optimum pulse length must lie between these extremes and Robinson's description of the formation of the sound field suggests that the pulses used with scanners now may be near this optimum choice. They are peaked sharply enough to prevent secondary maxima forming off axis, yet they are quasi-monochromatic and allow strong primary maxima to form on axis.

(vi) The analysis of the field of a plane piston can be used to obtain at least a qualitative understanding of the behaviour of focussing transducers and the effects of using arrays of small elements which are excited non-uniformly. If the transducer is split into many small elements each of which is excited by a different voltage, then the area contributing to the pressure at any time must be weighted by its velocity distribution. It is possible to change the sound beam shape by such 'shading' techniques, and such ideas may prove particularly useful in the design of multielemt arrays to improve the Multiscan performance. (Willson 1974).

5.7 A reconsideration of the A-scan

The analyses of echo formation by Freedman, and of transient sound fields by Robinson, imply that the description of the A-scan of Chapter 4 requires modification when the replica pulses are very short. Although the A-scan image of the echo from a plane appears to be shift-invariant in practice, if the transducer has a very wide bandwidth the replica components of the transmitted field are separable to a degree which depends on the distance from the transducer, and no single plane is isochronal to all the sound. The degree of shift-invariance found in practice was discussed in Chapter 4 and its importance will increase as the lengths of the replica components decrease, but it does not invalidate the use of the plane reflector as an object element for measuring resolution. It does however, suggest that axial resolution depends on distance from the transducer so that to completely specify a scanner's capability the axial resolution should be measured at all distances. Such measurements have not yet been found necessary but they may be required when wide bandwidth or strongly focussed or very large aperture transducers are used.

Freedman's analysis also suggests that any object may include more than one discontinuity in its Generating Function even when it is plane. The infinite plane is useful because it contains only a single discontinuity and it is isochronal to the first replica component of the transmitted sound so that a characteristic response of the scanner can be measured, Furthermore, it averages the transmitted sound over its surface and smooths out variations in pulse structure which are present across the beam. For smaller objects e.g. small plane discs,

the resolution is dependent both on the size (and shape) of the object and upon the position of the reflector relative to the sound beam axis.

These variations of resolution suggest that artefacts can be produced in A-scans particularly if the A-scan is processed by deconvoluting with a single, shift-invariant inverse filter (e.g. Robinson 1975: Norton-Wayne 1974). Artefacts may be caused by resolving individual transmitted replica pulses (equivalent to a distortion of the image produced by a degradation in the intrinsic resolution of the scanner) or by resolving the replica components of each of the discontinuities of the object's Generating Function. Although these latter artefacts contain potentially useful information about the object's shape, they must in general be considered a source of confusion in the interpretation of the image and therefore a limitation on the desired bandwidth of large transducers.

Chapter 6: A consideration of echo amplitudes.

6.1 Introduction

In Chapter 1 the information contained in an ultrasonic image was classified as geometrical information or physical information and it was postulated that the former could be derived from measuring only the positions of reflecting interfaces and their possible changes with time. These positional measurements are used extensively in A, B and TP scans and they are influenced by the factors considered in Chapters 4 and 5, where the ability of a scanner to obtain such geometrical information was described in terms of its intrinsic resolution and accuracy. The recognition of structures in an image is often considerably enhanced by the portrayal of physical information of various types. Physical information can be extracted by analysing the features of either a single echo or an ensemble of echoes. In the former case the echo structure i.e. its amplitude and shape, is used to depict the nature of a reflecting interface such as an organ boundary. In the latter case, the distributions of suitable parameters such as echo amplitudes or echo frequency spectra, over some region of tissues, are evaluated to provide criteria for tissue differentiation. The analysis of the structure of a single echo can be useful for probing the nature of interfaces much larger than the ultrasound wavelength (tissue macrostructure) while echo ensemble analysis is thought to be more applicable to smaller scale (and probably more distinctive) tissue characteristics (tissue microstructure).

Several authors have reported their development of systems that display echo amplitudes in a quantitative fashion so that tissues are more clearly distinguished (e.g. Baum 1975, Yokoi 1972, Coleman 1974). Such systems generally utilise either discrete colour or grey level displays to distinguish between echoes in chosen amplitude ranges. Other workers have reported the usefulness of quantitative analyses of the echoes from regions of tissues e.g. Mountford and Wells (1972), Chivers (1973). The recent advent of grey scale displays has demonstrated that image quality and diagnostic accuracy are improved when the small echoes which depict a tissue's internal geometry are displayed in a semi-quantitative manner, but the quantitative interpretation of grey scale displays has not been attempted and little physical explanation of the meaning of grey scale images has appeared in the literature. An approach to the quantitation of grey scale images is considered in Chapter 7, where a possible method of echo ensemble analysis is described. An attempt is made here to identify those processes contributing to the structure of echoes from a well-defined interface, and in particular to assess the influence of the scanner's characteristics on the information contained in the echo amplitude alone.

6.2 Factors that affect echo amplitude

There are several independent variables which can affect the amplitude of an echo. It is necessary to differentiate between those factors which are dependent only on the physical character of the object, and which therefore are of potential significance to the interpretation of the image, and those factors which are in part determined by the intrinsic character of the scanner. In the latter category a further distinction can be made between those factors which are dependent only on the scanner (and which are therefore measurable and can be allowed for), and those influences which are significantly dependent on the interaction of scanner with object. These distinctions can be understood by considering the process of image formation shown schematically in Figure 6.1. The Search Field is the acoustic disturbance generated by the transducer, and its precise spatial and temporal configuration is determined not only by the intrinsic structure of the emitted sound field but also by factors such as the scanning technique used and by the properties of the medium in which the sound propagates. The Object consists of the field of echo generators discussed previously, and the Echo field is produced by the Search Field - Object interaction and is the acoustic disturbance reflected back at the transducer. The Echo field is dependent on the medium between object and transducer, which in reception samples the Echo field to produce a signal which is processed and displayed to form the Image.

The simplest situation comprises a continuous plane wave Search field incident on an infinite, plane Object so that the echo amplitude is determined by the change in acoustic impedance

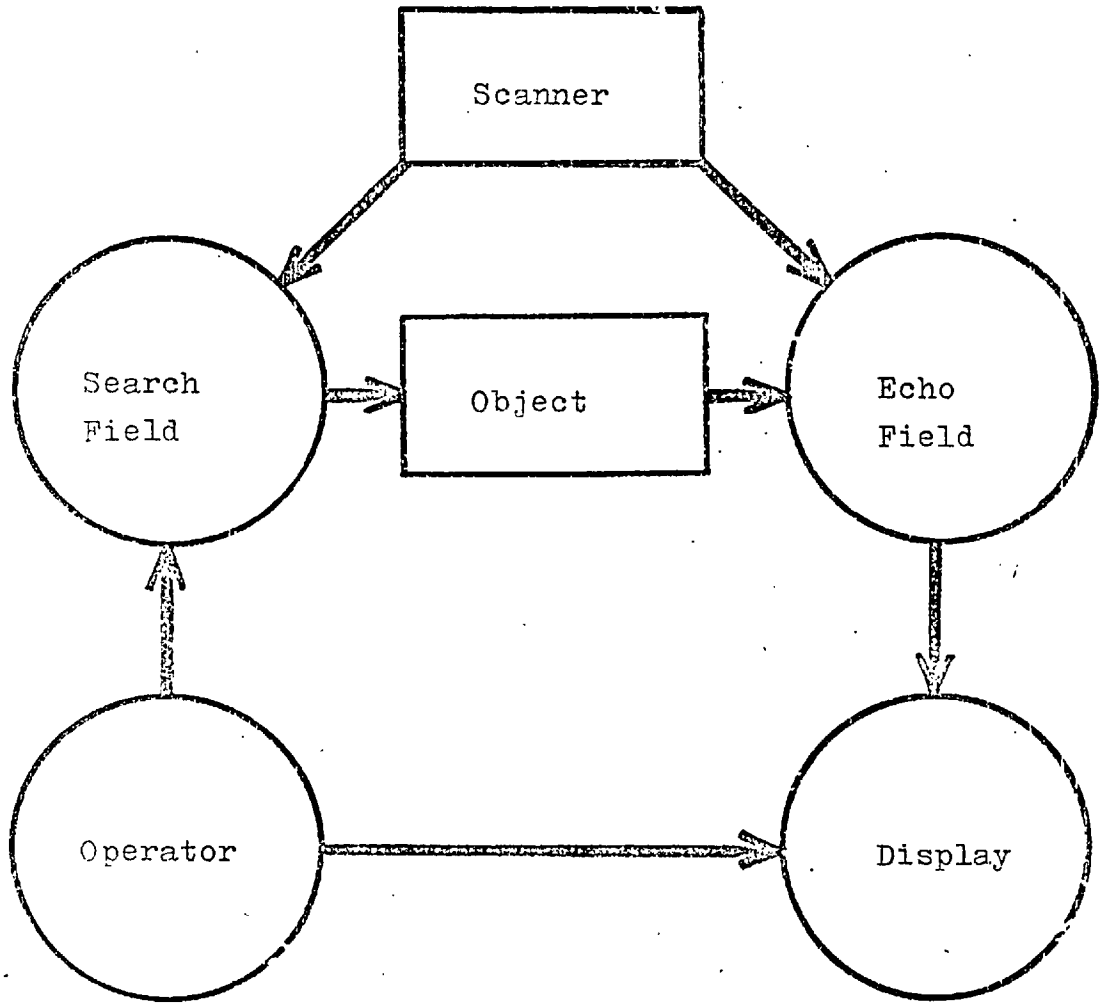


Figure 6.1 The basic stages of image formation by pulse-echo ultrasonography

across the interface, which is a useful measure of a change in the physical composition of the object. Quantitative analyses of echoes have usually extrapolated from this idealised, continuous plane wave situation by assuming that the echo amplitude from a real object indicates the change in impedance across a reflecting interface provided proper account is taken of the dependence of amplitude on the cosine of the angle of incidence of the sound beam, a correction which can be obviated by compound scanning.

In real objects the generation of the Echo Field is more complex, and the Search Field itself influences the relative importance of the object's features. Similarly, the sampling procedure in reception determines the shapes and amplitudes of the signals, and it is these limitations imposed on the usefulness of amplitude information by the intrinsic behaviour of the scanner which are of interest here. The factors considered below are therefore not intended to represent a complete description of the formation of echoes from real tissues, so that several simplifying assumptions can be made to limit the number of variables considered.

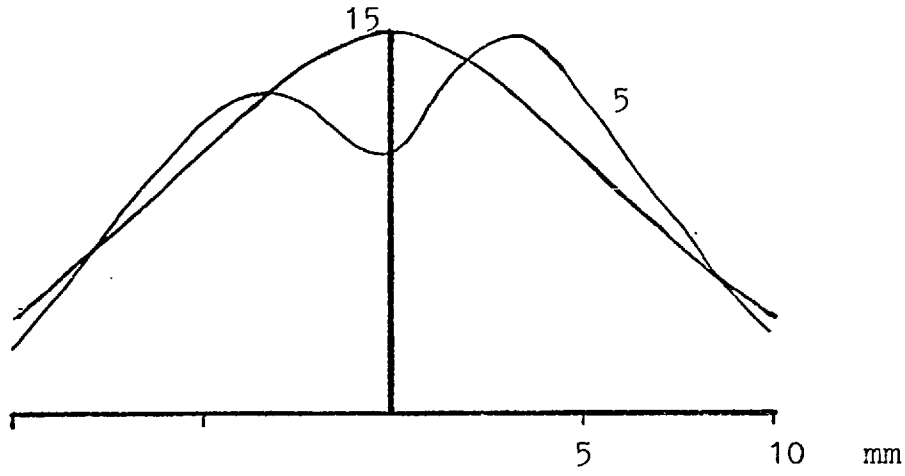
Since the purpose is to investigate the information contained in the echo from single, isolated interfaces, the medium in which the sound propagates is assumed to be homogeneous and isotropic, and the effects of attenuation are neglected. Absorption of sound in tissues will obviously modify the Search Field by reducing the sound pressure incident at every point, and by selectively filtering frequencies from the pulse, thereby changing its spectral content and possibly modifying the shape of the sound field. The importance of pulse and beam

shapes for echo amplitudes are discussed later, and in general these must be considered to be dependent on the medium surrounding the object. When the attenuation of sound varies only to a small degree over the range of frequencies of a sound pulse, these effects are of second order importance and the attenuation can be approximated by an exponential decay. Evidence for the validity of this is afforded by Figure 6.2 which compares beam profiles measured in water and castor oil. The normalised beam profiles show no differences in oil which attenuates dispersively. The amplitude of echo from an object will always depend on the sound intensity incident to the interface, and this depends on the emitted sound intensity, attenuation, and position along the sound beam axis. All these effects are disregarded below as they are self-evident but can often be allowed for when the received echoes are processed. The purpose of the analysis below is therefore that of deciding the information contained in the apparent reflection coefficient of an interface, which is analogous to the Target Strength concept used in sonar.

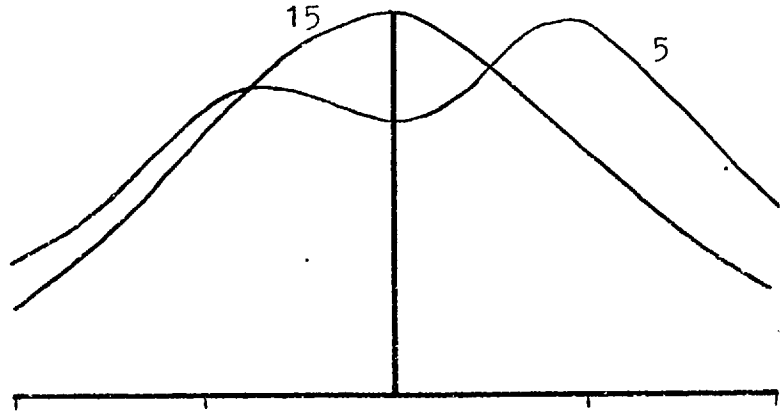
The signal received by the transducer can be considerably affected by the transfer properties of the electronic amplifiers and associated processing of the receiver and display, but these modifications are not explicitly considered here as they are well understood and accurately measurable. The amplifier transfer characteristics are selected by the designer and do not depend in any way on the object. Although the characteristics of the display are fundamental to the interpretation of quantitative measurements they do not determine the true information contained in an echo amplitude, and indeed should be designed only after the significance of this information has been evaluated.

Figure 6.2 Lateral beam profiles in different media

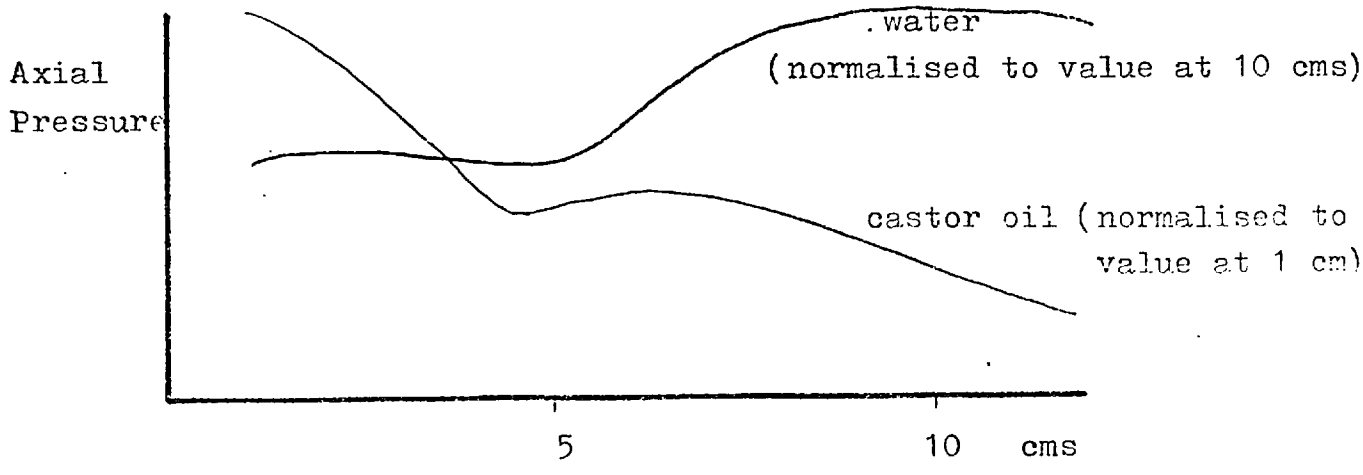
(a) in castor oil at 5 and 15 cms from transducer



(b) in degassed water at 5 and 15 cms



(c) Axial pressure plots in castor oil and water



6.3 Factors that affect apparent reflection coefficients

(a) Echo structure in pulsed conditions

A mechanism of echo formation was described in Chapter 5 which predicts that when a pulse of sound reflects from an object the echo consists of a number of component pulses, each generated at a range corresponding to a mathematical discontinuity in an area function, and each of similar shape to the incident pulse. Such replica pulses can account for the observed structures of not only the transient sound field transmitted from a transducer, but also the sound field scattered from an object whenever the Kirchoff integral is applicable. Thus the acoustic disturbance arriving at any point in an irradiated region may consist of resolvable transmission replica pulses, whilst all but the simplest objects will generate more than one replica reflection pulse towards the transducer. In Chapter 5 the Generating Function of the Object was used to describe the distribution of Freedman points and it was shown that the relative magnitudes of the discontinuities at which replica pulses are produced depend not only on the distribution of pressure within the Search Field but also on the precise projection of the Object towards the transducer. There may occur more than one discontinuity at any range, when the two replica amplitudes add, but in general a non-plane object will contain several generating discontinuities, and the number, relative spacings and magnitudes of these depend on the precise geometrical configuration of the Search Field towards the Object.

When replica pulses overlap they add vectorally and the resultant pulse has a structure that depends on the arrangement of the individual generating discontinuities and on the

transmitted pulse shape. Freedman described three types of echo distinguishable by the degree of overlap of the replica components. Where all the replica pulses are resolved, the echo envelope consists of a series of components whose envelopes are similar except in size; where there are few simultaneously overlapping pulses the envelope shape depends on the relative phases and amplitudes of the replica components; where there are many simultaneously overlapping pulses the shape of the envelope is governed by laws of probability. A single echo amplitude cannot be satisfactorily used to describe such pulses because their shapes vary, and the peak echo amplitude is dependent on the degree of overlap of the replica components, which is itself determined partly by the shape of the Object and partly by the intrinsic resolution of the scanner.

This description of echo formation shows that the Search Field Structure is an important determinant of echo amplitude and shape, whilst complex echo structures can be generated by a real object whose surface is not everywhere isochronal to the transducer. The lateral resolution of the scanner affects the number and relative weightings of the discontinuities contributing terms to the total signal, and it affects the degree of diffusion of echo generators in the image. The axial resolution determines the importance of the overlapping of replica pulses, whilst the receiver bandwidth, itself a major influence on axial resolution, affects the ability of the scanner to record the high frequency structure of echo complexes. It is therefore apparent that echo size and structure are considerably influenced by both the physical composition of an object and its geometry,

but that the geometrical factors included in Freedman's analysis are themselves dependent on the intrinsic behaviour of the scanner.

(b) Effect of angle

The angle of incidence of a sound wave to a surface is an important factor which determines the spatial distribution of reflected sound and in particular affects the apparent reflection coefficient of a surface. The amplitude of an echo usually decreases when the angle of incidence increases and an Angle Factor, $A(\theta)$, can be defined as the ratio of the echo amplitude at an angle of incidence θ (to the normal) to that for normal incidence. When $A(\theta)$ is dependent only on the reflecting surface then it is a property of the Object only. However, when $A(\theta)$ depends on the shape or structure of the Search Field, the intrinsic properties of the scanner help determine the apparent reflection coefficient of the Object.

The manner in which $A(\theta)$ depends on θ is well understood for plane waves incident on plane surfaces when the rules of geometrical (ray) optics apply. Many real surfaces are not smooth on the scale of a wavelength, and the surface area which contributes to the sound back at the transducer is neither large nor uniformly irradiated, so that tissues are not specular reflectors and diffraction effects are observable. In these circumstances the reflected sound fields cannot be accurately calculated using ray approximations and other procedures for estimating the apparent reflection coefficients of surfaces are necessary (e.g. Twersky 1950, Berry 1972). The Kirchoff integral can be used as an approximate description

of the sound reflected back to a point on the transducer if the distribution of particle velocities across the reflecting surface is known. This distribution depends on the distribution of pressure in the Search Field and the angle θ, and its precise form determines the directional pattern of the reflector. Even plane surfaces which are irradiated by a non-uniform sound wave will possess a directional pattern which extends over several degrees from the surface normal and whose shape is determined by the shape of the Search Field, and this is demonstrated below.

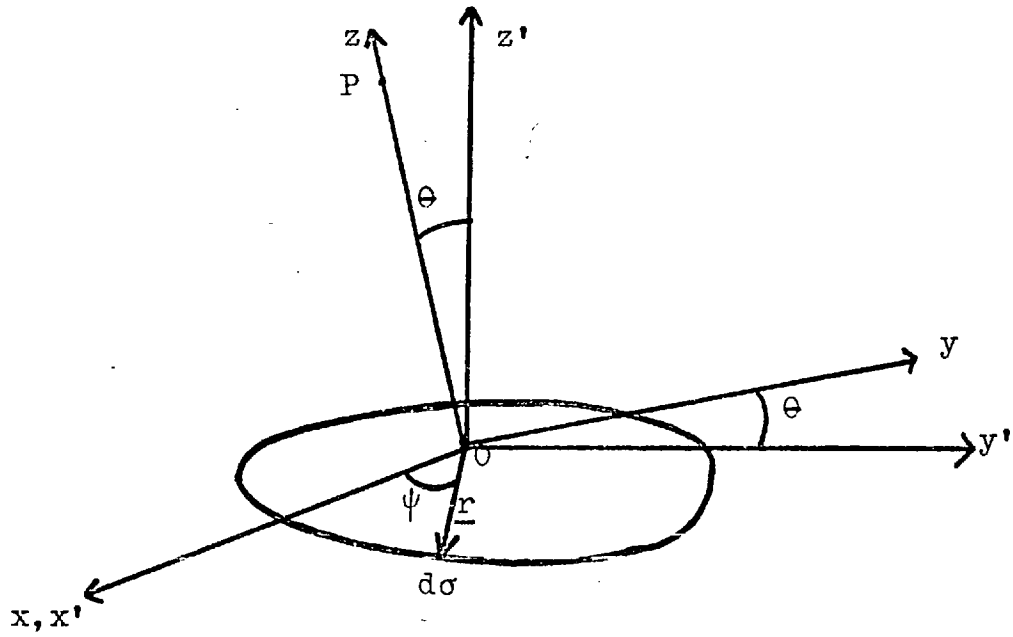
A rough surface can be defined as a surface whose height from some reference plane is not everywhere the same but which fluctuates about some mean height. Although it is often stated that tissues are rough or smooth, the validity of such a distinction depends on the size and frequency of these fluctuations relative to a wavelength of sound, which implies that classifications of surfaces as rough or smooth, or indeed as specular or non specular, can only be made with reference to a given range of sound wavelengths and to a given Search Field configuration. Rough surfaces are usually considered less specular than smooth surfaces because the deviations from the plane scatter more nearly uniformly in different directions, but the exact dependence on angle is governed by the nature of the deviations themselves. When these are regular on a scale of the order of a wavelength then the surface can behave as a reflection grating, producing severe interference lobes at discrete directions (though these should be smoothed out by using short pulses). Where the deviations are randomly distributed then the angular dependence can be found by using the

relevant probability distribution (e.g. Morse and Ingard 1968).

A further complication of the angular dependence of echo amplitudes is that the echo shape changes with angle. As the angle θ increases, the area of surface irradiated by the sound field becomes extended in range and the echo therefore stretches. At different angles the sound from different ranges interferes to different degrees, producing echoes with varying shapes. At some angles these pulses split to produce several distinguishable peaks which means that at these angles the reflector appears as two or more closely spaced reflectors. The amplitude of each peak is dependent on the shapes of the incident pulse and the sound beam profile. A single curve is therefore not sufficient to describe $A(\theta)$ when short pulses are used, and examples of pulse splitting are demonstrated below.

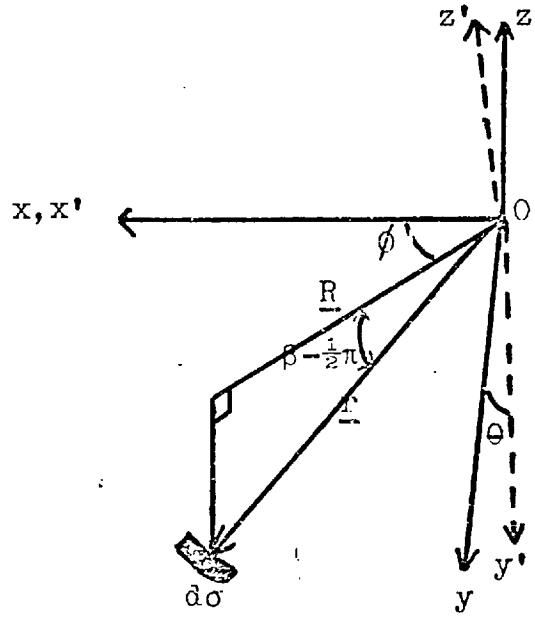
Many of the features of the behaviour of different surfaces and Search Fields can be illustrated by considering a reflecting annulus of width w. The annulus lies in the x'y' plane which is rotated by an angle θ to the xy plane as shown in Figure 6.3. The centre of the annulus O is the origin of both coordinate systems and a wave incident along the -z direction is reflected back into the half space above the annulus, and some of the sound is received by a transducer at P ((0,0,z) in the xyz coordinate system). The incident wave is assumed to be monochromatic with wave vector $\underline{k}$, to have no phase variations in the xy plane but to have an amplitude distribution p(R) which is radially symmetric about the z axis. In the plane of the annulus this pressure distribution becomes $p(r.\sin\beta)$. The particle velocity v in the wave has a component $v.\cos\theta$ normal to the annulus, where v is itself proportional

Figure 6.3 Coordinate system used to calculate Angle Factor



$d\sigma = (r\cos\psi, r\sin\psi, 0)$ in x'y'z' system

$P = (0, 0, z)$ in xyz $= (0, -z\sin\theta, +z\cos\theta)$ in x'y'z'



R is the projection of r in the xy plane.

Path difference between Pdσ and PO is Δ

$$\Delta = (r^2 + z^2 + 2rz\sin\psi\sin\theta)^{\frac{1}{2}} - z$$

$$\doteq r\sin\psi\sin\theta$$

to the pressure, p. Rotating the plane of the annulus introduces phase variations across the reflecting surface which depend on θ. The pressure back at P can be estimated by using the Kirchoff integral with the usual far-field conditions. The Angle Factor for an annulus whose inner radius is r_o is

$$A(\theta) = \frac{\int_{r_o}^{r_o+w} \int_{o}^{2\pi} p(r\sin\beta)\ \cos\theta\ e^{-2jkr\sin\theta\ \sin\psi}\ r\,d\psi\ dr}{2\pi \int_{r_o}^{r_o+w} p(r)\ r\ dr}$$

For a single annulus, $\sin\beta$ varies from 1 ($\psi = 0$) to $\cos\theta$ ($\psi = \frac{\pi}{2}$). If the angle θ is in the range $0 < \theta < \frac{\pi}{10}$, then $0.96 < \cos\theta < 1$, so that for physically realisable beam profiles, $p(r\sin\beta) \simeq p(r)$. In this case,

$$A(\theta) = \frac{\int_{r_o}^{r_o+w} p(r)\ J_o(2kr\ \sin\theta)\ r\ dr\ .\ \cos\theta}{\int_{r_o}^{r_o+w} p(r)\ r\ dr}$$

$A(\theta)$ depends on the rate at which $p(r)$ decreases over a distance w, and is therefore broader for focussed beams. A plane reflector can be considered as a series of concentric annuli each of which conforms to the approximations used above. The Angle Factor for an inclined plane is then approximately

$$A(\theta) = \frac{\int_{o}^{\infty} p(r)\ J_o(2kr\sin\theta)\ r\ dr}{\int_{o}^{\infty} p(r)\ r\ dr}$$

$$= \cos\theta\ F'\left(\frac{2\sin\theta}{\lambda}\right)$$

where F' is the Hankel Transform of p, appropriately normalised, and is related to the function F(q) used in Chapter 5 to describe the scanner's resolution. The Angle Factor for the plane is the product of cos θ (which does not vary much in the range $0 < \theta < \frac{\pi}{10}$) and a directivity function which is determined by the Search Field. As the beam profile p(r) is made sharper to obtain better resolution, so the Hankel Transform broadens and surfaces appear less specular. Thus the ability of a scanner to detect inclined surfaces and to resolve closely spaced interfaces are related. A measurement of $A(\theta)$ could be used as a complete specification of the scanners behaviour. By measuring the echo from an inclined plane at different angles, the scanner response, F', to various spatial frequencies, $\frac{2 \sin \theta}{\lambda}$ cycles/mm, can be constructed, whilst the angle that limits the detection of the plane could be a useful measure of sensitivity. However, the derivation above is not valid at large angles and contains several approximations, not least serious of which is the assumption of a continuous incident sound wave. Figure 6.4 and 6.5 show that the agreement with theory is reasonable at very small angles, but that pulse effects in particular detract from the quantitative validity of the theory. The beam profiles used in these measurements are shown in Figure 6.6.

The characteristics of surfaces which are 'regularly rough' can be illustrated with an array of concentric annuli ruled on a nylon sheet to a depth of several millimetres, and Figure 6.7 shows the results of measurements made of the echo amplitude produced from such an array aligned with its centre on the axis of the plane 1.5 MHz transducer of Figure 6.6. Figure 6.8 shows the results obtained with the focussed beam. The theoretical

Figure 6.4 Comparison of measured Angle Factor with theoretical prediction (plane reflector, focussed 1.5 MHz transducer)

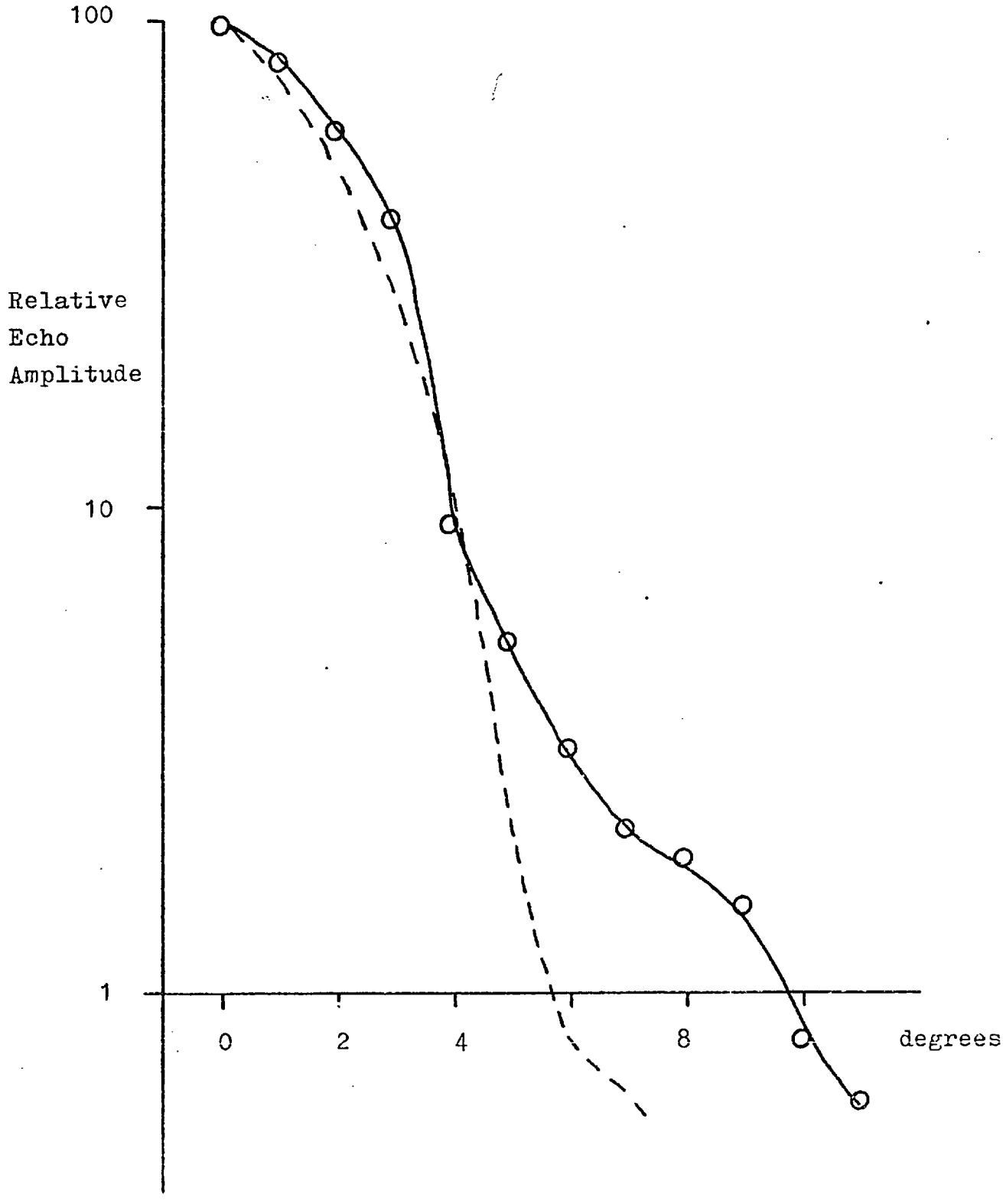


Figure 6.5 Comparison of measured Angle Factor with theoretical prediction (plane reflector, plane 1.5 MHz transducer)

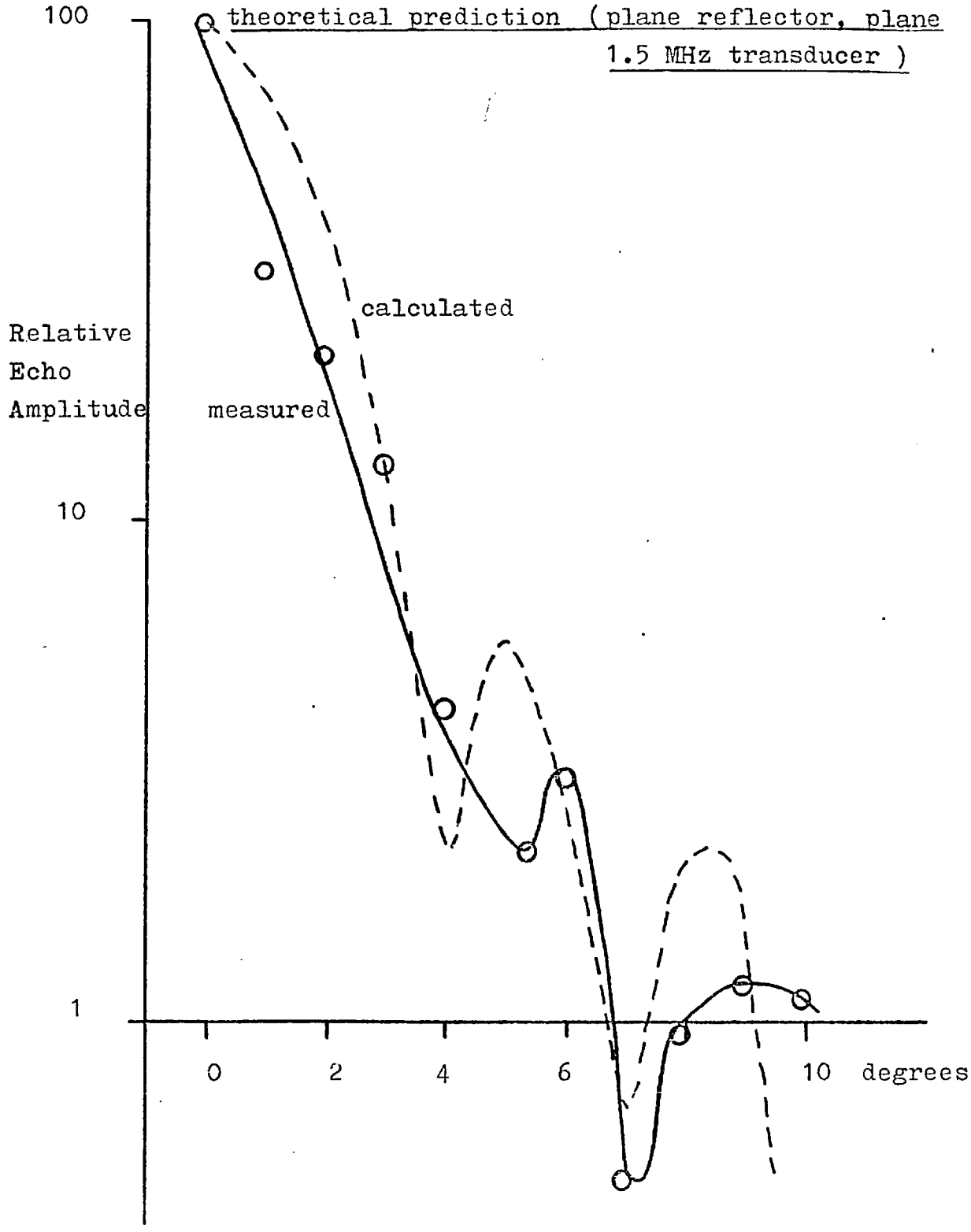
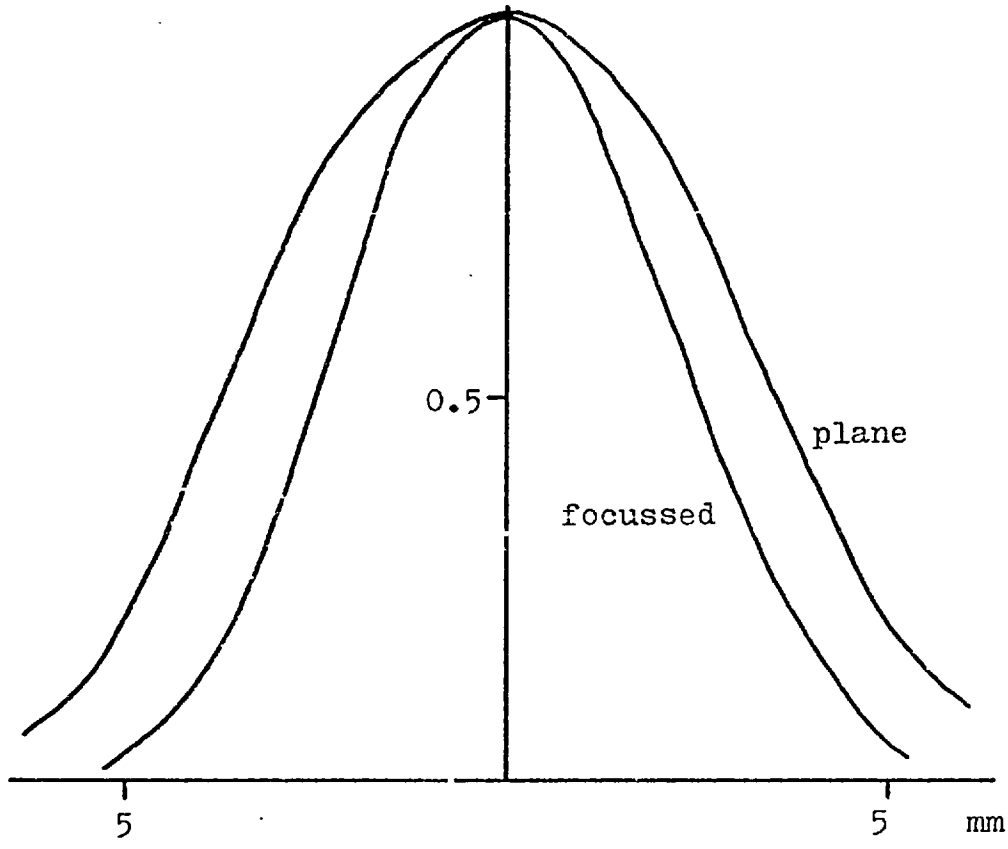


Figure 6.6 Lateral beam profiles of transducers used to measure and calculate Angle Factors.



Angle Factors were obtained by summing the contributions of several annuli, each weighted by the average pressure across the annulus. If these weighting pressures are denoted as p_n then the Angle Factor for the array is

$$A(\theta) \propto \sum_{n=o}^{N} p_n \frac{w \cot\theta}{2k} \left((2n+1) J_1(2(2n+1)kw\sin\theta) - 2n\, J_1(4n\, kw \sin\theta) \right)$$

The precise form of $A(\theta)$ depends on the weighting pressures and hence on the Search Field. The predicted secondary lobes of $A(\theta)$ are severely reduced in practice, presumably an effect of using short pulses. Pulse splitting is apparent at several angles. Figure 6.9 shows the measured angle factors for smooth surfaces coated with lead shot (average diameter 600 μm) and plastic microspheres (average diameter 50 μm). The principal lobes are similar to those of Figure 6.5 but the patterns at larger angles are different and Figure 6.9 suggests that coherent effects are obtainable with the larger spheres.

These results show that the apparent reflection coefficient of a surface is dependent on several features of the surface itself which are geometrical features unrelated to the physical composition of the medium. However, even smooth plane surfaces do not possess a unique Angle Factor since this depends on the nature of the Search Field and is directly related to the resolution. Rough surfaces can behave anomalously and the reflection coefficient even at normal incidence is dependent on the sound wavelength and pulse shape.

Figure 6.7 Angle Factors obtained for reflections from ruled annuli for plane transducer

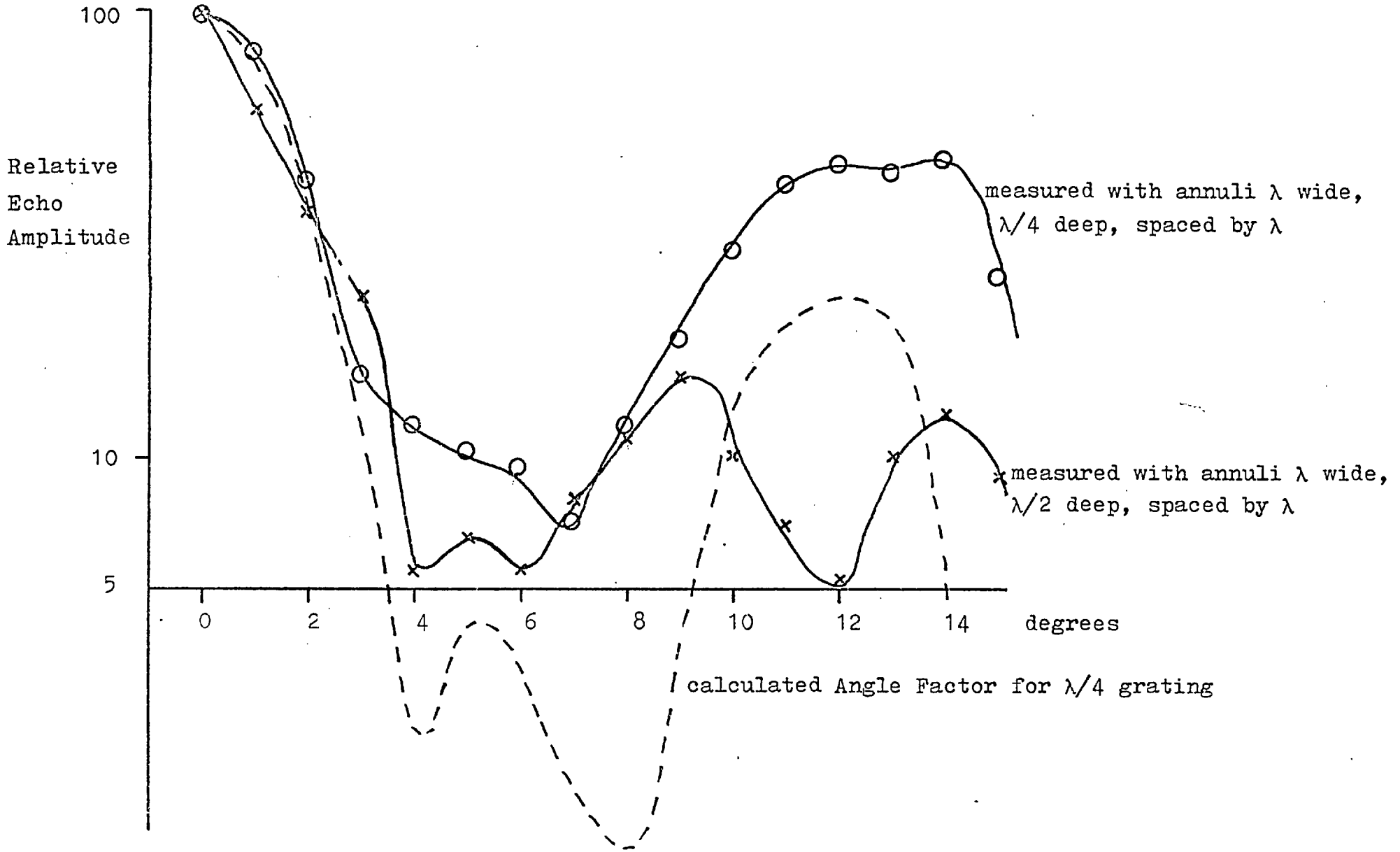


Figure 6.8 Angle Factors obtained for reflections from ruled annuli for focussed transducer

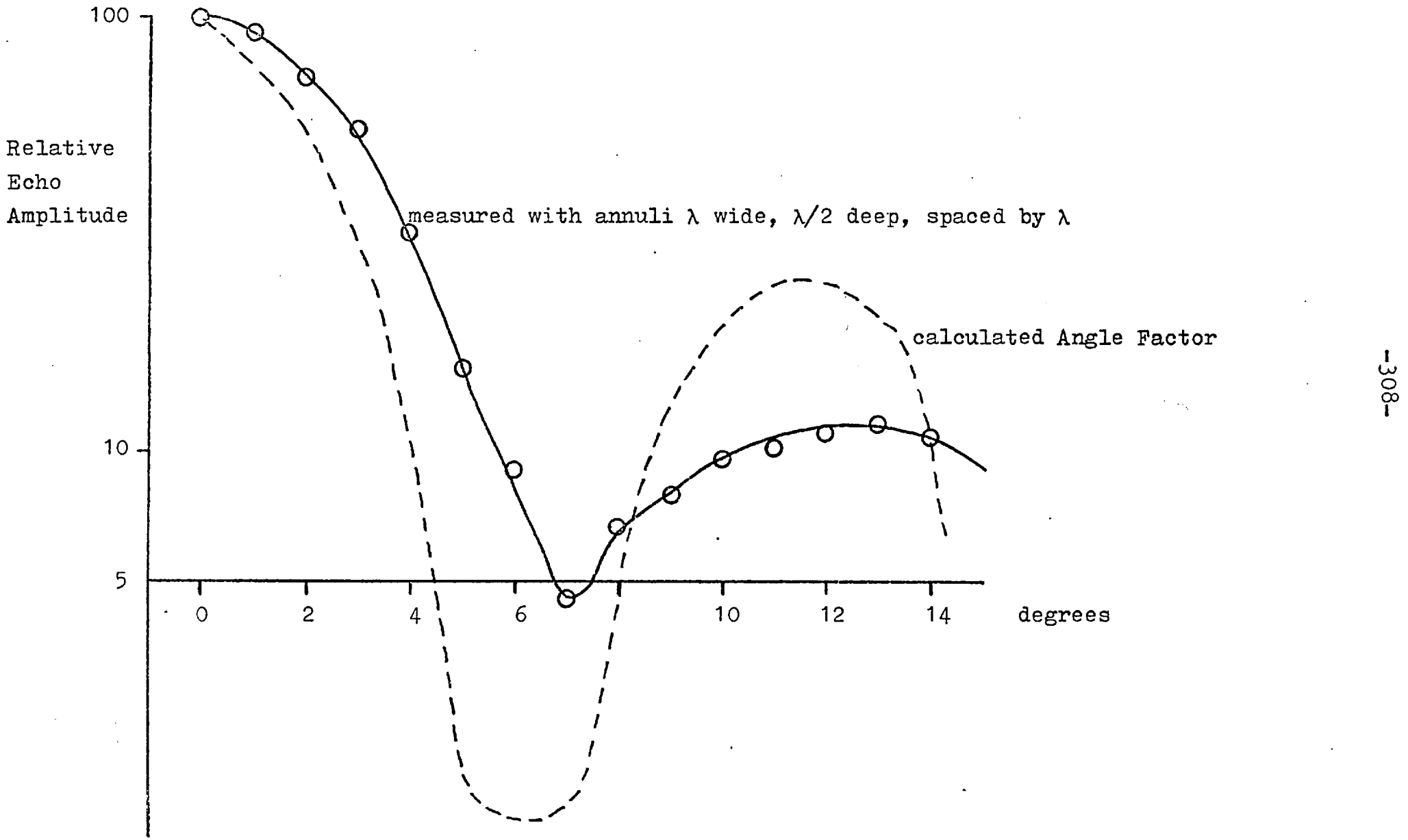
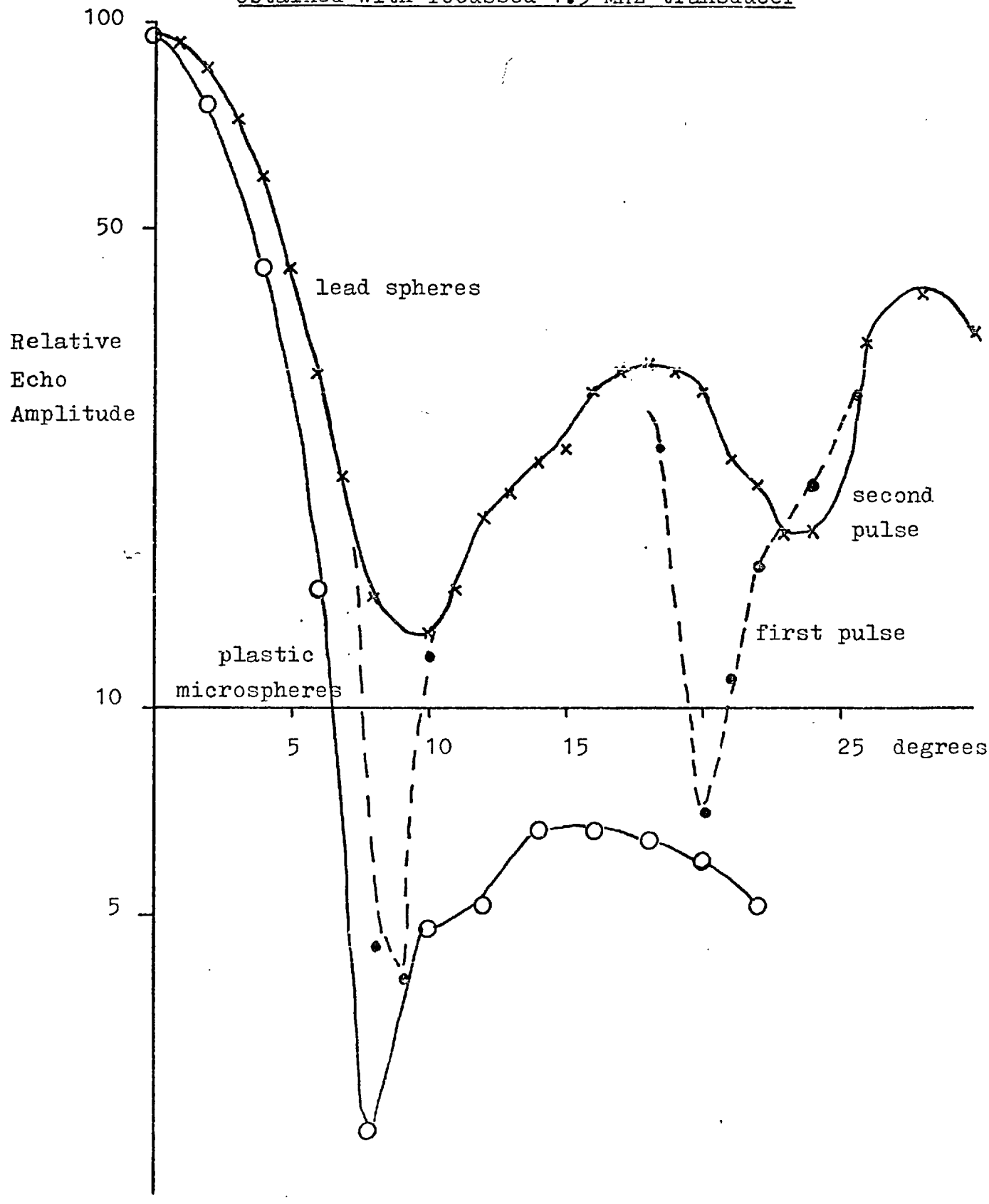


Figure 6.9 Measured Angle Factors for rough surfaces obtained with focussed 1.5 MHz transducer



Pulse splitting effects are apparent in the change of echo with angle. The first and second components of the echo complex show different variations with angle and coalesce at some angles.

(c) Effect of reflector area

The apparent reflection coefficient of a surface is dependent on the area of that surface which is irradiated and different areas produce echoes with different amplitudes even though the composition of the surface and the position of the sound beam remain unchanged. The effect of area on echo amplitudes was measured by aligning solid discs of different radii so that they were coaxial with a transducer at a distance z. Sets of discs were manufactured from brass, nylon and perspex but the Area Factor, the ratio of echo amplitudes produced by a disc of radius R to that produced by an infinite plane of the same material at the same distance, and which can be denoted as S(R), was found to be independent of the reflector material. This Area Factor was found to change with different transducers and therefore it depends on the intrinsic properties of the scanner.

Figure 6.10 shows the Area Factors for two transducers with the same radius (a) and emitting pulses of closely similar shape, measured at the same distance from the transducer face. S(R) increases smoothly in both cases to a value of unity, but the gradients of the curves are different because one of the sound fields is focussed. S(R) depends on the shape of the sound beam profile across the disc so that focussed transducers measure a much greater change in echo amplitude for a given change in reflector area than plane transducers.

When the Area Factor is measured near to the transducer, apparently anomalous effects can occur such that S(R) decreases as the disc size increases. While the general shapes of the curves of Figure 6.10 can be predicted by simply considering the energy

Figure 6.10 Measurements of the Area Factors of small disc reflectors for different Search Fields.

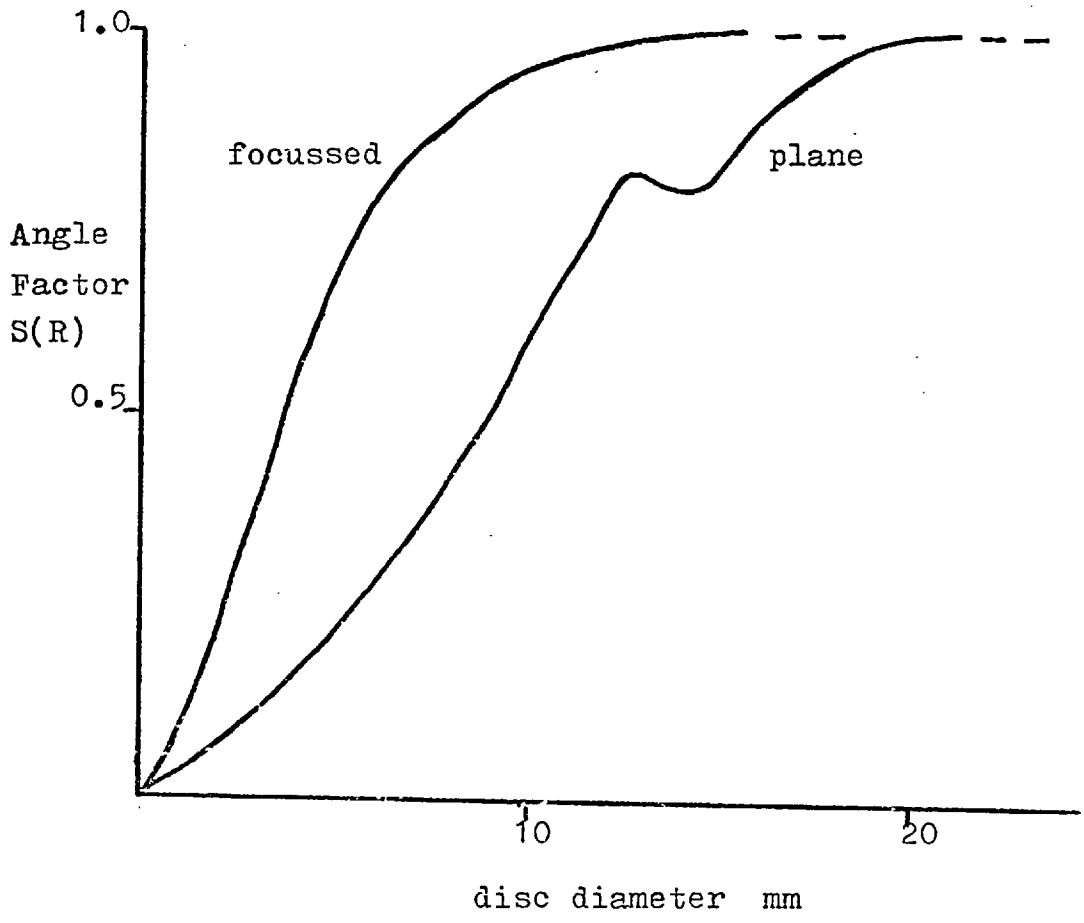
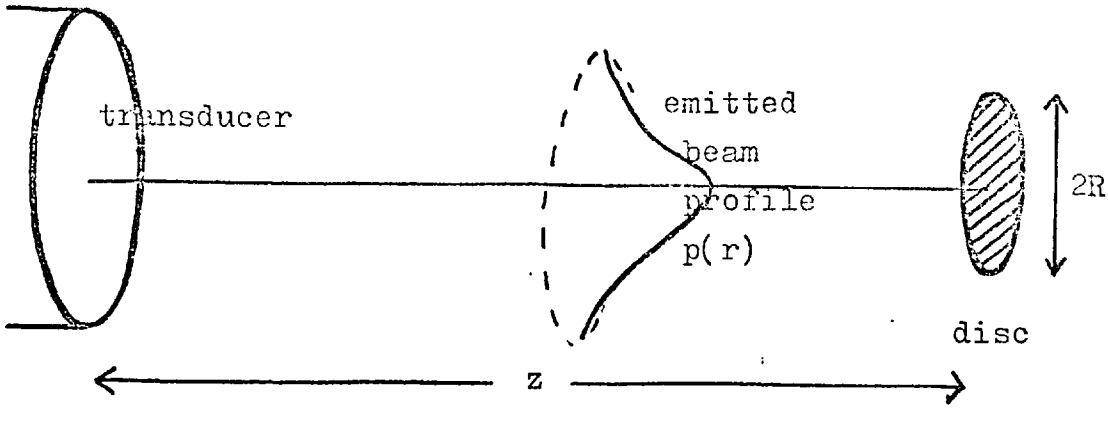


Figure 6.11 Coordinate system used to derive Area Factors



reflected back by the disc, in the region of the sound field used in practice interference effects must also be considered. Exact calculations of the Area Factor for point sources radiating spherical waves have been produced by Saneyoshi (1958) who also reported the observation of reduced echo amplitudes from large discs. An illustration of these effects with plane waves can be obtained by an approximate calculation of the sound pressure reflected back to a point on the transducer axis when a disc of radius R is irradiated by a wave whose beam profile is p(r) (Figure 6.11). The Area Factor measured at the axial point is approximately given by

$$S(R) \propto \int_0^R r\,p(r)\, e^{\frac{jkr^2}{2z}}\, dr$$

The shape of S(R) depends on the rate of change of p(r) (i.e. the degree of focussing) relative to the period of the phase factor which causes S(R) to oscillate in the manner of the Fresnel integrals. The shape of S(R) depends on p(r) and $\frac{R^2}{z\lambda}$, both of which are determined by the Search Field.

When the discs are a long way from the transducer, the exponential factor does not change very much with increasing r and

$$S(R) \propto \int_0^R r\,p(r)\, dr$$

The integral is the volume under the (two dimensional) beam profile. Measurements of S(R) under these circumstances could be used to compare the imaging ability of scanners since p(r) is related to the Point Spread Function considered in Chapter 5.

The area of disc that appears to have an Area Factor of 0.5, for example, is a useful inverse measure of the scanner sensitivity, whilst its radius affords a measure of the lateral beamwidth.

Figures 6.12 and 6.13 show the measured Area Factors for two transducers which were of the same design but had different radii. The measurements were performed at distances equal to half integral multiples of the continuous wave Near Zone limit, $\frac{a^2}{\lambda}$, so that the beam profiles across the discs were closely similar. The Area Factor rises more steeply with a small transducer but the two sets of curves can be made more alike by expressing the disc radii in terms of the transducer radius. This has the effect of ensuring that the phase factor is the same for both cases (e.g. at a distance $z = \frac{a^2}{\lambda}$, the exponent is $2\pi.(\frac{R}{a})^2$). The area of the transducer compared to the disc area is therefore an important determinant of the precise form of the Area Factor.

The Area Factor also depends on the pulse shape and wavelength because the Echo Field from the disc is scaled by the factor $\frac{R^2}{\lambda}$ and is shaped by the incident pulse shape. Each disc possesses its own directional pattern which is like the sound field from a circular transducer that is non uniformly excited, and the Near Zone of such a field shows lateral and axial pressure variations on a scale that depends on $\frac{R^2}{\lambda}$. The importance of such effects is determined by the pulse length. A further and probably more important influence on the Area Factor is the manner in which the transducer samples the Echo Field which can lead to anomalies of the type depicted in

Figure 6.12 Measurements of the Area Factors of disc reflectors obtained with different size transducers

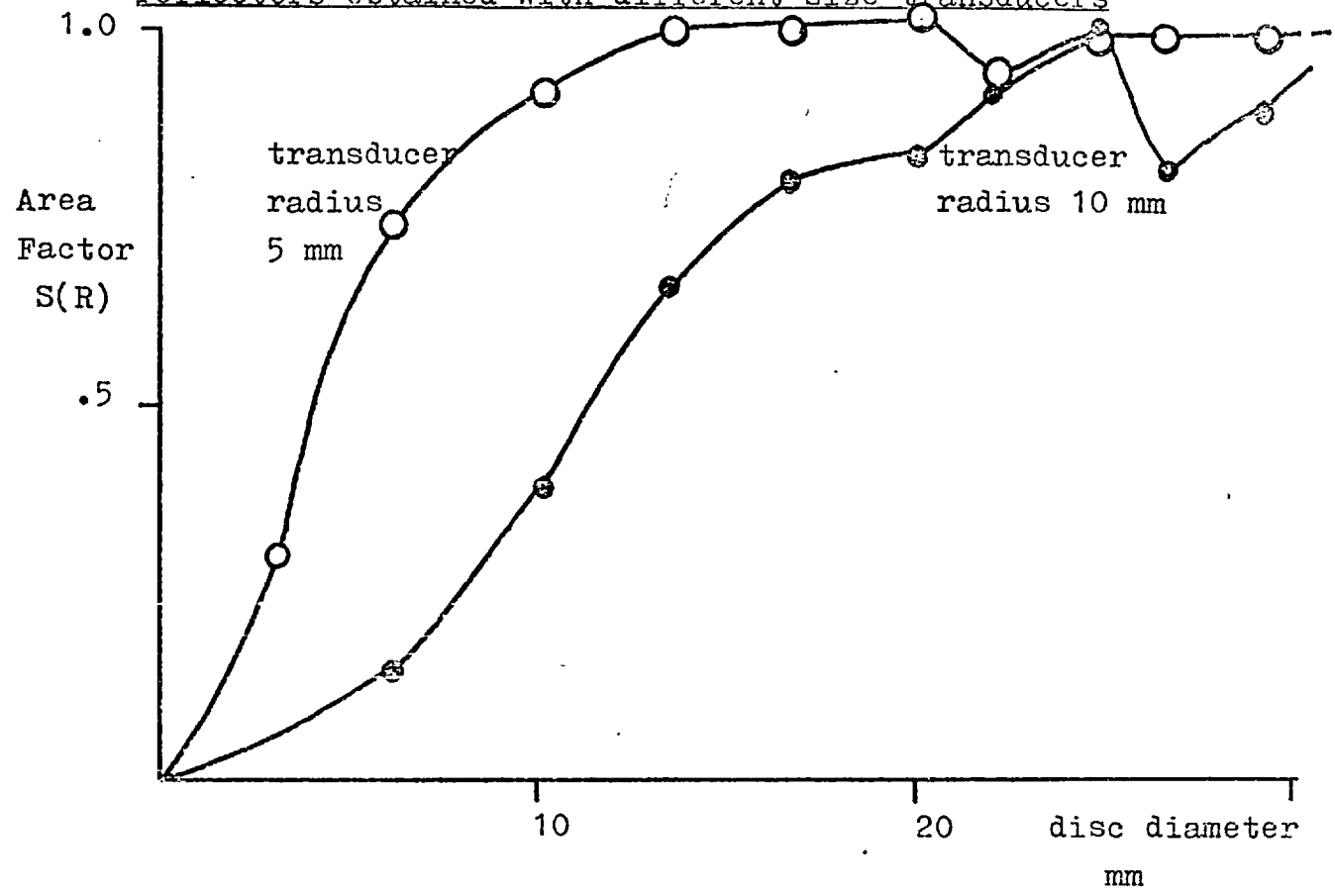
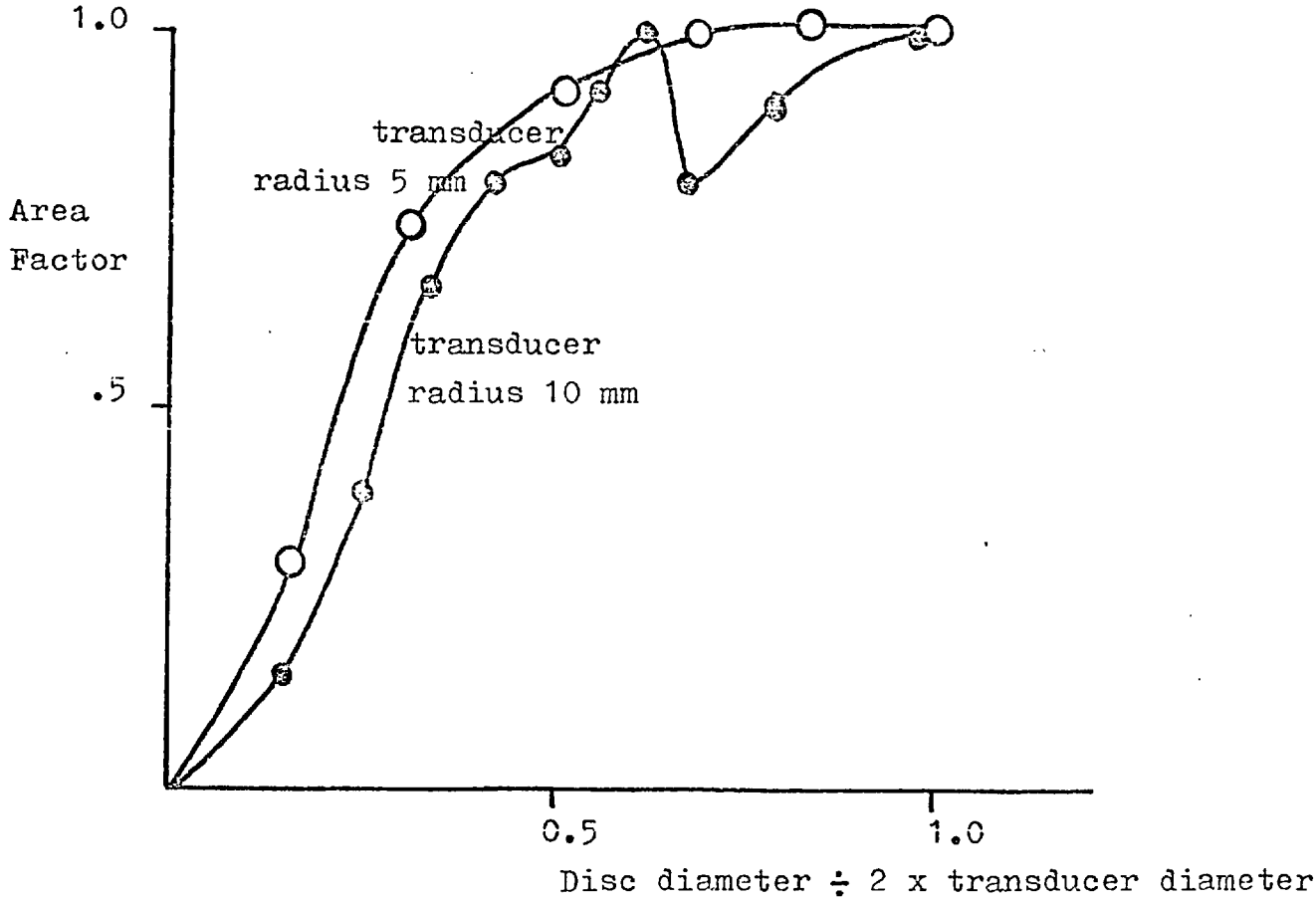


Figure 6.13 Area Factors re-plotted on normalised scale



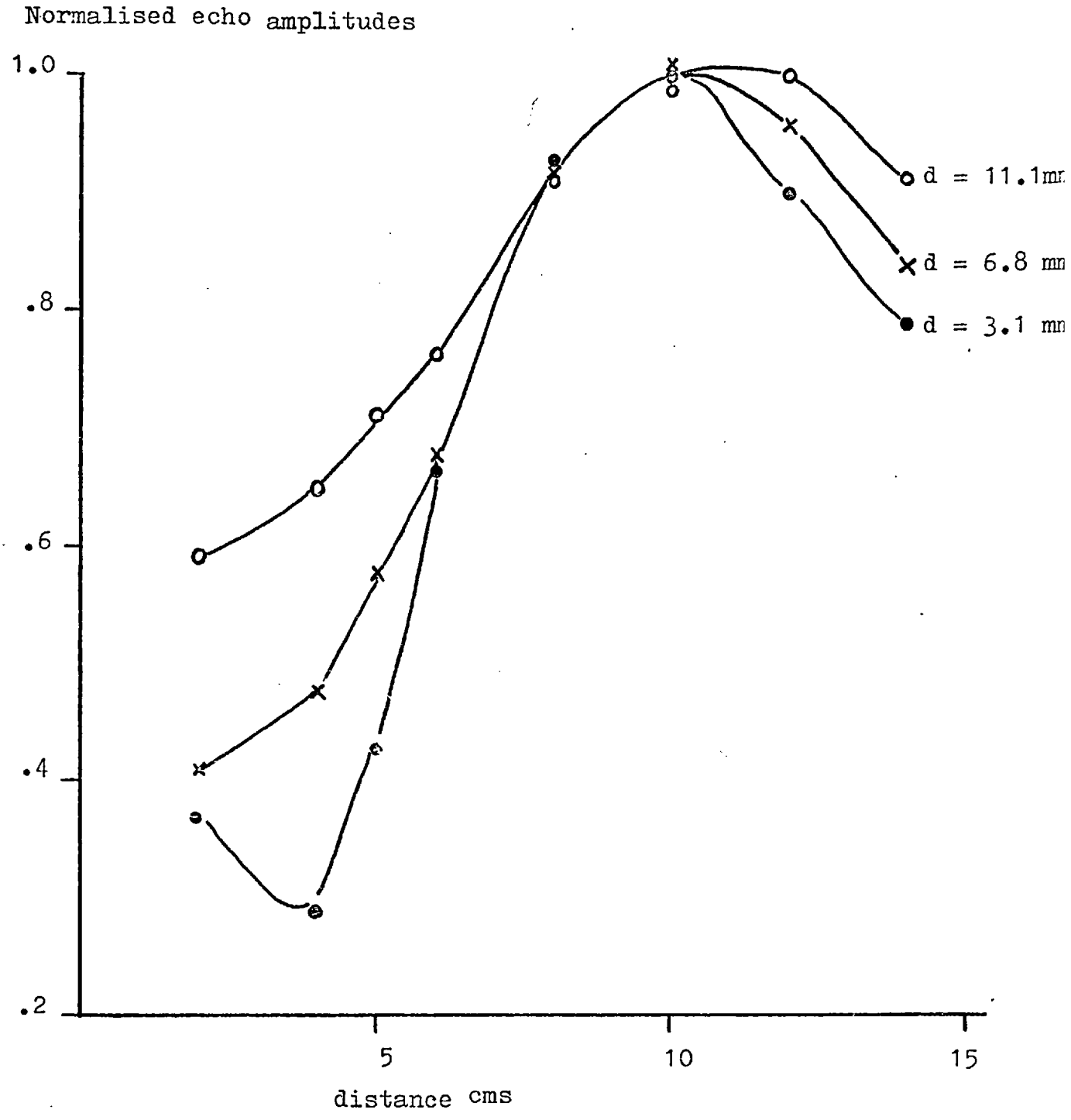


Figure 6.14 Measurements of the variation in echo amplitudes observed as small disc reflectors (diameter d) are moved to different distances from the transducer, normalised to the value at the focus at 10 cms.

Figure 6.12, when the wavefronts at the transducer are not plane. This is considered below.

Although the Area Factor is dependent on the shape of the Search Field, it may be possible to estimate the area of a reflector from the manner in which the echo amplitude changes with distance from the transducer. Figure 6.14 summarises the results of measurements of the variation of echo amplitude produced by moving different sized discs along the axis of a 1.5 MHz plane transducer, and by comparing measured variations with such curves it may be possible to estimate reflector dimensions. In general, however, the criterion for the size of a reflector, which determines whether it can be thought of as an infinite plane or not, is derived not just from the size of reflector compared to λ, but also the size compared to the beamwidth and λz.

(d) Effect of sampling the Echo Field

The sound field reflected from an object forms an Echo Field whose spatial and temporal distribution is dependent on the Search Field and object. The image produced by a scanner is a representation of the pressure in the Echo Field at the transducer face and for a quantitative analysis of echo amplitudes to be useful it is essential that the electric signal from the transducer is related in some prescribed manner to this pressure. The transfer function of a piezoelectric receiver which is derived in Appendix B shows that the pressure in a plane wave can be related to the voltage produced when that plane wave is normally incident to a transducer. Non-linearities in the pressure-voltage relationship, and pulse

distortion caused by the effect of the transducer impulse response in reception, may in principle be removed by suitable inverse filtering, and are therefore not fundamental limitations on the information available. Any transducer and receiver can therefore be calibrated so that the reflection coefficients of large plane reflectors can be compared to some standard reflector. However, no allowance can be made for variations in the phase or amplitude of the pressure across the transducer face, and the manner in which the transducer signal records such non-uniform wavefronts is an important limitation on the amplitude information obtainable. The experiment described below illustrates the effect of transducer area and wavefront shape on the echo amplitude recorded.

The lateral beam profiles, p(r), from a transducer (20 mm diameter, plane, 1.5 MHz) were measured at several distances with a small probe. An identical co-axial transducer was placed facing this transmitting transducer at a distance far enough away for the emitted wavefronts to be reasonably plane (10 - 20 cms). A tightly fitting sleeve was used to hold thin metal discs close to the face of this receiving device. Holes whose radii varied from 1.5 to 6 mm were drilled in the centres of these discs so that when each in turn was placed in front of the transducer face, the signal amplitude from the transducer varied with the size of the hole. Table 6.1 summarises the results of measurements of the voltages produced, V(R), as a function of hole radius R, expressed as percentages of the signal obtained with no masking disc. By subtracting the measurements obtained with different holes, the percentage contributions of various annuli of the transducer element to the unmasked

response of the whole transducer, were estimated. The forces on these annuli were then calculated using the approximation to the measured pressure profile shown in Figure 6.15.

For an annulus whose radii are R_1 and R_2 the force on the annulus compared to the total force on the transducer when no disc is present is $f(R_1,R_2)$.

$$f(R_1,R_2) = \frac{\int_{R1}^{R2} p(r)\ r\ dr}{\int_{o}^{a} p(r)\ r\ dr}$$

where a = transducer radius. If the forces on successive annuli are assumed to produce simple longitudinal strains in the receiving crystal, then the total force on an exposed area of the crystal can be found by adding the forces on the annuli which make up that area. The force on an exposed region of transducer face of radius R calculated in this way is F(R), and Figure 6.16 shows that there is a very close correspondence between V(R) and F(R). Figure 6.17 shows the way in which V and F vary with R for two different beam profiles, one more focussed than the other, whilst Table 6.2 shows the percentage contributions of different annuli to that signal obtained when the transducer is not shielded.

The correspondence between theory and experiment is not exact, particularly when the area of the transducer exposed is small. However, the deformation of the irradiated region is almost certainly not a plane, one-dimensional strain because extra deformation occurs at the edges of the exposed area. Such an edge effect produces an additional contribution to the

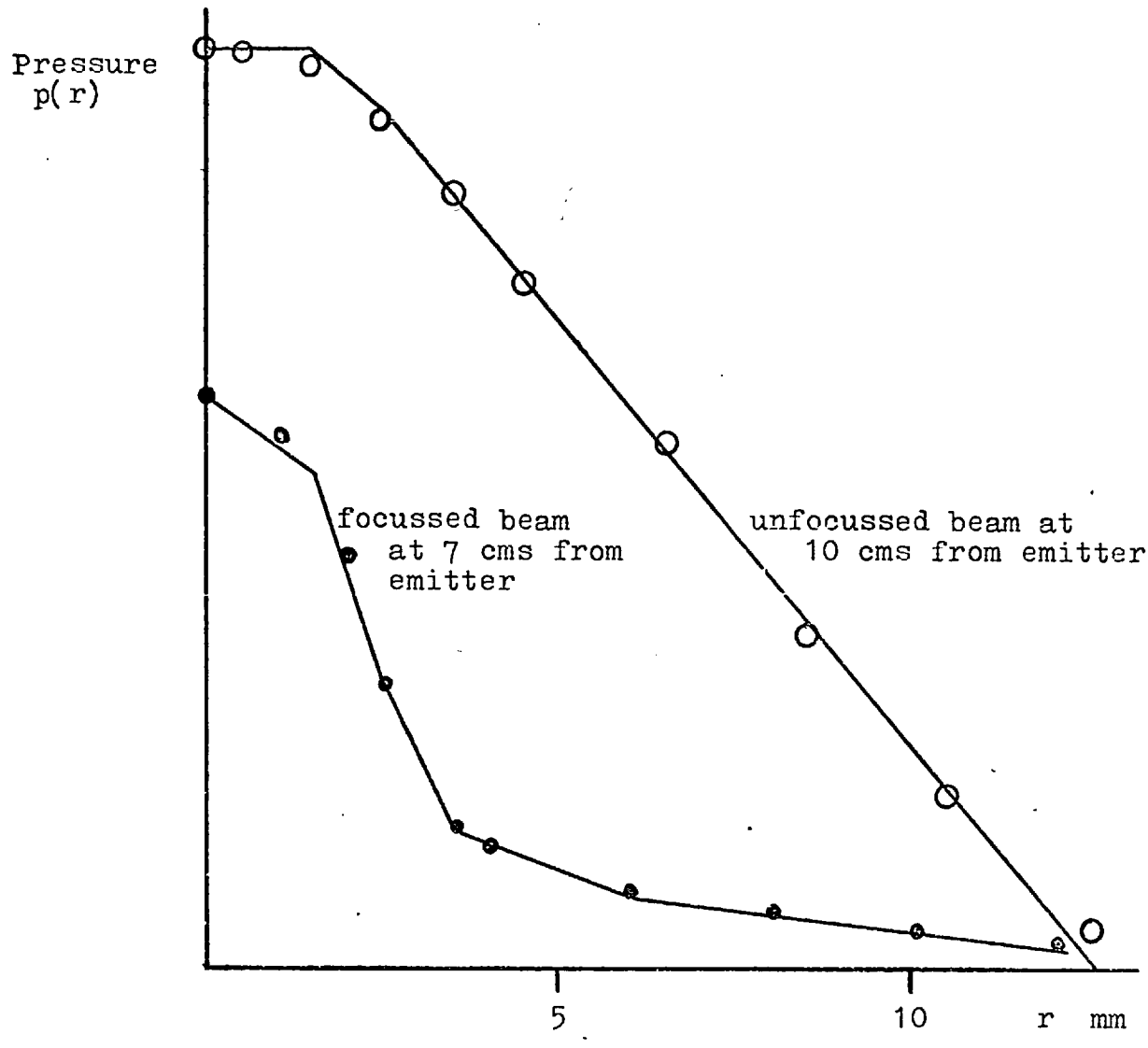


Figure 6.15 Comparison of the approximate pressure profiles used to calculate force on transducer (shown by series of straight lines) with measured beam profiles (• and o).

Table 6.1
Measurements of signal voltages for different radii of aperture as percentage of maximum response at two distances.

Radius of aperture R mm	$\frac{V(R)}{V_{max}}$ (plane transducer) at 10 cms	$\frac{V(R)}{V_{max}}$ (focuseed at 7 cms)
10.0	1.00	1.00
6.0	.66	.74
4.5	.45	.60
3.5	.33	.49
2.5	.22	.33
1.5	.12	.14

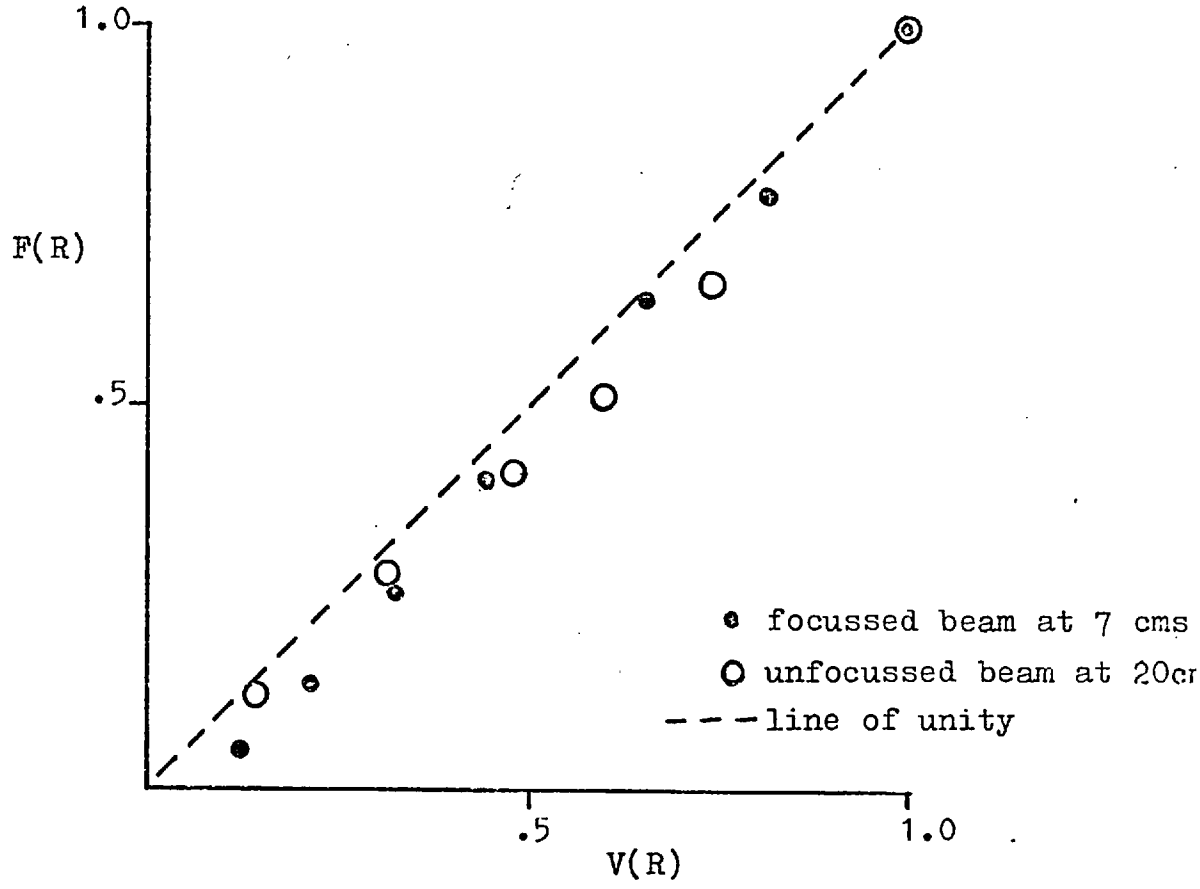
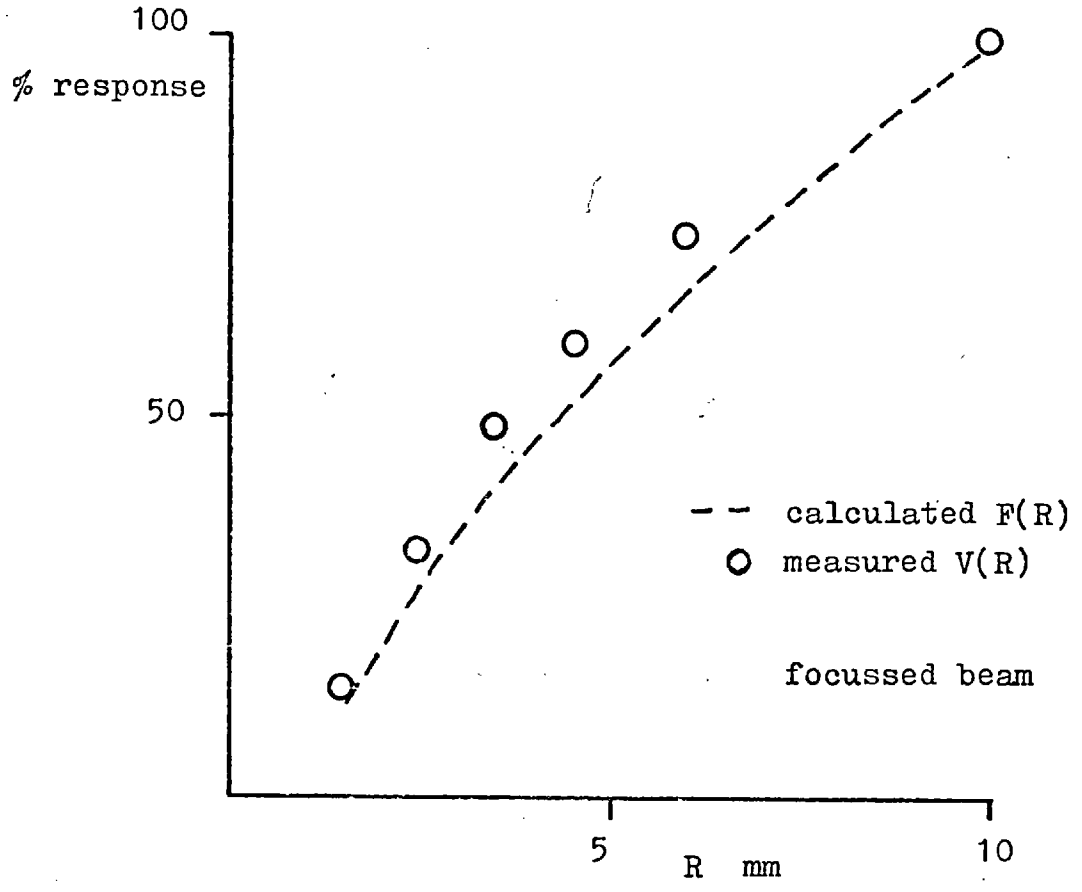


Figure 6.16 Comparison of measured voltage with calculated average pressure for two sound fields incident on transducer.

Table 6.2

Percentage contributions of different annuli in the transducer to the total signal for two different incident sound fields.

Inner Radius mm	Outer Radius mm	Annular Area mm^2	% contribution (unfocussed beam)	% contribution (focussed beam)
0	1.5	2.25	12.6	14.3
1.5	2.5	4.00	9.5	18.3
2.5	3.5	6.00	10.8	16.0
3.5	4.5	8.00	11.8	11.4
4.5	6.0	15.75	21.1	14.3
6.0	10.0	64.00	34.2	25.7



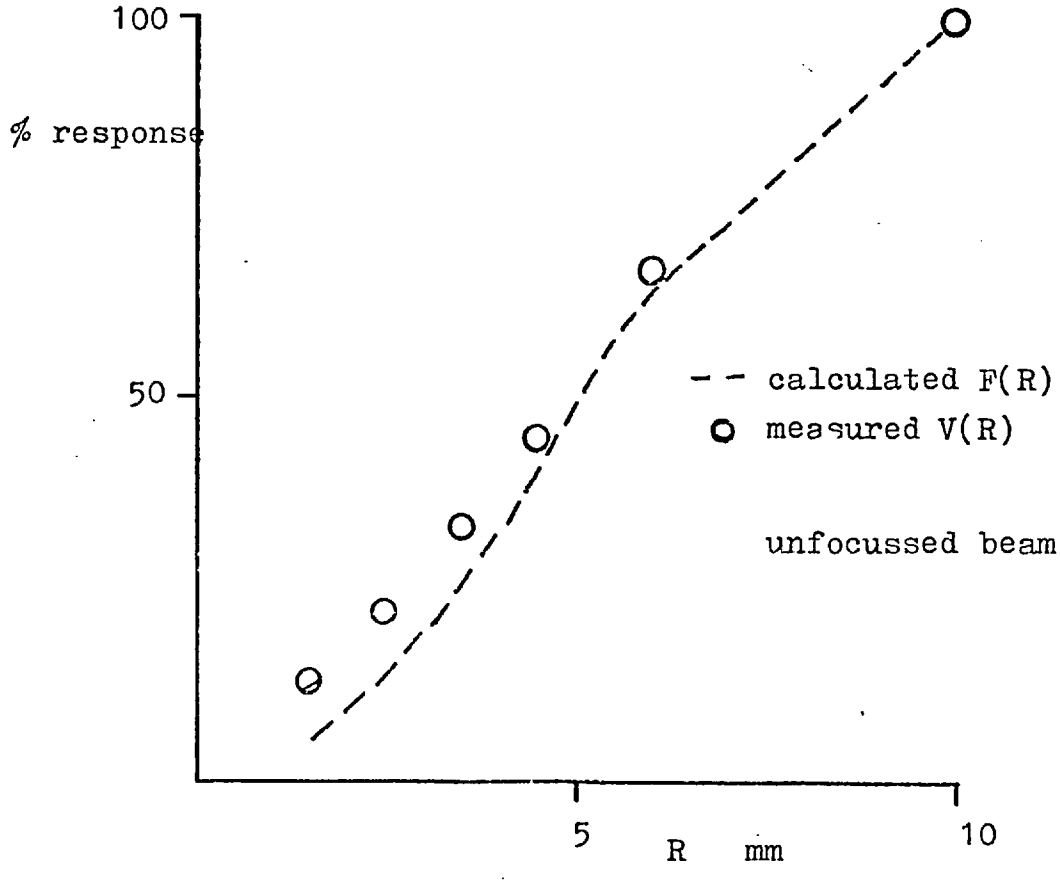


Figure 6.17 Comparison of measured V(R) with calculated F(R) for two sound fields.

total polarisation in the crystal, and this extra signal is relatively more important with small holes. Except for such small discrepancies the addition of the forces on the annular components of the transducer face appears to agree with the measured behaviour of the transducer. The receiving transducer element produces a voltage which is proportional to the total force and therefore to the average pressure, on its face. This implies that the relative magnitudes of two signals from a transducer will depend not just on the peak pressure in the pulse incident to the transducer but also on the shape of the incident wavefront. Two pulses with the same peak amplitudes may induce different voltages because they are different in shape or extent, whilst two reflectors formed from materials with different acoustic impedances but surrounded by the same medium, can produce the same voltage at the receiver. In particular, the spatially uniform pressure of a wave reflected from a weakly reflecting plane, can exert the same force on a transducer as a curved wavefront from a small interface whose composition is very different from that of the plane. This effect will be reduced when the transducer area is small, but in general, by averaging the Echo Field pressure over a relatively large area, the apparent impedance change at an interface is modified and information on the physical composition of the medium is lost.

6.4 Conclusions

In a quantitative analysis of echo amplitudes, the characteristic of the Object which is of interest is the physical composition of reflecting interfaces but it is clear that the relative amplitudes of echoes are dependent on several factors which are unrelated to this physical composition. Physical information is lost whenever the echo amplitude depends on geometrical variables that are independent of the material acoustic properties and it has been demonstrated that the distinction between Physical and Geometrical information is not useful except when the reflectors have simple shapes. The formation of replica pulses at discontinuities in the Object, the effect of angle of incidence of the sound beam, the influence of reflector shape and size, are factors that are unrelated to the density or elasticity of the Object, and such variables are therefore potentially sources of artefact in an image that records echo amplitudes quantitatively. Furthermore, the precise influence of such effects is determined by the design of the scanner, and particularly by the shape of the Search Field. The dependence of echo amplitude on angle is reduced when the sound beam is focussed, as is the size of the reflector which appears as an infinite plane. The shape of the pulse (in three dimensions) determines the direction and distribution of the Echo Field, whilst the area of the receiving transducer determines the size of the sample of the Field over which the pressure is averaged.

The usefulness of a scanner for obtaining quantitative information on the composition of the Object is partly determined by the Angle and Area Factors but these can be derived

from the Point Spread Function discussed earlier. Similarly, the importance of replica pulses can be related to the pulse shape and system bandwidth that were considered in Chapters 4 and 5. Whilst the influence of the design of the scanner may be described simply in terms of the transfer characteristics used to describe resolution and sensitivity, the intrinsic character of the Search Field remains a considerable limitation on the general usefulness of amplitude quantisation. Although several workers have reported applications of such analyses, there are hazards inherent in these procedures and considerable care must be taken to prevent incorrect interpretations of the amplitudes of isolated echoes.

Chapter 7: An analysis of grey scale images

7.1 Methods of tissue differentiation

The A scan produced by irradiating real tissues contains not only the distinct echoes produced at interfaces whose dimensions are much larger than a wavelength, and which correspond to abrupt changes in the physical composition of the tissue, but also many small, closely spaced pressure fluctuations in which separate echoes are not clearly distinguishable. These signals can be displayed on a B scan which has a dynamic range that is sufficiently wide, and scanners which successfully record these different amplitude echoes produce so-called grey scale images. The special requirements of a scanner for grey scale imaging have been extensively discussed in recent years (Kossoff, 1972, Hill, 1976). Considerable attention must be given to methods of increasing the sensitivity and dynamic range of the recording technique in order to depict the small echoes from inside tissues. For example, Kossoff (1972) compresses the echo amplitudes logarithmically, he enhances the small amplitudes further by differentiation, and records the B scan by an open shutter technique from a non-storage oscilloscope onto a film whose speed and spectral response are carefully selected. The advent of non-integrating scan converter tubes has obviated the need for some of these procedures, and partly because of the ease with which grey scale patterns can now be produced, they are widely acclaimed as an aid to interpreting scans and diagnosis.

At present, grey scale images are not quantitatively analysed although some authors have discussed the potential use of grey scale patterns for characterising different tissues

or as indicators of the changes in a tissue that are produced by disease (e.g. Rattenmaier, 1973). However, grey scale cannot be fully exploited as a method of differentiating between tissues unless the origin and nature of the scattering from inside tissues is properly understood. No attempt has been made at describing the scattering processes which give rise to the echoes shown in a grey scale image. With such a description it may be possible to extract diagnostically useful information about tissues from analysing B scan patterns, but without an understanding of the nature of these diffuse echocs, grey scale images can only be used as qualitative aids to diagnosis.

Other methods of characterising tissues by quantitative analyses of the echoes from inside tissues have not yet produced many results of practical significance. Chivers (1973) analysed the frequency spectra of the sound backscattered from a small region of tissue and found this depended on the sample's orientation as well as the type of tissue. Lele (1975) has similarly analysed the spectral composition of the sound produced from inside cardiac tissues and found the spectrum changed if the tissue was infarcted. Hill and Nicholas (1975) have reported that when monochromatic sound waves are scattered from inside tissues the intensity of sound is not equal in all directions, but is predominantly scattered into several discrete directions. The angular spectrum of the scattered wave may be of diagnostic significance (Hill, 1976). Wells and Mountford (1972) analysed the distribution of amplitudes in the train of echoes from inside livers and found the distribution was different when the liver was cirrhotic.

This statistical analysis of amplitudes must account in some way for the B scan appearance of a liver irradiated in the same way, and it should relate to the findings of any of the spectroscopic techniques, but no attempt has been made to establish connections between these different approaches. The discussion below is intended to indicate how these apparently dissimilar techniques may be related, and by properly describing the scattering from inside tissues, to outline a possible alternative method of analysing ensembles of echoes.

7.2 The inhomogeneous wave equation

Sound waves in homogeneous media can be described by the homogeneous wave equation (see Chapter 1) which predicts that plane waves of sound propagate without being scattered when the density ρ and compressibility K are everywhere uniform. Therefore any model which is constructed which allows tissues to have uniform acoustic properties can be used to describe the formation of distinct echoes from large interfaces only. A more suitable model of a tissue interior that can be used to predict scattering assumes that the macroscopic tissue properties only tend to their mean values when averages are taken over large tissue volumes. The density and elasticity of small tissue samples fluctuate about the mean value so that in a region of tissue the local acoustic properties differ from the average values in the rest of the medium. Sound waves will be scattered in such an inhomogeneous medium and the echoes from inside a tissue can be attributed to density - elasticity fluctuations. These fluctuations may be distributed randomly or regularly throughout the tissue.

The equation which describes the propagation of plane waves in an inhomogeneous medium has been derived by several authors (e.g. Morse and Ingard, 1968; Chernov, 1960). Suppose that in some region V the density of the medium is ρ' and its compressibility is $K' = (\rho' c'^2)^{-1}$ where c' is the wave velocity in V, whereas these quantities have values ρ, $K = (\rho c^2)^{-1}$ throughout the rest of the medium. The differential equation for the acoustic pressure either inside or outside the region V assuming small amplitude vibrations, is

$$\nabla^2 p - \frac{1}{c^2}\frac{\partial^2 p}{\partial t^2} = \frac{1}{c^2}\frac{\partial^2 p}{\partial t^2}\gamma(\underline{r}) + \mathrm{div}(\lambda(\underline{r})\,\mathrm{grad}\,p) \qquad \ldots.7.1$$

where $p = p(\underline{r},t)$, the acoustic pressure at position $\underline{r}$ at time t

$\gamma(\underline{r}) = \frac{K' - K}{K}$, the fractional difference between the bulk modulus inside V compared to outside

$\lambda(\underline{r}) = \frac{\rho' - \rho}{\rho'}$, the fractional difference between the density outside V compared to inside.

γ and λ are both zero outside V. The terms on the right of this equation represent sources of sound produced by scattering an incident sound wave from the non-uniformities in V. The echoes produced when a wave passes through tissues represent the energy scattered out of the wave by fluctuations in the tissues acoustic properties. Grey scale is essentially a technique of depicting the manner in which the density or elasticity of a medium fluctuates. The differential equation may be transformed to an integral equation and solved by using the time dependent Green's function (Morse and Ingard, 1968). Rewriting 7.1 as

$$\nabla^2 p - \frac{1}{c^2}\frac{\partial^2 p}{\partial t^2} = -f(\underline{r},t)$$

the sound scattered to any position defined by vector $\underline{r}$ is $p_s(\underline{r},t)$.

$$p_s(\underline{r},t) = \int \ldots \int f(\underline{r}',t')\, g(\underline{r},t:\underline{r}',t')\, d^3\underline{r}'\, dt' \qquad ..7.2$$

where $g(\underline{r},t:\underline{r}',t') = \dfrac{\delta\left(t - t' - \frac{|\underline{r}-\underline{r}'|}{c}\right)}{4\pi|\underline{r}-\underline{r}'|}$

The scattered sound field can be calculated by successive approximations, but when the fluctuations in the physical properties of the medium are small then the scattering is weak and the first Born approximation can be used to evaluate the integral. The total wave amplitude can be written as the sum of the incident sound pressure, p_i, and the scattered sound pressure, p_s, which is always much smaller. To first order, therefore,

$$p_s(\underline{r},t) = \int\!\!\ldots\!\!\int \left(-\frac{1}{c^2}\frac{\partial^2 p_i}{\partial t^2}\cdot\gamma(\underline{r}') - \operatorname{div}(\lambda(\underline{r}')\operatorname{grad} p_i)\right).$$

$$g(\underline{r},t:\underline{r}',t')\, d^3\underline{r}'\, dt' \qquad \ldots.7.3$$

The scattered pressure at any point is dependent on the spatial distribution and magnitude of the elasticity and density fluctuations, and on the incident sound pressure. Equation 7.3 could be used to calculate the scattered pressure in any direction for any incident wave, but here we confine the discussion to the solution for backscattered sound produced by a realistic pulse, which is the solution of interest for A scanning and for single lines on a B scan.

7.3 Solution for backscattering of pulses

The integral can be considerably simplified by making assumptions about the pulse which do not lead to a serious loss of accuracy. The incident sound pressure pulse can be expressed as an equivalent ensemble of plane waves with suitable amplitudes and directions by means of a three dimensional Fourier Transform. In the frequency domain ($\underline{k}$ - space) each plane wave has wave vector $\underline{k}'$ so that

$$p_i(\underline{r}',t) = \int_{-\infty}^{\infty} G(\underline{k}' - \underline{k}) e^{i(\underline{k}' \cdot \underline{r}' - w't)} \, d^3\underline{k}'$$

where $w' = c|\underline{k}'|$

$\underline{k}$ = the wave vector about which the distribution $G(\underline{k})$ is peaked

It is convenient to express the vectors in terms of a cylindrical coordinate system

$$\underline{k}' = (q,\phi,k)$$

$$\underline{k} = (0,0,k_o)$$

$$\underline{r}' = (\rho,\theta,z)$$

If the pulse is produced by a circular transducer then it is symmetric about the transducer axis, and if it propagates unchanged in shape then the variables can be separated so that

$$G(\underline{k}' - \underline{k}) = A(k - k_o)F(q)$$

Suppose that $k \gg q$ for all the $\underline{k}'$ of interest.
Mathematically this implies that the component vectors of $G(\underline{k}')$ point predominantly in the direction z away from the transducer, and that their components in directions orthogonal to z are much smaller than k. Physically, such a pulse corresponds to

a wave packet that does not spread away from the axis of propagation and which travels unchanged in shape with velocity c.

$$w't = ct(k^2 + q^2)^{\frac{1}{2}} \simeq kct$$

Assuming that $\frac{q}{k} \ll 1$, the pulse becomes

$$p_i(\underline{r}', t) = \int_0^{2\pi} \int_0^{\infty} \int_0^{\infty} A(k - k_o) F(q) e^{ipq\cos(\phi - \theta)} \cdot e^{+ ik(z - ct)} q\,dq\,dk\,d\phi \quad ..7.4$$

$$= a(z - ct)\, p(\rho)\, e^{ik_o(z - ct)}$$

$a(z)$ = the pulse envelope shape, whose Fourier Transform is $A(k)$. At time $t = 0$ the pulse is centred about $z = 0$.

$$p(\rho) = 2\pi \int_0^{\infty} F(q)\, J_o(\rho q)\, q\,dq$$

= the Hankel Transform of $F(q)$. $p(\rho)$ is the lateral beam profile in the sound field of the transducer, here assumed independent of z. $p(\rho)$ is related to the Point Spread Function introduced in Chapter 5 and to the Area Factor of Chapter 6. It is equivalent to the Angle Factor derived in Chapter 6 for a plane.

The approximation used above is equivalent to assuming that the width of the lateral pressure profile is much greater than the fundamental wavelength of the carrier wave in the pulse. It does not necessarily imply that the bandwidth of a pulse is restricted but it does require that the spatial frequencies of interest orthogonal to the axis are much smaller than those of interest along the axis. A realistic pulse in

the field of a large aperture, unfocussed but damped transducer has a beamwidth several times greater than the axial pulse wavelength, so the approximation is valid for many real pulses. Figure 7.1 shows typical values for $F(q)$ and $A(k-k_o)$ for such limited spectrum pulses.

Equation 7.4 can be substituted into the scattering integral (7.3) and the backscattered pressure calculated at the observation point $\underline{R}$ (Figure 7.2). Using the limited spectrum approximation again, and assuming that the observation point $\underline{R}$ is quite distant from the scattering region so that $\left|\frac{\underline{r}'}{\underline{R}}\right| \ll 1$, $|\underline{R}-\underline{r}'| \doteq R + \underline{r}'.\hat{\underline{n}} = R + z$

$$|\underline{R}-\underline{r}'|^{-1} \doteq R^{-1}$$

then to the first order,

$$p_s(\underline{R},t) = \int\cdots\int A(k-k_o)F(q).\frac{1}{4\pi R}(\ldots)e^{iq\rho\cos(\phi-\theta)}$$

$$e^{i2k(z+R)-ikct}\, q\,dq\,d\phi\,dk\rho\,d\rho\,d\theta\,dz \qquad \ldots 7.5$$

with $(\ldots) = k^2(\gamma(\rho,\theta,z)+\lambda(\rho,\theta,z))$

$$-i\left(q\cos(\phi-\theta)\frac{\partial\lambda}{\partial\rho} + \frac{q}{\rho}\sin(\phi-\theta)\frac{\partial\lambda}{\partial\theta} + k\frac{\partial\lambda}{\partial z}\right).$$

The ϕ and q integrations can be performed first, and the first two terms in the expansion of $\underline{k}'.\nabla\lambda(\underline{r}')$ can be dropped. The first term gives, on integrating over

$$\phi, I_1 = i\int_0^{2\pi} q\cos(\phi-\theta)\frac{\partial\lambda}{\partial\rho}\, e^{iq\rho\cos(\phi-\theta)}\, d\phi = 2\pi\frac{\partial\lambda}{\partial\rho}.\frac{\partial}{\partial\rho}J_o(q\rho)$$

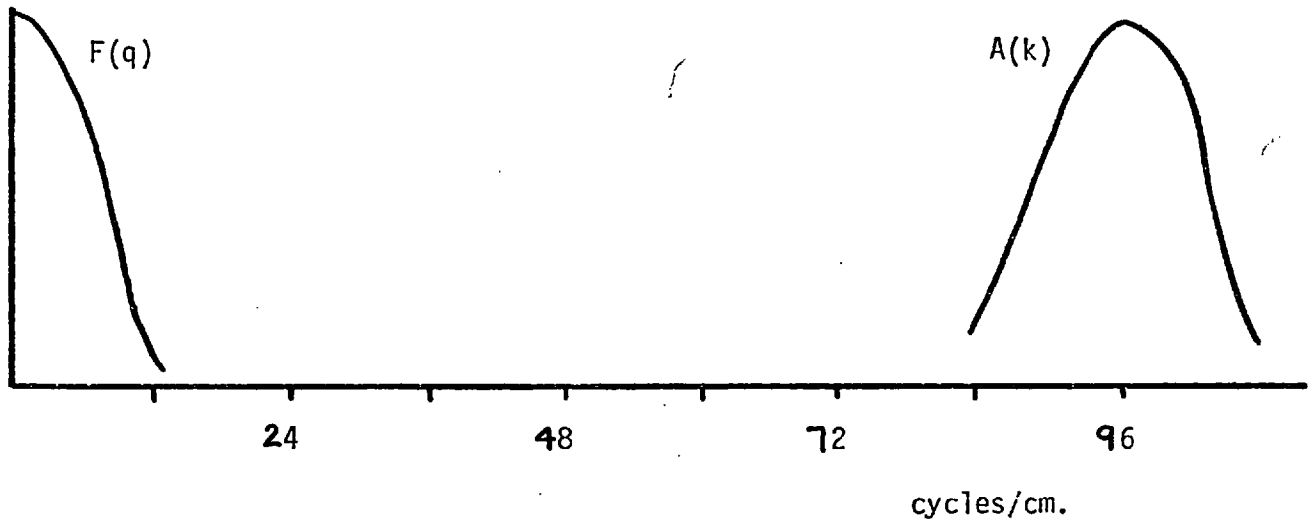


Figure 7.1 Typical frequency domain functions for a pulse from a plane 2.5 MHz transducer.

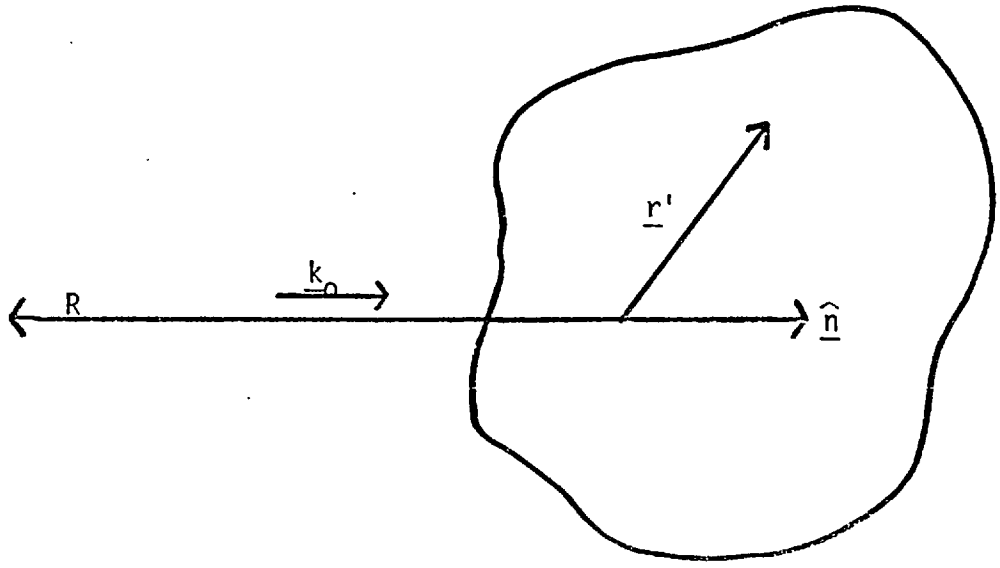


Figure 7.2 Coordinate system for derivation of p_s .

which on performing the integration becomes

$$I_1 = \frac{\partial \lambda}{\partial \rho} \cdot \frac{\partial p(\rho)}{\partial \rho}$$

If the beam profile varies smoothly and $\frac{\partial \lambda}{\partial \rho}$ is never too large then this term is only small. The size of $\frac{\partial p(\rho)}{\partial \rho}$ is indeed never large if the limited spectrum approximation holds as the restricted frequency content of $F(q)$ ensures that $p(\rho)$ cannot vary sharply.

The second term is

$$I_2 = \frac{q}{\rho} \int_0^{2\pi} \sin(\phi - \theta) e^{iq\rho \cos(\phi - \theta)} \, d\phi$$

$$= \rho^{-2} \frac{\partial}{\partial \theta} J_0(q\rho) = 0$$

Thus, to first order,

$$p_s(\underline{R}, t) = \frac{1}{4\pi R} \int \cdots \int p(\rho) A(k - k_0)(\gamma(\rho, \theta, z) + \lambda(\rho, \theta, z) \frac{-i}{k} \frac{\partial \lambda}{\partial z}(\rho, \theta, z))$$

$$e^{ik(2z + 2R - ct)} \, k^2 \, dk\rho d\rho \, d\theta \, dz \, .$$

Various sums and averages of the distributions γ and λ may be defined. An angle average, obtained by integrating the contributions of all the fluctuations of one type on an annulus centred on the transducer axis, of radius ρ and at distance z.

$$\bar{\gamma}(\rho, z) = \int_0^{2\pi} \gamma(\rho, \theta, z) \, d\theta \, , \quad \bar{\lambda} = \int_0^{2\pi} \text{etc.}$$

The contribution of each annulus to the total scattered pressure depends on its radius, ρ, and the sound pressure incident from the transducer. The integral of the contributions of all the annuli of each type at any distance z is

$$\langle \bar{\gamma}(z) \rangle = \int_0^\infty \bar{\gamma}(\rho, z)\, \rho\, p(\rho)\, d\rho, \quad \langle \bar{\lambda}(z) \rangle = \int_0^\infty \text{etc.}$$

Each z-dependent, area averaged contribution to p_s may be expressed as the sum of many components of different spatial frequencies along the transducer axis, by means of a Fourier Transform. The spectrum of frequencies is Γ.

$$\Gamma_\gamma(2k) = \int_{-\infty}^{\infty} \langle \bar{\gamma}(z) \rangle\, e^{i2kz}\, dz,$$

$$\Gamma_\lambda(2k) = \int_{-\infty}^{\infty} \langle \bar{\lambda}(z) \rangle\, e^{i2kz}\, dz$$

and $$-ik \int \frac{\partial}{\partial z} \langle \bar{\lambda}(z) \rangle\, e^{2ikz}\, dz = -2k^2 \Gamma_\lambda(2k)$$

If $\Gamma(2k) = \Gamma_\gamma(2k) - \Gamma_\lambda(2k)$, then (7.5) becomes

$$p_s(\underline{R}, t) = \frac{1}{4\pi R} \int_{-\infty}^{\infty} A(k - k_o)\, e^{ik(2R - ct)}\, \Gamma(2k)\, k^2\, dk$$

The Fourier Transform of the scattered pressure wave is

$$P(\underline{R}, w) = \frac{1}{2\pi} \int_{-\infty}^{\infty} p_s(\underline{R}, t)\, e^{iwt}\, dt$$

so that

$$P(\underline{R}, w) = \frac{1}{2Rc}\, A\left(\frac{w}{c} - k_o\right) \Gamma\left(\frac{2w}{c}\right) \cdot \frac{w^2}{c^2}\, e^{i\frac{2Rw}{c}}$$

$$\Rightarrow \quad |P(w, \underline{R})|^2 \propto \frac{1}{R^2} \cdot w^4 \left| A\left(\frac{w}{c} - k_o\right) \right|^2 \cdot \left| \Gamma\left(\frac{2w}{c}\right) \right|^2 \quad \ldots.7.6$$

Figure 7.3 Illustration of correspondence between A scan and B mode intensity measured as photographic density.

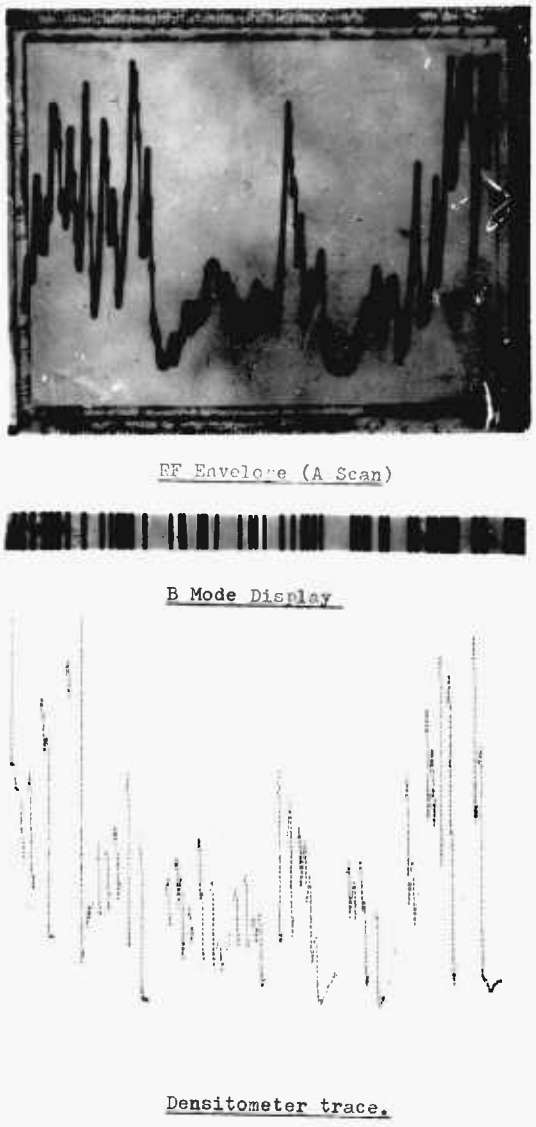
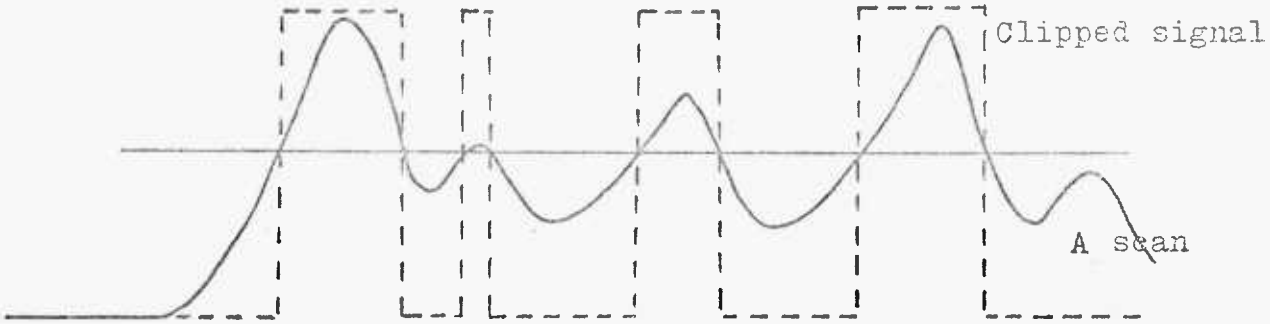


Figure 7.4 Illustration of a clipped A scan which corresponds to a bistable display processing



Equation 7.6 is a relationship between the power spectrum of the sound pressure waveform at the observation point and a function, Γ, that depends on the structure of the tissue irradiated but which also involves factors that depend on the pulse of sound used for the irradiation.

The mathematical assumptions invoked in the derivation of equation 7.6 have already been validated and are reasonably satisfied by real scanners. The physical model of scattering neglects effects of attenuation and multiple scattering, both of which may affect the quantitative validity of the results above. Simple attenuation introduces an extra factor of the form $e^{-\alpha z}$ into the expression for $p(t)$, which formally changes the frequency variable of Γ in the final result to the complex quantity $2(\frac{w}{c} + i\alpha)$ where α is an attenuation coefficient. The effect of attenuation can be removed by correct selection of the gain - depth compensation of the receiver. Furthermore, α is small compared to any of the values of $\frac{w}{c}$ of interest (e.g. if the attenuation 2 dB/cm at 1.5 MHz, $\alpha \sim .23$ cm^{-1}, whilst $\frac{w_o}{c} \sim 20\pi$ cm^{-1}), but even when it is large it is nevertheless a characteristic of the tissue and merely changes the physical interpretation of Γ.

The frequency composition of the scattered sound differs from the spectrum of the voltage in the receiver because the signal is again modified by the response of the transducer and amplifiers. The power spectrum of the electrical signal is therefore

$$|V(w)|^2 \propto \frac{w^4}{R^2} \cdot |H(\frac{w}{c} - k_o)|^2 \cdot |\Gamma(\frac{2w}{c})|^2 \qquad \ldots.7.7$$

where $H(k)$ is the same Impulse Response Function described in Chapter 4.

Furthermore, the demodulated signal is produced by taking only the envelope of the pressure wave, so that the power spectrum of the A-scan is $|V_E(w)|^2$, where the A-scan voltage is

$$V'(t) = V'_E(t)e^{iw_o t}$$

so that

$$|V(w)| = |V_E(w + w_o)| . \qquad \ldots.7.8$$

7.4 Implications for tissue characterisation by B scanning

Equation 7.6 is a quantitative relationship between the power spectrum of the sound pressure at the transducer and a property of the tissue, Γ. It is clear from 7.8 that Γ, which is a function that describes the structure of a tissue but also depends on the scanner, may be estimated by calculating the power spectrum of the A scan envelope and correcting for the frequency response of the scanner. A procedure for performing such calculations is outlined later in this chapter.

The A scan amplitude and B mode brightness are closely related even in systems using non-linear amplifiers. For example, the microdensitometer trace of Figure 7.3, obtained by scanning the negative of a film (Polaroid Type 105) exposed to the B mode of a NE4102 grey scale display, shows good correlation with the corresponding A scan. This suggests that there is a quantitative relationship between the tissue characteristics, Γ, and the power spectrum of the B mode brightness, which could form the basis of objective differential diagnosis. Indeed, both the qualitative impression of grey scale images on the eye and quantitative analyses such as those of Beckley *et al.* (1975) and Rattenmaier (1973) are directly related to the power spectrum of the B mode intensity. A bistable display can be considered at the clipped waveform of Figure 7.4 and the power spectrum of such displays are considered later.

The influence of the scanners' design on the grey scale image can be estimated from the analysis. The echo envelope smoothes out fluctuations in the tissue's properties along

the axis. Spatial frequency components outside the frequencies contained in the pulse envelope are attenuated although there is some compensating effect caused by the fourth power (Rayleigh) term, and we cannot hope to depict details whose spectra are outside the range of $A(\frac{w}{c} - k_o)$. When the pulse is long then its spectrum is sharply peaked around k_o and the smoothing is very severe. At carrier frequencies of 1.5 to 5 MHz, this implies that the signal contains information on structures which lie in the range 0 - 40 cycles per mm. only, suggesting that both A and B scans can derive structural information only on a scale whose spatial dimensions are approximately two orders of magnitude greater than single cell diameters. This information therefore relates to the ordering and distribution of reasonably large populations of cells, and therefore may be called semi-microscopic detail.

The integration of the contributions on any annulus is inevitable but the severity of the averaging over the area of the beam depends on $p(\rho)$. When the sound beam is broad, the number of scattering sites contributing to $p_s(R,t)$ is large (there is a large volume of interaction) whilst narrow beams enable much smaller numbers to be resolved. The grey scale intensity pattern shown on a display is not therefore an intrinsic property of the tissue, but it is a variable pattern that depends on $p(\rho)$, $H(k)$ and w_o. However, the requirements of a scanner for depicting the intrinsic property of tissue (the $\gamma(\underline{r})$ and $\lambda(\underline{r})$) as precisely as possible, are the same as those required for good B-scan resolution, and the descriptions of scanner performance in terms of $H(k)$ and $F(q)$ are useful here.

The nature of the scattering however, is itself dependent on the sound field used. In the derivation of equation 7.6, a component of $\underline{k}'.\nabla\lambda(\underline{r}')$ was dropped on the assumption that the gradient of the beam profile, $\frac{\partial p}{\partial \rho}$, was small. When the beam profile changes rapidly (as with a focussed transducer) this contribution is not negligible so there is an extra contribution to the scattering from the fluctuations in density. It may be possible to deduce the nature of a fluctuation from its behaviour in different sound fields. Even with a broad beam, the density and elasticity fluctuations scatter with different phases, so that phase sensitive detection methods may also help deduce more about the nature of the scattering.

7.5 A possible method of tissue characterisation.

There has been little evidence produced by other workers to substantiate claims that tissues possess characteristic structures whose dimensions may be determined by ultrasonic scattering techniques, although consistent claims have been made about the ability to recognise tissues from their grey scale image appearances. The analysis above indicates how a tissue property may be determined by measuring the spectrum of backscattered sound. The method of Chivers and Hill (1975) can be used to determine $|\Gamma(\frac{2w}{k})|$ directly, and from their results it is apparent that this tissue function changed with the orientation of the specimen. The usefulness of any method of identifying tissues is dependent on the nature of the tissue concerned. If the distribution of scattering inhomogeneities is isotropic and stationary then the tissue can be described by a single measurement in any direction from any position, although the result need not be specific to any single type of tissue. For such a medium, for example, the statistical analyses of Mountford and Wells (1972) are independent of the position in the organ from which the A scans are derived and the results should be invariant under rotation or translation of the transducer. However, the statistical properties of tissues may be only weakly stationary in which case the single spectrum analysis of Chivers and Hill can indicate results that vary with translation as well as rotation. The observed variation with angle indicates that tissues are not isotropic and the more recent work of Nicholas and Hill (1975) supports this conclusion. Their results demonstrate that the scattering from small volumes is not just a stochastic

phenomenon but suggest that coherent interference effects between the sound from different scattering sites may be used to indicate short range ordering in tissues. However, their rotation of the tissue sample about a single axis cannot be used to characterise a general three dimensional structure and is useful by itself only for a severely restricted class of structures.

The usefulness of these or any other procedures depends on the existence or non-existence of structural regularity, isotropy and stationarity, which are analogous to the requirements of stationarity and ergodicity which condition the use of standard statistical methods elsewhere. In order to fully determine the spatial distribution of scattering inhomogeneities it is necessary to uniquely invert a scattering integral, and this requires measurements other than single A scan measurements. In the notation of Section 7.3 the measurement of a single A scan power spectrum will yield information only on the variation of the function $\langle \bar{\gamma}(z) \rangle - \langle \bar{\lambda}(z) \rangle$ with z, which by itself cannot be used to obtain a unique $\gamma(\underline{r}) - \lambda(\underline{r})$, the ρ and Θ integrations enabling several different functions to possess the same averages. However, measurements of the variation of echo amplitude on a time gated C scan would give information on the ρ dependence, and measurements using asymmetric sound fields could be used to unravel the Θ dependence. Alternatively, the A scan power spectrum could be measured with different orientations of the sound field in the tissue, and quantitative information obtained about $(\gamma - \lambda)$ whether or not the inhomogeneities are distributed in a regular matrix or randomly.

There therefore appears to be some justification for investigating the power spectra of single A scans or single B mode lines, and although it was not the purpose of this thesis to report the results of experiments on tissue characterisation, it is worthwhile reporting a possible method of signal analysis which may be useful in practice and with which some preliminary results have been obtained.

The Wiener - Khintchine theorem relates a power spectrum to a time domain function, the Autocorrelation Function, by means of a Fourier Transform. The Autocorrelation Function is a well documented approach to the analysis of deterministic signals hidden in noise (e.g. Champeney, 1972) and it contains information about random as well as the periodic components of a signal. It is therefore particularly suitable to the analysis of signals which adhere strictly to neither category and which contain elements which are correlated over short times only. The joint probability density function of a stationary, ergodic process denoted by the function $p(t)$ gives the probability that the value is p_1 at t and p_2 at $t+T$. The Autocorrelation Function is the first moment of this joint density, and is generally written in the form

$$C(T) = \lim_{t' \to \infty} \frac{1}{2t'} \int_{-t'}^{+t'} p(t)\ p(t+T)\ dt$$

for real $p(t)$. It represents the correlation between the values of a function at different positions and summarises the statistical information about the various characteristic dimensions that describe the function. In this context these

correspond to characteristic lengths in tissue, and where there is local regularity in the parent function then there is an oscillation in the value of C(T). When normalised by dividing by the integral of the square of the parent function, $\frac{C(T)}{C(0)}$ is unity at the origin and tends to a constant value as T, the lag, increases. The significance of the shape of C(T) has been discussed elsewhere (e.g. Bendat and Piersol, 1966). The Wiener - Khintchine relations give

$$C(T) = \frac{1}{(2\pi)^{\frac{1}{2}}} \int_{-\infty}^{\infty} |P(w)|^2 \, e^{iwT} \, dw$$

where

$$P(w) = \frac{1}{(2\pi)^{\frac{1}{2}}} \int_{-\infty}^{\infty} p(t) \, e^{-iwt} \, dt$$

Thus, the area under the power spectrum, the autocorrelation function at zero lag, and the mean square amplitude are equivalent. The power spectrum contains no extra information than the Autocorrelation Function but both contain considerably more information than a first order statistical analysis of p(t). For a satisfactory estimate of C(T), however, different conditions must be satisfied than with a power spectrum measurement. For example, a sufficiently long sample of signal must be obtained to provide a reliable estimate of the asymptotic values of C(T) at large lags, but such errors and difficulties are understood in principle and have been summarised for example, by Blackman and Tukey (1958) and Jenkins and Watts (1968).

Preliminary experiments have been undertaken to demonstrate the feasibility of estimating the Autocorrelation Function of ultrasonic signals. Echoes were produced from inside samples of tissues suspended in a water bath and the envelope of the electrical signals from the transducer was recorded onto film from an oscilloscope on which the time base was adjusted so that 100 mm of the oscilloscope screen represented 5 mm of tissue. The photographic records were then traced using a pen whose coordinates were digitised with a spatial resolution of better than 1 mm, and the digital information was stored in a Hewlett-Packard 2100 mini-computer. In this way the pressure envelope was sampled with an equivalent resolution better than 1/20 mm.of tissue. Autocorrelation Functions were calculated on equi-spaced samples and power spectra were estimated by Fourier Transformation. The numerical techniques used followed closely the recommendations of previous workers, particularly Bendat and Piersol (1966), Blackman and Tukey (1958), and Dainty and Shaw (1974). The estimated discrete power spectrum was smoothed using a three point convolution with coefficients $\frac{1}{4}, 1, \frac{1}{4}$ (conventionally referred to as Hanning), but the choice of smoothing window does not appear to be critical and has been discussed by Blackman and Tukey. A computer programme was devised to perform such calculations on the HP2100 and some results are shown in Figure 7.5. These preliminary results have not been corrected for the smoothing of the pulse shape but they demonstrate that such calculations can be performed without specially dedicated spectral analysers, although the particular method of data handling used here is obviously not a practic-

able technique for any but experimental purposes. The curves shown in Figure 7.5 indicate the general shape of the Autocorrelation Functions found by analysing the signals from specimens of bovine liver, and they show that the Autocorrelation changes quite drastically when the specimen is rotated or when the transducer frequency is changed, confirming that bovine liver is not statistically isotropic. Furthermore, the change with frequency implies that the distribution and characteristic separation of echoes in a grey scale image varies with the frequency and bandwidth of transducer used.

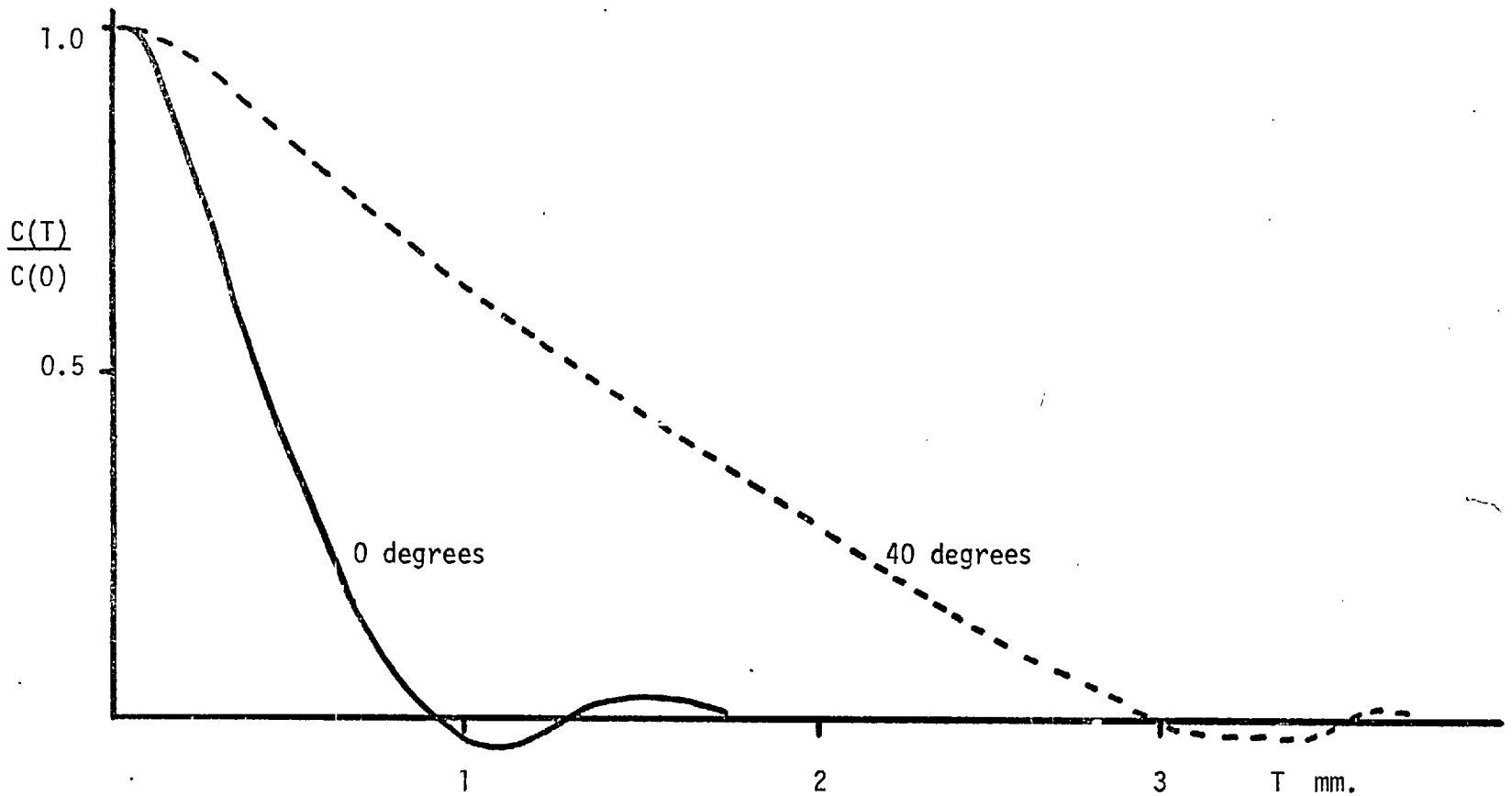


Figure 7.5a Autocorrelation Functions of envelopes of sound from bovine liver for different orientations of the specimen.

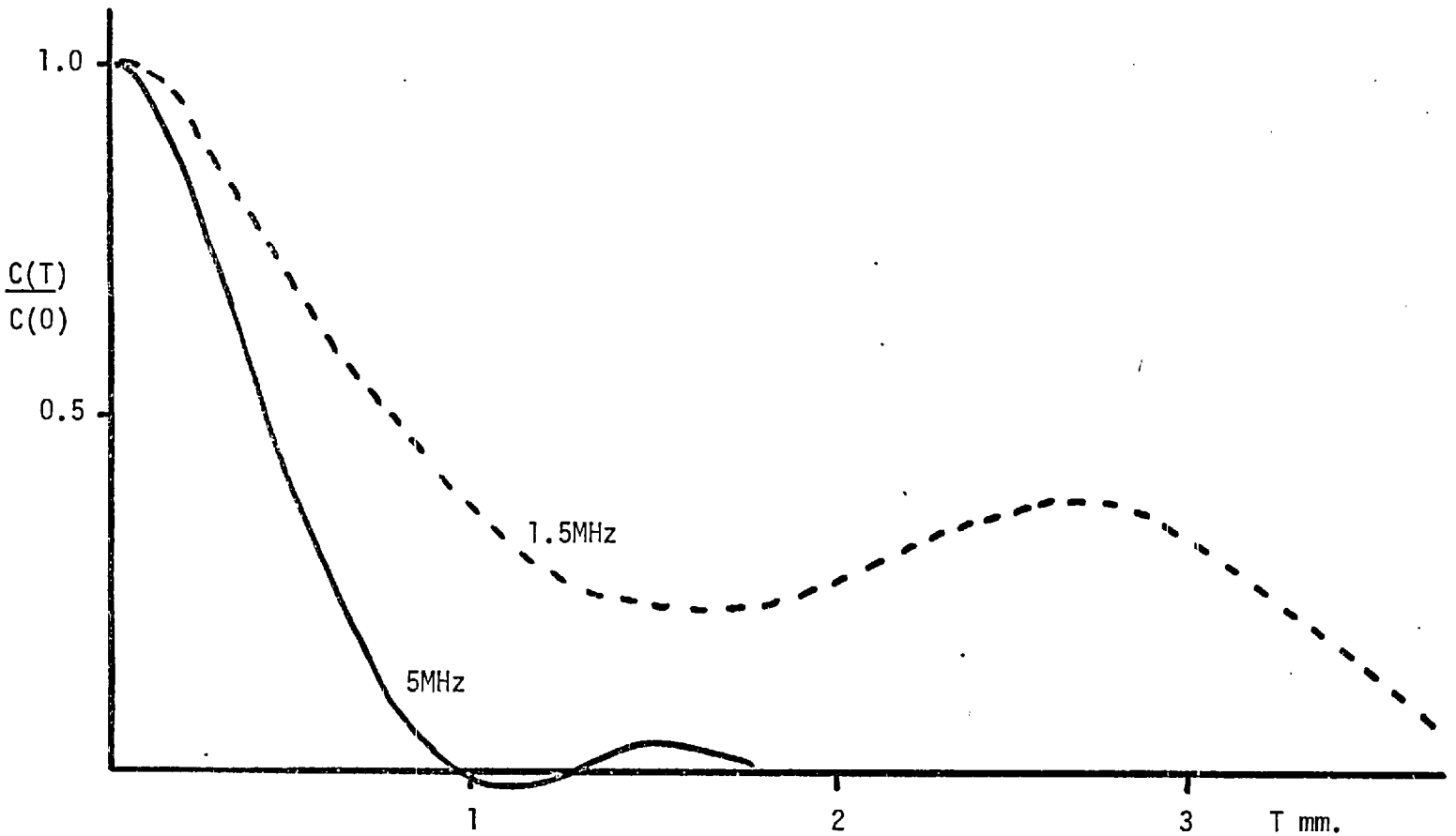


Figure 7.5b Autocorrelation Functions of envelopes of pressure from bovine liver for different transducer frequencies.

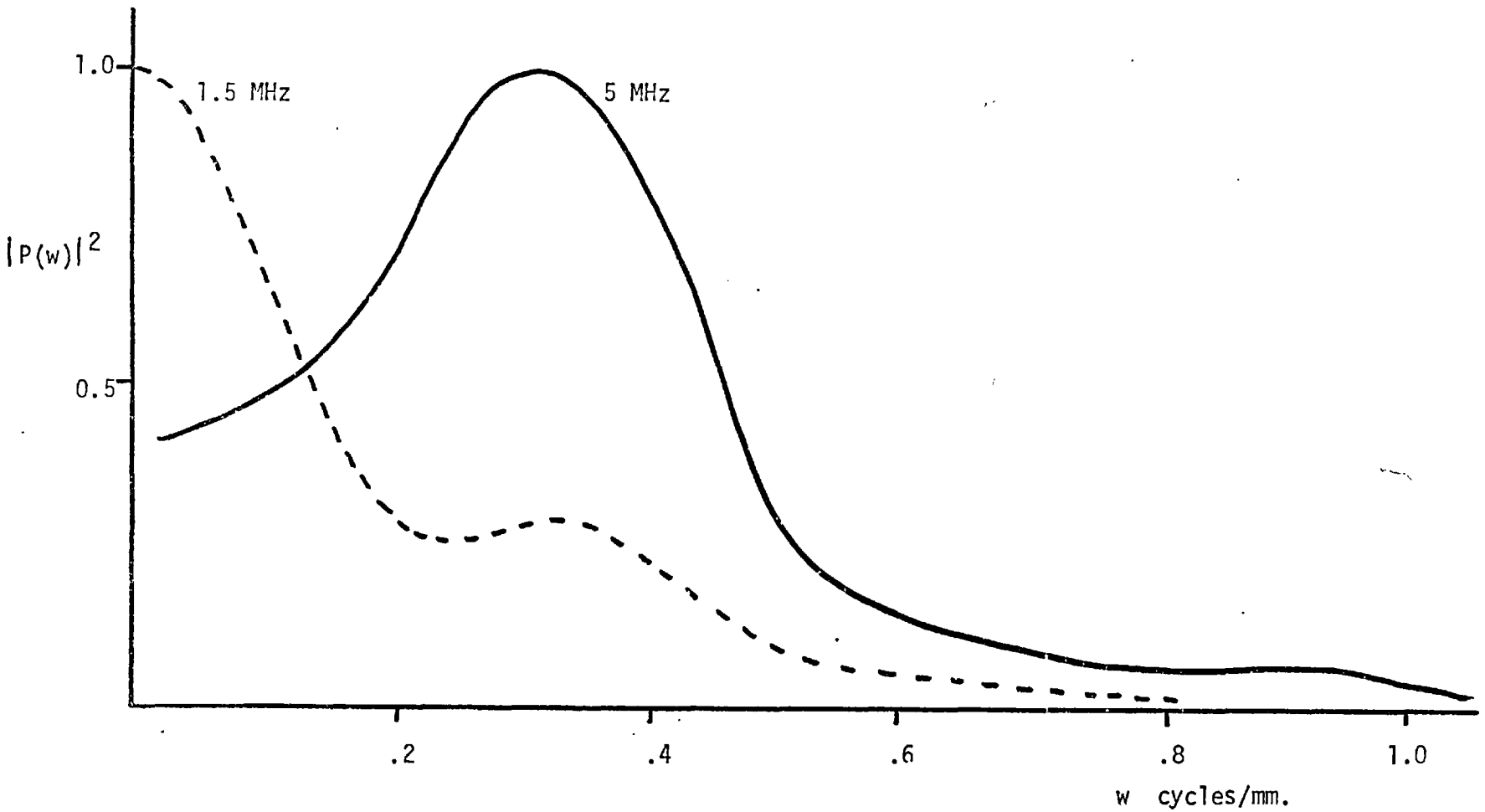


Figure 7.5c Power spectra of envelopes of sound from bovine liver at different frequencies.

7.6 Conclusions

A model of the scattering of realistic pulses of ultrasound from tissues was used to predict the kind of information obtainable by backscatter measurements, and although a method of implementing such measurements has been indicated with a procedure for calculating suitable parameters, no results have yet demonstrated the practical feasibility of identifying tissues from their scattering characteristics. It is necessary however to continue such measurements to identify those structures of tissues that are characteristic and to obtain anatomical correlations to the theoretical model. The analysis above, perhaps in conjunction with its natural extensions to the C scan, sector scan or other scanning geometries, may prove useful as the basis of a method of differential diagnosis. Certainly it goes some way towards explaining the origin and character of the echoes depicted in a grey scale image, and it shows the dependence of these on scanner design. It clarifies the use of quantitative analyses of grey scale images.

Equation 7.7 shows that the raw video envelope possesses an Autocorrelation Function of the form

$$C(T) = C_1(T) * C_2(T)$$

where * denotes a time domain convolution

$C_1(T)$ = the Autocorrelation Function of the second derivative of the pulse reflected from a plane interface

$C_2(T)$ = the Autocorrelation Function of $\langle \bar{\gamma}(z) \rangle - \langle \bar{\lambda}(z) \rangle$.

The B mode processing certainly modifies the spatial frequency spectra of grey scale signals, but the changes can be understood and corrections made if desired. For example, when the B mode brightness is simply the A scan amplitude clipped as shown in Figure 7.4 then the B mode power spectrum can be calculated (Van Vleck and Middleton, 1966). When the nature of the signal is known then further calculations can yield useful information. For example, the mean duration of signal maxima and minima, the average number of crossings of the signal through a reference level, or higher order probability functions, may each indicate the results of changes in the signal processing, and the significance of such parameters has been discussed by Beckmann (1968)

If Autocorrelation Functions do contain useful information that can be used to characterise tissues then further development of equipment to perform measurements of them will be justified. However, analogue autocorrelators operating in real time with adequate response are already available using either surface acoustic wave or charge coupled devices, so that instrumentation may be a minor obstacle to clinical implementation.

Chapter 8 Some further problems.

In this thesis several problems encountered in the evaluation of ultrasonic scanners, and related topics that are poorly understood, have been approached from directions that do not appear to have been previously investigated. Some of the limitations on the information obtainable by pulse echo techniques have been indicated and related to practical scanner design. It is therefore appropriate that some of the general conclusions of this survey of pulse echo methods are summarised and some of the problems outstanding are indicated.

A straightforward method of evaluating scanners would be to assess the quality of images produced by scanning patients in realistic conditions. Despite the difficulties of performing such measurements quantitatively, this method will no doubt remain important when equipment is chosen since clinicians are likely to be influenced more by the reputation and published scans from a manufacturer than by objective numerical criteria as proposed here. However, subjective impressions of image quality are not adequate indicators of how well a scanner performs in general circumstances, nor do they aid the scanner designer to compare different scanners quantitatively or specify precisely the limitations of any device.

Similar difficulties are inherent in the use of phantoms that are realistic (i.e. in some way tissue equivalent) which purport to represent typical objects of diagnostic significance, although the standardisation of such phantoms allows images to be meaningfully compared. However, realistic phantoms cannot represent all the objects of interest that occur in general, nor is it clear what features should be reproduced in a test object. Despite these difficulties, the requirement for checking ultrasonic scanners on an everyday basis has been largely

satisfied by the intuitive approach of physicists familiar with clinical imaging problems. Suitable methods have been developed for checking those characteristics that are known to affect images, and the measurements summarised in Chapter 3 are examples of these. Although the number of possible measurements is large, the accumulated experience of people in the field suggests that relatively few measurements is sufficient. However, it is also clear that some of the concepts used to compare scanners are not well understood. Although several attempts of measuring resolution have been made, and although most workers believe it is important, it is not clear what is really meant by resolution or how it should be defined. Programmes that use test objects fail to specify resolution properly, and the measurements made with any object do not give results that are intrinsic to the scanner alone.

The approach to resolution suggested here produces analytic methods of measuring intrinsic characteristics of the scanner which are themselves derived from basic definitions of relevant image parameters. These analytic methods do not conflict with the pragmatic requirements of clinicians. They use measurements of phantoms that are simple and easily realised and the particular definitions suggested herein enable indices of resolution to be calculated simply. Specifically, it has been shown that an A scan can be described by a transfer function that can be measured with a phantom that is merely a plane reflector. The definition of resolution proposed in Chapter 4 can be measured off the A scan display of a single echo but it has a well founded physical interpretation in terms of the spatial frequency response of the scanner.

Similarly, the object element of the B scan is identified as the point reflector, and the scanners response to a point describes its imaging capability, although the validity of general decomposition of B scans using linear analysis is shown to be undermined by the nature of the processes of echo formation. However, where stationarity and linearity can be established the overall imaging process can be modelled by a cascade of transfer functions, each component describing a separate, independent part of the total system. Such a model can be used to provide a useful insight into the system's behaviour especially when single components are changed.

Many of the factors that influence scanner resolution are well understood; obviously the shape of the emitted sound pulse determines resolution but a significant step in analysing behaviour is transformation of the pulse into a frequency spectrum. The limited spectrum approximation introduced in Chapter 7 shows that realistic pulses can be adequately described by two simple functions and our resolution criteria are voiced in terms of these. Single indices of resolution that describe the shape in the frequency domain are used because they give a better representation of the overall shape of the pulse in the space domain. However, these indices have been chosen to be calculable without performing an integral transformation.

The design of transducers has been briefly considered in this thesis to emphasise that the effective pulse shape in any direction depends on independent components such as the receiver and transmitter as well as transducer shape and size in all three dimensions, and to relate such design factors to system transfer functions. The continuous wave theories

of sound fields and transducer resonance that are often used to describe pulse echo systems have limited applicability in this context. The impulse response of a piezoelectric transducer and the transient sound field from an impulse excited radiator, are more clearly derived from the transient analyses emphasised in Appendices B and C. The interdependence of A and B scan resolution, as illustrated by the formation of replica pulses, appears not to have been stressed before. It is likely that these effects will become more important as transducer bandwidths increase. Pulse splitting will also produce image artefacts that have not been previously described.

Some consideration has been given to the significance of the information contained in echoes other than the positions of their origins. In particular, the importance of geometrical factors to echo amplitudes and shapes has been demonstrated, and the relationship between these factors and the design of high resolution scanners has been emphasised. There are other factors not considered here that help determine apparent reflection coefficients and these may also have to be considered when attempting to derive information about tissue boundaries. The significance of echo shape to the characterisation of well defined boundaries remains to be established. The overlap between Geometrical and Physical Information is reiterated in Chapter 7 where it is shown that the pattern of echoes in a grey scale image is a pulse smoothed version of the true scattering structure in tissue, but the relevant filtering function is closely related to the A and B scan transfer functions considered earlier. The grey scale images produced by mapping tissue interiors depend on the shapes of the beams used and even if the carrier frequency is not changed

the images produced with different transducers may be very dissimilar. The analysis of Chapter 7 should be extended to include the effects of overlying tissue but it represents a first attempt at constructing a realistic model of tissues.

There are of course limitations in the analysis given here; and areas of uncertainty remain to be explored. Having used objective definitions of resolution to characterise scanners, we have yet to explore how well such parameters are able to describe good or bad performance, or whether they correlate well with subjective criteria of image quality. Certainly the concept of the ideal image introduced in Chapter 4 is not sufficient to describe the optimum presentation of an image if only because our perception of images relies to some extent on features that are unconnected with sharpness. Although scanner performance can be assessed from the fidelity with which features of the object are reproduced in the image, it is not always clear what features of the object are diagnostically meaningful or how they should be presented for optimal recognition. Further research is required to evaluate what constitutes a good image from the subjective viewpoint so that the parameters used to describe objective performance, and the criteria for good or bad performance, are chosen sensibly. Without correlating objective and subjective appraisals of scanners, it has been assumed that the analytic criteria developed here are a subset of the total set of good performance requirements, and it seems reasonable to suppose that the object - image differences introduced by poor resolution correspond to a loss of information about the object. It is also clear that the requirements of good performance are conditioned partly by the object itself. For example, high

resolution scanners may detect variations in an organ outline which result in a loss of continuity of a boundary that might otherwise be recognised with low resolution.

The analysis of Chapter 7 indicates that useful information is contained in grey scale patterns but it is not clear how best to display such information, although this might be discovered by studies of pattern vision. It is not known, for example, whether differences in the spectral content of arrays of echoes are best portrayed directly in the frequency domain or in the space domain, in the A mode or the B mode, or how the eye recognises differences of this type.

A further problem is that we have chosen to evaluate scanners in isolation from not only the operator but also the effects introduced by regions of tissues. However, the distinction drawn between intrinsic and achieved resolution and the use of one to calculate the other, shows that estimates of behaviour in non ideal conditions can be obtained from simple measurements. For such calculations to be generally applicable however, more data is needed on tissue properties such as attenuation, velocity, and dispersion. In the next generation of scanners, more attention may be paid to further processing of images, in which case the echo forming mechanisms invoked in Chapters 5 and 7 must be carefully evaluated in real situations. A proper study of the Freedman analysis would require a detailed knowledge of the physical properties of tissues but the reward for such a study might be a diagnostically useful classification of reflectors and a sensible technique of enhancing images. It also seems to be likely that increasing interest will be shown in measuring quantitatively the acoustic properties of single tissues in vivo, "tissue

characterisation", so that the behaviour of sound at organ boundaries may then become less important. The possible reward here is the ability to make accurate differential diagnoses which could significantly extend the usefulness of ultrasonic pulse echo techniques in medicine.

Appendix A The Nuclear Enterprises NE4102 'Diasonograph'

The NE4102 is manufactured by Nuclear Enterprises Ltd., in Edinburgh and is at present the ultrasonic B-scanner most commonly found in routine clinical use in the United Kingdom. It embodies most of the features of the present generation of scanners in a semi-modular design that has found wide application in several fields of medicine.

The scanning gantry consists of a motor driven vertical column that supports a metal encasement which houses the transducer arm and positional resolvers. The transducer movement which defines the plane of scanning is monitored by two wire driven linear potentiometers in the case whilst rotation of the transducer in the plane of scan are monitored by a sine/cosine potentiometer attached to the transducer holder. The x,y signals corresponding to transducer position, and $\sin\theta$/$\cos\theta$ signals corresponding to its direction, are used to deflect the electron beam of a cathode ray tube.

The control module contains two cathode ray tubes able to show any two A, TP or B scans simultaneously. The display tubes are Hewlett Packard types 140B and 141B, the latter an integrating storage tube with variable persistence facilities.

Synchronisation of the time dependent functions of the various electronic circuits is provided by a multivibrator (the rate generator) whose frequency is either preset (nominally at 300 pulses per second, which is therefore the Pulse Repitition Frequency, PRF) or which depends upon the rate of change of the transducer coordinates. By differentiating the x,y or θ coordinate voltages, a measure of transducer velocity is obtained

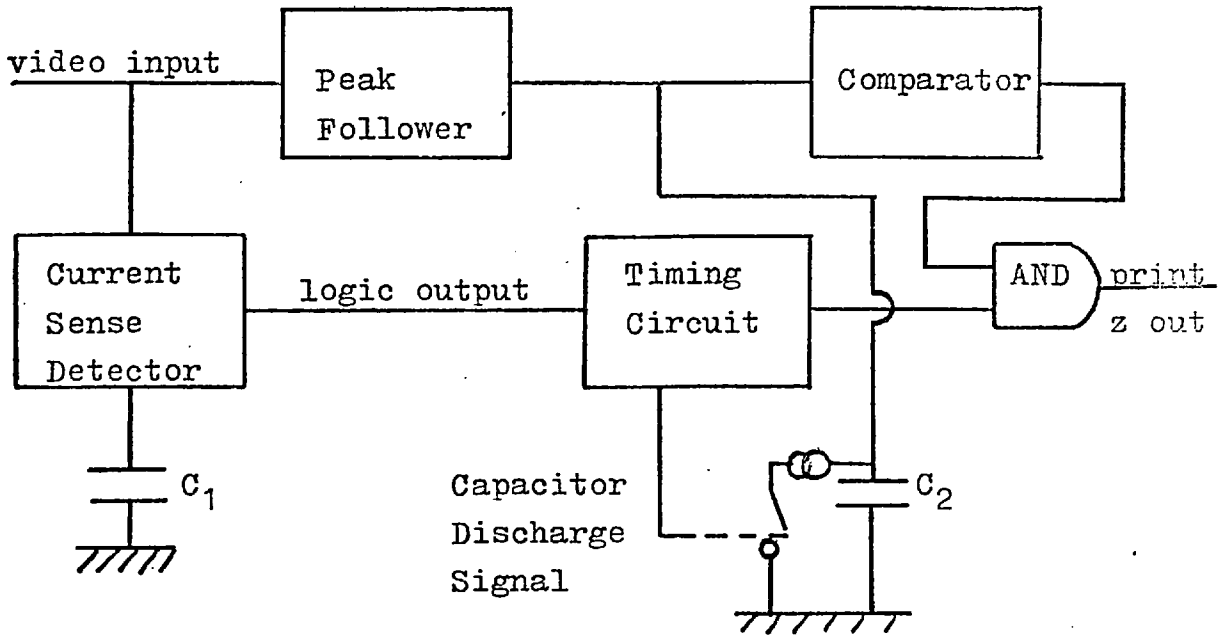


Figure A1 Block diagram of Diasonograph Echo Processing.

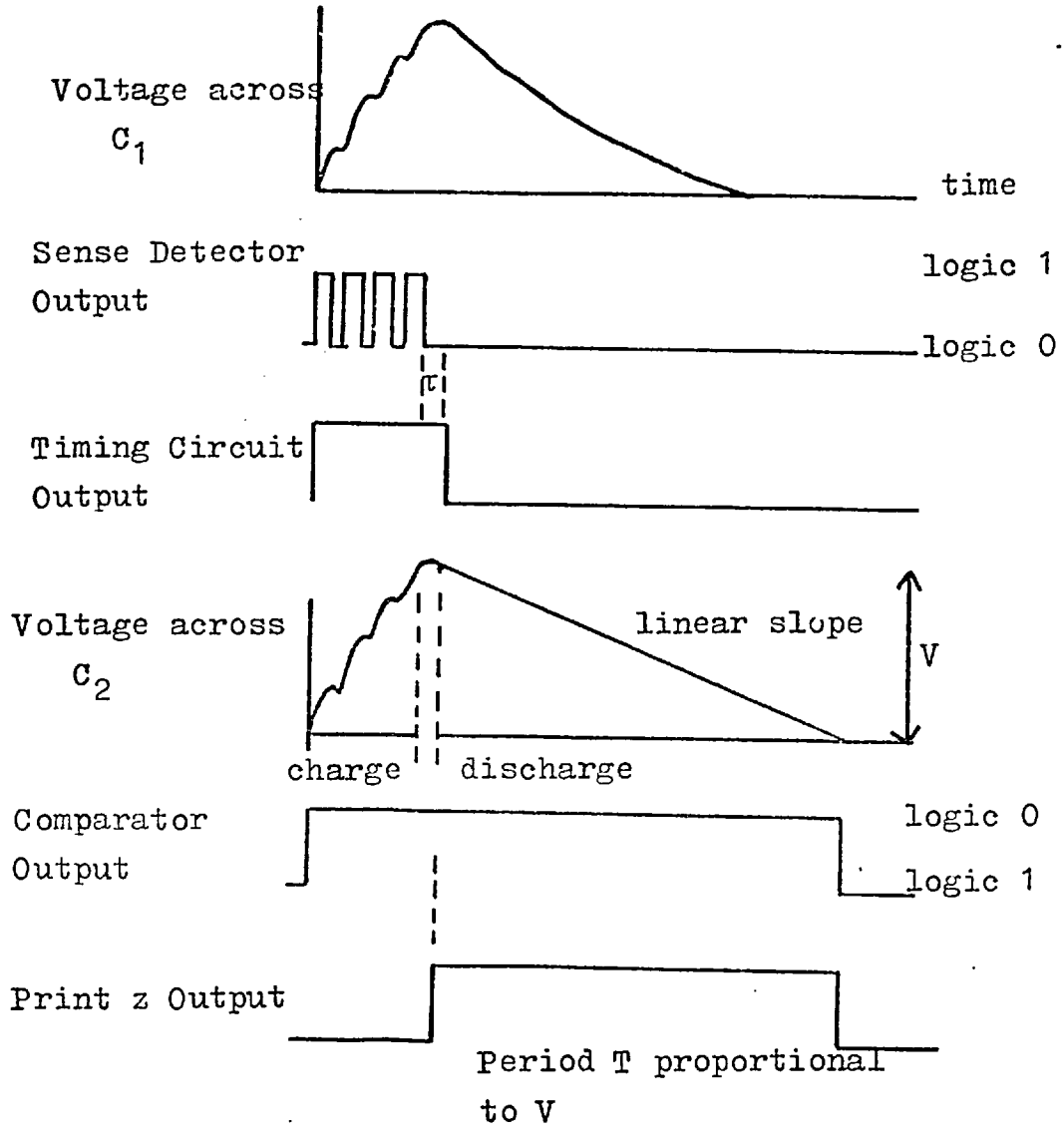


Figure A2 Video Circuit Waveforms of the Diasonograph

and this is used to modulate the PRF. In this 'Velocity mode' the variations in the PRF compensate for an uneven speed of scanning and therefore gives a more uniform time-integrated intensity on the display.

The rate generator provides trigger pulses for the transmitter which uses a thyristor to rapidly switch a power supply and thereby raise the potential difference across the transducer to 700 volts. The active element in the transducer is a lead zirconate titanate ceramic (PZT5) which is rigidly mounted to operate in the thickness expander mode. Each element is backed with an araldite-tungsten compound and is faced with an araldite layer which insulates the crystal and which is conically machined to provide a moderate degree of focussing over much of the useful range of the beam. The transducers supplied with each scanner are 1.5 MHz (20 mm diameter), 2.5 MHz (15 mm diameter) and 5 MHz (10 mm diameter).

The acoustic intensity emitted can be changed by attenuating the voltage impulse supplied to the transducer with an attenuator which is variable between 0 - 48 dB.

The electrical signals produced at the transducer in reception are amplified in a three-stage RF amplifier which is tuned to give a satisfactory response to noise. The frequency response curves of Figure 3.4 show that the 3 dB bandwidth is approximately $\pm$ 25% of a centre frequency, but the centre frequency can be selected to suit he transducer in use.

The gain of the amplifier cannot exceed 80 dB, when it saturates but it can be varied by changing the biasing currents through the bases of the transistors of the second stage of the

amplifier. The time dependence of this bias current controls the depth dependence of the amplification. The time-gain characteristic is determined by choosing an initial value (= 80 - "Initial Attenuation" in dB), a delay (a time during which the gain is constant) and a slope (which determines the rate of increase of gain with time, and is calibrated in dB/cm.). Small signals are removed by a suppression control which has a range of 20 dB.

After the amplification, the signals are full wave rectified and demodulated, and the echo envelope waveform is displayed as an A-scan. By changing the x time base velocity of the display tubes, the distance scale of the A-scan can be varied between $x\frac{1}{2}$ and x20.

The processing of echo signals for the B mode is designed to enhance range resolution and maintain echo amplitude information and it is shown schematically in Figures A1 and A2. The echo envelope waveform is applied to a capacitor C_1 via a current sense detector which is a binary that changes logic level as soon as C_1 begins to discharge. The output of this sense detector is applied to a timing circuit whose period is just greater than one half cycle of the sound carrier frequency. This produces a logic pulse which commences at the beginning of the echo envelope and returns to zero just after the last detected peak. Meanwhile the capacitor C_2 charges with the detected signal until the timing circuit output changes and causes a constant current discharge from C_2 to commence. The duration of this discharge is proportional to the peak echo amplitude. The timing circuit output also sets a bistable

which applies a bright up pulse to the cathode ray tube through a gating system. When the capacitor C_2 has discharged this bistable is reset so that the bright up pulse commences shortly after the echo peak and has a length which is proportional to the echo amplitude. These B-mode pulses vary in length between 100 and 350 nano seconds.

The B-scan is called the section scan on the NE4102 and the linear magnification of the display image is variable between $\frac{x1}{5}$ and x 1. On all modes it is possible to electronically generate two marker pulses which act as calipers for measuring distances. These can be separated and moved, and the time between their generation is converted into a distance which can then be read from a digital voltmeter. The conversion from time to distance is the caliper velocity which can be adjusted by the operator. Similarly, the system velocity, the conversion of times into tissue distances, is independently variable between 1400 and 1700 $msec^{-1}$. Both velocities can be read from the caliper voltmeter.

The images produced by the NE4102 are usually recorded with Polaroid 107 film.

Appendix B: Derivation of the transient response of a piezoelectric transducer

B.1 General Equations

The piezoelectric relations which form the basis of this derivation have been extensively discussed elsewhere (e.g. Mason, 1964) but a less general description may be used with simple crystal geometries. If the equations of state of an isolated transducer are considered (e.g. Cady, 1946) then contributions to the relevant thermodynamic potential may be derived in terms of independent elastic and electromagnetic fields and various material constants. It is assumed below that the coefficients which determine the piezomagnetic, pyroelectric, pyromagnetic, magnetoelectric and thermal expansion contributions are small enough to allow these effects to be ignored. Furthermore, the one dimensional description of a piezoelectric plate which vibrates predominantly in the thickness expansion mode allows the piezoelectric tensor (which in general is a third order tensor relating the second order tensors of stress or strain to electric field vectors) to be reduced to a scalar constant. Thus, two independent fields, the elastic strain $\underline{S}$ and electric field $\underline{E}$, are defined first in terms of scalar potentials (assuming that the strain deformation is irrotational).

$$\underline{S} = -\underline{\nabla} u, \quad \text{where } u = \text{elastic displacement}$$

$$\underline{E} = -\underline{\nabla} \phi, \quad \text{where } \phi = \text{electric potential}$$

For small perturbations, two dependent fields may be defined as linear functions of S and E. The weak field condition

ensures linear coupling of electric and mechanical variables and in practice considers only the direct piezoelectric effect, which is a reasonable assumption for the materials and acoustic intensities of interest here (Mason, 1964).

Elastic stress, $\underline{T} \alpha \underline{S}$

Electric displacement, $\underline{D} \alpha \underline{E}$

For plane thin plates, Hooke's Law and Newton's Equation may be utilised to derive a wave equation. The coupled equations are

$$T = - hD + \frac{c\partial u}{\partial x} \qquad (1)$$

where the first term is an additional stress due to electric polarisation, and the terms refer to X-components of the fields only,

$$E = \frac{D}{\sigma} - h\frac{\partial u}{\partial x} \qquad (2)$$

where the last term is an additional polarisation due to piezoelectric action. Newton's equation in a continuum relates the gradient of stress to the net force per unit volume

$$\rho \frac{\partial^2 u}{\partial t^2} = \frac{\partial T}{\partial x}$$

which combined with (1) gives

$$\frac{\partial^2 u}{\partial t^2} = \frac{c}{\rho}\frac{\partial^2 u}{\partial x^2} - \frac{h}{\rho}\frac{\partial D}{\partial x}$$

If the material has no free charge and is a nonmagnetic insulator, then Maxwell's equations give the divergence of electric displacement as zero.

$$\text{div } \underline{D} = 0$$

This condition assumes that the velocity of the elastic disturbance is much less than the velocity of any associated electromagnetic phenomena, which is the quasistatic approximation discussed in depth by Auld (1973). Since all the fields possess only an x component (for the ideal plate) then

$$\frac{\partial \underline{D}}{\partial y} = \frac{\partial \underline{D}}{\partial z} = 0$$

and therefore $\frac{\partial \underline{D}}{\partial x} = 0.$

$\frac{\partial^2 u}{\partial t^2} = v^2 \frac{\partial^2 u}{\partial x^2}$, an equation that predicts plane waves propogating in the x-direction with velocity V.

By taking Laplace Transform with respect to t only, assuming that all u and $\frac{\partial u}{\partial t}$ are zero at t = 0, then

$$\bar{u} = Ae^{-p\frac{x}{v}} + Be^{+p\frac{x}{v}} \qquad (3)$$

(where $\bar{u} = \int_0^\infty ue^{-pt}\, dt$)

Substituting (3) into the Laplace Transform of (1) gives

$$\bar{T} = \frac{cp}{v}\left(-Ae^{-p\frac{x}{v}} + Be^{p\frac{x}{v}}\right) - h\bar{D}$$

$\frac{c}{v} = \rho v = Z$, the characteristic acoustic impedance medium.

Guass' Law applied at the transducer surfaces gives

$\int \bar{D}\, dS = \bar{Q}$, where Q is the total charge of the transducer surfaces at x = 0, x = L.

The total force on a transducer surface is therefore F where

$$\bar{F} = pZ(-Ae^{-p\frac{x}{v}} + Be^{p\frac{x}{v}}) - h\bar{Q} \qquad (4)$$

Consider a transducer which conforms to the restrictions already imposed; the general transducer is backed with a material whose impedance in Z_B whilst it is faced with an impedance Z_F.

Using equation (4) in the non-piezoelectric media,

$$\bar{F}_{B,F} = pZ_{B,F}(-A_{B,F}e^{-p\frac{x}{v}} + B_{B,F}e^{p\frac{x}{v}})$$

The influence of reflected waves from the far front and backs of the system is removed by allowing the back and front media to be semi infinite in length. Inserting the conditions

$$\bar{u}_F \longrightarrow 0 \text{ as } x \longrightarrow \infty$$

$$\bar{u}_B \longrightarrow 0 \text{ as } x \longrightarrow -\infty$$

into (3) gives $A_B = B_F = 0$

The forces and displacements at the boundaries $x = 0$ and $x = L$ must be the same measured from either side

i.e. $\bar{F}_F = \bar{F}$, $\bar{u}_F = \bar{u}$ at $x = L$

$$\bar{F}_B = \bar{F} \text{ , } \bar{u}_B = \bar{u} \text{ at } x = 0$$

Thus, the following equations may be obtained, writing $\gamma = \frac{p}{v}$:

$$A + B = B_B \qquad (5)$$

$$Ae^{-\gamma L} + Be^{+\gamma L} = A_F e^{-\gamma L} \qquad (6)$$

$$pZ(-A + B) - h\bar{Q} = pZ_B B_B \qquad (7)$$

$$pZ(-Ae^{-\gamma L} + Be^{\gamma L}) - h\bar{Q} = pZ_F(-A_F e^{-\gamma L}) \qquad (8)$$

The voltage across the transducer may be obtained by integration of the field through the medium and then by Laplace Transform and substitution for $\bar{u}$:

$$\int_o^L \bar{E}\, dx = \int_o^L -\nabla \bar{V}\, dx = \bar{V}_o - \bar{V}_L$$

$$= -h(\bar{u}_L - \bar{u}_o) + \frac{\bar{D}}{\sigma}.L$$

Writing $\bar{V} = \bar{V}_o - \bar{V}_L$ and C_o = the static capacitance

$$= \frac{\sigma S}{L},$$

$$\bar{V} = -h(\bar{u}_L - \bar{u}_o) + \frac{\bar{Q}}{C_o}$$

$$\bar{V} = -h(Ae^{-\gamma L} + Be^{\gamma L} - A - B) + \frac{\bar{Q}}{C_o} \qquad (9)$$

B.2 Transmission Transfer Functions

Equations (5) - (9) are the equations used by Redwood (1961) to construct an equivalent circuit for the transducer. The general solution for transmission of sound may be obtained from the three simultaneous equations which relate A and B to $\bar{Q}$.

$$B = \frac{h\sigma\bar{Q}}{pLC_o}\left(\frac{e^{-\gamma L}}{Z+Z_F} - \frac{k_F e^{-2\gamma L}}{Z+Z_B}\right)\left(\frac{1}{1-k_F k_B e^{-2\gamma L}}\right) \qquad (10)$$

$$A = \frac{h\sigma\bar{Q}}{pLC_o}\left(\frac{k_B e^{-\gamma L}}{Z+Z_F} - \frac{1}{Z+Z_B}\right)\left(\frac{1}{1-k_F k_B e^{-2\gamma L}}\right) \qquad (11)$$

where $k_F = \frac{Z-Z_F}{Z+Z_F}$, $k_B = \frac{Z-Z_B}{Z+Z_B}$

Substituting (10) and (11) into (8) and (9) gives

$$\bar{T}_F = \frac{-hC_o\frac{\bar{V}\,Z_F}{Z+Z_F}\left(1 + k_B e^{-2\gamma L} - \frac{2Z}{Z+Z_B}\,e^{-\gamma L}\right)}{1 - k_F k_B e^{-2\gamma L} - \frac{h^2 C_o}{p}\left(\frac{(k_B e^{-\gamma L}-1)(e^{-\gamma L}-1)}{Z+Z_F} + \frac{(k_F e^{-\gamma L}-1)(e^{-\gamma L}-1)}{Z+Z_B}\right)} \qquad (12)$$

Equation (12) is of the form

$$\bar{T}_F = \bar{V}.\bar{H}$$

T_F, the output stress in the front medium, corresponds to an acoustic pressure emitted by the transducer. An inverse transform of the frequency domain product gives

$$T_F = V(t) * h_T(t)$$

a convolution relation between any exciting waveform, V, and an intrinsic transfer function of the transducer, $h_T(t)$

$$h_T(t) = L.T^{-1}\ (\bar{H}(p))$$

The inverse transform of (12) is a complex expression but considerable simplifications may be obtained in special conditions, which fortunately correspond to situations of realistic interest.

Firstly, the results of Cook (1956) may be derived and the assumptions implicit in his derivation may be deduced.

(a) Weakly Coupled Transducers

The electromechanical coupling coefficient, k, is conventionally used as a parameter to describe the degree of coupling between transducer fields, and in the notation of equations (1) and (2)

$$k^2 = \frac{h^2\sigma}{c} \qquad \text{(Blitz (1963))}$$

For a weakly coupled material,

$$k^2 \ll 1$$

$$h^2\sigma \ll c$$

$$h^2\sigma\frac{\partial u}{\partial x} \ll c\frac{\partial u}{\partial x}$$

Comparison of this inequality with equations (1) and (2) shows that with weak coupling, the mechanical deformation does not significantly affect the electric field. This is Cook's approximation in which application of a voltage to the transducer

causes a uniform stress throughout the crystal. In the derivation above, this leads to expression for A and B in (10) and (11) in which $\bar{Q}$ is simply replaced by $\bar{V}C_o$ because the electric field is not significantly different to that for a non piezoelectric dielectric of the same permitivity. In (12) this leads to a dropping of the third (bracketed) term in the denominator: this depends upon h^2 and is a second order small quantity.

$$\bar{T}_F = \frac{-hC_o\bar{V}}{2} \cdot \frac{(\frac{2\ Z_F}{Z+Z_F})(1 + k_B e^{-2\gamma L} - \frac{2Z}{Z+Z_B} e^{-\gamma L})}{1 - k_F k_B e^{-2\gamma L}} \qquad (13)$$

Equation (13) may itself be rewritten in terms of reflection and transmission coefficients of plane waves at boundaries. If α_{ij} = reflection coefficient of a wave travelling in medium i and incident upon medium j then

$$\alpha_{ij} = \frac{Z_j - Z_i}{Z_j + Z_i}$$

Similarly, the transmission coefficients $t_{ij} = \frac{2Z_j}{Z_i + Z_j}$

Let the subscript T denote the transducer. Because the reflection and transmission coefficients are always less than 1, then equation (13) may be expressed as a geometrical series:

$$\bar{T}_F = \frac{-hC_o\bar{V}}{2}\ t_{TF}\ (1 - \frac{(t_{BT}e^{-\gamma L} + t_{FT}\alpha_{TB}e^{-2\gamma L})}{1 - \alpha_{TB}\alpha_{TF}e^{-2\gamma L}})$$

$$\bar{T}_F = \frac{-hC_o\bar{V}}{2} t_{TF} \left(1 - \sum_{n=1}^{\infty} (\alpha_{TB}\alpha_{TF})^{n-1} \right.$$

$$\left. (t_{BT} e^{-(2n-1)\gamma L} + t_{FT}\alpha_{TB} e^{-2n\gamma L}) \right)$$

The intrinsic transfer function for a weakly coupled transducer, $h_T(t) = L.T^{-1} \left(\frac{\bar{T}_F}{\bar{V}}\right)$. Thus,

$$h_T(t) = \frac{-hC_o t_{TF}}{2} \left(\delta(t) - \sum_{n=1}^{\infty} (\alpha_{TB}\alpha_{TF})^{n-1} \left(t_{BT} \delta\left(t + \frac{L}{V} - \frac{2nL}{V}\right) \right.\right.$$

$$\left.\left. + t_{FT}\alpha_{TB} \delta\left(t - \frac{2nL}{V}\right) \right) \right)$$

(14)

This transfer function represents a series of Dirac impulses each separated by a time $t = \frac{L}{V}$, the transit time of the impulse through the transducer (assuming no dispersion), with amplitudes determined by the impedances of the front and back media.

(b) Rigidly backed transducers

Most transducers are constructed with rigid backings. The rigidly backed crystal was analysed by Redwood (1961) but the transfer function may be derived directly from (12). Rigid backing implies that the boundary at X = 0 is held fixed.

i.e. $A_B = B_B = 0$

$Z_B \dashrightarrow \infty$, $k_B \dashrightarrow -1$

These extra conditions substituted into (12) gives

$$\bar{T}_F = \frac{-phC_o\bar{V}}{2} t_{TF} \left(\frac{1 - e^{-2\gamma L}}{p - \frac{h^2C_o}{Z+Z_F}}\right) \cdot$$

$$x \left(1 + \frac{\left(\frac{h^2C_o}{Z+Z_F} + pk_F\right)e^{-2\gamma L}}{\left(p - \frac{h^2C_o}{Z+Z_F}\right)}\right)^{-1}$$

The last expression may be expanded by the binominal theorem. Using the notation for transmission and reflection coefficients defined above, and putting

$$\frac{-h^2C_o}{Z+Z_F} = a$$

$$\bar{T}_F = -\left(\frac{p}{p+a}\right)\frac{hC_o\bar{V}}{2} t_{TF} \left(1 - \left(\frac{p}{p+a}\right) t_{FT} \sum_{n=1}^{\infty} \left(\frac{p\alpha_{TF}+a}{p+a}\right)^{n-1} e^{-2\gamma L}\right) \qquad (15)$$

The inverse, time domain transform may be obtained by writing

$$a\left(\frac{1}{\alpha_{TF}} - 1\right) = \beta$$

and by using the Laplace Transform relationships

$$LT(t^{n-1} e^{-\alpha t}) = \frac{1}{(p+\alpha)^n}$$

$$LT(f(t-T) = e^{-pT} LT(f(t))$$

After multiplications and rearrangement (15) may be rewritten in the time domain in the form

$T_F(t) = V(t) * h_T(t)$, where

$$h_T(t) = \frac{-hC_o}{2} t_{TF}\left(\left(\delta(t) - \sum_{n=1}^{\infty} \alpha_{TF}^{n-1} t_{FT}\,\delta(t-n\tau)\right.\right.$$

$$\left.\left. - \sum_{n=o}^{\infty} \sum_{m=o}^{n} e^{-a(t-n\tau)} A_{mn}(t-n\tau)^m\right)\right) \qquad (16)$$

where $\tau = \frac{2L}{V}$

and A_{mn} are amplitude factors that depend only upon Z, Z_F and a.

$A_{oo} = a$

$A_{o1} = -2at_{FT}$

$A_{11} = a^2 t_{FT}$

$A_{o2} = -(2a-\beta)\ \alpha_{TF} t_{FT}$

$A_{12} = a(a-2\beta)\ \alpha_{TF} t_{FT}$

$A_{22} = a^2\beta\alpha_{TF} t_{FT}$

$A_{o3} = -2(a-\beta)\alpha_{TF}^2 t_{FT}$

$A_{13} = (a^2-4a\beta+\beta^2) a_{TF}^2 t_{FT}$

$A_{23} = 2(a-\beta)a\beta\alpha^2_{TF} t_{FT}$

$A_{33} = a^2\beta^2\alpha^2_{TF} t_{FT}$

This solution produces not just a sequence of Dirac impulse functions but also a sequence of exponentially decaying impulses of finite bandwidth.

B.3 Receiver transfer functions

The thickness mode plate may also be considered as a receiver and a solution obtained for the output voltage produced by any incident stress wave. The general solution may again be derived in the Laplace Transform frequency domain, but the difficulties of inverse transformation render this solution less useful than the solution for particular electrical boundary conditions. The results derived below were also derived by Redwood whose final expression was given in slightly different form but whose conclusions on the importance of the electrical loading are given for completeness.

(a) Open circuit response

When the electrical load across the transducer is infinite, then no current may flow in the transducer. Consider a transducer backed at $x = 0$ by a semi infinite material (Z_B), and consider a sound wave incident on the front surface at $x = L$ travelling in the $-x$ direction. The electrical boundary condition gives

$$\bar{I} = p\bar{Q} = 0$$

At $x = 0$, $A + B = B_B \quad (A_B = 0)$

$$pZ_T(-A + B) = pZ_B B_B \quad (\bar{Q} = 0)$$

At $x = L$, $Ae^{-\gamma L} + Be^{\gamma L} = A_F e^{-\gamma L} + B_F e^{\gamma L}$

$$pZ_T(-Ae^{-\gamma L} + Be^{\gamma L}) = pZ_F(-A_F e^{-\gamma L} + B_F e^{\gamma L})$$

$$\bar{V} = -h(Ae^{-\gamma L} + Be^{\gamma L} - A - B)$$

These equations may be rearranged to give $\bar{V}$ in terms of B_F, the incident pressure wave amplitude.

This gives

$$B_F = \frac{B}{t_{TF}} \left(1 - \alpha_{FT}\alpha_{BT}e^{-2\gamma L}\right)$$

and $$\bar{V} = -h\ t_{TF} \cdot B_F \frac{\left(\alpha_{BT}\left(e^{-\gamma L}-1\right) + e^{\gamma L} - 1\right)}{\left(1 - \alpha_{BT}\alpha_{FT}e^{-2\gamma L}\right)}$$

Expressing the denominator as a geometric series, and using the condition that at t = 0 the stress at the front face is related to B_F as

$$\bar{T}_F = pZ_F B_F e^{\gamma L}$$

then

$$\bar{V} = \frac{-ht_{TF}}{pZ_f} \bar{T}_F\ e^{-\gamma L} \left(\alpha_{BT}e^{-\gamma L} - \left(\alpha_{BT} + 1\right) + e^{\gamma L}\right).$$

$$x \sum_{n=0}^{\infty} \left(\alpha_{BT}\alpha_{FT}\right)^n e^{-2n\gamma L} \qquad (17)$$

Again this is of the form

$$\bar{V} = \bar{T}_F \cdot \bar{H}(p)$$

so the time domain relationship will be a convolution of the pressure waveform $T_F(t)$ with an intrinsic receiver impulse response obtained by inverse transformation of (17). Re-writing (17) gives

$$\bar{H}(p) = \frac{-ht_{TF}}{Z_F} \sum_{n=o}^{\infty} (\alpha_{BT}\alpha_{FT})^n \left(\frac{e^{-2np\frac{L}{V}}}{p} - \frac{(1+\alpha_{BT})e^{-(2n+1)\frac{L}{V}p}}{p} + \frac{\alpha_{BT}e^{-2p(n+1)\frac{L}{V}}}{p}\right) \quad (18)$$

But, $LT(u(t)) = \frac{1}{p}$ (where $u(t)$ is the unit step function of Heaviside) so that the inverse transform is a sequence of step functions delayed in time.

i.e.

$$h_R(t) = \frac{-ht_{TF}}{Z_F} \sum_{n=o}^{\infty} (\alpha_{BT}\alpha_{FT})^n \left(u(t-\frac{2nL}{V}) - (1+\alpha_{BT})u\left(t-\frac{L}{V}-\frac{2nL}{V}\right) + \alpha_{BT}\, u\left(t-\frac{2L}{V}-\frac{2nL}{V}\right)\right) \quad (19)$$

$$\therefore \quad h_R(t) = \frac{-ht_{TF}}{Z_F}\left(u(t) - (1+\alpha_{BT})\,u\left(t-\frac{L}{V}\right) + \alpha_{BT}(1+\alpha_{FT})\,u\left(t-\frac{2L}{V}\right) - \alpha_{BT}\alpha_{FT}(1+\alpha_{BT})\,u\left(t-\frac{3L}{V}\right) + \alpha_{BT}^2\alpha_{FT}(1+\alpha_{FT})\,u\left(t-\frac{4L}{V}\right)....\right)$$

$h_R(t)$ is the response for an impulse of pressure, $\delta(t)$ and may be used to predict the output for any input by convolution.

(b) Response for finite loading and rigid backing

In many practical situations, the transducer is connected to a finite electrical impedance. If the load is a resistance R then the current I that increases the charge Q on the surface of higher potential is $\frac{-V}{R}$. For a rigidly backed receiver, $A_B = B_B = 0$. Proceeding as before,

$$\bar{V} = \frac{-\frac{2h}{Z+Z_F}\,\bar{T}_F\,(1 - e^{-2\gamma L})}{(p + \frac{1}{RC_o})(1 + k_T e^{-2\gamma L}) - (\frac{h^2}{(Z+Z_F)Rp})(1 - e^{-2\gamma L})}$$

If $\frac{-h^2 C_o}{Z+Z_F} = a$ and $\frac{1}{RC_o} = \tau$, then the receiver response is

$$\bar{H}(p) = \frac{-2h}{Z+Z_F}\, p \sum_{n=o}^{\infty} \frac{(p^2 k_F + \tau(pk_F + a))^n}{(p^2 + \tau(p+a))^{n+1}} (e^{-2n\gamma L} - e^{-2(n+1)\gamma L}) \quad (20)$$

Note that when $\tau = 0$ $(R = \infty)$,

$$\bar{H}(p) = \frac{-2h}{Z+Z_F} \sum_{n=o}^{\infty} \frac{k_F{}^n}{p} (e^{-2n\gamma L} - e^{-2(n+1)\gamma L}) \quad (21)$$

$$h(t) = \frac{-2h}{Z+Z_F} \sum_{n=o}^{\infty} k_F{}^n \left(u(t - \frac{2nL}{v}) - u(t - \frac{2(n+1)L}{v})\right)$$

The implications of the transfer equations derived above are considered in Chapter 4.

Appendix C: The structure of the transient sound field from a plane transducer

(a) Near Field

The Kirchoff integral may be used to calculate sound fields due to non-monochromatic excitations as long as each frequency component in the pulse satisfies the conditions for its use separately. The velocity potential at a point P (Figure C.1) for any frequency w is

$$\phi(r) = \frac{1}{2\pi}\iint_S u_w \frac{e^{jkr}}{r}\, dS \qquad (1)$$

where $u_w(x,y,z)$ satisfies the time independent wave equation. If a general excitation $V(x,y,z,t)$ may be represented by a Fourier Integral

$$V(x,y,z,t) = \frac{1}{(2\pi)^{\frac{1}{2}}}\int_{-\infty}^{\infty} u_w(x,y,z)\, e^{-jwt}\, dw \qquad (2)$$

then combining (1) and (2), and changing the order of integration with $w = kc$ gives

$$\phi(r,t) = \frac{1}{2\pi}\iint_S dS \; \frac{1}{(2\pi)^{\frac{1}{2}}}\int_{-\infty}^{\infty} \frac{u_w e^{-jw(t-\frac{r}{c})}}{r}\, dw$$

Thus,

$$\phi(r,t) = \frac{1}{2\pi}\iint_S \frac{1}{r}\, .\, V(x.y.z.t-\tfrac{r}{c})\, dS \qquad (3)$$

which is the result derived by Born and Wolf (1975). The intrinsic structure of the transducer field is obtained by considering a step displacement of the transducer face of unit

magnitude at time 0. The velocity potential at a field point is

$$\psi(r,t) = \frac{1}{2\pi} \iint_S \frac{\delta(t-\frac{r}{c})}{r} \, dS$$

Robinson (1974) analysed the field using the cylindrical coordinate system of Figure C.1, where P is at distance z from the plane of the transducer and y off the central axis. In a homogeneous medium in which the velocity of sound C is independent of frequency, the first sound to arrive at P originates from the foot of the perpendicular from P on S (at Q). After the time $t_o = \frac{z}{c}$, the sound originates from a circle of points in the transducer face which has radius R

$$R^2 = r^2 - z^2 \qquad (4)$$

All points on this circle are at equal travel time, $\frac{r}{c}$, from the field point P. The circle expands with time until it no longer cuts the transducer face, but before this the circle degenerates into a sector which subtends an angle 2θ at Q. θ depends on the position of Q and changes from 2π to zero during the passage of the disturbance at P. The area of transducer face contributing to the sound at P at time t has as area

$$dS = 2\theta(r) R \, dR$$

From (4), $R \, dR = r \, dr$, so that

$$\psi(r,t) = \frac{1}{\pi} \int \delta(t-\frac{r}{c}) \, \theta(r) \, dr$$

$$= \frac{c}{\pi} \int \theta(r) \delta(ct - r) \, dr$$

$$= \frac{c}{\pi} \theta(ct) \qquad (5)$$

This derivation is everywhere linear so that the sound field produced by any other excitation can be calculated by using a convolution integral. If the transducer face velocity waveform is h(t) then the velocity potnetial at P is $\phi(r,t)$

$$\phi(r,t) = \frac{c}{\pi}\int_{-\infty}^{\infty} h(t-t')\ \theta(ct')\ dt' \qquad (6)$$

This integral shows that the velocity potential (and therefore the pressure) at any point depends upon the form of h(t). The pulse shape at any point depends not just on h(t) but also on $\theta(ct)$. The acoustic pressure at P due to an impulse is

$$TF\ (r,t) = \rho\frac{\partial\psi}{\partial t}(r,t) = \rho\frac{c}{\pi}\frac{\partial\theta}{\partial t}(ct) \qquad (7)$$

whilst for any other excitation the pressure is

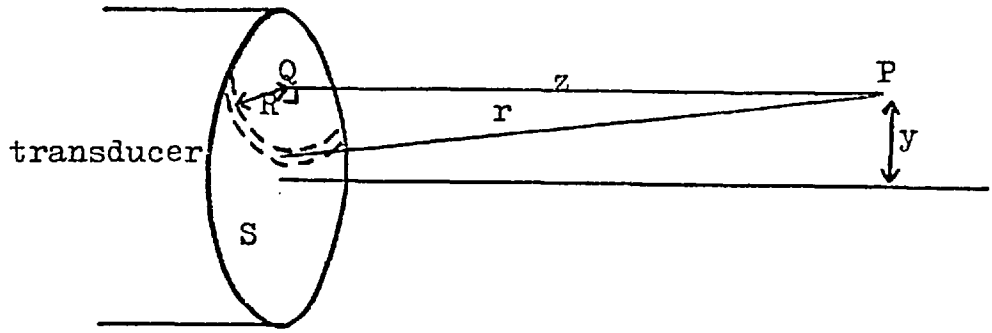
$$p(r,t) = TF(r,t) * h(t) \qquad (8)$$

The shapes of $\psi(r,t)$ and TF(r,t) depend on the variation of the angle subtended by circular elements at the projection of the field point P onto the transducer face. When the element is a whole circle $\theta = \pi$ and ψ is a constant, independent of the circle radius. Expressions for θ and ψ at other times may be derived using the geometry of Figure C.2 (Robinson, 1974). The annulus which contributes to the sound at P at time t is AB, where $\angle AQB = 2\theta$. If Q is distance y from O then when $R \leqslant a-y$, $2\theta = 2\pi$. If $a-y < R < a+y$, then by the cosine rule

$$y^2 + R^2 - 2yR\cos\theta = a^2$$

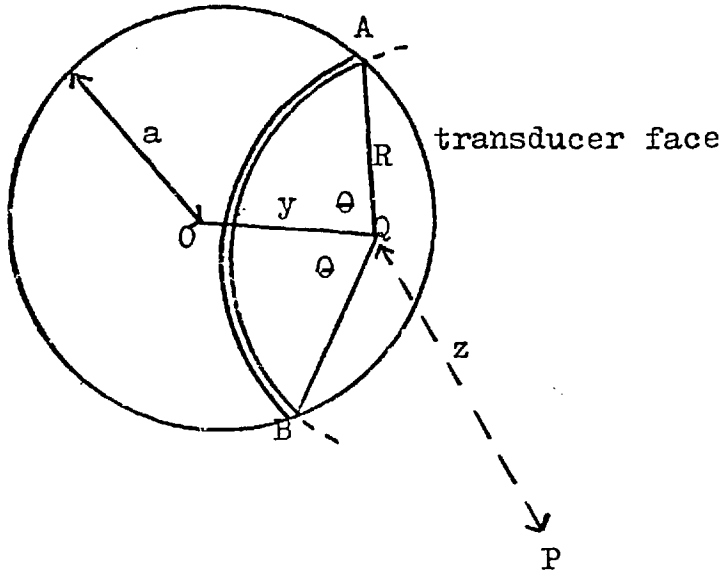
and $R^2 + z^2 = c^2t^2$

Figure C1 Cylindrical coordinate system used to calculate $\psi(r,t)$



The dashed annular area has radius R, centre Q, and is r from the field point P.

Figure C2 Definition of parameters used to calculate $\theta(ct)$



AB is the annulus contributing to sound at P at time t.

$\angle AQB = 2\theta$; if $R < a - y$, $2\theta = 2\pi$

if $a - y < R < a + y$, then

$$\cos\theta(ct) = \frac{y^2 + c^2t^2 - z^2 - a^2}{2y(c^2t^2 - z^2)^{\frac{1}{2}}}$$

if $y = a$ this reduces to $\frac{(c^2t^2 - z^2)^{\frac{1}{2}}}{2a}$

for $0 < R < 2a$.

$$\text{so that } \theta(ct) = \cos^{-1}\left(\frac{y^2 + c^2t^2 - z^2 - a^2}{2y(c^2t^2 - z^2)^{\frac{1}{2}}}\right) \qquad (9)$$

If $y > a$, θ is given by (9) if $y - a < R < y + a$.

The variations of ψ with position and time are summarised in Table C.1

A computer programme to calculate the velocity potential at any position in the field at different times was written in Fortran IV using the formulae derived above.
The results of a sample calculation for a plane 20 mm diameter transducer are shown in Figure C.3, and the qualitative features of such a field are discussed in Chapter 5 where implications for ultrasonic scanning are considered. A digital calculation such as this could be extended to include a convolution with any transducer face movement to obtain theoretical estimates of soundfield profiles for more narrow bandwidth excitations.

(b) Far Field

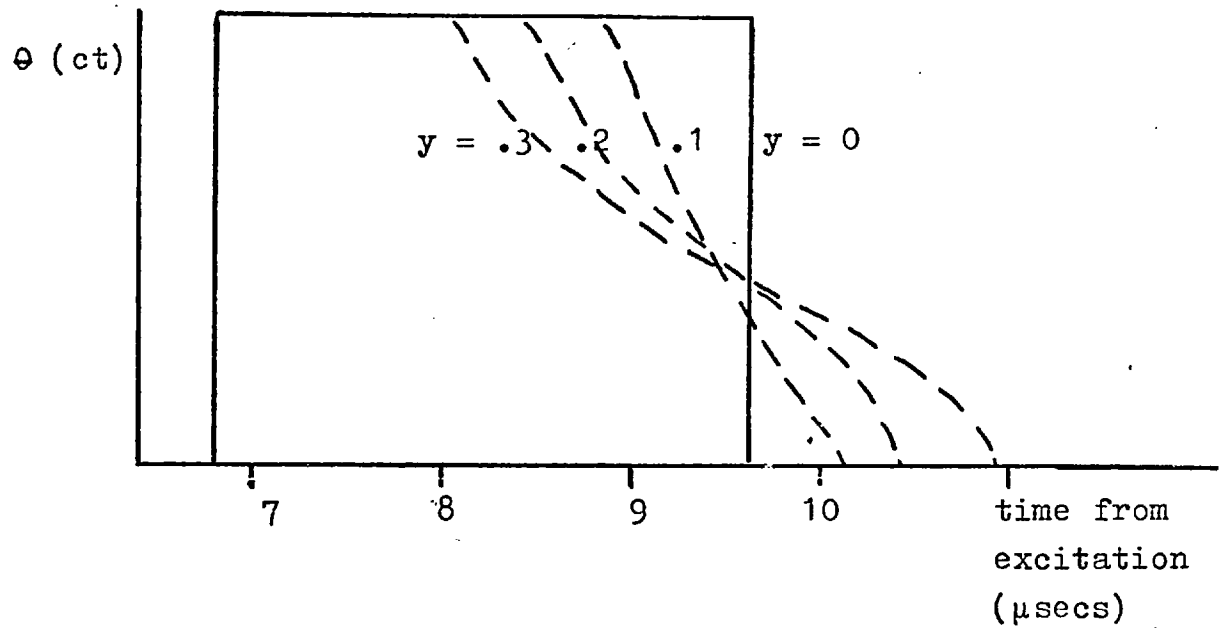
The pulse structure in the Far Field of a pulsed transducer has not been described very extensively in the literature. The result obtained below was derived for circular transducers to allow estimates to be made of the importance of changes in the structure of pulses in the far field, and although differences in the acoustic travel times from a field point to different parts of the transducer face decrease as the point moves away from the transducer, the analysis shows that pulses still change their shape at different bearings.

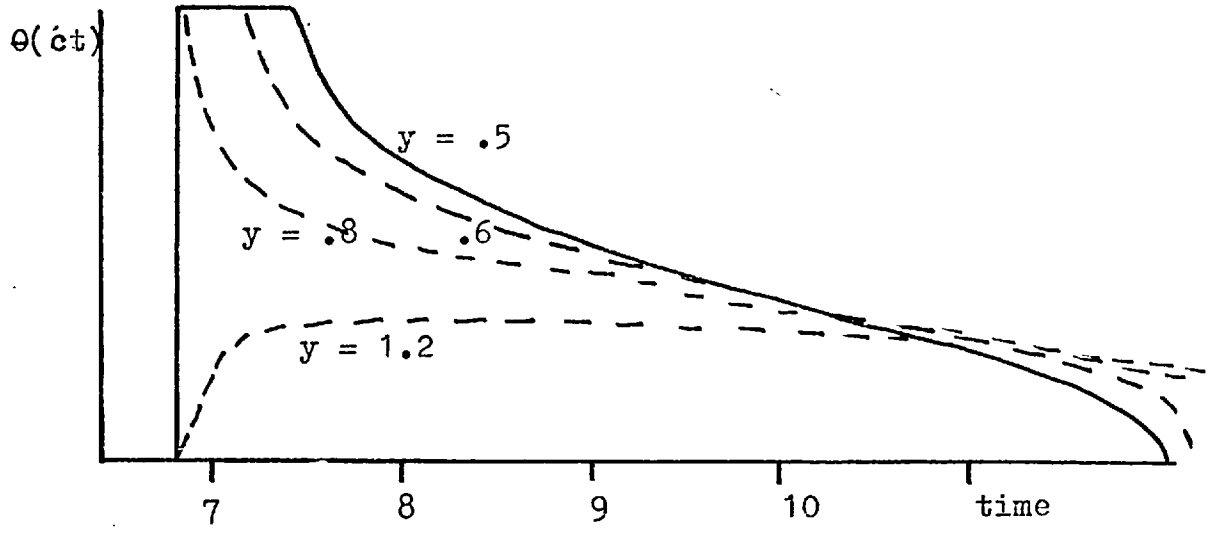
Table C.1

Region	time	ψ
$y < a$	$t < \frac{z}{c}$	0
	$\frac{z}{c} < t < \frac{((a-y)^2 + z^2)^{\frac{1}{2}}}{c}$	c
	$\frac{((a-y)^2+z)^{\frac{1}{2}}}{c} < t < \frac{((a+y)^2+z^2)^{\frac{1}{2}}}{c}$	$\frac{c}{\pi}\theta(ct)$
$y = a$	$t < \frac{z}{c}$	0
	$\frac{z}{c} < t < \frac{(4a^2 + z^2)^{\frac{1}{2}}}{c}$	$\frac{c}{\pi}\cos^{-1}\left(\frac{(c^2t^2 - z^2)^{\frac{1}{2}}}{2a}\right)$
$y > a$	$t < \frac{((a-y)^2 + z^2)^{\frac{1}{2}}}{c}$	0
	$\frac{((a-y)^2+z^2)^{\frac{1}{2}}}{c} < t < \frac{((a+y)^2+z^2)^{\frac{1}{2}}}{c}$	$\frac{c}{\pi}\theta(ct)$

$$\theta(ct) = \cos^{-1}\left(\frac{y^2 + c^2t^2 - z^2 - a^2}{2y(c^2t^2 - z^2)^{\frac{1}{2}}}\right) \qquad \text{(from (9))}$$

Figure C3 Calculated time profiles for the velocity potential at 10 mm from a plane transducer at different displacements from the transducer axis.





To calculate θ(ct) the following values were assumed ; z = 10 mm , c = 1.5 mm/μsec , a = 10 mm ; the values of y shown in the diagram are the lateral displacements divided by the transducer radius, 10 mm.

The Far Field pressure distribution for a monochromatic excitation is usually described in terms of a Directivity Function, $D(\theta)$, which relates the plane wave pressure at some bearing θ from the axis to the axial pressure. $D(\theta)$ is related to the Fourier Transform of the excitation distribution on the transducer face and is simply obtained by the Fraunhofer Diffraction integral (Born and Wolf 1975). For a pulsed transducer, let $P(t,\theta)$ be the pulse in any direction θ. Its Fourier Transform is $p(w,\theta)$

$$P(t,\theta) = \int_{-\infty}^{\infty} p(w,\theta)\, e^{-iwt}\, dw$$

From the definition of the Directivity Function,

$$p(w,\theta) = p(w,0)\ D(w,\theta)$$

$$\therefore\ P(t,\theta) = \int_{-\infty}^{\infty} e^{-iwt}\ p(w,0)\ D(w,\theta)\ dw$$

$$\text{But, } p(w,0) = \int_{-\infty}^{\infty} P(t',0)\, e^{iwt'}\, dt'$$

$$\text{so that } P(t,\theta) = \int_{-\infty}^{\infty} P(t',0) \int_{-\infty}^{\infty} D(w,\theta)\, e^{-iw(t-t')}\, dw\, dt' \quad (10)$$

Equation (10) is a general result that may be used with any transducer directivity.

In the far field of a circular disc of radius a,

$$D(w,\theta) = \frac{2J_1\left(\frac{wa}{c}\sin\theta\right)}{\frac{wa}{c}\sin\theta}$$

(see, for example, Gooberman (1968)).

If $\frac{a}{c} = k'$, then

$$P(t,\theta) = \int_{-\infty}^{\infty} P(t',0) \int_{-\infty}^{\infty} e^{-iw(t-t')} \frac{2J_1(k'w\sin\theta)}{k'w\sin\theta} \, dw \, dt'$$

Let $\mu = k'w\sin\theta$, so that $d\mu = k'\sin\theta \, dw$ (θ fixed)

$$P(t,\theta) = \int_{-\infty}^{\infty} P(t',0) \int_{-\infty}^{\infty} e^{\frac{-i\mu(t-t')}{k'\sin\theta}} \cdot \frac{2J_1(\mu)}{\mu} \cdot \frac{d\mu}{k'\sin\theta} \, dt'$$

However, $\int_{-\infty}^{\infty} t^{-1} e^{-iwt} J_n(w) \, dt = \frac{2i}{n}(-i)^n (1-w^2)^{\frac{1}{2}} U_{n-1}(w)$

$$(\text{if } w^2 < 1)$$

$$= 0 \quad (\text{if } w^2 > 1)$$

where $U_n(w)$ = Chebyshev Polynomial of second kind

$$U_o = 1$$

$$\therefore \quad P(t,\theta) = \int_{-\infty}^{\infty} P(t',0) \cdot \frac{4}{k'\sin\theta} \left(1 - \left(\frac{t-t'}{k'\sin\theta}\right)^2\right)^{\frac{1}{2}} dt'$$

$$\text{if } |t-t'| < \frac{a\sin\theta}{c} \qquad (11)$$

Equation (11) is a convolution integral which may be written in the form

$$P(t,\theta) = P(t,0) * TF(t,\theta)$$

where $TF(t,\theta) = \frac{4c}{a\sin\theta}\left(1 - \frac{c^2t^2}{a^2\sin^2\theta}\right)^{\frac{1}{2}}$ (12)

REFERENCES

Atkinson, P. and Berry, M.V. (1974). J. Phys. A.: Math., Nucl. Gen., 7, 1290.

Auld, B. (1973). Acoustic Fields and Waves in Sounds, Volume 1. (Wiley, Interscience).

Baker, B. and Copson, E. (1950). The Mathematical Theory of Huygen's Principle. (Oxford Books, Oxford).

Baum, G. (1974). in Diagnostic Ultrasound, ed. D.L. King. p. 282 - 289 (Mosby, New York).

Beckley, D., Ross, F. and Halliwell, M. (1975). Presented at Annual Meeting of British Medical Ultrasonics Group, Bristol (abstract to be published in Brit. J. Radiology).

Beckmann, P. (1968). Probability in Communication Engineering (Harcourt, Brace and World, New York).

Bellhouse, B.J. (1972). Cardiovascular Res., 6, 199 - 210.

Bendat, J. and Piersol, A. (1966). Measurement and Analysis of Random Data (Wiley, New York).

Berry, M.V. (1973). Phil. Trans. A 273, 611 - 658.

Blackman, R. and Tukey, J. (1958). The Measurement of Power Spectra (Dover, New York).

Blackwell, R.J. (1972). Biomed. Eng. 7, 356.

Blackwell, R.J., Lachelin, G., McIntosh, A. and Suter, P. (1973). Brit. J. Radiology, 46, 259 - 261.

Bom, N. (1972). New Concepts in Echocardiography (Stenfert Kroese, Leiden).

Bom, N., Lancee, C.T., Honkoop, J. and Hugenholtz, P.G. (1971). Biomed. Eng., 6, 500.

Born, M. and Wolf, E. (1975). Principles of Optics, 5th Edit. (Perganon Press, Oxford).

Bracewell, R. (1965). The Fourier Transform and its Application. (McGraw Hill, New York).

Brown, T.G. (1973). Proceedings, Ultrasonics International p. 208 (IPC Press, Guildford).

Cady, W.G. (1046). Piezoelectricity Volume I (McGraw Hill, New York).

Champeney, D.C. (1973). Fourier Transforms and their Physical Applications (Academic Press, London).

Chernov, L.A. (1960). Wave Propagation in Random Media (McGraw Hill, New York).

Chivers, R.C. (1973) Ph.D. Thesis, University of London.

Chivers, R.C. and Hill, C.R. (1975). Phys. Med. Biol., 20, 799.

Christie, A.D. (1973). Proceedings of the Second World Congress on Ultrasonics in Medicine, Rotterdam, p. 171. (Excerpta Medica, Amsterdam).

Coleman, D. and Katz, L. (1974). Arch. Ophthalmol., 91, 429.

Cook, E.G. (1956). I.R.E. Conv. Res. 4, pt. 9, 61 - 69.

Dainty, J.C. and Shaw, R. (1974). Image Science (Academic Press, London).

Dekker, D.L., Piziali, R.L. and Dong, E. (1974). Computers and Biomed. Res., 7, 544.

Doi, K., Strubler, K. and Rossmann, K. (1972). Phys. Med. Biol., 17, 241.

Edler, I. and Hertz, C.H. (1956). Acta. Chir. Scand., 111, 230 - 231.

Effert, S. and Domanig, E. (1959). German Med. Monthly, 4, 1 - 3.

Effert, S., Bleifeld, W., Dempmann, F. and Karitsiotis, T. (1964). Brit. J. Radiology, 37, 920 - 927.

Eggleton, R.C., Townsend, C., Herrick, J., Templeton, G. and Mitchell, J.H. (1970). IEEE Trans. on Sonics and Ultrasonics. SU - 17, 3.

Feigenbaum, H. (1972). Echocardiography (Lea and Febiger, Philadelphia).

Freedman, A. (1962). The Formation of Acoustic Echoes in Fluids. Admiralty Underwater Weapons Establishment, Portland. Establishment Reports 64/62 - 67/62.

Freedman, A. (1970a). J. Acoust. Soc. America, 48, 221.

Freedman, A. (1970b). J. Acoust. Soc. America, 48, 135.

Gehkre, J. (1975). Proceedings of the British Medical Ultrasonics Group, Bristol. (to be published).

Gehkre, J., Jayakumar, R., Raphael, M. and Pridie, R.B. (1974). Presented at the 7th World Congress on Cardiology, Buenos Aires.

Gehkre, J. and Leeman, S. (1975). Phys. Med. Biol., 20, 844.

Gehkre, J., Leeman, S., Raphael, M. and Pridie, R.B. (1975). Brit. Heart. J., 37, 911.

Ghista, D.N. and Rao, A. (1972). J. Biomechanics, 5, 295 - 307.

Gibson, D. (1976). Proceedings of the 7th L.H. Gray Conference on Medical Images, Leeds. (in press).

Gooberman, G.L. (1968). Ultrasonics: Theory and Application (English Universities Press, London).

Gramiak, R. and Waag, R.C. (1975). Cardiac Ultrasound (Mosby, New York).

Gramiak, R. and Waag, R.C. (1973). Proceedings of the Second World Congress on Ultrasonics in Medicine, Rotterdam, p. 244 (Excerpta Medica, Amsterdam).

Greene, M.E., Clark, J., Mohr, D. and Bowland, H. (1973). Med. and Biol. Eng., March, p. 126.

Gustafson, A. (1967). Am. J. Cardiology, 19, 32 - 41.

Hall, A.J. (1974). Contact B Scanners - Registration checking and error correction. University of Glasgow, Department of Ultrasonic Technology, Report 7/74.

Hall, A.J. and Fleming, J.E. (1972). Med. and Biol. Eng., 10, 631 - 642.

Hall, A.J. and Fleming J.E. (1975). Abstracts, Second European Congress on Ultrasonics in Medicine. Munich.

Hickling, R.D. (1962). J. Acoust. Soc. America, 34, 1582.

Hill, C.R. (1976). Brit. J. Radiology, 49, 238 - 243.

Holmes, J.H. (1974). in Diagnostic Ultrasound, ed. D.L. King, p. 1 - 16 (Mosby, New York).

Jenkins, G.M. and Watts, D.G. (1968). Spectral Analysis and its applications (Holden Day, San Francisco).

Joyner, C.R., Reid, J.M. and Bond, J.P. (1963). Circulation, 27, 503 - 511.

King, D.L. (1973). Circulation, 47, 843.

Kossoff, G. (1963). J. Acoust Soc. America, 35, 905 - 912.

Kossoff, G. (1972). Ultrasonics, 10, 221.

Kossoff, G., Robinson, D., Liu, C. and Garrett, W. (1964). Ultrasonics, 2, 29.

Kossoff, G. and Robinson, D. (1972). Radiology, 104, 123.

Lancee, C.T. (1973). Abstracts, Second World Congress on Ultrasonics in Medicine, Rotterdam.

Landam, L.D. and Lifshitz, E.M. (1970). Course of Theoretical Physics Volume 6: Fluid Mechanics. (Perganon, Oxford).

Lele, P.P. and Serapati, N. (1975). Abstracts, Second European Congress on Ultrasonics in Medicine, Munich.

Leyton, C., Froude, J., Gent, G., Pridie, R.B., McDonald, A. and Brigden, W. (1972). Presented to the 6th European Congress on Cardiology, Madrid.

Madiera, H., Ziady, G. and Pridie, R.B. (1972). Proceedings of American Institute for Ultrasound in Medicine, Philadelphia.

Mallard, J.R. and Christie, A. (1968). Abstracts, Second International Conference on Medical Physics, Boston, Mass.

Mason, W.P. (1964). Piezoelectric crystals and their applications to ultrasonics. (D. Van Nostrand, Princeton).

McDicken, W.N. (1976). Diagnostic Ultrasonics (Crosby, Lockwood and Staples, London).

McDicken, W.N., Bruff, K and Paton J. (1974). Ultrasonics, 12, 269.

McSherry, D.H. (1973). Proceedings of the Second World Congress on Ultrasonics in Medicine, Rotterdam, p. 325 (Excerpta Medica, Amsterdam).

Meeker, T.R. (1972). Ultrasonics, Jan, 26.

Meindl, . (1976). Presented at the 7th L.H. Gray Conference on Medical Images, Leeds. (to be published).

Montgomery, J. (1972). UKAEA, AWRE Applied Physics Division Publication GRO/44/83/105.

Morse, P.M. and Feshbach, H. (1953). Methods of Theoretical Physics Volume I (McGraw Hill, New York).

Morse, P.M. and Ingard, K.N. (1968). Theoretical Acoustics (McGraw Hill, New York).

Mountford, R.A. and Wells, P.N.T. (1972). Phys. Med. Biol., 17, 14.

Nicholas, D. and Hill, C.R. (1975). Nature, 257, 305.

Norton-Wayne, L. (1975). Signal Recovery by Deconvolution. City University Department of Systems Science, Publication 81.

O'Neill, H.T. (1949). J. Acoust Soc. America, 21, 516.

Pridie, R.B. (1971). Thorax, 27, 759.

Pridie, R.B., Benham, R. and Wild, J. (1972). Clin. Radiol., 23, 160 - 173.

Pridie, R.B. and Weir, J. (1973). Proceedings of British Medical Ultrasonics Group, London.

Rachly, C.E., Whalen, R.E. and McIntosh, H.D. (1966). Circulation, 34, 579 - 584.

Rayleigh, Lord (1896). Theory of Sound Volume II (Dover Publications).

Redwood, M. (1961). J. Acoust. Soc. America, 33, 527 - 536.

Rettermaier, G. (1973). Proceedings of the Second World Congress on Ultrasonics in Medicine, Rotterdam, p. 199 (Excerpta Medica, Amsterdam).

Robinson, D.E., Lees, S. and Bess, L. (1974). IEEE Trans. on Acoustics, Speech and Signal Processing, ASSP - 22, 395.

Robinson D.E. and Williams, B.G. (1975). Proceedings of the Second European Congress on Ultrasonics in Medicine, Munich, p. 96 (Excerpta Medica, Amsterdam).

Ross, F.G.M. (1972). in Ultrasonics in Clinical Diagnosis, ed. Wells, P.N.T. (Churchill Livingstone, Edinburgh).

Saneyoshi, J. (1958). Bulletin of Tokyo Institute of Technology Series B, 3, 103.

Segal, B, Likoff, W. and Kingsley, B. (1966). J. American Medical Association, 195, 161 - 166.

Skudrzyk, E.J. (1971). Foundations of Acoustics (Springer Verlag).

Somer, J.C. (1968). Ultrasonics, 6, 53.

Somer, J.C. (1973). Proceedings of Second World Congress on Ultrasonics in Medicine, Rotterdam, p. 304 (Excerpta Medica, Amsterdam).

Taylor, D.E.M. and Wade, J.D. (1973). Cardiovascular Res., 7, 14 - 21.

Thurstone, F.L. and Von Ramm, O.T. (1973). Proceedings of Second World Congress on Ultrasonics in Medicine, Rotterdam, p. 43 (Excerpta Medica, Amsterdam).

Tiersten, H.F. (1969). Linear Piezoelectric Plate Vibrations (Plenum Press, New York).

Twersky, V. (1950). J. Acoust. Soc. America, 22, 539.

Van Vleck, J.H. and Middleton, D. (1966). Proc. IEEE, 54, 2 - 19.

Waag, R.C. and Gramiak, R. (1973). Proceedings of the Second World Congress on Ultrasonics in Medicine, Rotterdam, p. 239 (Excerpta Medica, Amsterdam).

Wagner, R.F., Weaver, K.E., Denny, E.W. and Bostrom, R.G. (1974). Medical Physics, 1, 11.

Watmough, D., Crippin, D. and Mallard, J. (1974). Brit. J. Radiology, 47, 24 - 33.

Wells, P.N.T. (1969). Physical Principles of Ultrasonic Diagnosis (Academic Press, London).

Wells, P.N.T. and Mountford, R.A. (1972). Phys. Med. Biol., 17, 261.

Wells, P.N.T. (1975). Ultrasound in Med. and Biol., 1: 4, 369.

Whittingham, T.A., Davison, J.M., Lind, T. and Farr, V. (1973). J. Obst. Gynaec. Brit. Commonwealth, 80, 769.

Whittingham, T.A. (1975). Proceedings of the Second European Congress on Ultrasonics in Medicine, Munich, p. 59 (Excerpta Medica, Amsterdam).

Wigle, E.D., Marquis, Y. and Anger, P. (1967). Can. Med. Ass. J., 97, 299 - 301.

Willson, K. (1974). M.Sc. Report, University of London.

Willson, K., Gehkre, J., Gore, J., Leeman, S., Oliver, R. and Pridie, R.B. (1975). Proceedings of Second European Congress on Ultrasonics in Medicine, Munich (Excerpta Medica, Amsterdam).

Winters, W.L., Ricetto, A., Grineriez, J., McDonough, M. and Soulen, R. (1967). Brit. Heart. J., 29, 788 - 800.

Yokoi, H. and Ito, K. (1972). Toshiba Review, 76, 1. (Tokyo Shibawa Electric Co. Ltd., Tokyo).